The Static and Dynamic Behaviour of Carbon Fibre Composites used in Golf Club Shafts

by

Carl Slater

A thesis submitted to The University of Birmingham

For the degree of DOCTOR OF PHILOSOPHY

School of Metallurgy and Materials

College of Engineering and Physical Sciences

The University of Birmingham (UK)

July 2011

Contents

Abstract

The static and dynamic properties of carbon fibre composites of varying orientation, stacking sequence and geometry has been analysed in terms of modulus and material loss factor up to strain rates applicable to golf club shafts.

No noticeable change in modulus or damping was seen at strain rate applicable to golf club shafts. All panels tested strain rate sensitivity onset occurred at around 0.4 s^{-1}, which is above the maximum observed during a golf swing (0.1 s^{-1}).

The strain rate sensitivity was found to be sensitive to aspect ratio (for strain rates above 0.4 s^{-1}). Two 20° panels of the same fibre interfacial area, but with different aspect ratios (length/width) showed different strain rate sensitivities. The short wide panel (aspect ratio 1.5) showed a higher stiffness and lower strain rate sensitivity when compared to a panel with an aspect ratio of 2.6.

A model was created to predict the modulus and damping of lay-ups for laminates and golf club shafts. The model was validated against three composite systems at varying orientations and stacking sequences. The software agreed well with laminate experimental data (data sets showed a RMSD of less than 5 %). From this an optimising software was developed to provide the user with a stacking sequence that will optimise modulus, damping or the product of both.

This thesis also evaluated commercial shafts in order to determine the models applicability to this application. Commercial shafts were tested for both stiffness and damping, where a number of aspects such as inter-ply resin rich regions and seam were observed as possible areas for discrepancy with the models prediction.

Shafts were fabricated in order to analyse these aspects in greater deal, and to determine the models limits for this application. The model accurately predicted the stiffness of the shafts however the model failed to predict the damping of the shafts when comparing to the average values taken. When damping was compared to the areas where no seams were present, the model agreed well except for in two cases, which have been attributed to shafts flaws (cracks or excess inter ply resin). The model presented in this research consistently characterised the stiffness of fabricated shafts, however the seams proved too dominant a feature to be neglected in the prediction of damping.

Acknowledgements

There are many people to who I owe a lot for their help during my time as a PhD student. Firstly I need to thank my supervisor, Dr Martin Strangwood, from who I have had unbelievable support and helped my not only with my PhD but also given me genuine prospects for a future career, and I am sure I would not be aiming to continue a career within the University if it was not for his input, support and guidance.

Thanks also needs to be given to my industry supervisor, Dr Steve Otto, and my second academic supervisor, Prof Claire Davis. Both of which have offered fantastic advice and support.

To all my co-workers in the office; Dan, Millie, Heiko, Dave, Amrita, Hamid, Rachel, Xi, Mark, Frank, JP, George, Daniel. For always creating a great office to which I looked forward to coming into everyday.

To the lab technicians Mick Cunningham, Dave Price and John Lane, of who I am convinced are the foundations of the department, and stop the building from falling down if it wasn't for all the hard work they put in.

Finally, and most importantly, my family. Thank you for all the support throughout my time at University. If it wasn't for your support I would have not got the opportunity to come to university and stay on to do a post graduate. Most of all my girlfriend, Tan, what a star. I sure that I could not have got through all the pressures of the PhD if I didn't have you waiting for me at home. I'm sure you were as relieved as me when this was submitted.

I could write a thesis on thanking everyone, and I am sorry if I have missed anyone out.

Nomenclature

* In order of first appearance

CFRP - Carbon Fibre Reinforced Polymers

GFRP - Glass Fibre Reinforced Polymers

CFC - Carbon Fibre Composite

UTS - Ultimate Tensile Strength

E - Young's Modulus

ρ - Density

CoM - Centre of Mass

GoG - Centre of Gravity

I - 2nd moment of Inertia

F - Force

L - Cantilever Length

d - Deflection

EI - Flexural Rigidity

M - Bending Moment

f - Fundamental Bending Frequency

C_1 - Constant attributed to Clamping

r_o - Inside Radius

r_i - Outside Radius

Vf - Volume Fraction

E_x, E_y - Longitudinal and Transverse Modulus (with respect to the laminate)

E_1, E_2 - Longitudinal and Transverse Modulus (with respect to the fibre orientation)

G_{xy} - Shear Modulus (with respect to the laminate)

G_{12} - Shear Modulus (with respect to the fibre orientation)

θ - Fibre orientation away from the loading axis

$\boldsymbol{C}_{ij}$ - Stiffness Matrix

$\boldsymbol{T}_{ij}$ - Transformation Matrix

$\overline{\boldsymbol{C}}_{ij}$ - Transformed Stiffness Matrix

$\boldsymbol{A}_{ij}$ - Extensional Stiffness Matrix

$\boldsymbol{B}_{ij}$ - Extensional/Bending Coupling Matrix

$\boldsymbol{D}_{ij}$ - Bending Stiffness Matrix

h_k - Distance to laminate mid-plane from the k^{th} ply

η - Loss Factor

T_g - Glass Transition Temperature

RRR - Resin Rich Region

η_x, η_y, and η_{xy} - loss factor for x, y and shear respectively (with respect to the laminate)

w = Weighting factor of a ply

RMSD - Root Mean Square Deviation

CLT - Classical Laminate Theory

Laminate Script

This section will explain the short-hand script used to define a laminates stacking sequence.

$[\theta]_4$ - The unit is repeated four times, all with fibres orientation at θ° [θ θ θ θ].

$[\pm\theta]_4$ - Is a four ply laminate with fibres orientation both in + and - and balanced [θ -θ -θ θ].

$[\theta_a\ \theta_b]_{2s}$ - Is a four ply laminate. The *s* denotes it is symmetric about the last ply and the unit is repeated twice [θ_a θ_b θ_b θ_a].

List of Figures

List of Tables

1. Introduction

The interaction between a golfer and their equipment is extensive, and has led to the development of equipment as effects that dramatically enhance golfers' games are sought. For a golfer to be able to swing consistently, they need to have confidence that the club they are using will provide them with a reproducible action including delivery of the face to the ball, which is mainly dictated by the shaft. Of the three components that make up the golf club, it is the shaft that transmits the swing from the golfer to the ball; the grip is merely a handle for the golfer, and the head, although important in its own right, cannot work to its potential unless it is addressed to the ball correctly.

1.1. History of the Shaft

From the 17th to the 19th century golf club making was a craft mainly dominated by the British. Therefore British hardwoods were the predominant material used in this period. Woods, such as danga, greenheart, lemonwood, lancewood and ash, were all being used for shafts throughout England and Scotland. As access to various woods was regional, club makers also showed regional variations in their products, with the shaft materials used depending heavily on location [1].

As golf became more popular, and golfers preferred certain woods because of their "feel", hickory started to be favoured. Whilst being low in density (600 g/cm^3) and relatively high in modulus, hickory also shows a great deal of resistance to warping, unlike the other woods previously used in shafts. The first recorded reference to a hickory shaft was in 1828 and this type of shaft dominated until the late 19th century [1].

Major disadvantages of the hickory shaft were its relatively low strength and the property variability of this natural product. Thus, if a shaft broke, replacement by another hickory

shaft would often not give the club the same "feel" as the original shaft. Shafts based on metallic alloys demonstrate much more uniform properties coupled with higher strength so that these materials replaced hickory and other woods for mass-produced shafts showing greater reproducibility (early 1900's). The processability of metallic alloys allowed for variables such as taper, wall thickness and outer diameter to be altered readily, therefore changing stiffness and the position of the kick point.

By the 1950s golf club manufacturers started experimenting with synthetic non-metallic materials for the shaft. Glass fibre reinforced polymers (GFRP) were first used in 1954 [2, 3], and were originally used to wrap around a steel shaft in order to reduce its mass; eventually being used for the entire shaft. Although having low density, GFRPs have poor torsional resistance and a low fracture toughness due to their highly anisotropic mechanical properties, and therefore the GFRP shaft only lasted in the market for little over a decade. In the late 1960s carbon fibre reinforced polymer (CFRP) or carbon fibre composite (CFC) shafts with greater strength and stiffness values were produced, and by 1974 the "graphite" shaft was being mass-produced. This gave the shaft its more desirable properties (low density, and high modulus, yield stress, ultimate tensile strength and ductility), with little trade off [4, 5].

1.2. Metallic Shafts

1.2.1. *Alloys Used in Commercial Golf Shafts*

Although steel shafts are the most common metallic alloy shafts, many other metallic alloy shafts are available; these include; Al-based alloys, Mg-based alloys, Ti-based alloys and Cu-based alloys. Table 1.1 shows some material properties for the alloys used in commercial shafts. It can be seen that no one material has all the desired properties for a shaft; steels for

example have a far greater modulus to other metallic alloy systems, however they also have the greatest density, Aluminium-based alloys conversely have a much lower density, but both modulus and ultimate tensile strength (UTS) values are much lower than those for steels and titanium-based alloys. Other requirements of the material include; damping, formability, cost, corrosion resistance and joinability. Properties are typically determined through simple uniaxial tensile tests at room temperature, and at constant low strain rates (0.01 min^{-1} or 2mm/min depending on strain or displacement controlled testing[6]).

Table 1.1: Material properties for alloys used for golf shafts [7]

Alloy	**Density, ρ (g/cm^3)**	**Young's Modulus, E (GPa)**	**Yield Stress, σ_y (MPa)**	**Ultimate Tensile Strength, UTS (MPa)**	**Ductility (%)**
C-Mn (mild) Steel	7.85	210	210-350	400-500	15-35
High Strength Steel e.g. 4340	7.85	207	860-1620	1280-1760	12
316 Stainless Steel	7.85	195	205-310	515-620	30-40
Cu-Be	8.25	128	200-1200	450-1300	4-60
Al-Cu	2.77	73	75-345	185-485	18-20
Mg-Ti	1.78	45	200-220	260-290	15
Ti-3Al-2.5V	4.5	105-110	750	790	16
Ti-6Al-4V	4.43	110-125	830-1100	900-1170	10-14
Ti-15V-3Al-3Sn-3Cr (β - Titanium)	4.71	85-120	800-1270	810-1380	7-16

The demands of the shaft are different depending on the club it will be used for, typically drivers will be subjected to much higher loads and therefore the yield stress (σ_y) and modulus

are of primary importance, whereas the effect of mass of the shaft (within the range seen between a steel and composite shaft) may be less of a concern [8]. For putters however, the forces acting on the club are minimal and therefore weight distribution is a higher priority, with σ_y and UTS becoming less of an issue, with irons and wedges requiring intermediate properties.

1.2.2. *Fabrication of Metallic Shafts*

1.2.2.1. Seamless Shafts

For the ductile materials seen in Table 1.1, drawing is often used to produce a seamless shaft. Although less ductile materials can be used in this process, they would require softening before shaping and subsequent heat treatment to full strength, thus increasing the cost of the production and reducing production rate.

Drawing involves forming a rough tube from the billet material by either piercing or uneven rolling for the less ductile metals, this tube is then forced through a hardened die which works in conjunction with an internal mandrel; this is used to control the outer radius and wall thickness, as seen in Figure 1.1 [7]. By widening the gap between the dies, and moving the mandrel forward and back, a large range of tapered shafts can be manufactured. Stepped shafts can be produced by making a simple tapered shaft and then shaping the tube between two dies. Typical butt tip and butt diameters are around 8.5 and 15.3 mm respectively [9, 10].

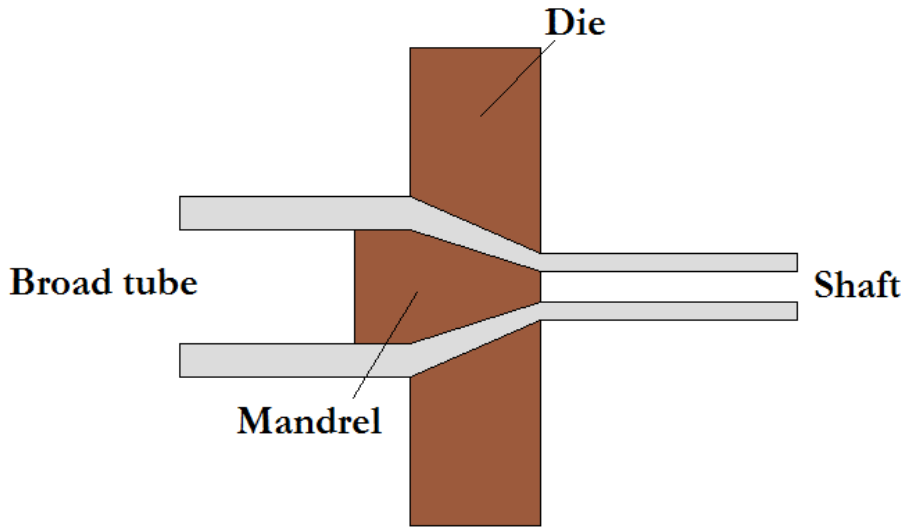

Figure 1.1: Schematic diagram to show a metal shaft fabricated by drawing.

1.2.2.2. Welded Shafts

For high strength alloys, where drawing becomes very expensive, sheet welding is a preferred method. Flat sheets of the alloy are cut to produce either a stepped (although the previous method mentioned is more common for stepped shafts) or tapered shaft (Figure 1.2). The sheets are passed through a die, similar to that for drawing, this forms a tubular shape which is welded (typically tungsten inert gas (TIG) welding, as this forms a small weld bead, and a smaller heat affected zone, than other welding processes). The weld bead is then subsequently filed/polished flush with the surface in order to reduce the effect the thicker section will have on the stiffness.

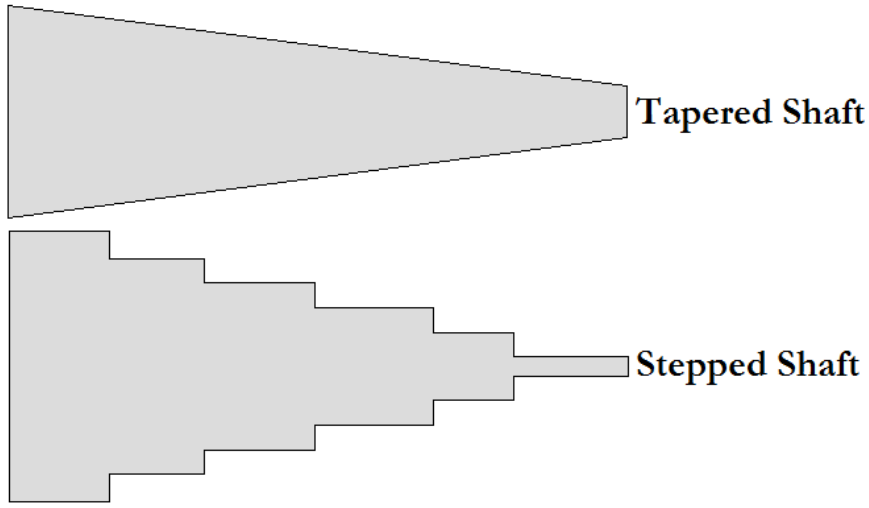

Figure 1.2: Flat sheet metal cut-outs used to make welded shafts.

1.3. Deflection of the shaft during a swing

Due to inertia forces acting on the shaft and the fact that the shaft axis and head centre of mass (CoM) are not collinear, the shaft is subjected to three different deformations. These are toe up/toe down, lead/lag and twisting (Figure 1.3 and Figure 1.4).

At the top of the backswing, the weight of the head causes the shaft to bend down. As the club is accelerated at the start of the downswing inertial forces oppose the motion of the head so that it lags behind the hands, once the mass of the head is acting in the same direction as the swing (once the club goes through the vertical), the head starts to catch up and the shaft will start to unbend, ideally impact will occur at the unbend point as at this point the club has the greatest amount of kinetic energy and the minimal amount of stored energy. Past this point the shaft will go into a lead position and the kinetic energy is reduced. The unbend point is also dictated by the golfer's swing style. This will normally result with the shaft in a slight lead position at impact. Figure 1.5 shows the three main swing styles [8, 11], it can be seen that a different deflection at impact can be seen in the three different styles (Table 1.2).

Both the one and two peak style show a greater acceleration loading the shaft compared to the ramp like style, this results in a greater amount of peak deflection in the toe-up/down direction, whereas the ramp like style shows a much greater acceleration prior to impact. Just prior to impact the shaft undeforms resulting in an additional velocity [12]. This extra kinetic energy, which has arisen from the stored strain energy of the downswing, is referred to as the kick velocity. This results in a greater clubhead velocity. It is also important to notice the kick velocity at impact, with the "ramp-like" swing showing a noticeable increase over the other two swing types.

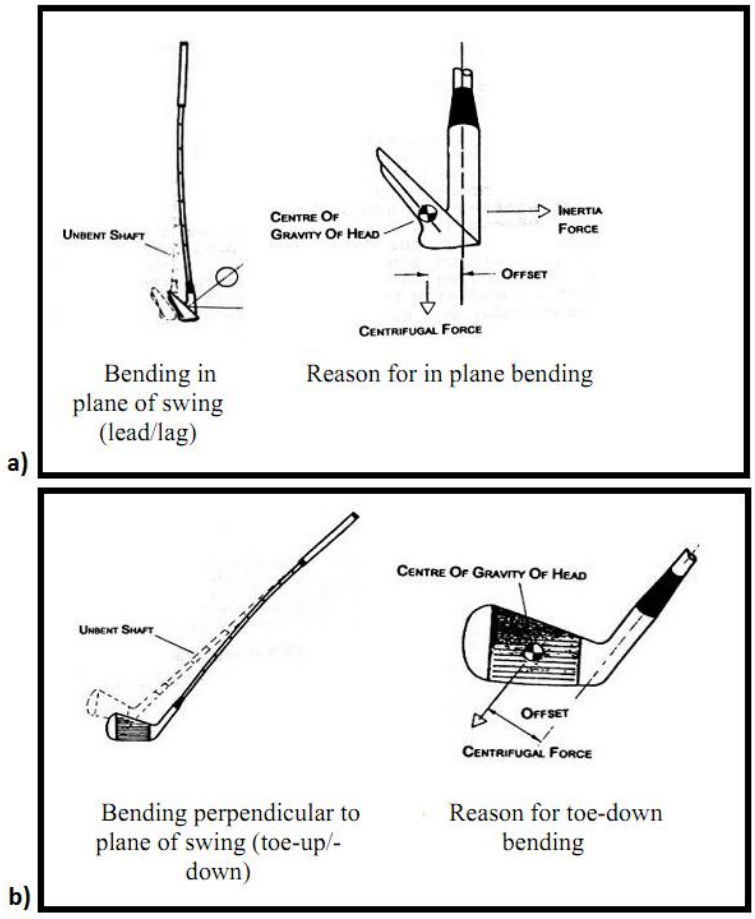

Figure 1.3: Schematic diagram to show a) lead/lag deflection and b) toe-up/toe-down deflection. (adapted from Horwood [13]).

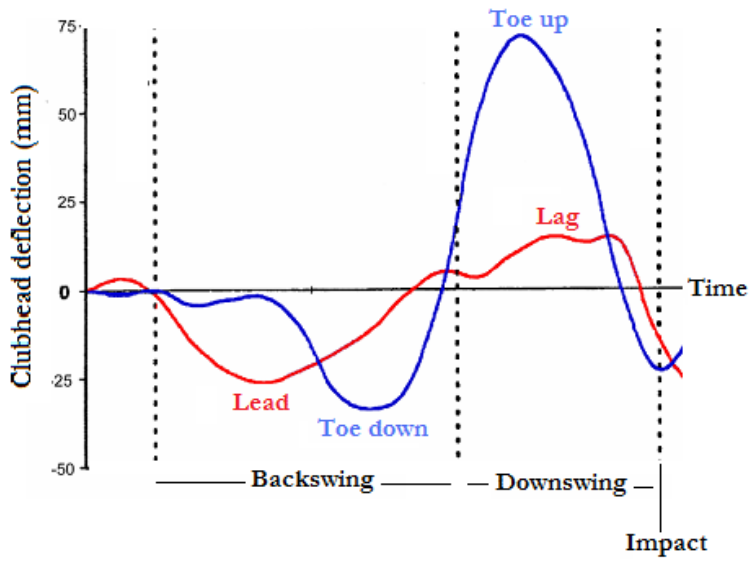

Figure 1.4: Deflection of the shaft in the toe up/toe down and lead/lag directions (adapted from Newman, Clay & Strickland [14]).

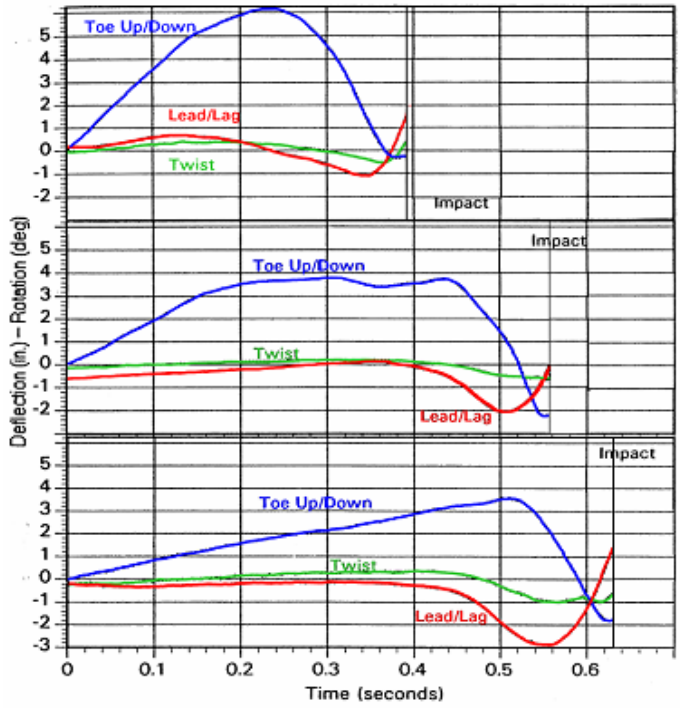

Figure 1.5: Three main swing styles: 'One-peak' (top), 'double-peak' (middle) and 'ramp-like' (bottom)(Adapted from Butler and Winfield [11]).

Table 1.2: Showing swing variables for the three swing types shown in Figure 1.5.

Variable	One Peak	Two Peak	Ramp-like
Load up time (s)	0.391	0.557	0.630
Peak deflection (mm)	158.23	97.2	92.5
Time to peak deflection (s)	0.234	0.304	0.51
Lead/Lag deflection at impact (mm)	39.2	2.8	38.14
Toe up/down deflection at impact (mm)	-5.3	-54.8	-43.8
Twist angle at impact (°)	0.413	-0.341	-0.472
Maximum twist angle (°)	0.55	0.677	1.021
Kick velocity at impact (mm/s)	2288	2288	2501
Toe up/down velocity at impact (mm/s)	335	426	500

Braunwart [15] carried out a comprehensive study on the bending modes present in a shaft for both free-free (Figure 1.6) and clamped-free clamping conditions (Figure 1.7). In this study, finite element modelling (FEM) was used to accurately predict the first three bending modes of a single shaft (accurate to 0.9 %). However, this was carried out on both steel shafts and "graphite" shafts, and for the carbon fibre composite shaft, a constant modulus was used along the shaft. This is not to be expected due to tip stiffening as well as the presence of seams. These tests were carried out at relatively low strains and strain rates. The frequency response of the carbon fibre composite shafts was also predicted (a maximum of 10%

discrepancy between experimental and FEA results), however without accurate material data, then at higher strains/strain rates it is expected that the error of the model may increase.

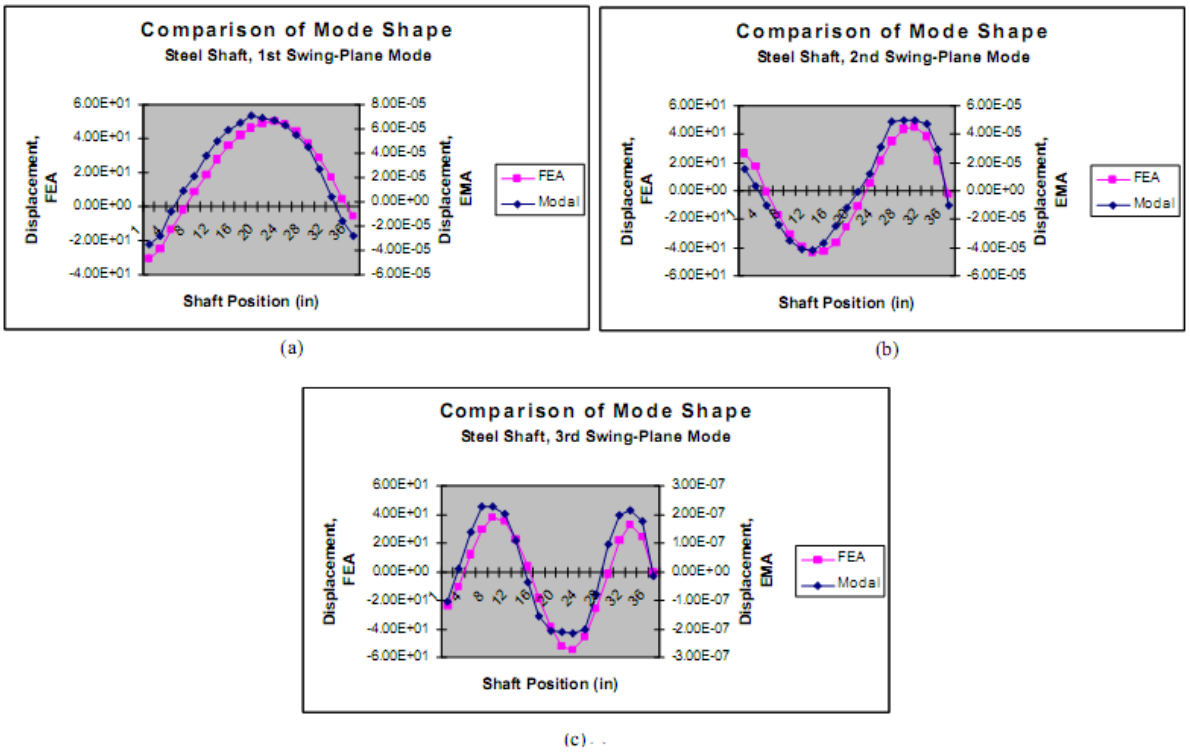

Figure 1.6: FEA and experimental modal analysis of a shaft in free-free clamping condition [15].

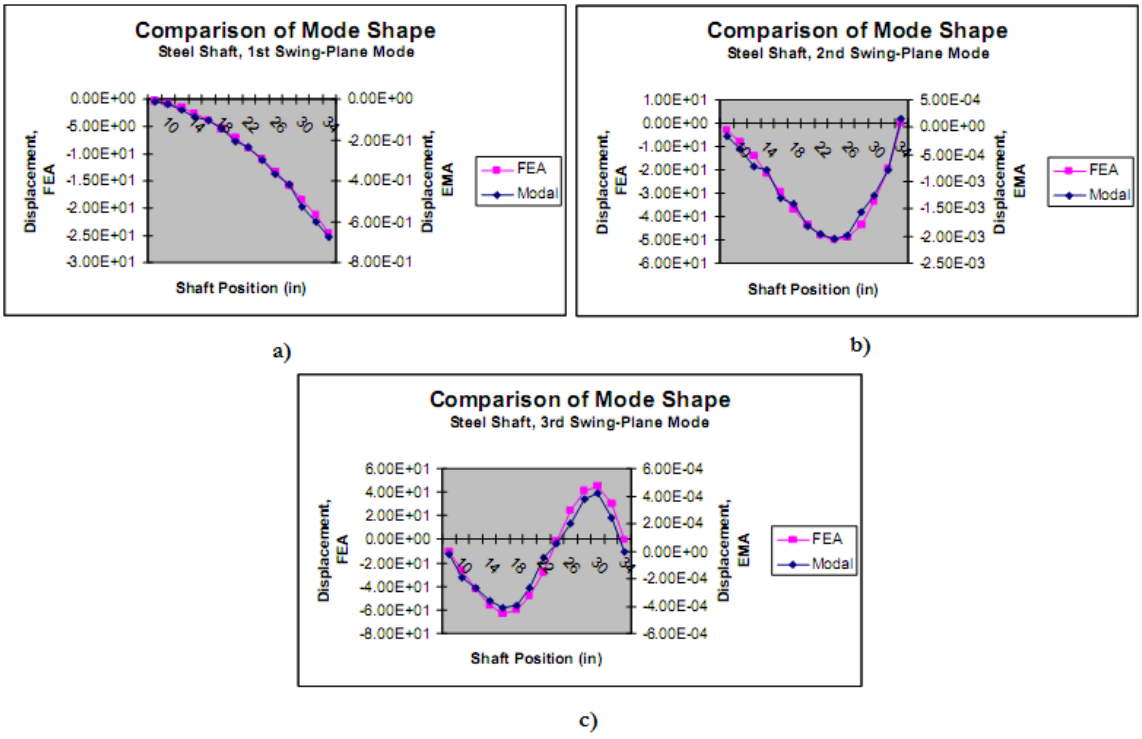

Figure 1.7: FEA and experimental modal analysis of a shaft in clamped-free clamping condition [15].

Friswell *et al.* [16] also used FE modelling with experimental modal analysis (EMA), on a single steel shaft and showed good agreement with Braunwart on modal shapes produced. This study also showed that a torsional coupling mode is present for all modes after the first in the clamped-free condition, which was attributed to the off-axis centre of mass of the head.

1.4. Current Testing Methods

1.4.1. *Deflection Test.*

In order to determine the flexural rigidity (commonly called “flex”) of a shaft a cantilever deflection test is carried out. This helps manufacturers group shafts into 5 stiffnesses; Ladies,

Flex, Regular, Stiff and X-Stiff. It should be noted however that there is no universal grading of shafts, and many shafts if manufactured by a different company may be assigned a different stiffness grading [1].

The deflection test simply involves a mass of 2.72 kg being attached to 76 mm away from the tip whilst being clamped at the butt, this provides a static stiffness measurement [17]. Equation 1.1 is used to give a numerical figure to this test, whereas in reality only the deflection distances are compared [1].

$$EI = \frac{FL^3}{3d},$$

Equation 1.1

Where E is the Young's modulus of the material, I is the 2nd moment of inertia, F is the force being applied, L is the cantilever length and d is the deflection distance.

However this only provides the overall stiffness of the shaft, and means that the effects of changes in the moment of inertia along the shaft, e.g. due to tapering and changes in wall thickness, on stiffness will not be determined. Broulliette [18] measured experimentally changes in stiffness along a shaft and analysed this to give stiffness values along the shaft's length. The clamp was initially placed in position L_1 and the deflection measured. The clamp is then moved to a new position (L_2) and again the deflection is read, this procedure is continued until the whole length of the shaft is covered (L_n). The stiffness along the shaft length is then given by Equation 1.2.

$$EI_n = \frac{\frac{1}{3}F\left(L_n^3 - L_{n-1}^3\right)}{\delta(L_n) - \frac{1}{3}\frac{M_{n-1}L_{n-1}^2}{EI_{n-1}}},$$

Equation 1.2 (Broulliette [18])

where EI_n, M_n and $\delta\ (L_n)$ is the flexural rigidity, bending moment and the deflection at the cantilever length n respectively.

1.4.2. *Frequency Testing*

Another measurement of flexural rigidity is the fundamental bending frequency. This provides a quasi-static approach to the testing, and takes into consideration the mass of the head.

A 205 g mass is attached to the tip of the shaft and excited, which can be carried out in a Golfsmith Precision Shaft Frequency Analysis Machine, and provides values in cycles per minute (cpm) or Hertz (Hz).

Figure 1.8: Schematic diagram showing the frequency testing method.

Equation 1.3 therefore allows the comparison for shafts of similar stiffness but varying weight. Whereas this is not possible with Equation 1.2.

$$f = \frac{C_1}{2\pi}\sqrt{\frac{EI}{\rho AL^4}} \quad ,$$

Equation 1.3

where C_1 is a clamped constant (3.52 in the clamped-free condition seen in Figure 1.8), ρ is the density of the material, A is the cross-sectional area, and L is the cantilever length.

This assumes constant dimensions along the shaft, when in reality the taper of the shaft has a large effect. However, this method is seemingly adequate for comparative purposes. This method also allows for the detection of seams (described later in Section 1.7.3.1), by measuring the frequency around the shaft's circumference, a seam is generally attributed to a lower frequency of up to 7 cpm [4].

1.4.3. *Bend Point*

Also referred to as the kick point or flex point, can be measured in three different ways. The shaft can be placed under uniaxial compression [17]; the shaft can be clamped at the butt and loaded at the tip; or loaded at the butt and clamped at the tip [19]. Figure 1.9 shows the second method. By creating a straight line between the butt and the tip, the kick point can easily be found by the point at which the shaft deviates most from this.

Bend point position is generally divided up into three categories, low, mid and high, which corresponds to around 40, 50 and 60 % distance away from the tip respectively as a proportion of the cantilever length.

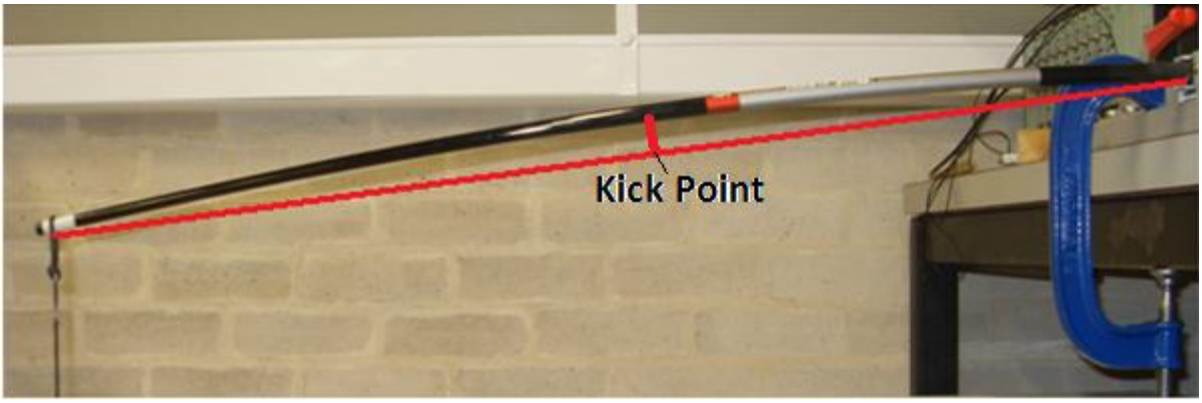

Figure 1.9: Image showing the kick point of a shaft.

1.4.4. *Torsional Testing*

Torsional rigidity is the shaft's resistance to twisting about its longitudinal axis. During a downswing the non-aligned nature of the shaft axis and the head centre of mass gives rise to a torque that twists the shaft and can cause non-square impact of the face on the ball. Inertia forces act on the COM and the grip the golfer imparts on the club resists this motion and results in a degree of twisting, depending on the torsional stiffness of the shaft. A high level of twisting during the swing reduces the likelihood of a square impact, and thus accuracy may be lost.

Current testing for this involves subjecting the shaft to a moment of around 1 foot lb (approx 0.67 m kg) and measuring the degree to which the shaft has twisted. Typically, commercial shafts twist through 2 - 5° for this loading [4].

1.5. Effects of Shaft Characteristics on Launch Conditions

1.5.1. *Influence of Shaft Dimensions on Stiffness*

For a parallel-sided shaft Equation 1.4 can be used to calculate the bending stiffness. It can be seen that stiffness is heavily dependent on the inner and outer radii of the tube, as well as the length [20]. The length is somewhat restricted by anatomical constraints, and shorter shafts may result in a lower clubhead speed (Section 1.5.2).

$$Bending\ Stiffness = \frac{3\,E\,\pi\,(r_o^4 - r_i^4)}{4\,l^3},$$

Equation 1.4

where E is the Young's modulus of the material, r_o is the outer radius, r_i is the inner radius and l is the length of the shaft.

Although Equation 1.4 is only valid for parallel-sided shafts, it is apparent that, for a tapered shaft, as the outer and inner radii decreases, as long as wall thickness remains constant then the stiffness will decrease. Modifying the stiffness profile along the shaft in this way allows the position of the bend point to be altered (Section 1.4.3). Example of different types of taper can be seen in Figure 1.10; by introducing tip stiffening, the bend point position will be moved closer to the butt, and vice versa for butt stiffening. The taper can, therefore, have a major effect on the overall tip deflection (Figure 1.11), assuming constant modulus, therefore only applying to metallic shafts.

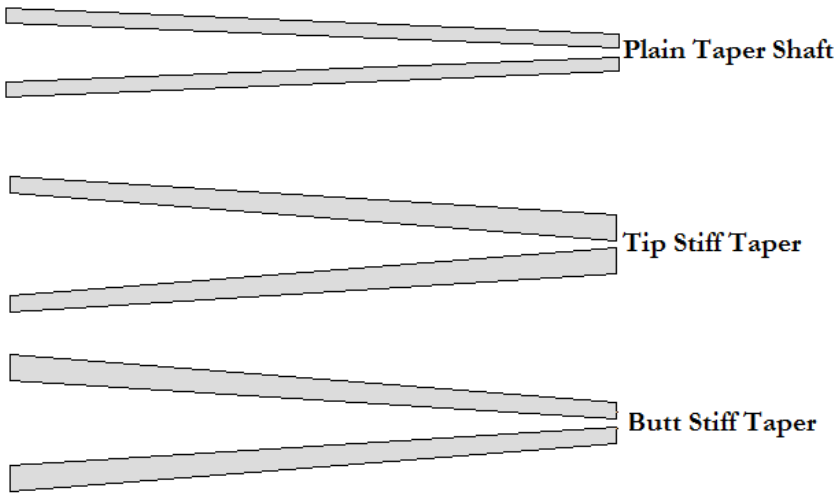

Figure 1.10: Different types of taper to move the bend point [7].

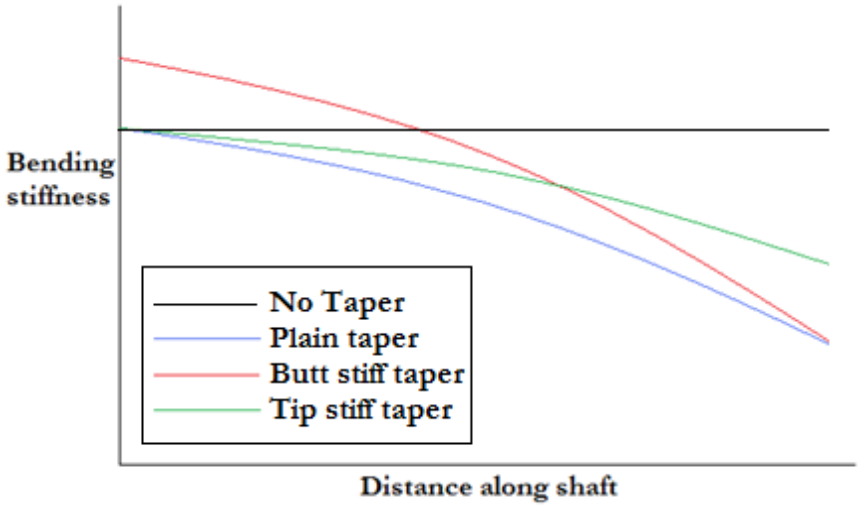

Figure 1.11: Bending stiffness profiles of shafts with different tapers [7].

However stepped shafts are very common when fabricated from metals, where the sequence of constant diameter sections leads to different bending stiffness profiles (Figure 1.12).

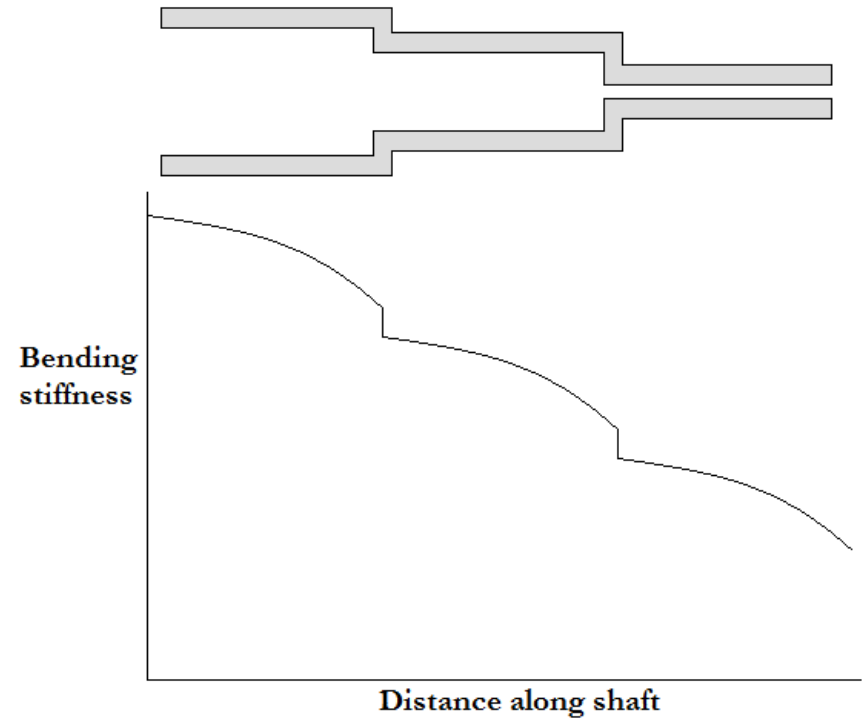

Figure 1.12: Stiffness profile of a stepped shaft.

1.5.2. *Effect of Shaft Length on Clubhead Speed*

Mathematically, if angular velocity remains constant, then as shaft length increases, so will clubhead speed [21]. Both Kenny et al., [22] and Mizoguchi and Hashiba [23] showed that with increasing shaft length (from 46 - 50 inches and from 45 - 48 inches respectively) an increase in clubhead velocity is expected. Whereas Kenny et al., found only an increase of 1.74 m/s with an increase in 4 inches, Mizoguchi and Hashiba present data which show an increase in speed of between 0.25 and 2.32 m/s per inch depending on the player. Kenny *et al.* used computer simulation to determine the effects of shaft length on clubhead speed, however Mizoguchi and Hashiba used actual golfers. As much lower change was seen for Mizoguchi and Hashiba it would appear that the players alter their swing to accommodate the new club, a similar effect was seen by Betzler [21], where a range of shaft stiffnesses that where otherwise nominally identical shows no change in launch conditions. Although there seems to be evidence to support the theory that an increase in shaft length increases clubhead speed, it remains to be seen if it is likely to improve a drive, as neither of these studies involve any accuracy measurements. As shaft length increases the inertia the player has to overcome increases (increase in inertia will be 15 and 7 % for Kenny et al. and Mizoguchi and Hashiba respectively, assuming the mass of the head is significantly greater than the mass of the shaft), therefore it is likely that the swing will be less stable and result in a decrease in accuracy [1, 13, 16, 24].

Shafts however, have been restricted on their length. The R&A state that "the length of the club must be at least 18 inches (457.2 mm) and, except for putters, must not exceed 48 inches (1219.2 mm)." [25, 26].

1.5.3. *Effect of Stiffness and Kick Point on Dynamic Loft*

The static loft of a club is the angle from the club face to the vertical if the shaft was rigidly clamped vertically. However this is rarely how the club is presented to the ball at impact. As mentioned in Section 1.3, the shaft is likely to be slightly deflected upon impact; this represents loss in kinetic energy being transferred to the ball, as the shaft is storing some elastic energy [8, 27]. The angle at which the face actually presented to the ball is deemed its dynamic loft. The shaft affects this in two ways; stiffness, and kick point.

Kick point: As mentioned earlier, the kick point of a shaft tends to be positioned between 40 and 60 % of the shaft length away from the tip. As the kick point moves closer to the tip ('low' kick point), a greater amount of dynamic loft will typically be seen (Figure 1.13). This can be attributed to the shorter radius of curvature as the shaft unbends, therefore for the same lead position at impact, the face angle will be slightly greater.

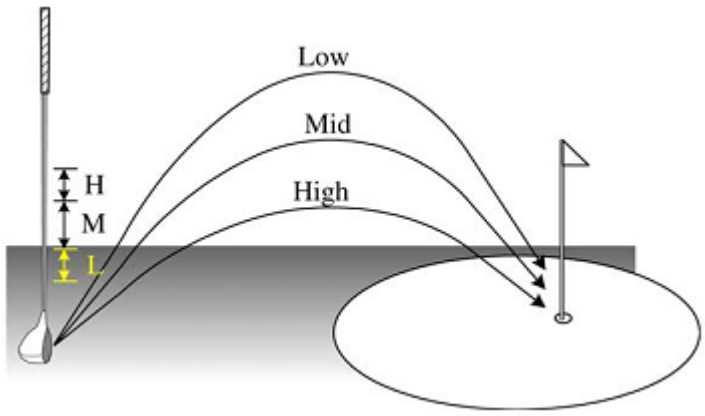

Figure 1.13: The effect of kick point on dynamic loft [17].

Stiffness: The fundamental bending frequency (related to stiffness) can have a noticeable impact on the dynamic loft of a shot. A typical club will have a bending frequency of around 4 Hz [4, 27], meaning one oscillation will occur every 0.25 s (longer than a typical downswing, (Figure 1.14), however due to the gripping and inertial forces acting on the shaft,

the oscillation time is likely to increase. However, mathematically the optimal downswing/oscillation time needs to coincide to present the ball with an unbent shaft [21, 28-30].

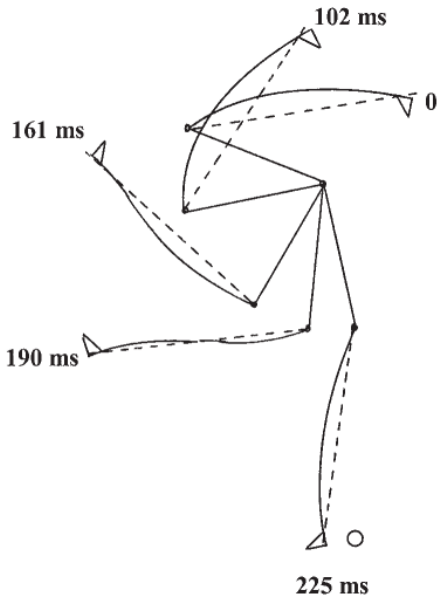

Figure 1.14: Schematic showing the deflection on a shaft during a typical swing, with the unbend point occurring between 190 -225 ms [30].

1.5.4. *Effect of Shaft Stiffness on the Deflections of a Shaft during a Swing.*

Shaft deflection at impact has been shown to be dependent on the loading characteristics or swing style (Section 1.3). Betzler [21] studied the effect of shaft stiffness on the deflections of a shaft during a swing. In this study three nominally identical clubs (apart from stiffness) were swung by 15 male golfers with handicaps < 5. The flexural rigidity of the shafts used were 38, 48 and 58 Nm^2 and represent a good range of stiffnesses of shafts available in the market [4, 5, 10, 31] and deemed a ladies, regular and x-stiff stiffness rating respectively by the manufacturer. Shafts were fitted with strain gauges at the kick point in both the lead/lag and toe-up/toe-down directions. Each player swung each club 6 times in a random order, not

knowing which stiffness they were holding, thus reducing any conscious adaptation prior to the first swing. Results indicated that both peak strain and peak strain rate increased with decreasing shaft stiffness, however both the loading pattern and defection at impact showed no noticeable difference between shafts. No correlation was also seen between peak strain and clubhead speed, with the player exhibiting the highest peak strain showing an average clubhead speed at impact.

It is important to note that peak strains and strain rates reached in this study were 6500 μm/m and 0.1 s^{-1} and will be used to determine whether the assuming linear elastic properties within this region are adequate in predicting the dynamic properties of the shaft.

1.6. Shaft Variability

According to the rules of golf (R&A, 2005, Appendix II - Rule 2b) [26]:

"At any point along its length, the shaft must:

i. Bend in such a way that deflection is the same regardless of how the shaft is rotated about its longitudinal axis; and
ii. Twist the same amount in both directions."

Therefore any deliberate asymmetry is strictly forbidden, thus ensuring the shaft cannot be designed in order to correct for wayward swing, for example. However "small spines" are deemed within manufacturing tolerances, and therefore a 'seamed' shaft will still conform to the Rules of golf.

During all the manufacturing methods spoken about in previous sections, variations will be found around the shaft's circumference:

- Drawn metallic shafts typically exhibit slight variations in wall thickness, due to the movement in the mandrel, leading to a thick wall section, with a thinner wall section 180° from it. Although the effect of this is normally minimal in comparison to other defects (such as weld lines), as the thick and thin sections somewhat counteract each other.
- Welded shafts have an obvious spine, the weld line. Depending on the size and extent of the heat affected zone (HAZ) will determine the effect it has on the stiffness, although the weld will typically increase the stiffness but can be minimised by polishing the weld bead flat.
- The greatest effect of seams can be seen in CFC shafts formed from pre-preg. As stated in Section 1.7.3.1, seams are formed when a ply starts or finishes. Huntley [4] investigated intrabatch variations of nominally identical shafts. Several observations were made:
    - Frequency variations of up to 5.1% were seen in a single shaft around its circumference, and can be attributed to variations in the wall thickness and modulus of the material. This is much higher than variations found in filament wound shafts (0.1%). Outer diameter differences did not alter stiffness by more than 0.8%.
    - A 34% variation in Young's modulus was found in sections taken from around the circumference, although specimen width did not meet with ASTM D790-92 standards. The low modulus regions of the shafts affect the stiffness of the shafts for a much greater distance around the circumference, thus frequency shows a lower variance compared to the modulus

- Average frequency values were found to vary by 2.8% between shafts in the same batch shafts, which was mainly attributed to mass variations of 2.5 g (4.1%). Although it can be seen from Figure 1.15 that if this set of shafts were selected and orientated randomly (as when a club is fitted), the range of frequencies expected can vary by up to 6 %.

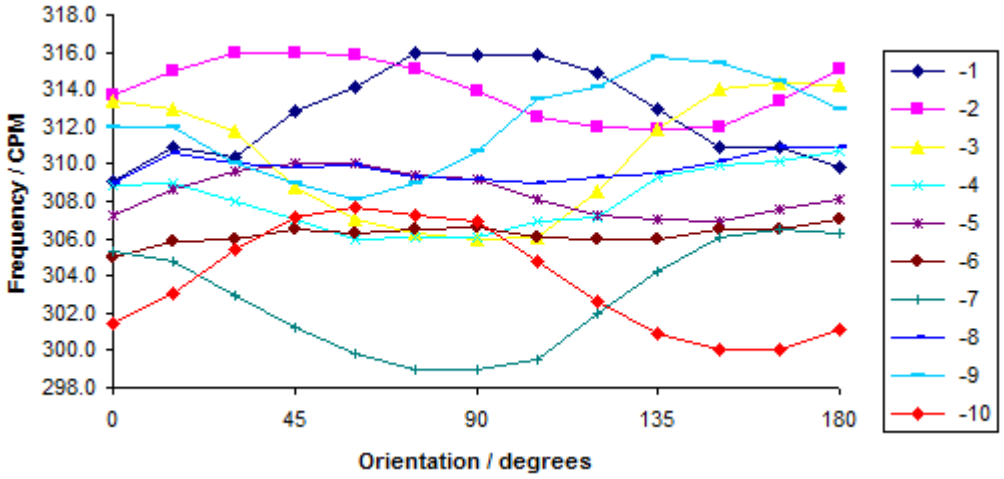

Figure 1.15: Intrabatch frequency variation of 10 nominally identical shafts [4].

1.7. Carbon Fibre Composites (CFCs)

Carbon fibre composites were originally developed for aerospace applications, due to their high specific modulus and specific strength. However, in more recent times, CFC technology has found its way into sporting applications, as well as automotive and civil engineering (Figure 1.16).

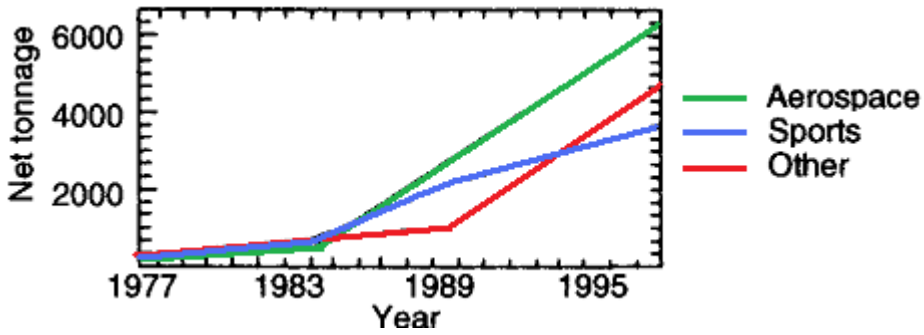

Figure 1.16: The amount of carbon fibres produced every year for different areas of application (adapted from Stabb [32]).

1.7.1. *Carbon Fibres*

In a graphite structure strong covalent bonds hold together carbon atoms in a hexagonal arrangement to form a layer, this is the source of the fibres' high modulus. These layers are held together by relatively weak van der Waals forces. However, there are no true graphite fibres, the term graphite simply refers to the fact that the fibres contain >99% carbon, whereas carbon fibres contain between 80-95% carbon [33]. The remaining 5-20 % being remaining hydrogen or nitrogen from the fibre precursor or oxygen to aid in the fibre-matrix interaction.

Carbon fibres are typically made from one of three precursor materials, polyacrylonitrile (PAN), pitch and rayon. For PAN-based fibres the method can be broken down into five stages [33, 34]:

- Spinning of the PAN into a precursor fibre.
- Stretching of the precursor
- Heating the precursor to 205 – 240 °C for 24 hours whilst being held under tension in an oxidising atmosphere.

- Carbonisation in an inert atmosphere at around 1500 °C, this will stabilise the PAN fibres and release the non-carbon elements present. At this point carbon fibres have been produced.
- To produce graphite fibres, the fibres are heat treated at 3000 °C again in an inert atmosphere, this begins to optimise the atomic structure orientation, and continue to purify the carbon content.

Table 1.3 shows some typical properties for different types of fibres used in composites. Although much higher in cost, the PAN-based fibres provide superior modulus in the direction of the fibre, and a lower density. Kevlar fibres however do have a lower density and greater strength, however the trade-off is a lower modulus, in both directions.

Table 1.3: Properties of different fibres [2].

Property	**Carbon polyacrylonitrile (PAN)-based type I**	**Carbon polyacrylonitrile (PAN)-based type II**	**E Glass**	**Aromatic Polyamide Kevlar 49**
Diameter (μm)	7.0 - 9.7	7.6 - 8.6	8 - 14	11.9
Density (kg m^{-3})	1950	1750	2560	1450
Young's modulus (GPa)	390	250	76	125
Young's modulus 90° to fibres (GPa)	12	20	76	/
Tensile strength (GPa)	2.2	2.7	1.4 - 2.5	2.8 - 3.6
Elongation to fracture (%)	0.5	1	1.8 - 3.2	2.2 - 2.8
Coefficient of thermal expansion (K^{-1})	≈$9x10^{-6}$			

1.7.2. *Matrix*

The second constituent of a CFC is the matrix. Although contributing very little to the longitudinal strength and modulus, the matrix increases shear and transverse properties, as well as binding and protecting the fibres, allowing for more efficient load transfer.

1.7.2.1. Thermosets

The most common matrices used in CFCs are epoxy and polyester resins (Table 1.4), due to the high level of cross-linking in such thermosetting polymers, which results in a tightly bound three dimensional network surrounding the fibres and effective load transfer [3, 34]. As cross-linking heavily dictates the mechanical properties of the matrix, the curing cycle is an important aspect into obtaining the optimal properties of the composite. As well as the properties highlighted in Table 1.3, epoxies show superior characteristics in terms of shrinkage on curing, and distortion temperature than other thermosets, which allows for the production of pre-pregs., due to their ability to partially cure (also known as staging). Once a thermoset has been mixed it is said to be in the α stage, this is where no cross-linking has occurred. Depending on the thermoset, stage β will show different properties, however, usually, the resin will become less ductile, and be less easy to manipulate; for this reason once stage α has occurred, thermosets are usually staged, which involves decreasing the temperature so that the polymer is in a position of latency to prevent the polymer from reaching the β stage for a defined period of time. For epoxies this involves the use of sub-zero temperatures under which the resin can last for 6 - 12 months in this state, remaining malleable until it is ready to be fully cured [35]. This is a valuable attribute and the main reason for their vast usage in industry [36].

Table 1.4: Properties of two different thermosetting resins [2].

Property	**Epoxy Resins**	**Polyester Resins**
Density (kg m^{-3})	1100 - 1400	1200 - 1500
Young's modulus (GPa)	3 - 6	2 - 4.5
Poisson's ratio	0.38 - 0.4	0.37 - 0.39
Tensile strength (MPa)	35 - 100	40 - 90
Compressive strength (MPa)	100 - 200	90 - 250
Elongation to fracture (%)	1 - 6	2
Coefficient of thermal expansion (K^{-1})	≈ 5 x 10^{-5}	1 x 10^{-4}

The degree of cross-linking is a large determinant to the characteristics of the polymer (Figure 1.17). During cross-linking of a polymer four main significant changes will occur [37].

- Become more dimensional stable.
- Rate of creep is reduced.
- Solvent resistance is increased.
- Reduced heat distortion due to a higher T_g.

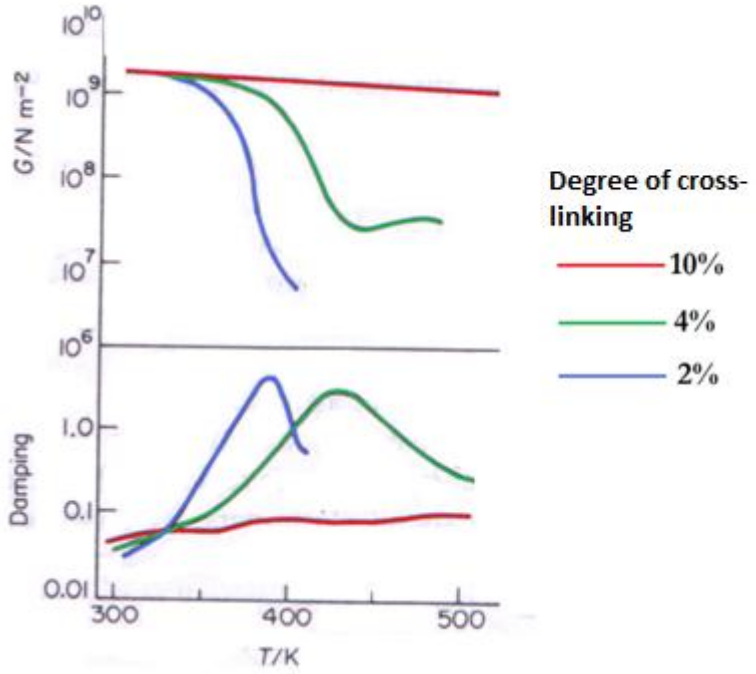

Figure 1.17: The effect of cross-linking and temperature on shear modulus and damping [37].

1.7.2.2. Thermoplastics

Some thermoplastics are also used as matrices in composites, e.g. nylon 6.6, polypropylene, and PEEK. Although containing no cross-links as in thermosets, thermoplastics derive their mechanical properties from the entanglement of long carbon-carbon chains, with the extent of entanglement being a function of the molecular weight of the side groups. Whether amorphous or semi-crystalline, thermoplastics tend to have anisotropic properties, this is due to the heat flow upon cooling orientating the chains or lamellae within the material. The main disadvantage of thermoplastics is the ease of impregnation of fibres [38]. Even above the polymer's T_g (glass transition temperature) thermoplastics remain highly viscous and so it is difficult to evenly distribute the matrix around fine fibre arrays [3]. In contrast thermosets have a relatively low viscosity, which, once the polymer has been mixed, decreases slightly (Figure 1.18) due to the increase in local temperature from the exothermic cross-linking and poor thermal conductivity; this stage makes impregnation of fibre arrays more uniform.

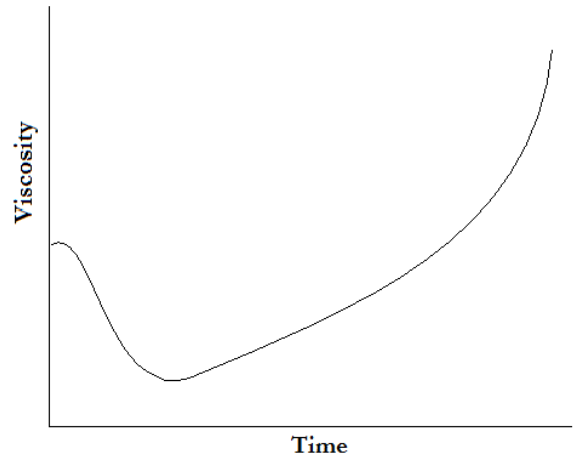

Figure 1.18: Viscosity changes of an epoxy with time at a constant temperature [35].

1.7.3. *Fabrication Considerations*

1.7.3.1. Fabrication Methods

There are two major fabrication methods for components from CFCs, pre-preg. or filament winding [39].

The pre-impregnated fibre method (pre-preg.) starts with sheets of fibres in a semi-cured matrix. This restricts the matrix material to a thermoset, usually an epoxy. The sheets are cut to the desired shape and laid on top of one another. The ability to lay plies in different orientations allows the stiffness and strength of the material in different parts of the component to be varied and optimised. The laying up process is usually performed manually and therefore one main limitation on the shape and quality of the product is the skill of the worker. Due to the semi-cured nature of the pre-preg., the sheets can be quite easily manipulated into three dimensional shapes. The layered pre-preg. is then placed under vacuum (either vacuum bag or autoclave, depending on quality, cost and size) (Figure 1.19). The mould is then heated up to around 125 °C (depending on the matrix material) gradually, then left for around an hour, curing at such a high temperature ensures no further cross-linking will occur during the usable life of the component, whilst also allowing flow between plies, increasing bonding and reduces defects such as pores.

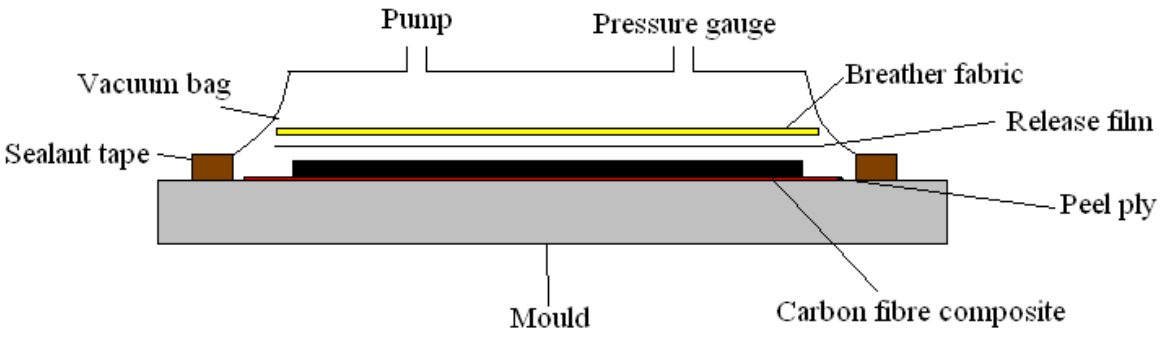

Figure 1.19: Schematic diagram of a pre-preg. being cured in a vacuum bag.

The disadvantages of this method are, defects due to contamination are relatively high due to the high level of human contact during the fabrication of the component, and voids can appear between plies where air has been trapped during the laying up. Another significant disadvantage of this method for the manufacture of golf shafts is the formation of seams. A seam is formed when the start or end of a ply is not at the edge of the component; this will occur in a tube where more than one ply has been used, as in golf shafts. The area at the end of a ply is not entirely filled by adjacent plies, this gap is usually then filled by the flow of matrix resin, creating a low strength/stiffness resin rich region (Figure 1.20). This defect can be located by carrying out frequency analysis around the shaft's circumference (Section 1.4.2.).

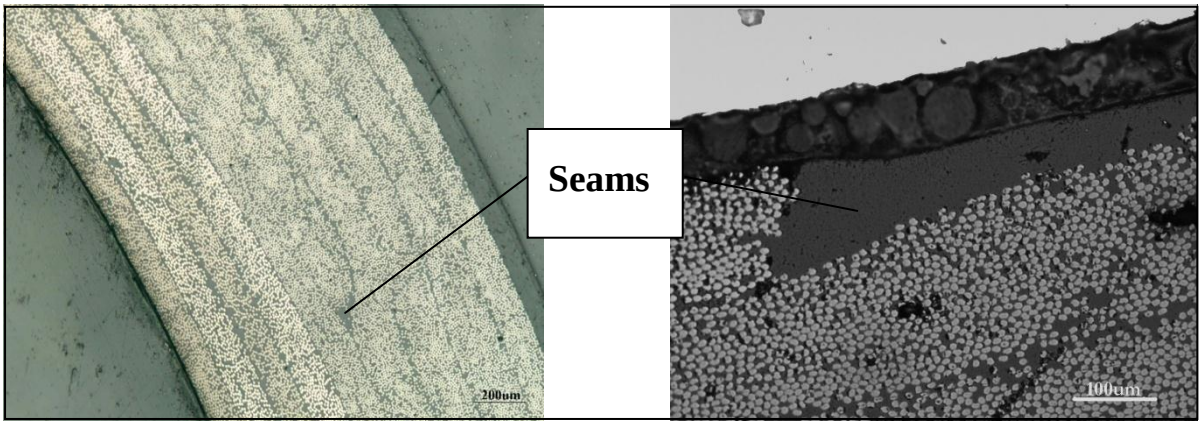

Figure 1.20: Micrographs showing a seam in a golf shaft.

The second method for CFC manufacture is filament winding, as shown is Figure 1.21. In this method the fibres are obtained dry from the supplier. The fibres are pulled from the spool through a resin bath and then around the mandrel. Due to the fibres being coated individually, the final component tends to have a higher volume fraction (V_f) of resin than the pre-preg. method. As the fibres are fed through the resin bath from the feeder arm, orientation can be

manipulated by altering the feeder arm direction and the speed at which the mandrel turns, however 0° fibres are not possible, and this route is restricted to very simple shapes, like tubes. The advantage of this method is that defects are smaller than in the previous method as human contact is minimised, there are also no seams present in this method, giving uniform properties around the whole circumference of the tube.

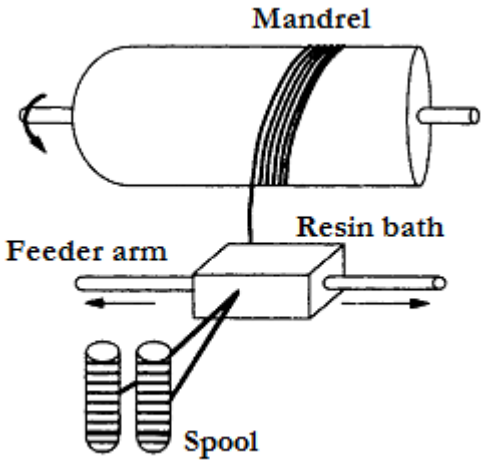

Figure 1.21: Schematic diagram of the filament winding method (adapted from Stabb [32])

1.7.3.2. Volume fraction (V_f)

Another variable that the manufacturer has control over is the fibre volume fraction. At very low volume fractions, the fibres do not support the load, but act more as voids. As load is mostly borne by the 'voided' matrix strength and modulus decrease as the number of fibres increases until V_{min} (Figure 1.22). V_{min} is the point at which the fibres start to carry the applied load and therefore any further increase will result in an increase in tensile strength and modulus. For a long fibre composite, a critical fibre volume fraction, V_{crit}, exists; the volume fraction, V_f, needs to exceed this value in order to provide the component with improved properties compared with just matrix material.

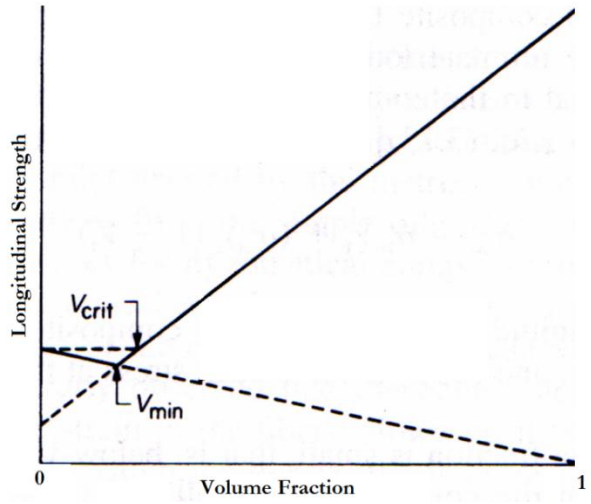

Figure 1.22: The affect fibre volume fraction has on the longitudinal tensile strength [33]

1.7.3.3. Fibre-Matrix Interface

The stronger the bonding between fibre and matrix the more efficient the load transfer is from matrix to the fibres [40]. Carbon fibres are usually heated in oxygen which forms reactive functional groups and therefore bond with the unsaturated resin, creating a good interfacial bond [41]. In the absence of this treatment, the resin would not wet the fibre nor spread along the fibre so that the load bearing area is reduced, lowering modulus and strength [42, 43]. If strong bonding between the two constituents is present then if a fibre breaks the fibre is still supported and load is still transferred. A strong bond will also give the composite a higher transverse modulus, which is essential when dealing with off-axis loading, however the high bond strength leads to poor toughness as fibre fracture is promoted over fibre pull-out [33].

Fibre / matrix interface strength can be easily tested through several methods, but the fibre pull-out test (Figure 1.23) is most widely used [3]. This involves embedding a single fibre into the matrix, and subjecting it to a uniaxial test. It can be seen from Figure 1.24 that there are three stages in this test; initial debonding; propagation of the debond; and fibre pull-out [44]. The first two stages are a good indication of the bonding strength between the fibre and

the matrix; the final stage is attributed solely to the frictional forces between the fibre and the matrix (Figure 1.25). Typical values for the debonding shear stress are 5 – 100 MPa, referring to the seconds stage of Figure 1.23 [3]. However preparation for this test can be difficult and fibre push-out tests are increasingly being used, which is essentially the same, from a thin slice of the composite, the fibres are displaced so it protrudes out of the reverse side. This also eliminates any problems that are made with the assumptions in the calculations concerning the fibre end that is embedded in the matrix for the pull-out test [45]. However, fibre push-out is likely to increase the bond strength as Poisson's ratio effects cause greater interaction with the surrounding matrix [46].

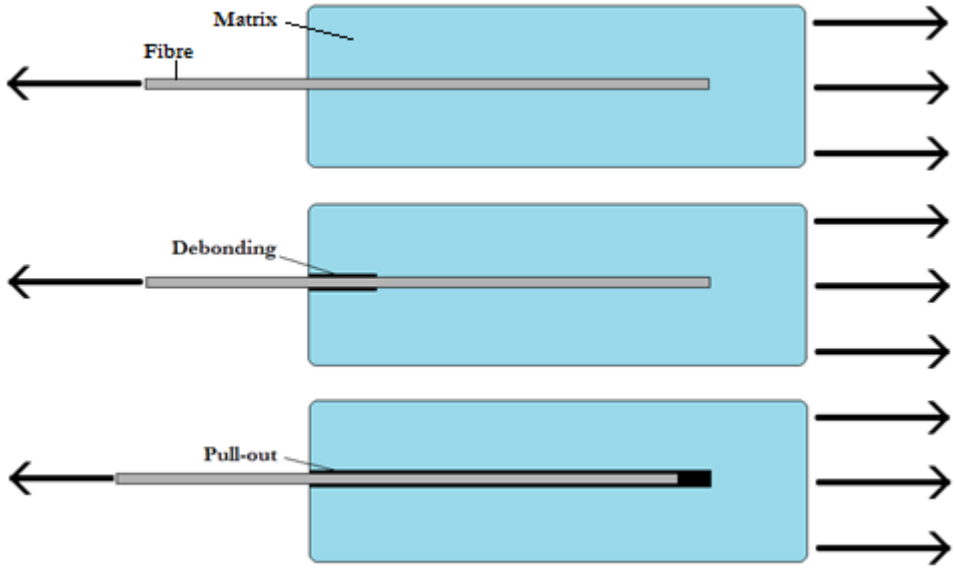

Figure 1.23: Schematic showing the uniaxial fibre pull-out test.

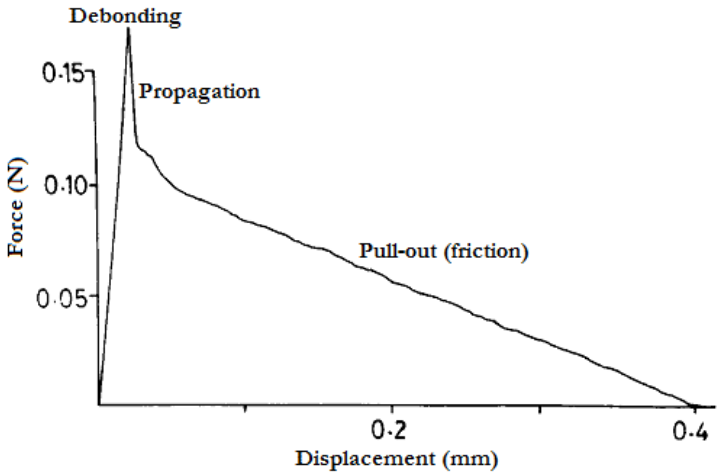

Figure 1.24: Shows a typical fibre pull-out trace for carbon fibre (adapted from Piggott and Andison [47])

1.7.4. *Effect of Fibre Orientation and Stacking Sequence on the Mechanical Properties of Composites*

Fibre orientation and stacking sequence are important considerations when fabricating components from CFCs. While maintaining mass, the mechanical properties of composite can show a wide range of properties, and conversely through optimising the orientation a reduction in mass is usually possible whilst maintaining the desired mechanical properties. This section aims to highlight the influence the fibre orientation has on a range of properties and emphasize how and why stacking sequence changes these properties.

1.7.4.1. Fibre Orientation

Altering orientation is the simplest method changing stiffness of a laminate without changing geometry. As fibres are oriented further from the loading axis the laminate becomes more matrix dominant and by doing so affects the load transfer from the fibres to the matrix.

In a simple uniaxial tensile test, fibres that are orientated along the tensile axis (usually deemed 0°) are clamped at either end. This therefore makes the specimen more fibre-dominated, giving a higher Young's modulus (Figure 1.25); as the fibres are orientated away from the tensile axis, modulus decreases rapidly. This is due to the load transferring between fibres across the matrix, making the specimen more resin-dominated, so much so that fibres at 90° show negligible difference in mechanical properties compared with the pure matrix. However, shear modulus increases from 0° to 45° and then decreases to 90°. For this reason golf shaft manufacturers tend to introduce internal layers of ±45° plies where they have less of an impact of bending stiffness but dramatically improve the torsional rigidity of the shaft [17].

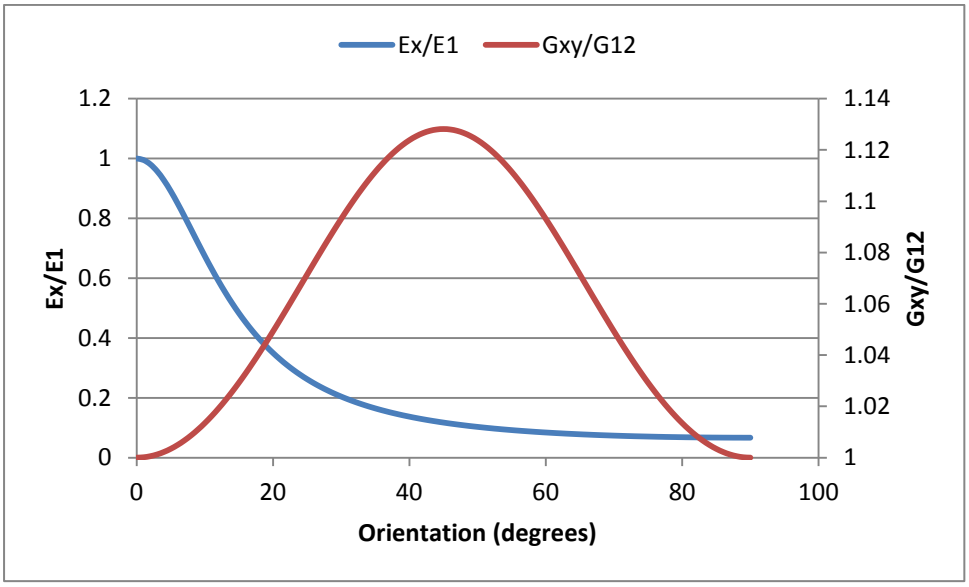

Figure 1.25: Showing the change in Young's and shear modulus with orientation (Ex/E1 refers to the normalised longitudinal modulus, and Gxy/G12 refers to the normalised shear modulus).

This change in load transfer can be observed in the fracture mechanics of different lay-ups (Figure 1.26). At orientations between 0 and 4° from the load axis, the composite will show longitudinal failure [48]. From 4 to 24° fracture will be largely by matrix / fibre interface

failure; between 45 and 90°, transverse failure will occur, and between 24 and 45° the composite will show a combination of transverse and shear fracture [2, 49, 50]. This change in mode of failure shows that the mechanics of the load transfer have altered. However, this only considers simple lay-ups on a single orientation.

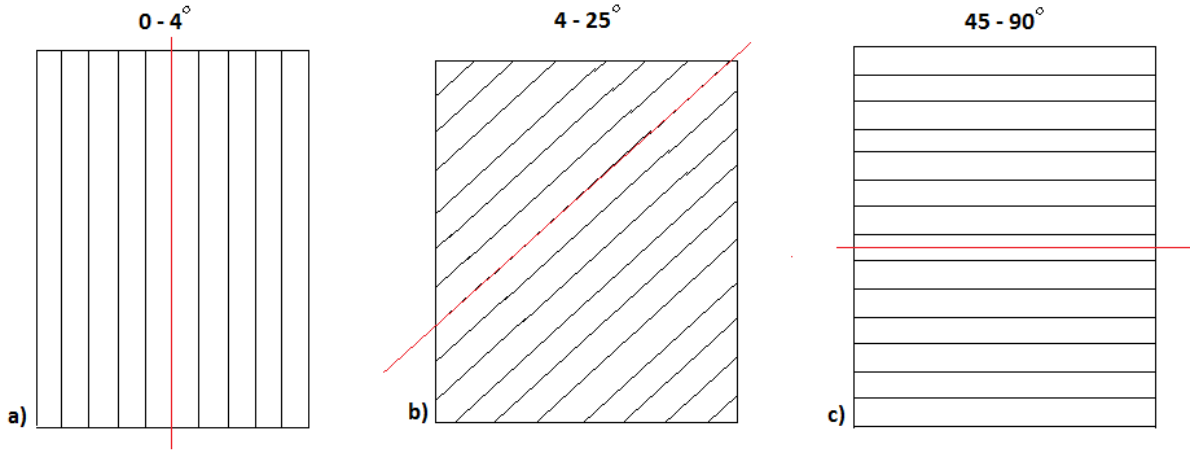

Figure 1.26: Schematic diagram showing the different failure mechanisms in unidirectional laminates a) longitudinal, b) fibre/matrix interface and c) transverse.

1.7.4.2. Stacking Sequence

In order to optimise a composite laminate's mechanical properties whilst reducing the number of plies (reduce mass), not only orientation of a ply needs to be considered, but the position within the laminate requires design (particularly in bending).

It is evident that a single ply shows highly anisotropic properties. This anisotrophy can be controlled through stacking plies of varying orientations, however several assumptions are made when analysising a laminate; the laminate must be flat and thin, and no through stress or edge effects are present. The plies are also assumed to be perfectly bonded, however they act as inividual entities [2, 3].

The longitudinal and shear stresses of a beam in bending can be seen in Figure 1.27. This figure shows with a constant modulus, the normal stress is zero at the mid-plane of the beam, thus the plies in this plosition contribute very little to the bending stiffness of the beam. This is shown in Equation 1.5 where the maximum stress of a beam in bending is proportional to the distance from the neutral axis squared, therefore normal stress is zero at the mid-plane. In order to maximise stiffness of a laminate, the position of the plies with orientation closest to the loading axis should be positioned furthest away from the mid-plane

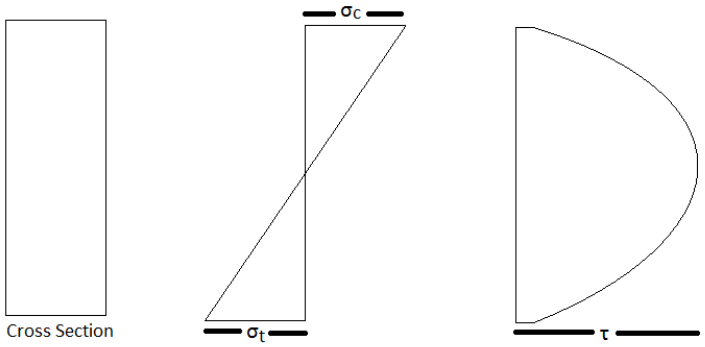

Figure 1.27: Normal stress and shear stress variations through the thickness of a homogeneous rectangular cross-section during bending [33] .

$$\boldsymbol{\sigma = \frac{6M}{bd^2}}$$

Equation 1.5

where σ and M are the normal stress and bending moment of the beam respectively. b is the beam width and d is the distance to the mid-plane.

In order to reduce the level of anisotropy two design criteria can be met when choosing the stacking sequence of a laminate:

- Balancing the plies: When the presence of an off-axis ply is countered by its negative then the laminate is deemed balanced. For example a laminate with a lay-up of [30, 45, 45 30] is not balanced, however [-30, 45, -45, 30] is balanced. By balancing a laminate the tensile-shear interaction effects are negligible.
- Symmetric lay-up: In order to retain shape during curing and also later when stressed, it is important to therefore ensure that the mechanical properties are symmetric about the mid-plane of the laminate. An example of distortion shapes can be seen in Figure 1.28. For example a [0, 0, 90, 90] laminate is not symmetric, however [0, 90, 90, 0] is. Usually a simpler form of notation of a symmetric is the use of the subscript "s", stating its symmetric about the mid-plane i.e. [0, 90, 90, 0] is the same as $[0, 90]_s$. The advantages of a predicting the behaviour of a symmetric laminate will become clear in Section 1.8, as being symmetric no coupling between tensile stresses and flexural stress exist.

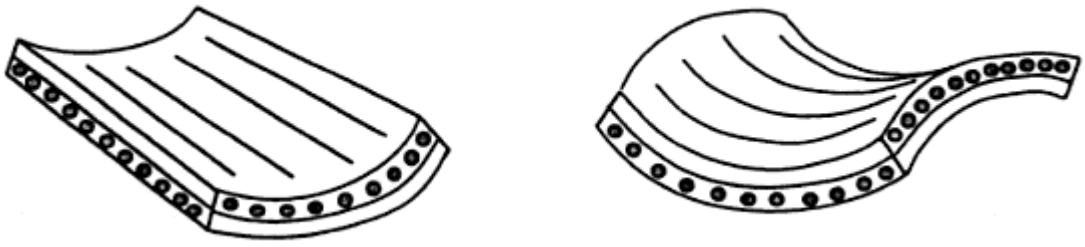

Figure 1.28: Distortion shapes due to no symmetric laminates [3].

The advantages of using these two design criteria depend entirely on the stress state of the laminate in service, for example a laminate designed to bend in a specific direction, or a tube subjected to internal stress may be optimised without using these criteria.

The effect of stacking sequence can clearly be seen in a study by Gubran *et al.,* [51] where a selection of parallel sided shafts were fabricated with changing the stacking sequence of two orientations (0 and 90°). Table 1.5 shows the natural frequencies for the shafts in this study. It can be seen that when the 0° plies are situated on the outer surface of the shaft then a higher natural frequency is for all bending modes. This was also noted by Ni and Adams [52] where the outer ply of a laminate of orientation $[\theta\ 0\ 60\ -60]_s$ (where θ is the ply of varying orientation), as orientation tended towards 0° the longitudinal modulus increases and longitudinal damping decreased (showing a more fibre dependent structure) as seen in Figure 1.29, however if the variable ply was to move to the innermost position, a negligible difference in modulus and damping can be seen.

Table 1.5: The effect of stacking sequence on the bending mode frequencies [51].

Stacking Sequence (°)[1]	**Bending Mode Frequencies (Hz)**		
	1st	**2nd**	**3rd**
[0 0 90 90]	346	1093	1931
[90 90 0 0]	330	1047	1855
[90 0 0 90]	339	1072	1897
[0 90 90 0]	338	1070	1893
[90 0 90 0]	335	1059	1875
[0 90 0 90]	342	1082	1913

[1] The stacking sequence order refers to the orientation of the outermost though to the innermost ply.

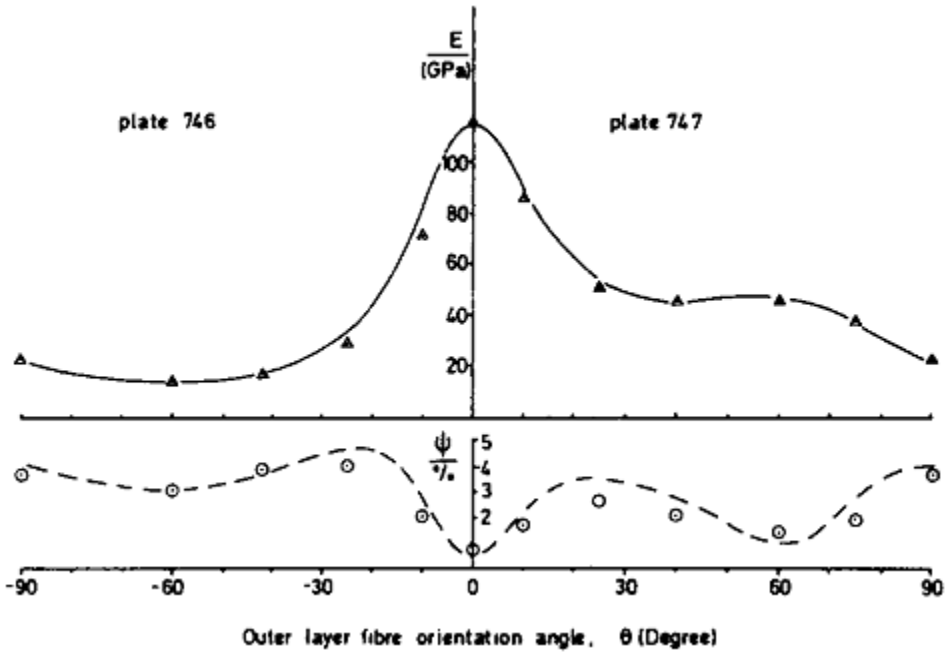

Figure 1.29: Change in longitudinal modulus and damping with outer ply orientation of a [θ 0 60 -60]$_s$ laminate [52].

Laminates with 0° plies have shown to show very fibre dependent properties. Ha and Springer [53] stated that a $[0,\pm45,90]_s$ fabricated from Fiberite T300/976, will still show a fibre-dominated response even though only 25% of the sample is actually 0°, reducing its sensitivity to temperature and strain rate dramatically. The strain rate sensitivity was shown to be greater in matrix dominant laminates, therefore it will be important to observe if the strain rate sensitivity is reduced when a minimal amount of 0° plies are introduced.

1.8. Analysis of Anisotropic Laminates

For this section the co-ordinate system seen in Figure 1.30 is used. Laminate theory has, for some years, been the backbone of composite design [54-65]. One of the main advantages of fibrous composites is the ability to control the properties of laminates very effectively [33]. This section concentrates on how the mechanical properties can be tailored by altering fibre

orientation and stacking sequence. Mechanical properties of the longitudinal, traverse and shear directions are needed to carry out this analysis, and thus the effect of altering volume fraction and the constituent materials are also taken into consideration. This method treats each ply separately thus give a better representation compared to assigning a laminate with one set of anisotropic values [66] (see also Section 1.7.4).

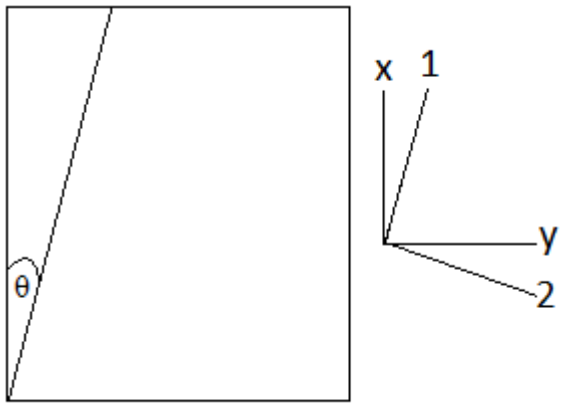

Figure 1.30: Schematic diagram to show co-ordinate system used. The z and 3 axes are perpendicular to the x-y plane.

The relationship between the strain and stress in a system can be seen in Equation 1.6. C_{ij} represents the stiffness matrix. If however it is assumed that there are no through-thickness stresses, which is reasonable for thin walled laminates, then Equation 1.6 can be reduced to Equation 1.7 [33, 67-70].

$$\begin{Bmatrix}\sigma_1\\ \sigma_2\\ \sigma_3\\ \tau_1\\ \tau_2\\ \tau_3\end{Bmatrix} = \begin{Bmatrix} C_{11} & C_{12} & C_{13} & C_{14} & C_{15} & C_{16} \\ & C_{22} & C_{23} & C_{24} & C_{25} & C_{26} \\ & & C_{33} & C_{34} & C_{35} & C_{36} \\ & & & C_{44} & C_{45} & C_{46} \\ Symmetric & & & & C_{55} & C_{56} \\ & & & & & C_{66} \end{Bmatrix} \begin{Bmatrix}\epsilon_1\\ \epsilon_2\\ \epsilon_3\\ \gamma_1\\ \gamma_2\\ \gamma_3\end{Bmatrix}$$

Equation 1.6

$$\begin{Bmatrix}\sigma_1\\ \sigma_2\\ \tau_{12}\end{Bmatrix} = \begin{Bmatrix} C_{11} & C_{12} & 0 \\ C_{12} & C_{22} & 0 \\ 0 & 0 & C_{66} \end{Bmatrix} \begin{Bmatrix}\epsilon_1\\ \epsilon_2\\ \gamma_{12}\end{Bmatrix} = |C| \begin{Bmatrix}\epsilon_1\\ \epsilon_2\\ \gamma_{12}\end{Bmatrix}$$

Equation 1.7

where:

$$C_{11} = \frac{E_1}{1 - v_{12}v_{21}}$$

$$C_{12} = \frac{E_1 v_{21}}{1 - v_{12}v_{21}}$$

$$C_{22} = \frac{E_2}{1 - v_{12}v_{21}}$$

and $C_{66} = G_{12}$

However, there is no interaction between normal and shear stresses so that, in order to find the resultant strains, the induced stresses first need to be recognised, i.e., the three stresses (σ_1, σ_2 and τ_{12}) need to be resolved onto the x-y plane. If θ is the angle between 1 and x, the transformation matrix is as follows:

$$\begin{Bmatrix}\sigma_1\\ \sigma_2\\ \tau_{12}\end{Bmatrix} = \begin{Bmatrix} c^2 & s^2 & 2cs \\ s^2 & c^2 & -2cs \\ -cs & cs & c^2 - s^2\end{Bmatrix}\begin{Bmatrix}\sigma_x\\ \sigma_y\\ \tau_{xy}\end{Bmatrix} = |T| \begin{Bmatrix}\sigma_x\\ \sigma_y\\ \tau_{xy}\end{Bmatrix},$$

Equation 1.8

Where $c = \cos\theta$ and $s = \sin\theta$.

This is also carried out for the strains:

$$\begin{Bmatrix}\epsilon_1\\ \varepsilon_2\\ \gamma_{12}\end{Bmatrix} = \begin{Bmatrix} c^2 & s^2 & cs \\ s^2 & c^2 & -cs \\ -2cs & 2cs & c^2 - s^2\end{Bmatrix}\begin{Bmatrix}\epsilon_x\\ \epsilon_y\\ \gamma_{xy}\end{Bmatrix} = |T'| \begin{Bmatrix}\epsilon_x\\ \epsilon_y\\ \gamma_{xy}\end{Bmatrix}.$$

Equation 1.9

Therefore, by using Equation 1.7, Equation 1.8 and Equation 1.9, the transformed stiffness matrix can be formed (Equation 1.10):

$$\begin{Bmatrix}\epsilon_x\\ \epsilon_y\\ \gamma_{xy}\end{Bmatrix} = |T'|^{-1}\,|C|\;|T|\begin{Bmatrix}\sigma_x\\ \sigma_y\\ \tau_{xy}\end{Bmatrix} = \bar{C}\begin{Bmatrix}\sigma_x\\ \sigma_y\\ \tau_{xy}\end{Bmatrix}.$$

Equation 1.10

The transformed stiffness elements are as follows [3]:

$\bar{C}_{11} = C_{11}c^4 + C_{22}s^4 + (2C_{12} + 4C_{66})c^2s^2,$

$\bar{C}_{12} = C_{12}(c^4 + s^4) + (C_{11} + C_{22} - 4C_{66})c^2s^2,$

$\bar{C}_{22} = C_{11}sc^4 + C_{22}c^4 + (2C_{12} + 4C_{66})c^2s^2,$

$\bar{C}_{16} = (C_{11} - C_{12} - 2C_{66})c^3s - (C_{22} - C_{12} - 2C_{66})cs^3,$

$\bar{C}_{26} = (C_{11} - C_{12} - 2C_{66})cs^3 - (C_{22} - C_{12} - 2C_{66})c^3s,$

and $\bar{C}_{66} = (C_{11} - C_{22} - 2C_{12} - 2C_{66})c^2s^2 + C_{66}(c^4 + s^4).$

Agarwal *et al.* [33] show in detail how the transformed elastic constants are derived from the transformed stiffness matrix by the use of the ABD matrices, which refer to the extensional stiffness, coupling stiffness and bending stiffness matrices respectively. In the case of zero bending extensional coupling (balanced and symmetric) B can be neglected. The elements are:

$A_{ij} = \sum_{k=1}^{n}(\bar{C}_{ij})_k(\omega_k - \omega_{k-1})$,

$B_{ij} = \frac{1}{2}\sum_{k=1}^{n}(\bar{C}_{ij})_k({\omega_k}^2 - {\omega_{k-1}}^2)$,

and $D_{ij} = \frac{1}{3}\sum_{k=1}^{n}(\bar{C}_{ij})_k({\omega_k}^3 - {\omega_{k-1}}^3)$,

where h_k is the distance from the mid-plane to the kth ply and n is the number of plies.

This now allows for the elastic components (Equation 1.11) to be calculated for laminates fabricated for varying orientation, and as it can be seen above the weighting factor $({\omega_k}^3 - {\omega_{k-1}}^3)$ of D_{ij} means that the stacking order will have a large influence on the flexural properties, whereas for A_{ij} each ply has the same influence.

$$E_x(tensile) = \frac{1}{H \times a_{11}}$$

$$\text{and } E_x(flexural) = \frac{12}{H^3 \times d_{11}},$$

Equation 1.11 (Adams and Bacons, 1973 [68])

where a_{ij} and d_{ij} are from the inverse A_{ij} and D_{ij} matrices respectively, and H is the laminate thickness.

1.9. Viscoelasticity

Viscoelastic materials, as the name implies, show characteristics typical of both an elastic body and a viscous solution. A completely elastic material, which obeys Hooke's law, can be represented by a spring, where the displacement is proportional to the force being applied, but not to the rate at which it was applied (Figure 1.31(a)); this is an energy storing system and will fully recover upon unloading. A viscous liquid, on the other hand, can be represented by a dashpot (Figure 1.31(b)), where displacement is more dependent on the shear strain rate than to strain itself. This type of system dissipates energy.

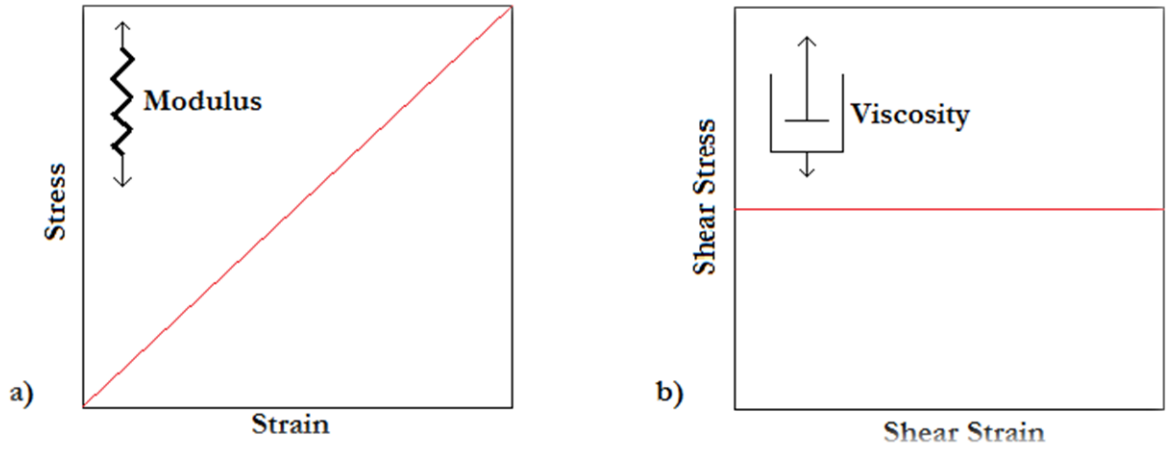

Figure 1.31: Showing the (a) spring and (b) dashpot systems acting in a viscoelastic material.

1.9.1. *Creep, Recovery and Relaxation in Polymers.*

When a viscoelastic material is subjected to a constant stress, strain will gradually increase with time, this is referred to as creep. Once the stress has been removed the material will start to recover, metals will immediately recover slightly and show no further change in strain with time, however, for polymeric materials strain will continue decreasing with time, and in some cases will show a full recovery given a long enough period. Relaxation occurs when a

viscoelastic material is subjected to a constant strain, this will result in a gradual decay in the stress [71].

The reason behind these phenomena is attributed to the molecular motion of the polymeric chains. As a chain is stretched, rotation of function groups needs to take place to accommodate this, a simple motion if a single chain is considered, but more complex is a poly-chain system [72]. Due to friction and internal forces [73, 74] the rotation action is delayed, and much like a traffic jam, a function group is unable to move until there is space in front of it. In addition, chain entanglement increases internal friction and slows molecular motion. This means that, upon initial application of a stress, the strain will continue to increase with time (creep). This deformation is not necessarily plastic, and, when the process if reversed, there is a time element to the recovery of the system as well.

Upon rapid loading chain rotation is limited and chain disentanglement will not occur, thus contact points where chains are tangled act as a cross-link and will stiffen the system [73]. At low loading rates stress relaxation will occur during loading, giving a much lower modulus (Section 1.9.2).

1.9.2. *Strain Rate Sensitivity*

One of the key variables that can manipulate the performance of viscoelastic materials is the loading or strain rate. High loading rates are common in many applications, and sports are no exception, although loads are not that great in comparison with structural applications, such as aerospace. The impact nature of many sports means that the equipment is usually loaded in fractions of a second.

Hsiao and Daniel [75] studied the effects of strain rate (up to 120 s^{-1}) on the compressive and shear modulus of a unidirectional carbon/epoxy composite (IM6G/3501-6). Compression

tests on the 90° oriented composite showed a large increase in both modulus and strength in comparison to the static case. This is also seen in shear tests, but to a lesser extent, both of these tests were resin-dominated. However, when the 0° samples were tested, the fibre-dominated system prevented any great effect of strain rate, with modulus showing no noticeable difference up to 0.4 % strain at strain rates up to 110 s^{-1}. This is backed up by Groves *et al.* [76, 77] who showed an increase in specimen stiffness for all samples for strain rates up to 3000 s^{-1}, in both tension and compression.

Testing of IM7/977-2 carbon/epoxy matrix composites [78] in tension at strain rates varying from low (10^{-5} s^{-1}), through intermediate (1 s^{-1}) to high (400 - 600 s^{-1}). Fibre-free matrix showed very little significant change in modulus from the low to intermediate strain rates, but an increase of 250 % from intermediate to high, which was the same as in 90° laminate. Gilat *et al.* [79] continued their work and investigated different epoxy resins; PR-520 and E-862 showed increases of 210 % and 250 % respectively from static testing to a strain rate of 460 s^{-1}, the sensitivity to strain rate occurred significantly after an intermediate strain rate (2 s^{-1}), however few data points were obtained below this value. Vinson and Woldesenbet [80] reported similar observations in the dependence of resins at strain rates of 400, 600 and 800 s^{-1}. Both these studies were based on epoxies with a modulus of approximately 4 GPa.

McClung and Ruggles-Wrenn [81] reported the effect of strain rate on the mechanical properties of unreinforced PMR-15 resin. As well as showing the characteristic increase in Young's modulus with increasing strain rate (strain rate range, 10^{-6} - 10^{-3}), changes in creep, stress relaxation and recovery were all noted.

With increasing strain rate, the amount of creep occurring also increases (by almost 1 % at 6 hours when strain rate was increased from 10^{-6} - 10^{-4}). For faster loading (upper strain rate)

re-orientation of functional groups under the applied stress does not occur during loading (as for lower strain rates) but occurs post-loading leading to increased creep. Similarly, for stress relaxation under a constant strain, greater stress reduction occurs for faster loading rates as insufficient time is available during loading for re-arrangement into a lower energy state [82, 83].

Recovery was shown to occur more quickly and to a greater degree at higher strain rates, the work carried out by McClung and Ruggles-Wrenn [81] showed full recovery only when loaded at a strain rate of 10^{-3} s^{-1} or greater. This can be attributed to the reduced molecular motion occurring during deformation, so that, when the load is removed, the little motion that had occurred can be fully recovered. However, if rotation and reorientation has occurred during loading then further energy will be required to reverse the motion [84].

Another important phenomenon was that, upon the reduction of strain rate during a loading cycle, the stress strain curve continues as for reduced strain rate immediately, thus the modulus does not show any effect to prior strain rate, only of instantaneous strain rate [85-87].

1.9.3. *Damping*

Energy absorption by means of mechanical damping is of the upmost importance in reducing vibrations that may result in reduction in a part's in service life [88, 89]. In this respect, high damping materials are used, which usually is accompanied by a reduction in component stiffness. CFCs, however, due to the constituent parts representing a high stiffness, low damping reinforcement and a low stiffness, high damping matrix, are able to give higher combinations of stiffness and damping depending on volume fraction [90].

There are three main levels of damping; light, heavy and critical (Figure 1.32). When a system still shows a sinusoidal oscillation, the amplitude of which is decaying with time, this is called light damping. If no oscillation occurs however, and the system slowly returns to an equilibrium, this is referred to as heavy or over-damping. At the point where no oscillations occur and the system returns to equilibrium the quickest, this state is called critical damping. Material damping due to internal friction is only very small and therefore the material is lightly damped.

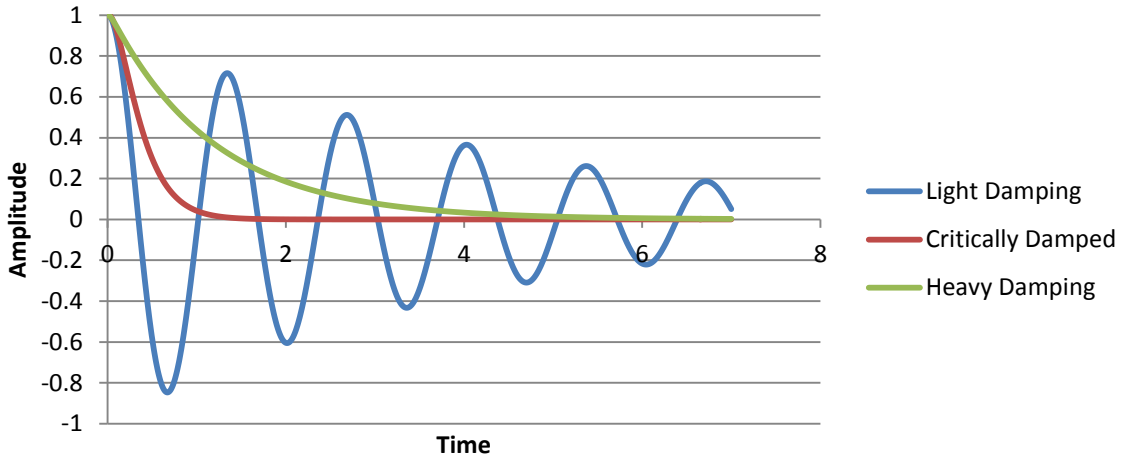

Figure 1.32: Schematic diagram of the three levels of damping.

Chapter 1.9 stated that a viscoelastic material shows both elastic and viscous properties. When a viscous fluid is subjected to a sinusoidal load the strain response will be 90° out of phase from the stress, as opposed to an elastic material which has both stress and strain in phase. A viscoelastic material however, will exhibit a response in between an elastic and a viscous response, with phase difference (δ) ranging from 0 – 90°.

All materials dissipate energy during cyclic loading through internal friction/hysteresis. The methods by which this can be measured dealt with in detail later in this chapter. Figure 1.33 shows this loss coefficient (η) plotted against Young's modulus for a range of materials. In

general η decreases with increasing E. Ceramics typically show low damping as dislocations are heavy pinned, however internal cracks will result in higher internal friction and increase η. Polymers will typically show high damping above their T_g, due to the large amount of molecular chain motion during loading; as polymers become more dense, modulus increases and chain motion is less, lowering η [91]. Composites allow for a high modulus to be maintained whilst having a relatively high loss coefficient.

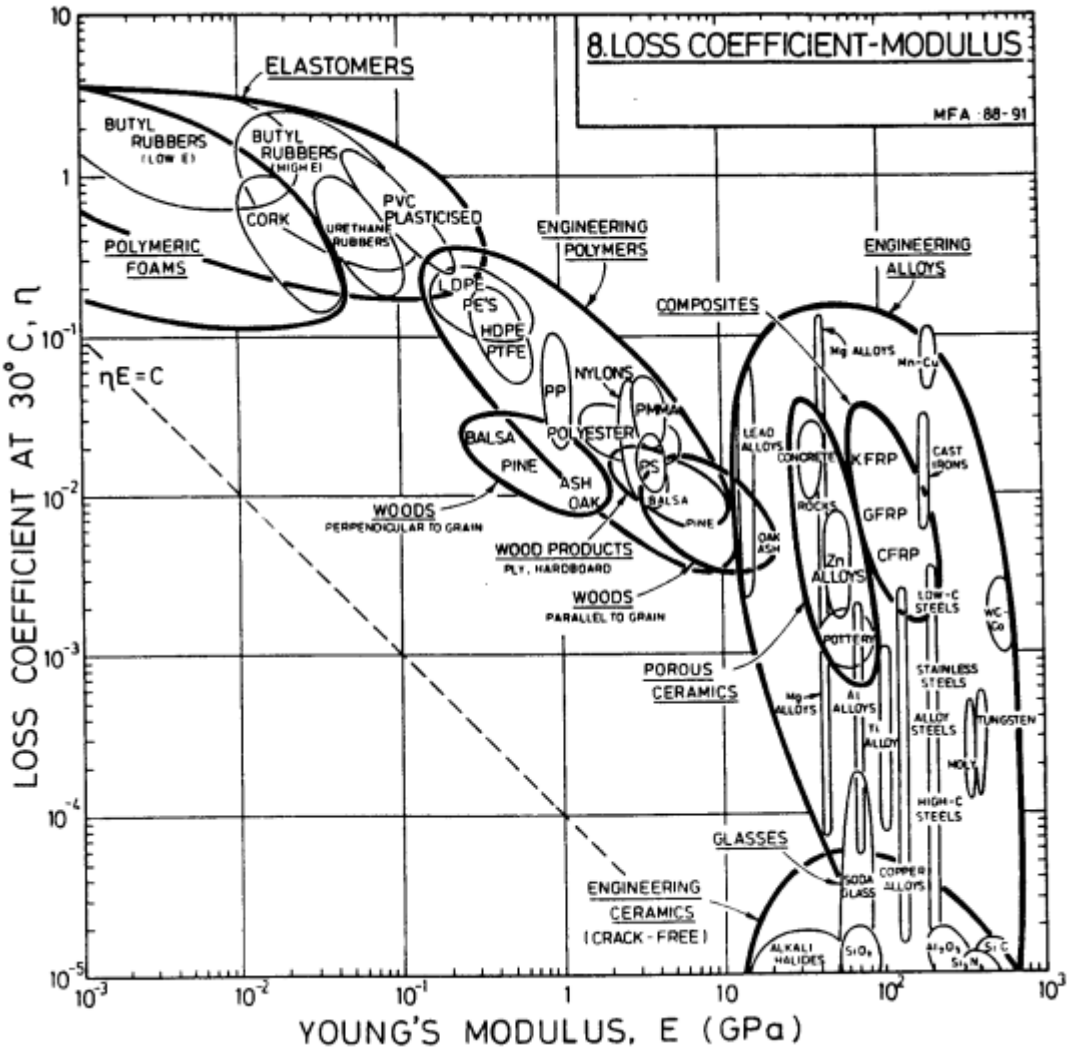

Figure 1.33: Loss coefficient/Young's modulus chart [92].

1.9.3.1. Calculating Light Damping.

Using an example of a simple mass/spring system, where the mass is displaced by Δx, then, for a given spring stiffness (k) which is proportional to Δx, and damping function (b) which is proportional to the velocity ($\dot{x}$), it is obvious that there will be an oscillatory motion that decays with time.

The damping function can therefore be calculated by the following process [93]:

As $F = ma = m\ddot{x}$ and $F = -kx - b\dot{x}$, then combination results in Equation 1.12.

$$\ddot{x} + \gamma\dot{x} + \omega_o^2 x = 0 ,$$

Equation 1.12

where $\frac{k}{m} = \omega_o^2$ and $\frac{b}{m} = \gamma$.

The complex form of Equation 1.5 is Equation 1.13.

$$\ddot{z} + \gamma\dot{z} + \omega_o^2 z = 0 ,$$

Equation 1.13

where *z* is a complex function expressed as by Equation 1.14

$$z = Ae^{i(pt+\delta)}.$$

Equation 1.14

Differentiating Equation 1.14 and substituting into Equation 1.13 gives Equation 1.15.

$$(-p^2 + \gamma ip + \omega_o^2)z = 0.$$

Equation 1.15

As neither γ nor p can be zero, in order to satisfy Equation 1.15, then p itself must be complex ($p = n + is$). Substituting p into Equation 1.15 gives Equation 1.16.

$$-n^2 + s^2 - 2nis + \gamma in - \gamma s + \omega_o^2 = 0.$$

Equation 1.16

As both the real and imaginary parts need to equal zero, then $s = \frac{\gamma}{2}$ from the imaginary parts, this can be substituted back into the real part to give:

$$n^2 = \omega_o^2 - \frac{\gamma^2}{4}.$$

Equation 1.17

Substituting this back into Equation 1.14 gives Equation 1.18. It can now be seen that n is the frequency of the oscillation and therefore will be referred to from now as ω_f. From Equation 1.17 it can be seen that the frequency of oscillation will increase under the presence of damping, however under very low damping, ω_f will be very close to ω_o.

$$z = Ae^{i(nt + ist + \delta)} = Ae^{-\frac{\gamma}{2}t}e^{i(nt + \delta)}.$$

Equation 1.18

Transposing Equation 1.18 back into the real plane gives Equation 1.19, which shows that x comprises of both a oscillatory function ($\cos(\omega_f t + \delta)$) and a decaying function ($Ae^{-\frac{\gamma}{2}t}$).

$$x = Ae^{-\frac{\gamma}{2}t} \cos(\omega_f t + \delta).$$

Equation 1.19

If the material damping is dictating the decaying function, then the material loss factor (η) can be used to calculate γ as Equation 1.20.

$$\frac{1}{\eta} = \sqrt{\frac{\omega_f^2 + \frac{\gamma^2}{4}}{\gamma^2}}.$$

Equation 1.20

1.9.3.2. Determining Loss Factor by Practical Methods.

The loss factor can be determined by three main methods:

- As mentioned earlier during a simple uniaxial tensile test, a hysteresis loop is produced, and the area between the loading and unloading curve represents the energy lost in a single cycle (ΔU). This can be converted into a material constant (Specific damping capacity, S.D.C) by Equation 1.21.

$$S.D.C = \frac{\Delta U}{U_L},$$

Equation 1.21

where U_L is the energy stored during the loading cycle.

- *Half power bandwidth:* By applying a swept sine signal through an electromagnetic shaker onto a clamped-free or free-free specimen provides data on the acceleration/velocity of the specimen for a range of excitation frequencies, and by using Equation 1.22 it can be seen that the lower trace (marked with red) in Figure 1.34 shows much greater damping to the trace marked with blue.

$$Q^{-1} = \frac{f_u - f_l}{f_n},$$

Equation 1.22 (Bert, 1973)

where Q is a damping coefficient, f_u and f_l are the upper and lower half power frequencies respectively, and f_n is the natural frequency. f_u and f_l are determined as 1/√2 of the peak acceleration.

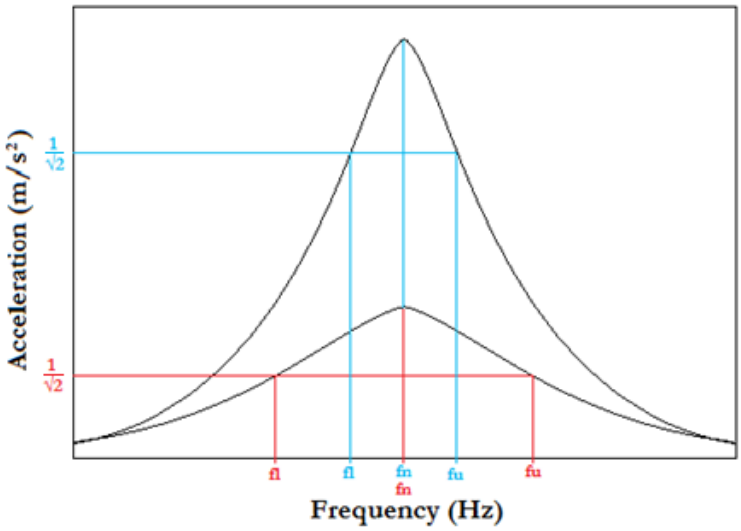

Figure 1.34: Half power bandwidth trace to determine damping [94].

- *Free decay:* After a component has been excited and is oscillating at its natural frequency, the amplitude will decay every oscillation (Figure 1.35). This logarithmic decay can also be used in calculating the energy lost (Equation 1.23).

$$\eta = \frac{ln\frac{A_n}{A_{n+1}}}{\pi},$$

Equation 1.23

where η is the loss factor, A_n is the amplitude of the nth peak, and A_{n+1} is the amplitude of the next peak.

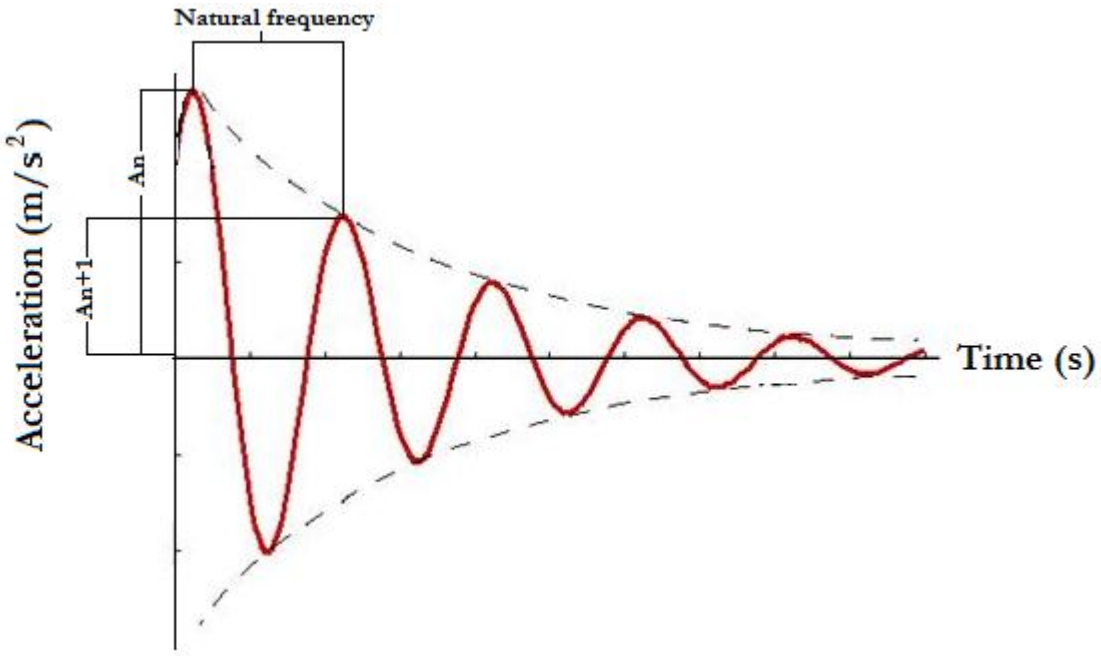

Figure 1.35: Free decay trace to determine damping

Equation 1.24 allows the different techniques to be compared.

$$\eta = tan\,\delta = \frac{E''}{E'} = \frac{1}{Q},$$

Equation 1.24 [92, 95]

where δ is the angle between the storage (E') and loss (E'') moduli.

Deng and Ye [96] studied the effects of strain rate and temperature on *tan(δ)*. This was carried out in a Dynamic Mechanical Analyser (DMA) in three-point bending where the storage and loss moduli were measured under relatively small loads (10 N). Both 0° and 90° specimens showed very little sensitivity to temperature up to around 65 °C, but the storage

modulus almost halved when the temperature was raised from 60 to 80 °C. This rise in temperature affects *tan(δ)* also, raising it from 0.01 to 0.2 and from 0.03 to 0.25 in the 0° and 90° panels respectively (Table 1.6). Damping shows very little sensitivity up to temperatures around 60 °C (coinciding with the glass transition temperature of the matrix). However, it is apparent that damping increases at a greater rate than stiffness decreased suggesting *tan(δ)* is much more dependent on environmental and loading parameters than E. This may be attributed to the araldite used as matrix material has gone through its glass transition temperature and thus the gripping is less efficient than at room temperature. In the 0° oriented panel, damping was dependent on the adhesion of the fibres to the matrix at lower V_f, however the difference in the 90° oriented panel was marginal, suggesting that the mechanical properties of the 90° oriented panel are almost entirely resin-dominated. In addition to this, by increasing the frequency (strain rate) the amount of damping significantly dropped for the 90° oriented composite, by around 30%, this was not seen for the 0° oriented panel where a minimal increase was seen (Figure 1.36)

Table 1.6: Changes in storage modulus and tanδ with orientation, temperature and fibre treatment [96].

Orientation	Treated/Untreated	Temperature (°C)	Storage Modulus (GPa)	Tan(δ)
0	Untreated	20-65	100	0.01
0	Treated	20-65	108	0.01
0	Untreated	80	40	0.2
0	Treated	80	40	0.2
90	Untreated	20-65	8.5	0.03
90	Treated	20-65	8.8	0.03
90	Untreated	80	2	0.25
90	Treated	80	1.5	0.25

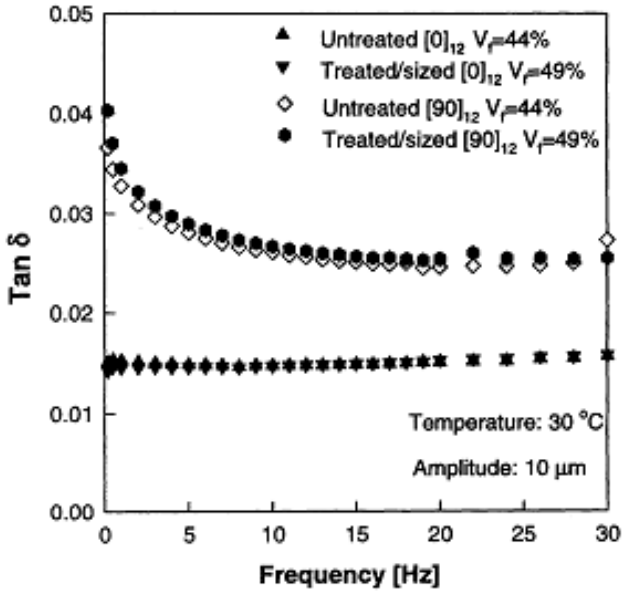

Figure 1.36: The effect of frequency on the longitudinal and transverse damping of CFC [96].

1.10. Summary of Literature Review

This literature review has outlined the principle of shaft fabrication and the effect the mechanical properties has on a golfer's swing. Since the introduction of carbon fibre reinforced composite shafts in the 1960's shaft characterisation methods has not accounted for the viscoelastic effects of such materials. This brings about several factors for consideration:

1) Current shaft characterisation is either static or quasi-static and would not fully characterise the dynamic shaft properties if the material was found to be strain rate sensitive over the region found in a swing.
2) The roles of using shafts of different stiffnesses has shown little effect on launch condition once a player has become accustomed to it, however the effects of a shaft that may stiffen during a swing has yet to be analysed.

3) In order to determine if shaft stiffening during the swing is likely to occur, a range of strains and strain rates applicable need to be analysed. From literature it would appear that strains and strain rates would not be likely to exceed 6500 μm/m and 0.11 s^{-1} respectively.
4) The strain and strain rate sensitivity of carbon fibre composites has not been fully characterised in the intermediate region that is applicable to golf club shaft, with literature showing that modulus shows no increase at levels of strain rate of 10^{-3} s^{-1} but will show an effect at strain rates as low as $2s^{-1}$, but little is known in the region between.
5) Shafts fabricated by pre-preg lay-up have shown a typical characteristic of a seam where a ply has started or finished within the laminate. This creates a void which during the curing process is filled with resin, and thus the region around this "resin rich region" shows a significant decrease in stiffness. It is also likely that as these sections are more resin dominant that they would show greater viscoelastic effects and thus cannot be ignored in the characterisation of the dynamic performance of a golf shaft.
6) Current testing methods do not measure the damping behaviour of a shaft, however this factor is also strain rate sensitive therefore it appears that along with the damping properties of the commercially available shafts the strain rate dependence of this factor also needs investigating for rates applicable to a golf shaft.
7) As a unidirectional composite is orientated so that the direction of the fibres become further away from the loading axis, the greater the laminates dependence on the matrix properties. It can be seen from literature that the matrix material is predominantly the contributing factor to a composites viscoelastic nature. It is

important therefore that the strain rate dependence is characterised for a range of fibre orientations.

8) Stacking sequence has a major effect on the stiffness and damping of the resultant laminate. With different ply orientations having a varying effect depending on its position away from the neutral axis.
9) No current non-finite element model is available to predict both stiffness and damping for a given composite lay-up and used this to optimise a stiffness/damping function in the design of a composite laminate.

2. Aims and Objectives

The literature review has led to the following aims and objectives for this research:

1) Are the current static and quasi-static test methods of shaft characterisation satisfactory at defining the mechanical properties of the shaft during a swing?

Through fabricating carbon fibre reinforced composite laminates of varying orientation, geometry and stacking sequence and analysing any changes in stiffness and damping through this range of testing (up to the maximum strain rate seen in a gold club shaft), the viscoelastic nature of these laminates can be quantified.

Due to the presence of resin rich regions within a shaft, fabricated panels also need to encompass this feature in order to determine the significance of seams with reference to the viscoelastic nature of a shaft.

Once the viscoelastic properties of the composite has been quantified over the relative range this will allow for the production of a model to answer the following questions:

2) Can a non-finite element model be used to accurately predict the stiffness and damping of a laminate?
3) Can this model accurately predict the stiffness and damping of a shaft (including the presence of a seam)?
4) Can this model be used to optimise orientation and stacking sequence to obtain a preferential stiffness/damping ratio?

3. Experimental

3.1. Effect of Strain Rate on Stiffness

3.1.1. *Panel Fabrication*

Two types of carbon fibre/epoxy pre-preg (T800/VTM264 and T800H/MTM28-1) both with a fibre volume fraction (V_f) of 0.55 were used to fabricate fifteen panels with different lay-ups; all panels were symmetric about the central neutral axis. The lay-ups were vacuum bagged and cured using a thermal cycle that ramped up to 125 °C at 0.5 °C min^{-1}, held for 1 hour and then cooled down at 3 °C min^{-1}. Tables 1a and b show the panel dimensions and density. Panels 7 and 8 represent lay-ups that can be found in commercial golf shafts (Slater and Betzler, 2009). Artificial seams were introduced to panels 13 - 15 by inserting 3 layers of VTA260/PK313 epoxy resin adhesive with a 13 g m^{-2} polyester knitted mesh seam between the 2nd and 3rd as well as 6th & 7th ply (Figure 3.1); this increased these panels' density.

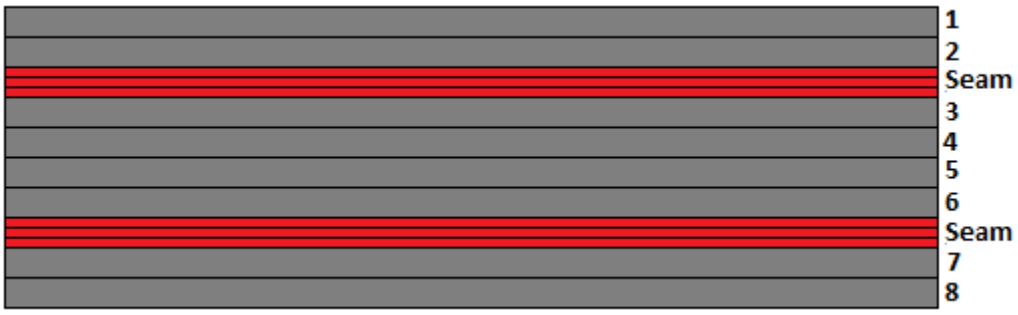

Figure 3.1: Schematic diagram showing the locations of the seam and ply numbers in a panel.

Table 3.1: Dimensions of panels fabricated from T800/VTM264.

Panel No.	Lay-up (°) *	Width (m)**	Height (m)**	Density (g cm^{-3})
1	0-90	0.075 (±0.001)	0.0029 (±0.0002)	1.46
2	0-±45-90	0.075 (±0.001)	0.0030 (±0.0002)	1.43
3	0 (1), ±45 (14), 0(1)	0.078 (±0.002)	0.0033 (±0.0001)	1.45
4	±45 (7), 0 (2), ±45 (7)	0.077 (±0.002)	0.0031 (±0.0001)	1.46
5	10	0.076(±0.002)	0.0032 (±0.0002)	1.49
6	20	0.076 (±0.002)	0.0033 (±0.0001)	1.49
7	±25(3), ±45(10), ±25 (3)	0.078 (±0.002)	0.0031 (±0.0002)	1.47
8	±25 (3), ±45(16), ±25 (3)	0.074 (±0.001)	0.0038 (±0.0001)	1.49
9	±45	0.077 (±0.002)	0.0029 (±0.0002)	1.49

*number in brackets signifies number of plies, if no number is stated then an even number of each is laid up alternately.

**number in brackets signifies the variance along each panel.

Table 3.2: Dimensions of panels fabricated from T800H/MTM28-1

Panel No.	Lay-up(°)	Width (m)	Height (m)	Density (g cm^{-3})
10	0-90	0.075 (±0.001)	0.0029 (±0.0002)	1.46
11	±30	0.074 (±0.001)	0.0038 (±0.0001)	1.43
12	±45	0.077 (±0.002)	0.0029 (±0.0002)	1.45
13	0-90 with seam between 2^{nd} & 3^{rd} and 6^{th} & 7^{th} ply	0.076(±0.002)	0.0017(±0.0002)	1.63
14	30 with seam between 2^{nd} & 3^{rd} and 6^{th} & 7^{th} ply	0.077(±0.002)	0.0016(±0.0002)	1.58
15	45 with seam between 2^{nd} & 3^{rd} and 6^{th} & 7^{th} ply	0.076(±0.002)	0.0017(±0.0002)	1.58
16	±20	0.074 (±0.001)	0.0038 (±0.0001)	1.46
17	±20	0.1 (±0.002)	0.0029 (±0.0002)	1.46
18	Pure Resin	0.075 (±0.001)	0.003 (±0.0002)	1.1

3.1.2. *Static Testing*

The panels were clamped in a three-point bending test set-up (0.2 m span). Mass was added in 0.5 kg up to 5 kg increments and left for 1 minute before taking the deflection reading

using a Solartron C55 linear transducer (Figure 3.2). The linear transducer works through an internal capacitive sensor, the linear travel of the needle is monitored as the capacitance of the circuit is a function of the spacing between a fixed point within the transducer and the needle. This signal is internally converted to a digital output reading as a distance.

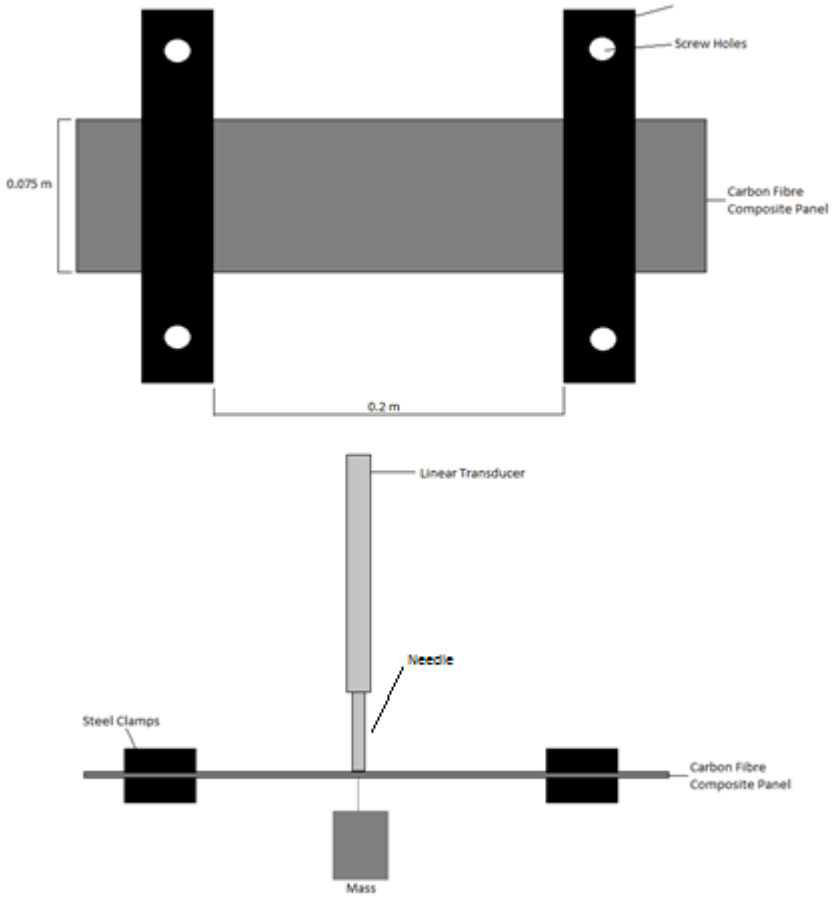

Figure 3.2: Clamping conditions for the static testing of the carbon fibre composite panels.

3.1.3. *Slow Strain Rate Testing*

Four Kyowa uniaxial strain gauges (type KFG) were attached to the back of the panel around the centre. Macro images were taken to determine the precise strain gauge positions (Zeiss MRc5 and Axiovision 4 software). For slow strain rate testing, a high quality polyurethane

covered golf ball was dropped from varying heights (50 to 400 mm in 50 mm steps) onto the centre of the panel. A Brüel & Kjær type 4393 accelerometer with Brüel & Kjær Pulse Labshop V7 was attached to the underside of the panel, beneath the impact point, used to give the force of the impact (Figure 3.3).

The strain gauges work by passing a very small electric current through a metallic resistive foil embedded within the strain gauge. As this foil undergoes some deformation, the change in dimensions causes a change in the resistance; it is this change in resistance that can be quantified to calculate strain (using Equation 3.1). Strain gauges were affixed using the manufactures strain gauge cement supplied.

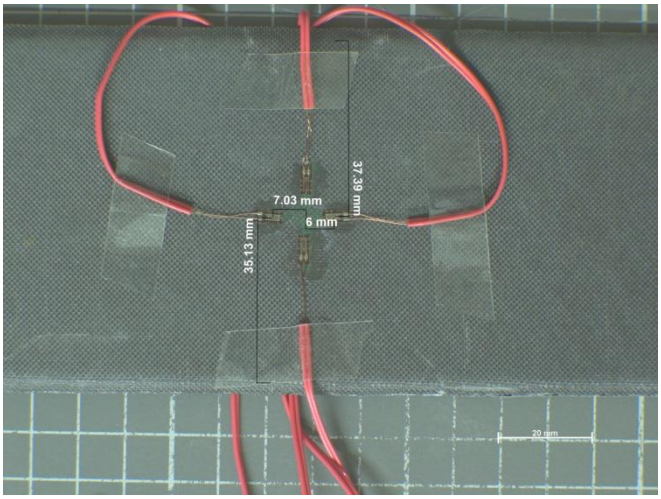

Figure 3.3: Image depicting the location of the strain gauges on the reverse of the carbon fibre composite panels.

$$\frac{\Delta R}{R} = K\varepsilon$$

Equation 3.1

Where ΔR and R are the change in resistance and initial resistance respectively, ε is the strain and K is a gauge factor or constant associated with the design and metal foil used (about 2.1 for the gauges used in this research).

Figure 3.4a and b show typical strain gauge traces from slow strain rate testing. The longitudinal gauges were deemed to be the two gauges located along the loading axis. This signal gave the values of maximum strain as well as strain rate. It can be seen that a linear extrapolation for strain rate (red line) agrees very well with 90 % of the loading curve, and thus during the deformation period this strain and strain rate represents the deformation very well.

a)

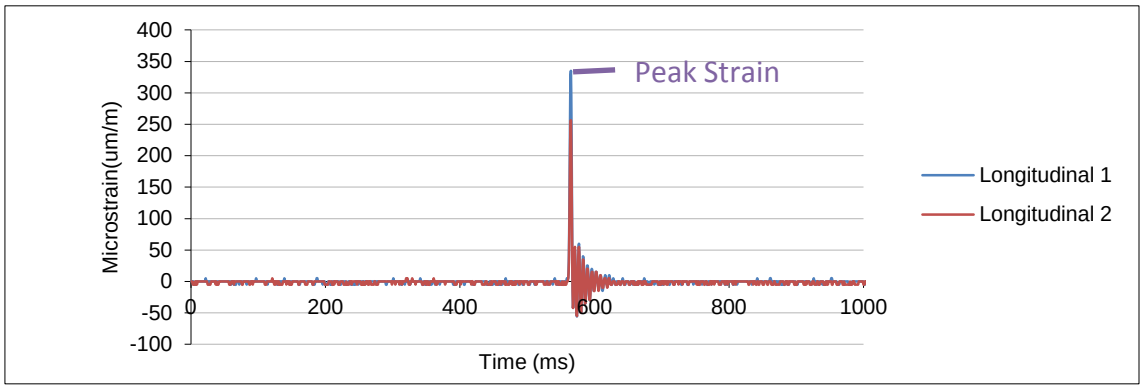

b)

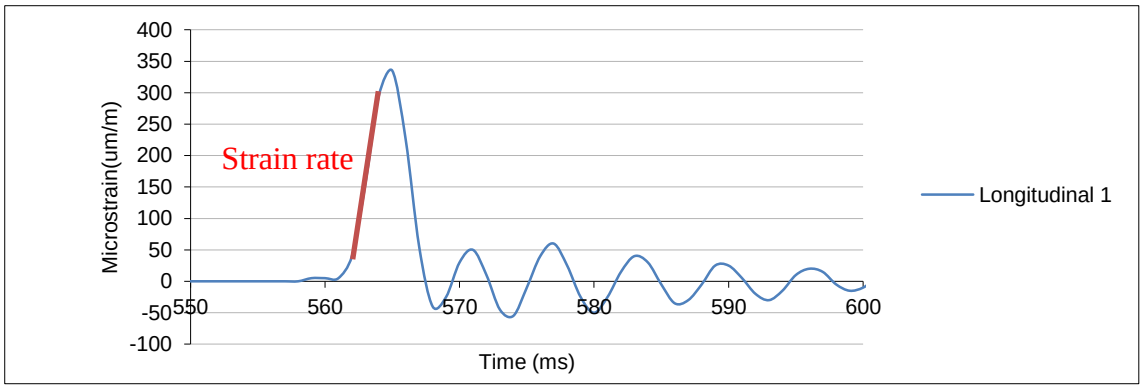

Figure 3.4: Strain gauge traces from slow strain rate testing showing a)the two longitudinal strain gauges and b)how strain rate was calculated.

To calculate the stress and therefore the modulus of the material a Brüel & Kjær type 4393 accelerometer with Brüel & Kjær Pulse Labshop V7 was used. The accelerometer calculates the force through a piezoelectric device. This device contains a crystal, which when stressed by accelerative forces, results in a small voltage being created. The change in voltage

multiplied by a manufacturers constant (embedded within the software) produces the output as a change in g (change in acceleration compared to gravity), this therefore allows for the calculation of the force of impact (the trace of force looks identical to that of Figure 3.4b), the force was calculated from the peak acceleration.

Once the force has been calculated the maximum stress can be calculated by using Equation 3.2 for a 3 point bend scenario:

$$\sigma = \frac{\frac{FL}{8}z}{I}$$

Equation 3.2

Where F is the force measured, L is the span of the 3 point test length, z is the distance of the surface of the panel to its neutral axis (half the thickness of the panel) and I is the second moment of area.

3.1.4. *High Strain Rate Testing*

The CFRP panels were clamped vertically (using the same rig as in static testing) and an ADC Super Cannon 2000 fired the same golf balls at 6 speeds (18 - 35 ms^{-1}) at each panel until at least two central impacts were achieved. Impacts were imaged using a Phantom V7.1 high-speed camera (20,000 fps) to determine the inbound velocity. Between each time a ball was fired, a 5 minute interval was left so that the panel could fully recover from the viscoelastic deformation. This time span was determined from repeat tests that showed good reproducibility after this period, no further appreciable changes occurred if the panel was rested for a longer period. The strain gauges and accelerometer was used in the same manner as for slow strain rate testing.

3.2. Effect of Strain Rate on Damping

Table 3.3 shows 16 panels fabricated for damping testing. Panels were 120 by 30 mm and fabricated from T800H/MTM28-1 unidirectional carbon fibre composite. Panels were cured in the same manner as stated in Section 3.1.1.

Table 3.3: Table of panels fabricated for damping measurements (the subscript refers to the number of repeat units).

Panel No.	Lay-Up (°)
18	$[0]_4$
19	$[10]_4$
20	$[20]_4$
21	$[30]_4$
22	$[40]_4$
23	$[50]_4$
24	$[90]_4$
25	$[0\ 90]_2$
26	$[10\ 90]_2$
27	$[30\ 90]_2$
28	$[50\ 90]_2$
29	$[10\ 0]_2$
30	$[20\ 0]_2$
31	$[30\ 0]_2$
32	$[40\ 0]_2$
33	$[50\ 0]_2$

Panels 18 - 24 were clamped in cantilever at a length of 100 mm, with two 10 g neodymium magnets were attached to the free end. An electromagnet was used to impart a sinusoidal oscillation onto the panel, this was achieved by connecting the electromagnet to an amplifier and a signal generator where both frequency and magnitude could be altered (Figure 3.5). Each panel was fitted with a Kyowa uniaxial strain gauge (type KFG) to monitor the oscillation. A Casio Exilim EX-F1 camera operating at 1200 fps was used to image the

vibrating panel. The images were analysed using Tracker 3.0 software from Open Source Physics.

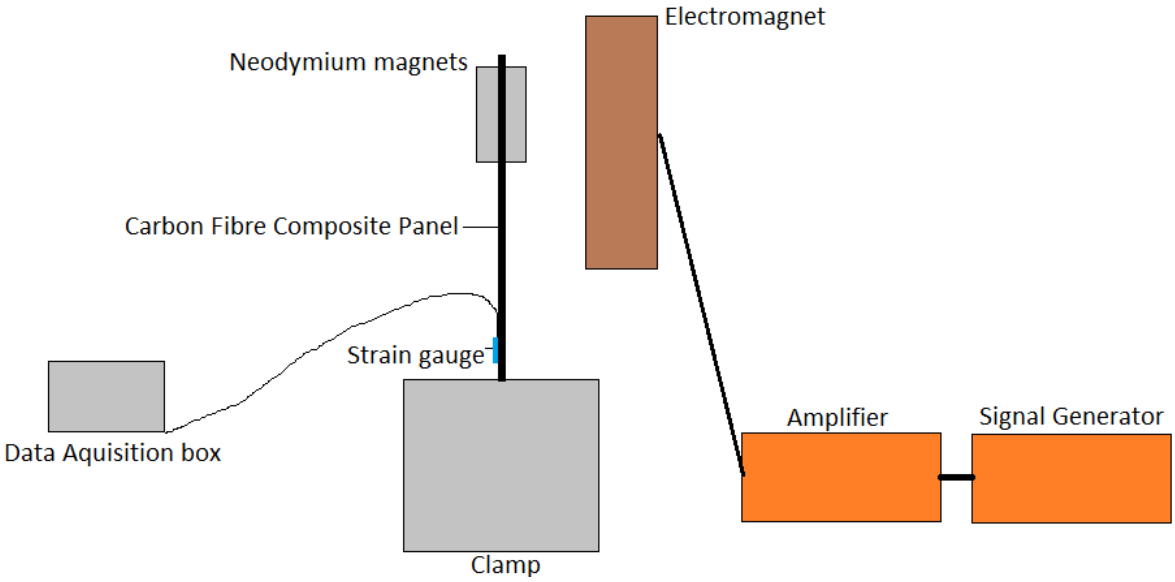

Figure 3.5: Experimental setup for measuring damping

The signal from the strain gauge was analysed using a Fast Fourier Transform (FFT), and the half power bandwidth method was used to determine the loss factor. Example traces of these can be seen in Figure 3.6. Figure 3.6a shows the strain gauge trace, as with the effect of strain rate on stiffness testing, a linear extrapolation has been taken from 90 % of the curve (shown by the red line). Figure 3.6b shows the trace once it has undergone a Fast Fourier Analysis where the half power bandwidth method is used, for this the natural frequency (central green line) is required as well as the two values which intersect the $Peak/\sqrt{2}$ line (red line), these are deemed the upper (right green line) and lower (left green line) bounds.

a)

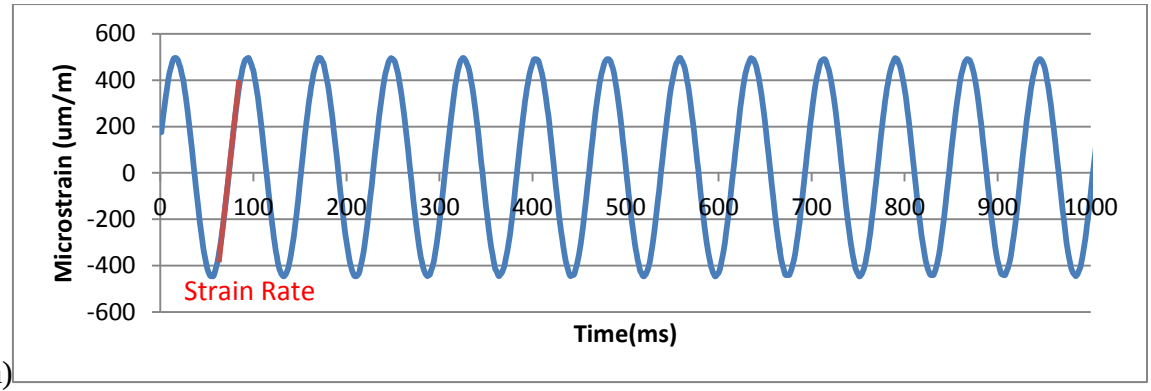

b)

Figure 3.6: Shows a) the strain gauge traces from an oscillating panel and b) the resultant FFT trace from which damping is calculated.

3.3. Golf Shaft Testing

3.3.1. *Shaft Fabrication*

Shafts were fabricated by using oriented sections of T800H/MTM28-1 (600 x 140 mm, which produces a 4 ply thick wall). The pre-preg. was then sectioned further to produce 600 x 80 mm and 600 x 60 mm panels which were laid on top one another to reduce off-axis twisting during rolling. This was then wrapped around a mandrel consisting of a 3 mm steel rod centre and a 10 mm outer diameter silicone tube. The silicone tube was prepared with Frekote WOLO, a release agent, before the pre-preg. was applied. A list of the fabricated shafts can be seen in Table 3.4, where for a shaft with a 0° orientation refers to all the fibres are orientated along the length of the shaft.

Table 3.4: List of fabricated shafts and their orientations.

Shaft Number	Orientation (°)
1	0
2	0
3	0
4	±30
5	±30
6	±45
7	±45
8	±45

To ensure that the pre-preg. did not crease (especially for the off-axis fibres), a mass was added to the end of the pre-preg. A schematic diagram of this can be seen in Figure 3.7. The shaft was cured in a vacuum bag in a Carbolite oven, which was heated up to 125 °C at 0.5 °C min^{-1}, held at 125 °C for 1 hour and then cooled down at 3 °C min^{-1}.

Figure 3.7: Schematic diagram to show the fabrication of a CFC shaft (the arrows depict the mandrel rolling direction).

3.3.2. *Fabricated and Commercial Shaft Deflection Testing*

A selection of commercial shafts where chosen for testing in order to provide a range of characteristics. These shafts had a range of stiffnesses, lengths and tapers. Each shaft had its outer diameter measured every 50 mm to profile the taper using a pair of Mitutoyo callipers.

Table 5: List of commercial shafts selected for deflection testing. All shafts where classified as regular stiffness by the manufacturer.

Shaft Batch	**Number of Shafts**	**Manufacturers Stiffness Rating**	**Notes**
A	3	Regular Flex	
B	6	Regular Flex	Triangular section
C	1	Ladies Flex	
D	1	Regular Flex	
E	1	Regular Flex	Triangular section
F	6	Regular Flex	
G	1	Stiff Flex	
H	1	Regular Flex	Parallel sided

Using a single column Instron 3345 with a 5 kN load cell, each shaft was deflected in a 2 point bend set up at 10 mm/min to 15 N, and returned to 0 N at the same rate, creating a hysteresis loop. Tangential stiffness was determined over the last 5% of the loading curve. Each test was carried out every 50 mm from the tip, and every 15° around the circumference 250 mm from the tip at a cantilever length of 485 mm (Figure 3.8). Fabricated shafts were clamped at a cantilever length of 415 mm as they are much shorter shafts and thus ensures a large enough region inside the clamp.

Figure 3.8: Experimental set-up for commercial shaft testing.

Shaft batch B were also tested in the conventional method [17], using a Golfsmith Precision Shaft Frequency Analysis Machine, at a given cantilever length of 1 m with a 205 g mass attached to the end. The shafts were then excited and the fundamental bending frequency was measured. This is repeated at 15° increments around the circumference of the shaft from 0° to 180° (0° was defined as the orientation with the manufacturers label on top).

3.4. Optical Analysis

Fibre orientation in commercial shafts, fabricated shafts and fabricated panels was determined from a longitudinal section of each panel and shaft (for high angled fibres a transverse section was also taken) mounted in DuroFix. Sections were removed using a Struers Minitom at 100 rpm, this reduces damage to the composite compared to more quicker, more abrasive methods. Sections taken from the shaft were taken 70 mm from each end, which were used to obtain tip and butt microstructures. The samples were polished to a 1 µm diamond polish finish and observed under a Leica DMRX optical microscope using KS300 image analysis software. Fibres were analysed in each ply for area fraction, length, width and aspect ratio. In addition, ply thickness was measured. Each ply was analysed in 10 locations across the sample, which analysed over 150 fibres, and ply thickness was measure 5 times at each location.

4. Material Characterisation

4.1. Optical Analysis

In order to determine fibre angle and volume fraction, firstly the 0° fibres needed to be characterised. Figure 4.1 shows a high magnification image of the fibres from the 0° panel. It can be seen that these fibres are kidney-shaped; this complicates the process for determining orientation compared with circular cross-section fibres.

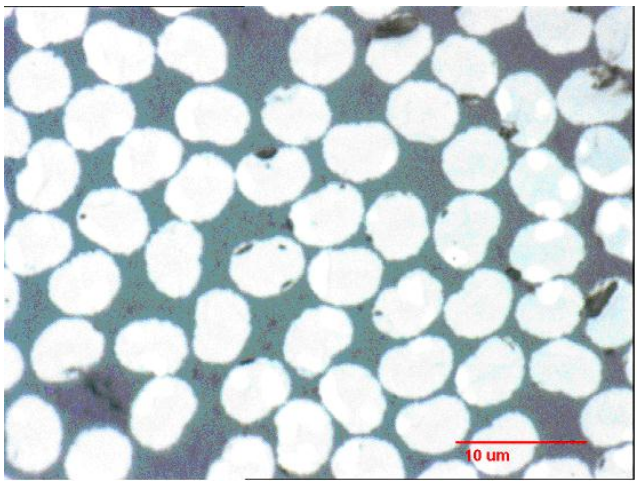

Figure 4.1: Optical image of fibres from the 0° panel.

When a fibre is orientated so that its axis is not perpendicular to the surface of a sample, the resultant cross-section becomes altered. This can be used to calculate the orientation of the fibre. Figure 4.2 shows the resultant projected cross-section on a 2-D section for fibres on- and off-axis. As the fibres are only oriented in a single plane, one dimension of the cross-section remains constant (this is deemed to be *feret min*). If the fibre cross-section is circular this gives a good idea of the original fibre dimensions regardless of orientation. As the cross-section of the fibres used in this study are of a kidney shape, the *feret max* (the value which

alters with orientation, see Figure 4.2) of the off-axis fibre needs to be compared to that of a 0° fibre, in order to establish a measure of the fibre orientation, as detailed below (Equation 4.2). The feret max of the fibres (in a 0° orientation) used in this study is 5.0 µm (± 0.15 µm). The distribution can be seen in Figure 4.3.

The use of Equation 4.2. requires that an accurate value for feret max in the 0° ply, whereas for circular cross-sections it would be sufficient to take the diameter perpendicular to the feret max as the original diameter. The equivalent ellipse area has been calculated from:

$$A = \frac{\pi r^2}{\cos\theta}$$ ***Equation 4.1***

where r is the fibre radius, and θ is the fibre orientation.

It can be seen in Table 4.1 that using an equivalent ellipse area over-estimates the area in all cases, re-emphasising that care needs to be taken when using this method of analysis for kidney shaped fibres.

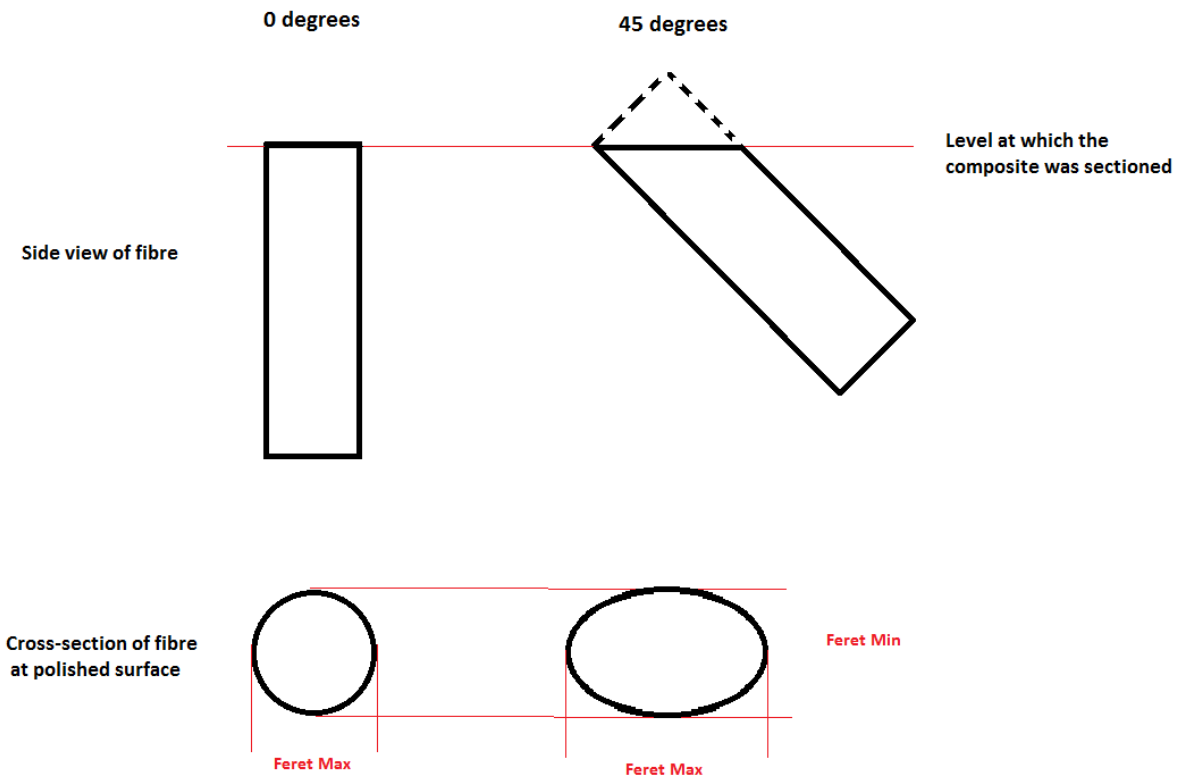

Figure 4.2: Schematic diagram showing the effect of fibre orientation of feret max for cuircular cross-section fibres.

$$\cos\theta = \frac{feret\ max\ of\ 0°\ ply}{feret\ max\ of\ off-axis\ ply}$$

Equation 4.2

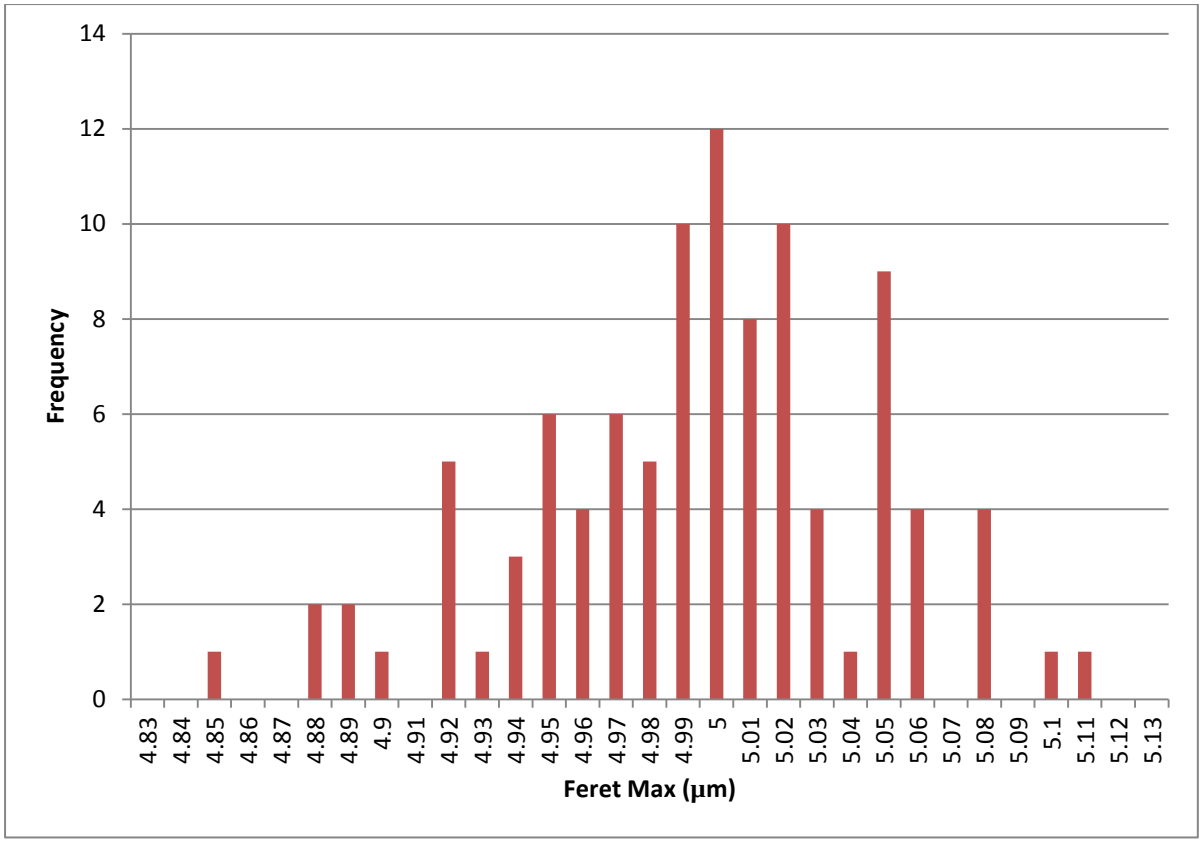

Figure 4.3: Histogram of the variation of feret max of 100 0° fibres

The variability in the fibres' diameter (± 0.15 µm) makes assessing orientation from 0 - 20° much less accurate, as changes in *feret max* for this change in angle will only be of the order approximately 0.3 µm, as seen in Figure 4.4 (changing the *feret max* of the off axis fibre by up to 50 %). Figure 4.5 shows the relationship between *feret ratio* and fibre orientation, reiterating the issue of using this method to identify the off-axis fibres below 20° due to the fibre variability, for cases such as this a transverse section was analysed. Fibre cross-sections were calculated to be 17 μm^2 (±1.5 μm^2), with a perimeter of around 14 µm (±1 µm), as seen in Table 4.1. Figure 4.6 shows two more images of off-axis laminates. For the 90° plies samples were mounted perpendicular to the loading axis. The fibres seen in the 90° ply of Figure 4.6b shows the fibres have finite extent, this should not be the case if the fibres were

truly 90°. This discrepancy can be attributed to either an inaccuracy in the mounting and subsequently grinding of the laminate section before analysis, or to an irregularity in CFC's known as fibre waviness. Fibres can show fibre waviness depending on the manufacturing process, which is the misorientation of the fibre at specific point along its length [47], although this is usually small in pre-preg lay-ups, less than 1° [97], compared to the fibre waviness of either two or three dimensional woven laminates. This could also account for the scatter observed in the *feret max* in Figure 4.3.

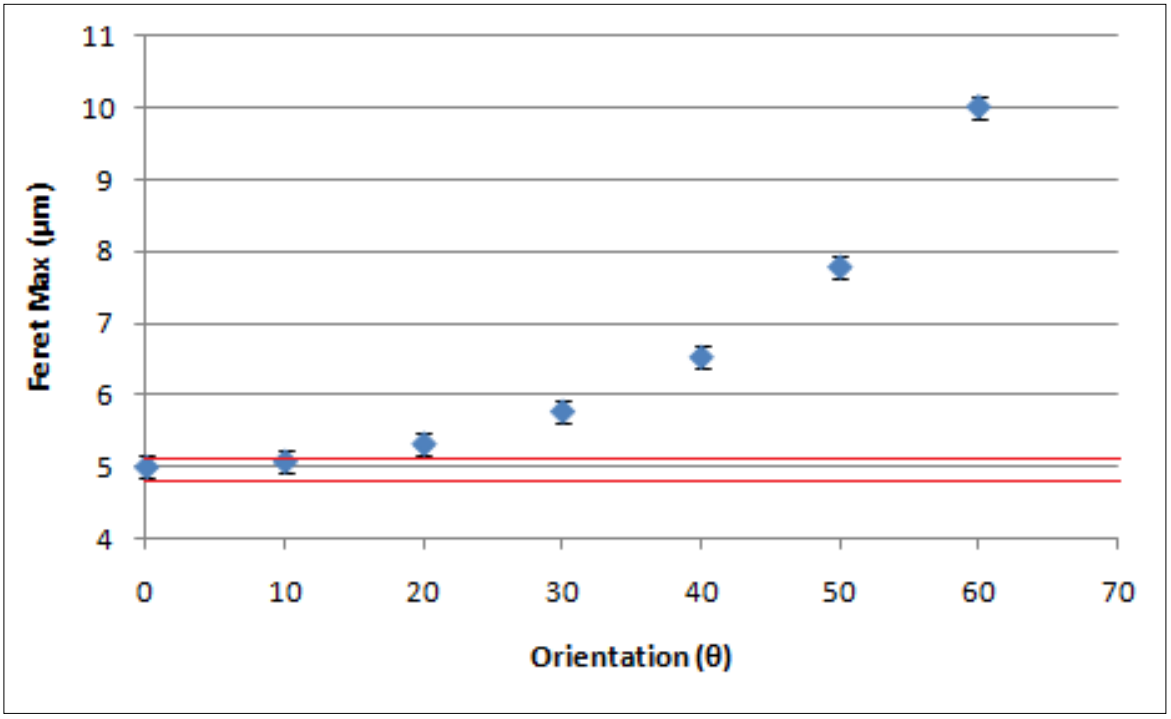

Figure 4.4: Relationship between feret max and fibre orientation using Equation 4.2.

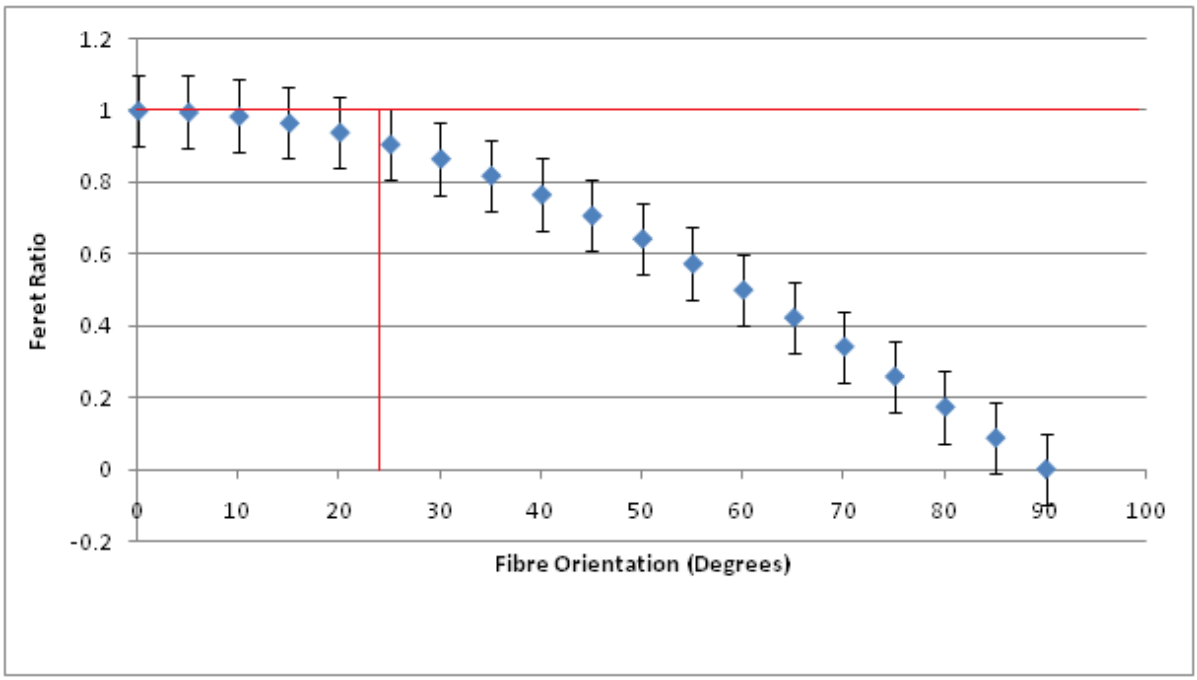

Figure 4.5: Relationship between feret ratio and fibre orientation using Equation 4.2.

Table 4.1: Summary of fibre geometry from optical analysis

Fibre Orientation (°)	Average maximum diameter (µm) (± 0.1)	Feret ratio (± 0.02)	Average fibre area (µm²) (± 0.3)	Equivalent Ellipse Area (µm²)
0	5	1	17.4	19.6
10	5.1	0.98	18.1	20
20	5.4	0.92	18.6	21.07
25	5.7	0.88	19.9	22.4
45	7.0	0.71	22.1	26

a) 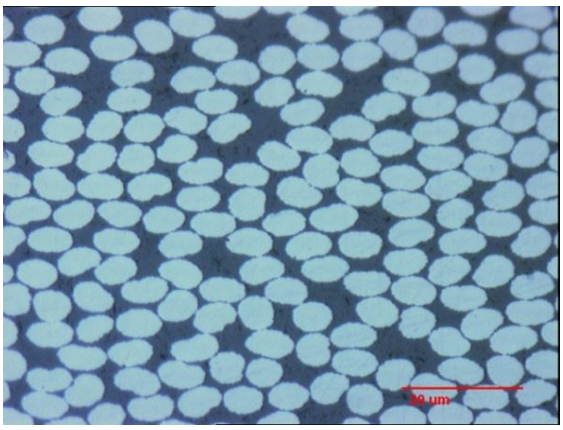 ***b)*** 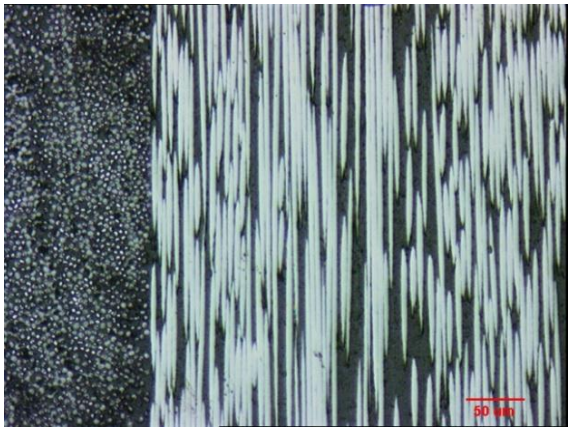

Figure 4.6: Optical images of a) 45° ply and b) 0-90° interface.

All panels were checked to ascertain that they had 55 % (±2 %) volume fraction and average ply thickness of 180 µm (± 10 µm). This ensured good repeatability and consistency across all fabricated components.

4.2. Mechanical Properties

In order to predict changes in modulus and loss factor with strain and strain rate, the composites used were fully characterised in terms of mechanical properties variation with fibre orientation. Eight panels were fabricated from MTM28-1/T800H of varying orientations (0, ±10, ±20, ±30, ±40, ±50, ±60, and 90°). Classic Laminate Theory (CLT), CoDA 3.1 software [98] was used to predict a theoretical modulus for the composite system. Figure 4.7 shows the predicted and experimental Young's modulus achieved from a uniaxial tensile test using a Zwick Z100 to a strain of 0.4%. In order to obtain the theoretical moduli, experimental values of E_1, E_2, G_{12}, and v_{12} were input based on the 0° panel

Table 4.2). The program was also used to estimate the static flexural modulus of the panels 1-9 (see Chapter 3.1), it can be seen that there is good agreement between predicted and experimental values (Root Mean Square Deviation (RMSD) of 0.00092).

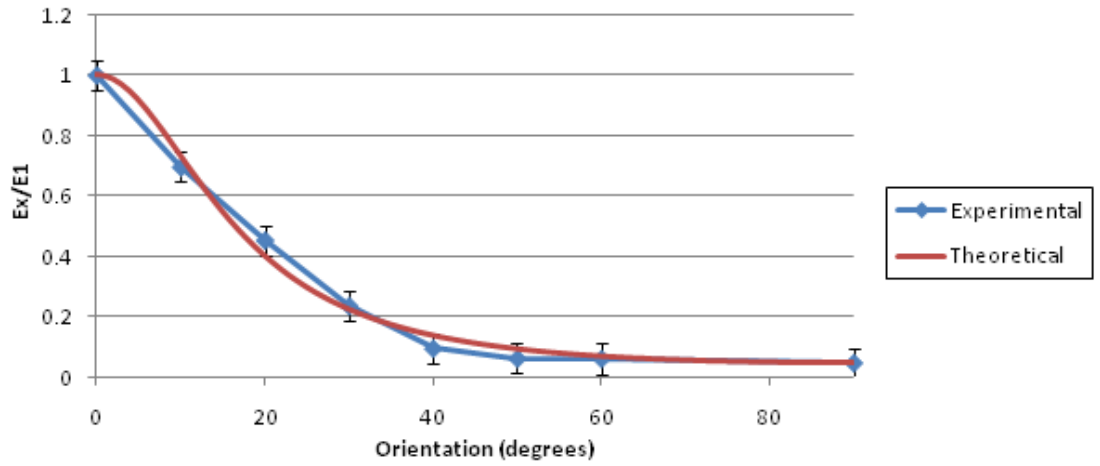

Figure 4.7: Predicted and experimental relative modulus as a function of fibre orientation away from the loading axis.

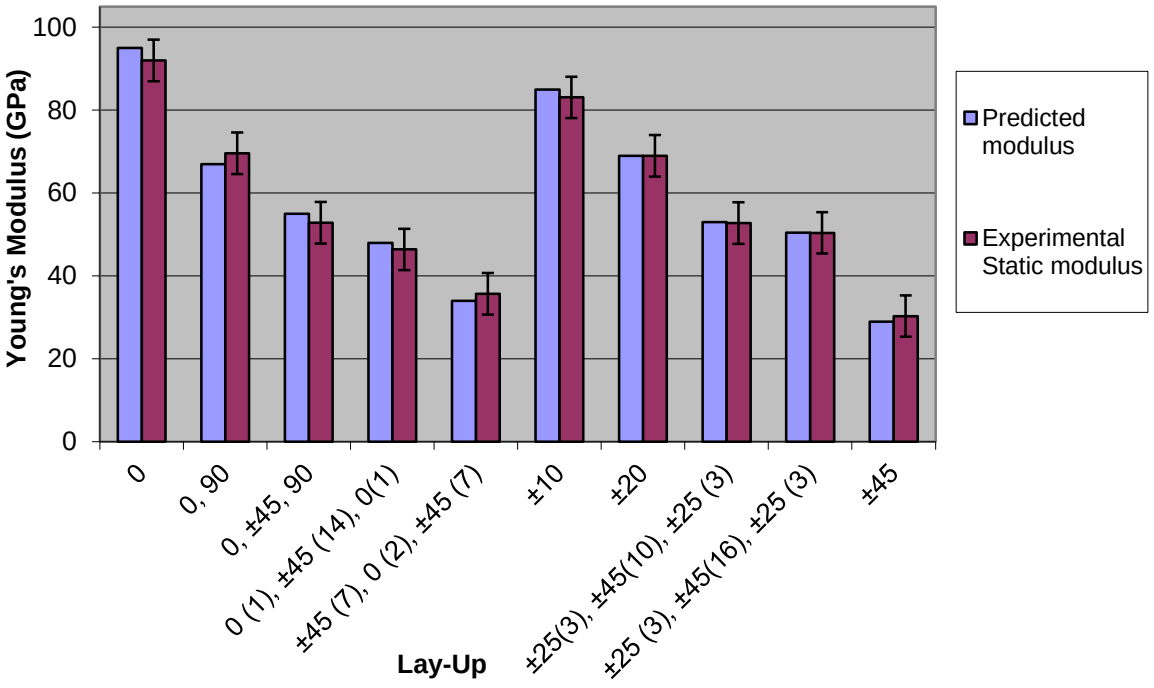

Figure 4.8: Predicted and experimental flexural modulus variation with stacking sequence.

Table 4.2: Mechanical properties of the two different composite systems used in this study

	VSM264/T800	**MTM28-1/T800H**
Ex (GPa)	**95 (±2)**	**165 (±2)**
Ey (GPa)	**8 (±0.5)**	**10 (±0.5)**
Gxy (GPa)	**5 (±0.5)**	**8 (±0.5)**
vxy	**0.25 (±0.03)**	**0.28 (±0.03)**
ηx	**0.008 (±0.0005)**	**0.0007 (±0.0005)**
ηy	**0.012 (±0.001)**	**0.0083 (±0.001)**
ηxy	**0.00105 (±0.001)**	**0.003 (±0.001)**

5. Laminate Testing

5.1. Characterisation of Composite Panels - Modulus

Currently commercial golf club shaft testing is primarily carried out either statically or quasi-statically [17]. However due to the viscoelastic nature of CFC's the sensitivity of modulus to strain rate needs to be examined [75-77]. This will help to determine whether static / quasi-static methods of characterisation are still valid for indicating the dynamic performance of a shaft.

This chapter aims to characterise the strain-rate sensitivity of flat panels of CFC in terms of stiffness. This will be carried out by using a range of orientations, stacking sequences and aspect ratios (See Chapter 3.1, Tables 3.1 and 3.2).

5.1.1. *Effect of Strain Rate on Modulus*

Figure 5.1 and Figure 5.2 show the percentage change in Young's modulus with increasing strain rate for the panels fabricated from T800/VTM264. For panels containing layers with a 0° orientation (Figure 5.2) there is very little noticeable change in modulus seen throughout the range of strain rates studied; this is considering a 5 % increase is needed for the effect to be deemed to be significant. However, Figure 5.1 shows that in the absence of 0° fibres, the onset of strain-rate dependency begins in the range of 0.4 to 0.7 s^{-1}. Increasing the off-axis angle (± 10 to ± 45°) appears to lead to a greater strain-rate dependency with a similar point of onset (another possibility is that the panels shows a consistent strain-rate dependency but differing points of onset, however this is not consistent with literature [75, 78].This trend agrees well with Gilat *et al.* (2002) [78], who also showed that the dependence did not saturate until around 400 s^{-1}. A continuation of the strain rate dependence beyond the range

tested experimentally here would be expected. However, the range that is applicable to golf club shafts has been covered fully (up to 0.1 s^{-1} [21, 99]).

From Figure 5.1, it can be clearly seen that as the angle between the fibre and loading axis increases the plies start to show properties more characteristic of the resin. For panels which show a high resin-dominated response (such as the ± 45°), a strain-rate dependence akin to that of the resin indicating that this is dominating strain-rate sensitivity for these conditions. On impact, when the outer surface is in tension and the inner surface is in compression the free chain sections within the epoxy reorganise, this results in the cross-links lengthening (tension), buckling (compression) and rotating (both tension and compression), creating more pseudo cross-links (or chain interactions in the absence of molecular bonding, but still constrain the polymer chain). As mentioned previously (Chapter 1.9) when loading an epoxy quickly, the motion and rotation of the functional groups becomes limited because of these pseudo cross-links, and thus an increase in modulus is seen.

From Figure 5.1 and Figure 5.2, although a ± 45° panel was shown to be the most strain-rate dependent out of the panels fabricated, the introduction of 0° plies, reduced this effect drastically, to the point where there was no noticeable change in modulus at higher strain rates until above 3 s^{-1}. The 0° plies that were introduced only constituted 50% (by volume) of the panel. This trend can also be seen in the 0-90° and 0-±45-90 panel, where it is assumed that the 90° plies will show the characteristics of pure matrix material. Little or no strain-rate sensitivity has been detected through this range for the 0-90° and 0-±45-90 panels, therefore the presence of 50 and 25% respectively of 0° plies has reduced the viscoelastic effect of the matrix resin. The maximum strain rate achieved is chiefly dictated by the stiffness of the panel, panels with much higher stiffnesses (such as the [0-90-0-90]2s panel) deflected at

much lower rates and as such strain rates much greater than $1s^{-1}$ could not be achieved in some cases.

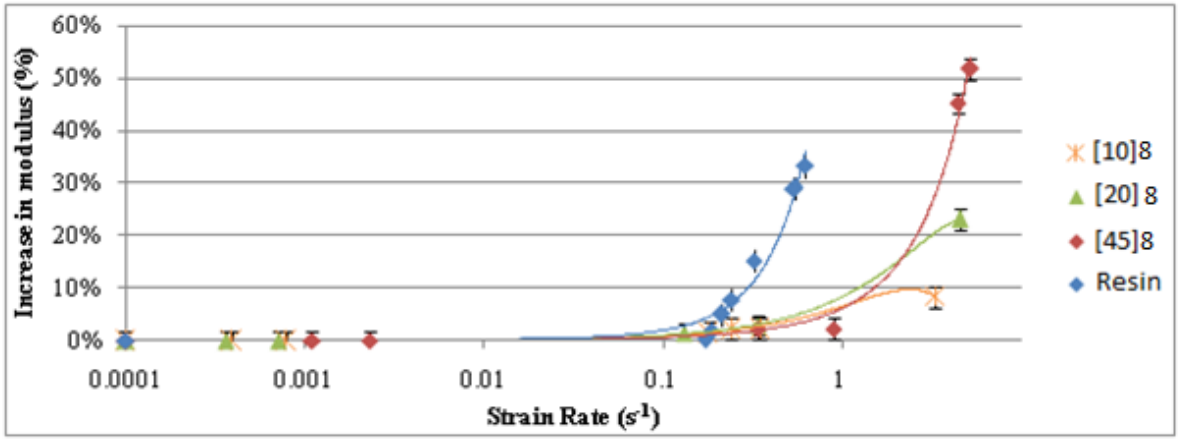

Figure 5.1: Strain-rate dependence of modulus on panels which contain 0° plies.

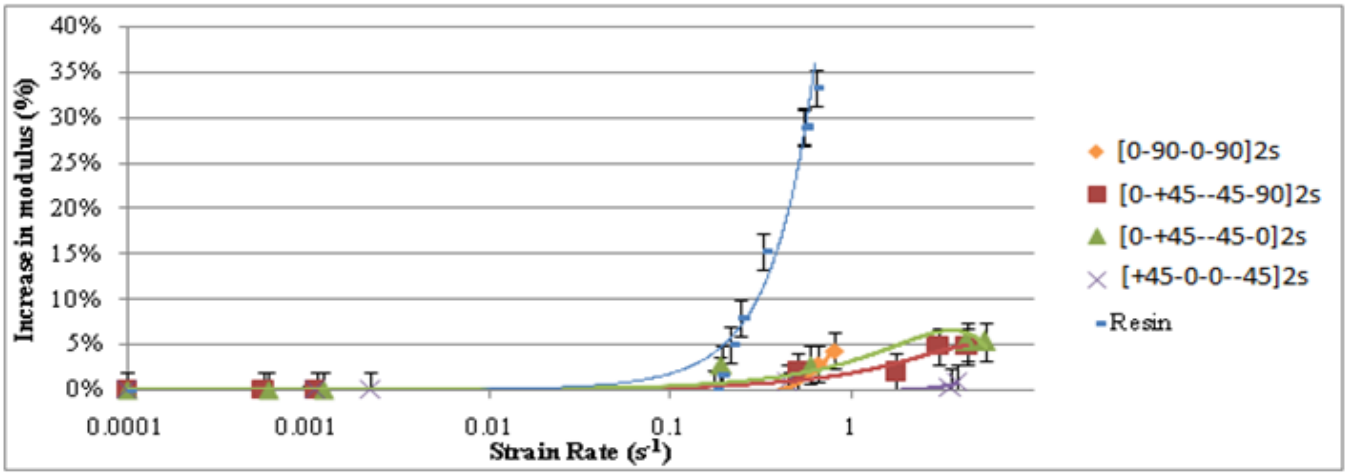

Figure 5.2: Strain-rate dependence of modulus on panels which contain 0° plies.

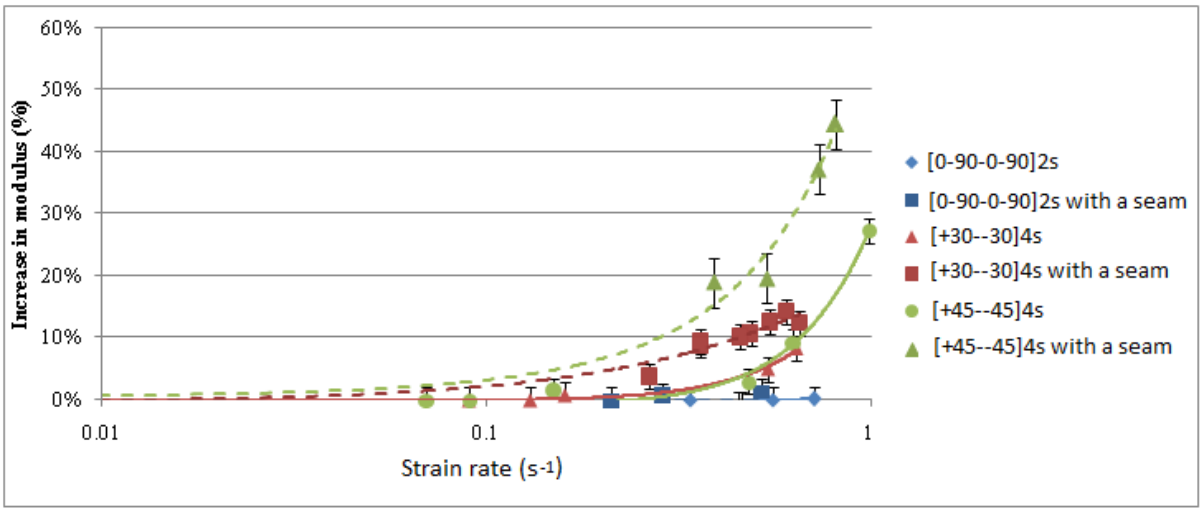

Figure 5.3: Strain rate dependence of modulus on panels which contain seams, panels were fabricated from T800H/MTM28-1.

The panels measured in Figure 5.3 were fabricated from T800H/MTM28-1, which shows a greater strain rate dependence than the T800/VTM264 (Figure 5.1). Figure 5.3 also shows the effect of seams on the strain rate sensitivity of the panels (seams were located between the 2nd & 3rd and 6th & 7th plies) The effect of the seam on strain-rate dependency is similar (shown by the similar gradients) but the point at which the strain-rate dependency occurs is reduced, this can be seen more noticeably in the ±45° panel, and to a lesser extent for all other lay-ups. The 30° panel with a seam clearly shows a reduced strain-rate sensitivity (modulus/strain rate gradient) compared to the 45° panel with a seam, however onset appears to be similar. This is attributed to the initial moduli of the panels, as the 45° panel with a seam is more dependent on the resin properties than the other panels. |Therefore, an increase in modulus of the epoxy due to the dynamic impact will contribute to a much greater degree to the modulus of the 45° panel with a seam than to the 30° panel also with a seam. The resin shows the same increase in modulus at the same point, however it is the laminates dependence on the resins properties that dictates the panels' susceptibility to this change.

The seams introduced into the panels contribute a volume fraction of about 0.2; seams of this magnitude are not likely to exist in CFRP shafts. This can be compared to 0.05 found in commercial shafts in areas with a large number of seams, and some areas around the circumference may show no seams at all [4]. Although seams have been seen to have significant effect on shaft stiffness, they are not likely to significantly change any strain-rate dependency of the shaft at the strain rates applicable to golf club shafts. This is due to the un-reinforced resin showing little change in modulus below 0.25 s^{-1}, and the addition of fibres in orientations between 0 and 45° appears only to reduce the strain-rate sensitivity (gradient of change in modulus/strain rate) and delay its onset.

For all panels tested there was no change in modulus when strain rates were in the range experienced in human golf swings (< 0.1 s^{-1} [99]). This indicates that the limits of linear stress-strain behaviour are not exceeded when a human swings a golf club and that static testing is sufficient to characterise the first bending mode of a shaft in a golf swing.

5.1.2. *Aspect Ratio*

In this research aspect ratio has been defined as the ratio between the cantilever length and the panel width (normal to the loading direction).

The testing carried out in this research has been based around a three-point bending condition, where the laminate is rigidly clamped at either end along the length of the panel. This creates a system by which the clamping condition of the fibres is very sensitive to the orientation of the fibres and the laminate's length and width. Table 5.1 shows how the lay-up of a laminate alters the clamping of the fibres. The clamping conditions can be separated into three groups (Figure 5.4);

- Doubled clamped: Continuous fibres are clamped at both ends of the laminate.

- Single clamped: Fibres clamped at one end of the laminate but due to their orientation reach the free edge of the laminate before the opposite clamped region.
- Unclamped: In some cases of large off-axis orientations some fibres will not be clamped at either end and thus load must be transferred through resin.

Table 5.1: Clamping condition for panels for strain-rate dependency testing.

Lay-Up	Dimensions (Length x Width)	% Doubled Clamped Fibres	% Single Clamped Fibres	% Unclamped Fibres
0°, 90°	0.2 x 0.075 m	50.0%	0.0%	50.0%
0°, ±45°, 90°	0.2 x 0.075 m	25.0%	18.8%	56.2%
0° (1), ±45° (14), 0°(1)	0.2 x 0.075 m	12.5%	32.8%	54.7%
±45° (7), 0° (2), ±45° (7)	0.2 x 0.075 m	12.5%	32.8%	54.7%
±10°	0.2 x 0.075 m	53.0%	47.0%	0.0%
±20°	0.2 x 0.075 m	2.9%	97.1%	0.0%
±25°*(3)*, ±45°*(10)*, ±25° *(3)*	0.2 x 0.075 m	0.0%	53.6%	46.4%
±25° (3), ±45°(16), ±25° (3)	0.2 x 0.075 m	0.0%	50.1%	49.9%
±45°	0.2 x 0.075 m	0.0%	37.5%	62.5%
±30°	0.2 x 0.075 m	0.0%	65%	35%
Wide ±20°	0.15 x 0.1 m	45.4%	54.6%	0.0%

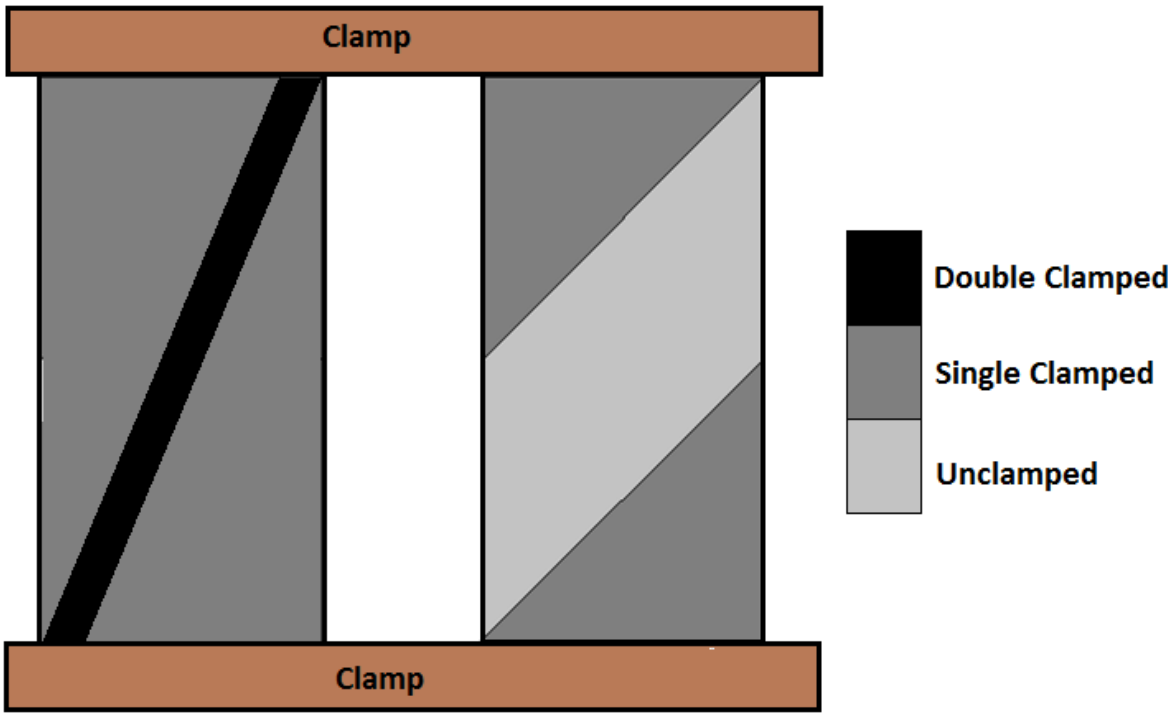

Figure 5.4: Schematic diagram showing how fibres can be either double, single or unclamped.

All initial panels were clamped with a span of 0.2 m and were 0.075 m wide. From optical analysis (100 fibres), the average fibre cross-sectional perimeter was 14 (± 0.2) μm with a volume fraction of 0.55; these give a total fibre / matrix interfacial area per unit volume of 454118 m^2/m^3. By altering the width of a panel (for the same span), both the interface area and the percentage of clamped fibres will change, therefore, in order to monitor the effects of percentage clamped fibres on strain-rate sensitivity, constant interfacial area needs to be maintained.

Figure 5.5 shows the results from two 20° panels with the same interface area, however one panel was made wider (100 mm), and clamped at a shorter span (0.15 m). This altered the clamping of the fibres, as shown in Table 5.1 and Figure 5.6. This change significantly reduces the strain-rate sensitivity, which now more closely resembles a ± 10° orientation

(Table 5.2), this is mirrored with the clamping condition, both the regular ± 10° and the short wide ± 20° showing close to a 50% split between double-clamped and single-clamped fibres.

As the panel aspect ratio is increased, as in this case, off-axis fibres will extend for a reduced distance along the laminate's length, in turn causing the matrix to transfer the load between fibres. The greater the distance between the unclamped end of a fibre and the end of the laminate, the more the laminate is dependent on the matrix material, and therefore will show an increased strain-rate dependency.

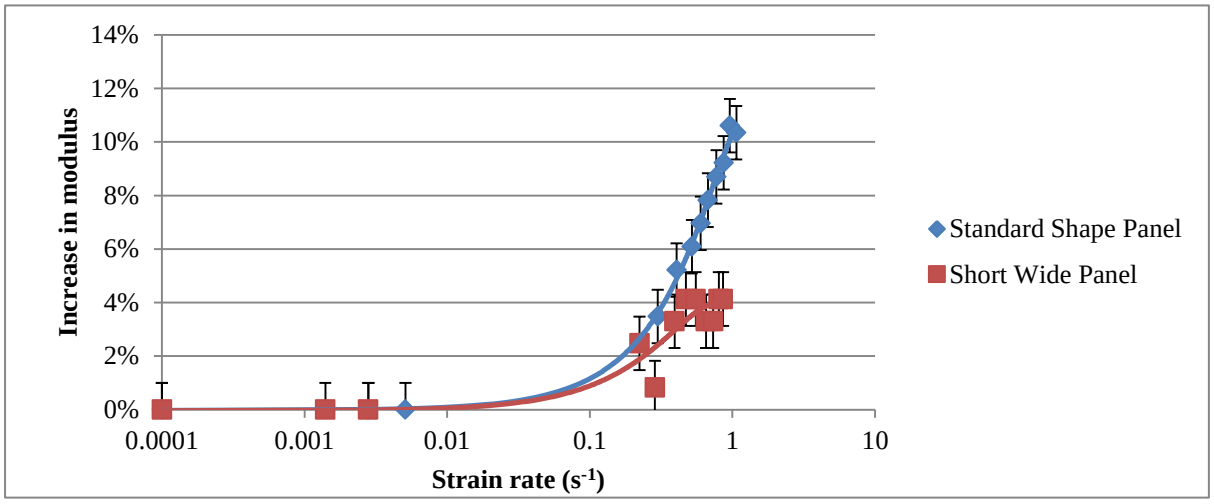

Figure 5.5: The effect of changing the percentage of clamped fibres on the modulus of 20° lay-up panels as a function of strain rate.

Table 5.2: Increase in Young's modulus at 1 s^{-1} for laminates of different orientation and geometry.

Panel	Increase in modulus at 1 s^{-1}
Standard 10° panel	5.1 %
Standard 20° panel	11 %
Short wide 20° panel	4.2 %

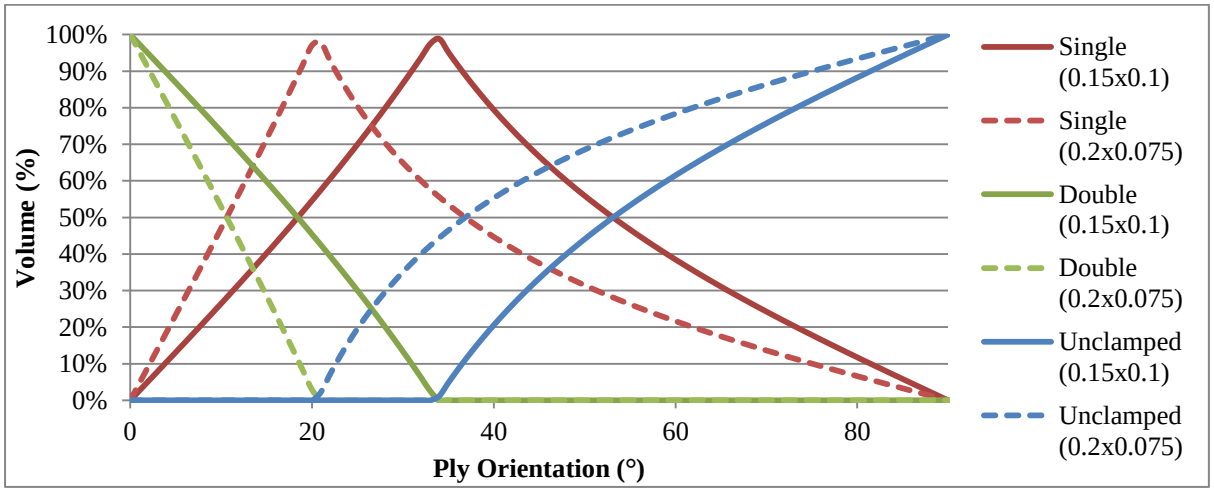

Figure 5.6: The effect of fibre orientation and laminate dimensions on the clamping conditions of a laminate.

The strain rate dependence is a non-linear function of fibre angle, demonstrated in Figure 5.6. For a panel of given dimensions, as ply orientation moves away from 0° this results in fibres becoming only clamped at one end. If fibres from opposite ends of the panel are only clamped at one end then shearing through the matrix between these plies would be expected.

At a critical angle, θ_{crit}, any greater increase in fibre orientation away from the loading axis will result in the formation of unclamped fibres. This occurs when:

$$tan(\theta crit) = \frac{\text{Panel Width}}{\text{Panel Length}}$$

This should result in a much greater strain-rate sensitivity and a tendency to behaviour similar to that of the matrix resin as complete shearing through the matrix between two unclamped fibres occurs.

The effect of aspect ratio has been investigated in many areas of composite material such as buckling, stiffness, fatigue, crack initiation and damping. Chen and Matthews [100] investigated the effect of plate aspect ratio on stiffness and fatigue of composite plates (also in 3-point bending). It was shown that increasing the aspect ratio from 1 to 3, decreased stiffness values by 24 %, however a smaller change was seen from 2 to 3 than from 1 to 2, suggesting the effect is reduced. It is also important to note that both the 2:1 and 3:1 aspect ratio plates showed a much greater influence of strain than the plate with an aspect ratio of 1:1. This was also reported by Jones (1975) [57] where stiffness was measured in vibrating plates in 3-point bending with aspect ratios ranging from 0.5:1 to 5:1. It was shown that there is a significant increase in deflection for aspect ratios between 0.5:1 and 2:1, with the effect showing saturation at around an aspect ratio of 3:1. This indicates how the behaviour of a composite system is sensitive to both orientation and aspect ratio. At low aspect ratios laminates, where a high proportion of the fibres are doubly (3-point testing) or singly (cantilever) clamped, are much more fibre dependent, as the load is transferred with minimal interaction from the matrix material. As aspect ratio increases, and the proportion of unclamped fibres increases, this increases the amount of dependence on the matrix. At aspect ratios greater than 3:1 however, no further decrease in stiffness is witnessed as a fibre/matrix

load transfer system is dominating the laminates properties and will continue to do so at greater aspect ratios. The point of saturation will alter depending on fibre orientation, with 0 and 90° laminates showing negligible changes in mechanical properties with aspect ratio.

For the same lay-ups, laminates have been shown to have an increased dependence on the matrix as aspect ratio increases. In this study, the two ± 20° panels with differing aspect ratios (2.666:1 and 1.5:1) showed different trends in strain-rate sensitivity (Table 5.2 and Figure 5.5). It is therefore important to compare directly only panels with similar aspect ratios, although it has been shown that the changes are negligible for aspect ratios greater than 3:1 [100, 101].

5.2. Characterisation of Composite Panels - Damping

5.2.1. *Effect of Strain and Strain Rate on Damping*

The previous section has shown that laminate modulus can be altered (based on a 5 % threshold) by subjecting composite panels to strain rates above 0.4 s^{-1} (also reported in Slater and Betzler, 2009[102]), and literature has measured golf club shafts being subjected to strain rates of up to 0.1 s^{-1} [99].

This section aims to determine whether loss factor (η), or the amount of energy lost due to internal friction, is also affected by the strain rates applicable to golf club shafts by using a novel testing method to excite composite panels fabricated from a range of lay-ups.

Frequency testing of 6 panels (±10, ±20, ±30, ±40, ±50 and 90° - See Chapter 3.2 for details) showed no noticeable effects of strain/strain rate on loss factor (Figure 5.7) up to about 0.5 s^{-1}; this range is applicable to golf club shafts and would suggest that static testing is sufficient

to characterise the dynamic damping of a shaft. The panels did however show an increase in dependence with increasing orientation away from the loading axis (Figure 5.8).

Polymeric damping arises from the molecular motion of the polymer chain during deformation. During the linear elastic region of a polymer's tensile stress/strain cycle, very little rotational movement of the polymer chain occur, and deformation can be attributed to the stretching of bonds. During non-linear deformation, pendant groups attached to the polymer chains rotate and move over one another so that energy is lost through internal friction, which can be observed by its characteristic hysteresis loop during a stress/strain cycle. Jones (2001) [103] studied the damping and moduli of various polymers and the resultant effect on the tensile behaviour due to their structure. For polymers which show a predominantly linear elastic response to small strains, damping will remain constant even when subjected to a high strain amplitude (damping is not likely to be zero as internal friction is not truly zero and additional losses will arise from the test method used). However, some elastomers (such as polyurethane) will show a linear response at low amplitudes (strains ≤ 0.1) but a non-linear response at higher amplitudes due to the increase in chain slippage.

From the stress/strain plot obtained from the tensile test of the T800H/MTM28-1 system a linear elastic region can be seen until around 0.5 % strain (Figure 5.9). Linear elastic behaviour would suggest just a stretching of the molecular bonding along the polymer chain with no rotation, and as such, so little or no damping would be expected.

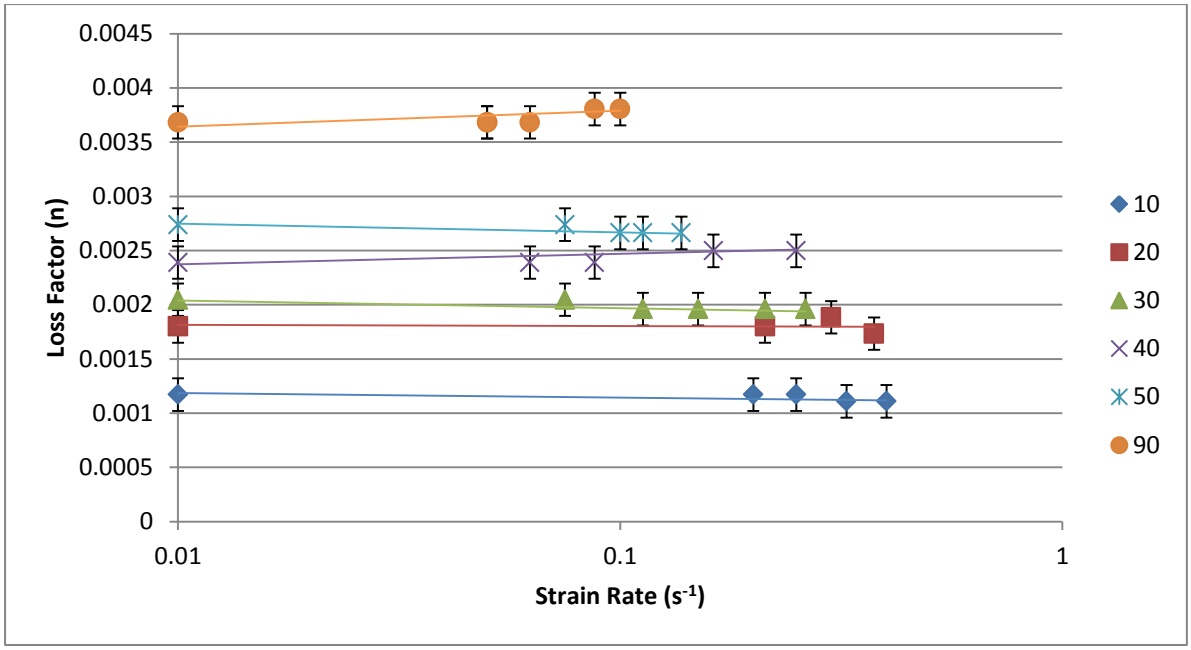

Figure 5.7: The effect of strain rate on loss factor on different fibre orientations.

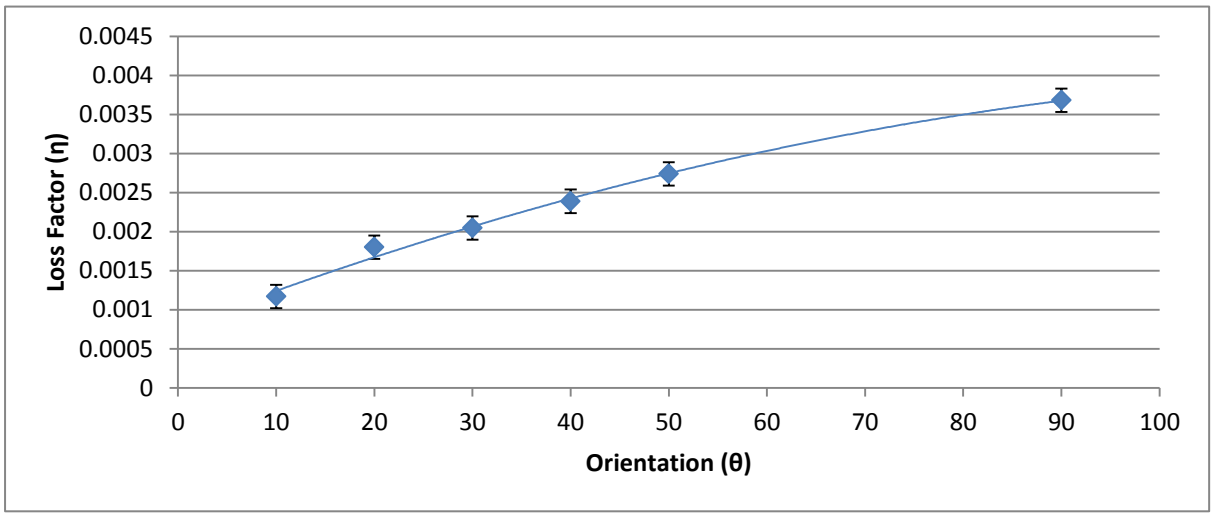

Figure 5.8: Experimental values for loss factor with changing ply orientation of a 4 ply laminate.

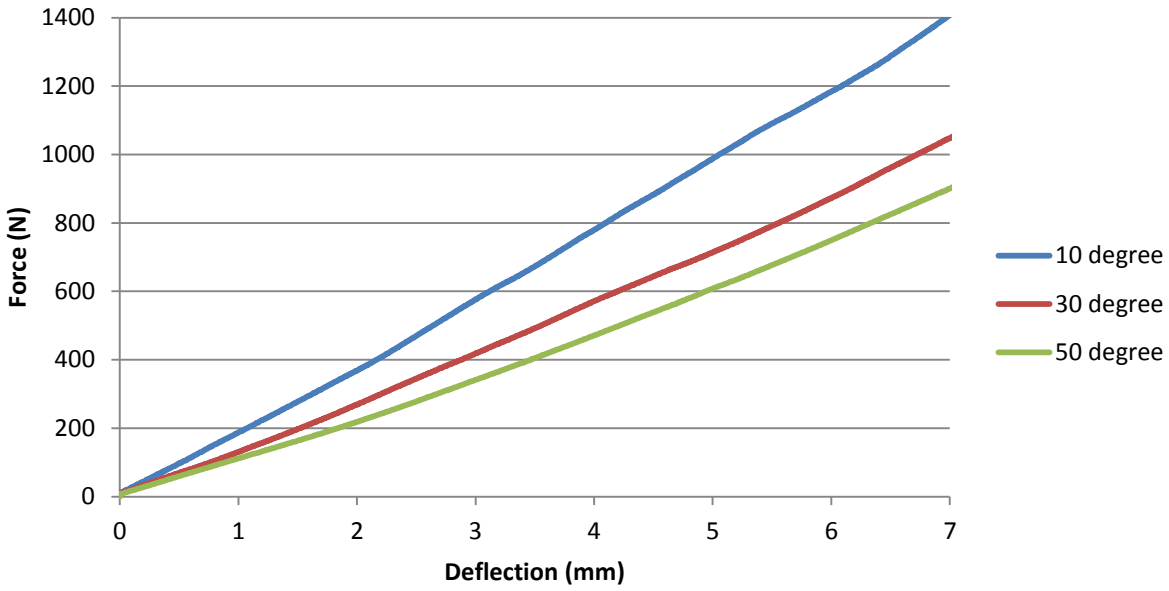

Figure 5.9: Force/deflection curves for three of the panels used for damping analysis.

Within a laminate the total damping is the summation of the three directional loss factors in the x, y and shear directions (η_x, η_y, and η_{xy} respectively, See Chapter 6), each deriving its value from different interactions within the composite. Figure 5.10 shows the effect of doubling each of the three factors based on the base values of the composite system used in this study (Figure 5.10a) and using the equation used by Ni and Adams (1984) [104] for calculating damping for unidirectional laminates (this will be covered more thoroughly in Chapter 6).

- η_x (Figure 5.10b) derives its value from the fibres and is normally the lowest loss factor as the internal friction of carbon fibres is exceptionally low (for a 0° laminate). By altering the value of η_x only orientations between 0-20° can be seen to change compared to the base values. As η_x is derived from the fibres, this curve is similar to

that of modulus' dependence on orientation. Changing η_x can be achieved by changing the fibres used.

- η_y (Figure 5.10c) derives its value from the matrix and is usually the most dominant of the loss factors (for high values of θ), with the total η showing a very similar trend to that of η_y with orientation, especially at large angles. The losses within a matrix have already been covered in Chapter 1.9, and will be almost an order of magnitude greater than η_x. As total η is so dependent on η_y, then if η_y is strain or strain-rate dependent this effect is likely to be seen in the laminate as well. Changing η_y can be achieved by changing the matrix system.

- η_{xy} (Figure 5.10d) derives its value from shearing of both the matrix and the fibre/matrix interface. If a weak fibre/matrix interface exists then η_{xy} is likely to be high, due to slippage between fibre and matrix. Such a high value of η_{xy} would be similar to that shown in Figure 5.10d. It may be possible for interfacial friction large enough to give an η_{xy} value greater than that of η_y and a peak in the total η will be seen for 45° orientations [101]. However, if a strong fibre/matrix interface is present, with little/no slippage, then η_{xy} will be dependent on the shear damping properties of the matrix material. Fibre pullout or push-out tests, as well as lap joints can be used to measure η_{xy} [104].

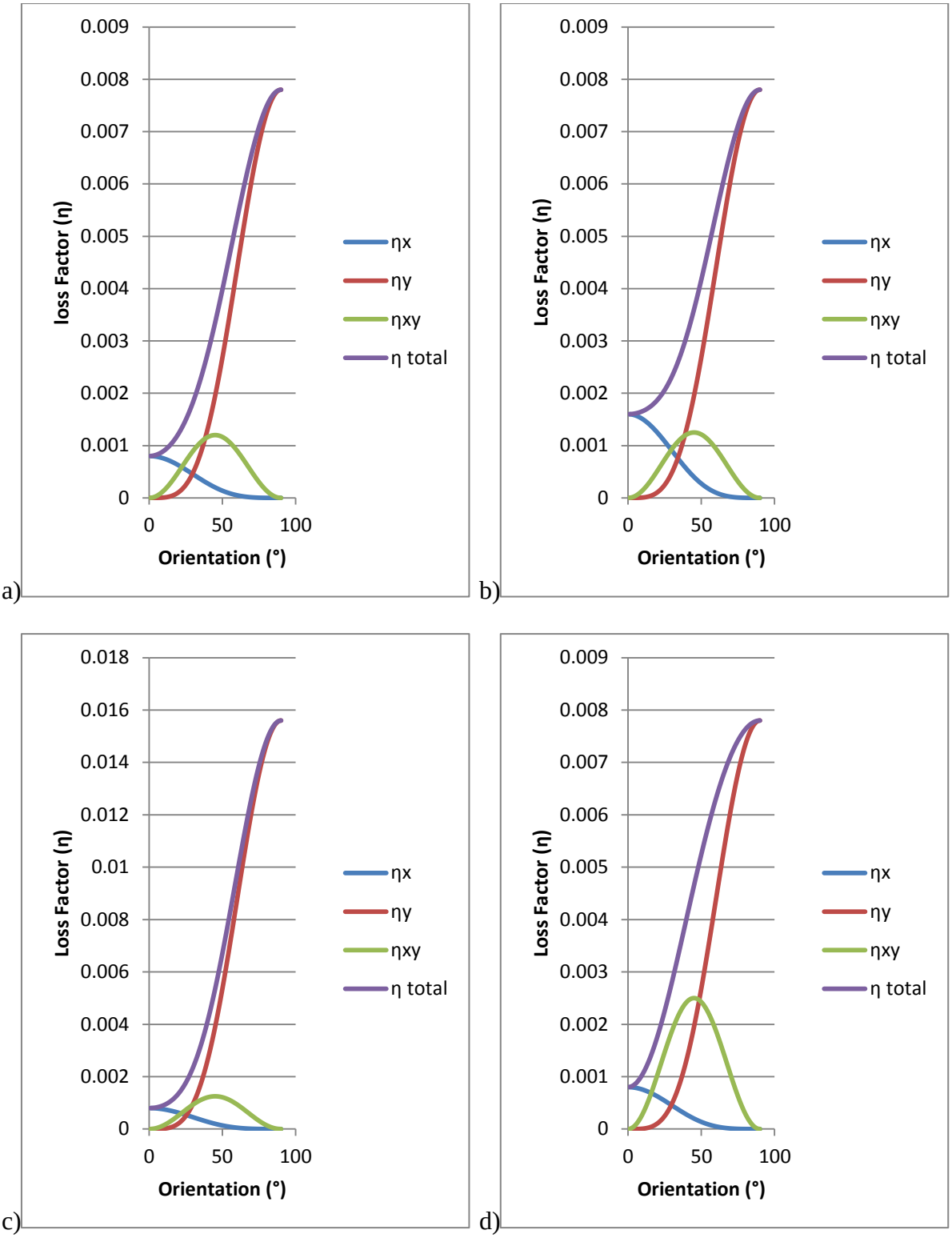

Figure 5.10: The influence of doubling η_x (b), η_y (c) and η_{xy} (d) on the total η based on the composite system used in this study (a), and how it changes with fibre orientation (based on work done by Ni and Adams, 1984 [104]).

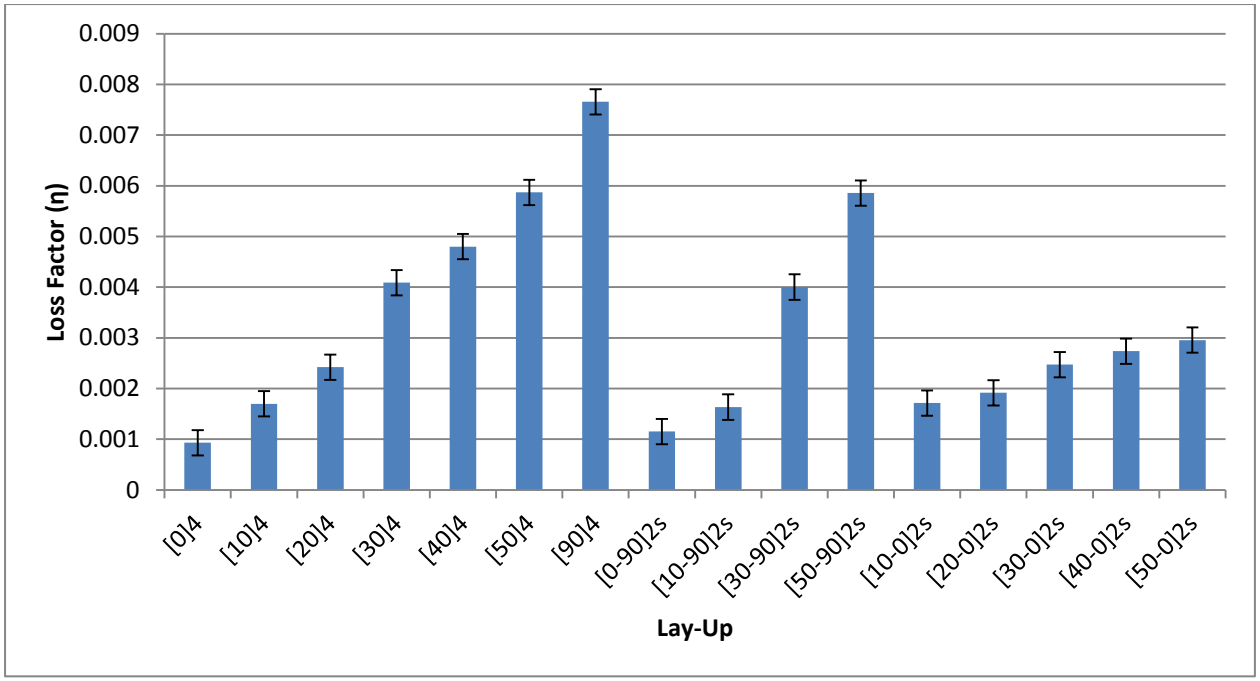

Figure 5.11: Loss factors with changing stacking sequence.

Figure 5.11 shows how η changes with stacking sequence. A clear dependence of loss factor on θ can be observed, however what is also apparent is, as with modulus, that loss factor is sensitive to the position of the ply within the laminate. The stress state of the laminate during bending results in greater strains at the outer surfaces, and as such these plies are likely to contribute more to the overall elastic behaviour of the laminate. For example, although the $[50\ 90]_{2s}$ panel has 50 % 90° plies, the loss factor value is still similar to that of the $[50]_4$ laminate (modulus values also vary by less than 0.5 %). Interestingly, if the more flexible plies are on the surface of the laminate (for example the $[50\ 0]_{2s}$ laminate) then a reduction in loss factor can be seen compared to that of a laminate composed fully of the outer ply orientation ($[50]_4$ in this case). It would seem that the improved load bearing capabilities of the internal plies (although closer to the neutral axis) are superior than those of a 4 ply laminate of the off-axis construction and thus now become an active part of the laminate structure. It is therefore important not to assume that by introducing a high damping layer

than the overall damping will increase in the laminate, and careful analysis of the surrounding plies needs to be understood first. Figure 5.12 shows the relationship between the loss factor and modulus of the panels tested in this study, although a general trend of an increase in modulus shows a lower loss factor, some stacking sequences allows minor alterations to this trend.

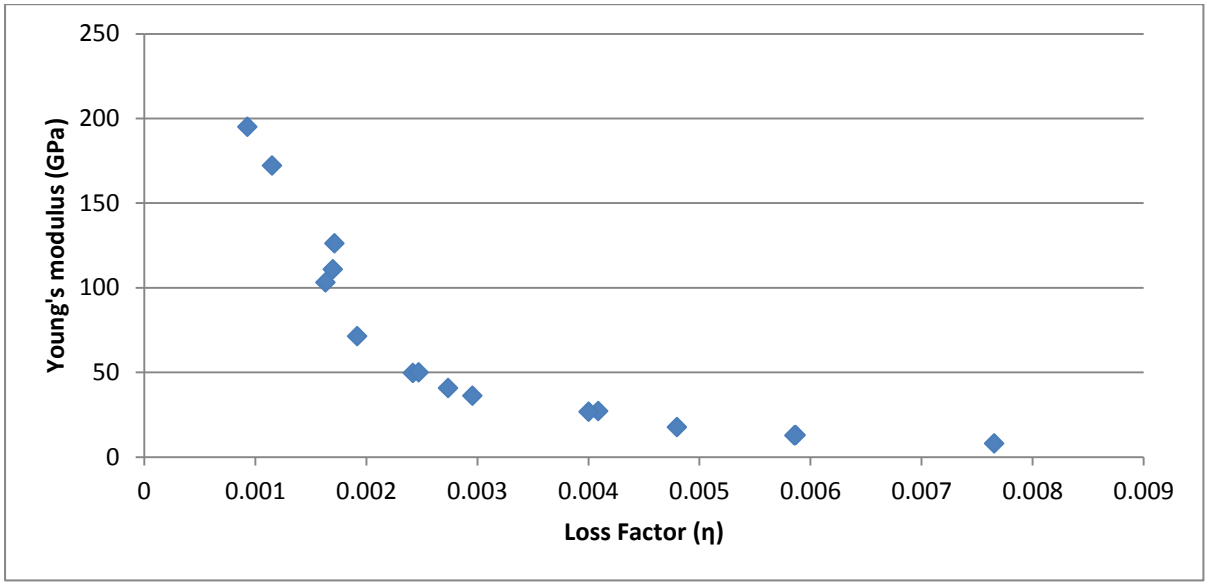

Figure 5.12: The experimentally determined relationship between Young's modulus and the loss factor of the panels used in this study.

5.2.2. *Aspect Ratio*

Along with orientation and stacking sequence, aspect ratio can be seen to have a significant role in the total η of a laminate. Figure 5.13 shows how the loss factor of panels with "regular" aspect ratio (2.16) compares with panels deemed "wide" (aspect ratio of 1.6). The wide 45° panels are shown to have a loss factor similar to that of the regular 30° panel (about 0.004), compared to the expected value of about 0.0054 if the panel had a regular aspect ratio. The reason behind this has been covered in Section 5.1. It is evident as well that the 90° panels show no noticeable difference in loss factor, regardless of aspect ratio, consistent with

the proposed effect of the clamping conditions of the fibres on laminate elastic behaviour. In a 90° ply 100 % of the fibres are unclamped; as such, the fibre clamping conditions will not change with aspect ratio, and therefore neither should η.

The effect of changing the fibre/matrix interfacial area within a panel has not been covered in this study, and the effect of changing this is strongly dependent on G_{xy} and η_{xy}. The model proposed later in Chapter 6 is therefore applicable only for panels of similar aspect ratios to that from which the initial material constants were derived.

From this it can be seen that, in the context of golf club shafts, aspect ratio will play a greater role in changing η than strain rate. The aspect ratio of a golf club shaft can be calculated from the dimensions of the unravelled layers of pre-preg used to fabricate the shaft (approximately 2.2 for an 8 ply shaft of 1m length and 15 and 8 mm outer diameters for the butt and tip respectively). These effects can be seen in work carried out by Berthelot (2005) [101], where an increase in the aspect ratio from 5 to 100 in a ± 30° composite, increases η by 0.0045 (≈20 %) for a Kevlar reinforced composite and 0.003 (≈30 %) for a glass fibre reinforced polymer (GFRP) whereas by increasing frequency from 50 to 600 Hz for the same orientation increased η by 0.005 (≈22 %) and 0.003 (≈30 %) for the Kevlar reinforced composite and GFRP respectively. Although both aspect ratio and strain rate can be seen to have an effect by Berthelot, it has been established that strain rate needs a minimal level to become effective (which has not been covered by this test method), in contrast to aspect ratio which shows a gradual change in properties for off-axis fibre orientations.

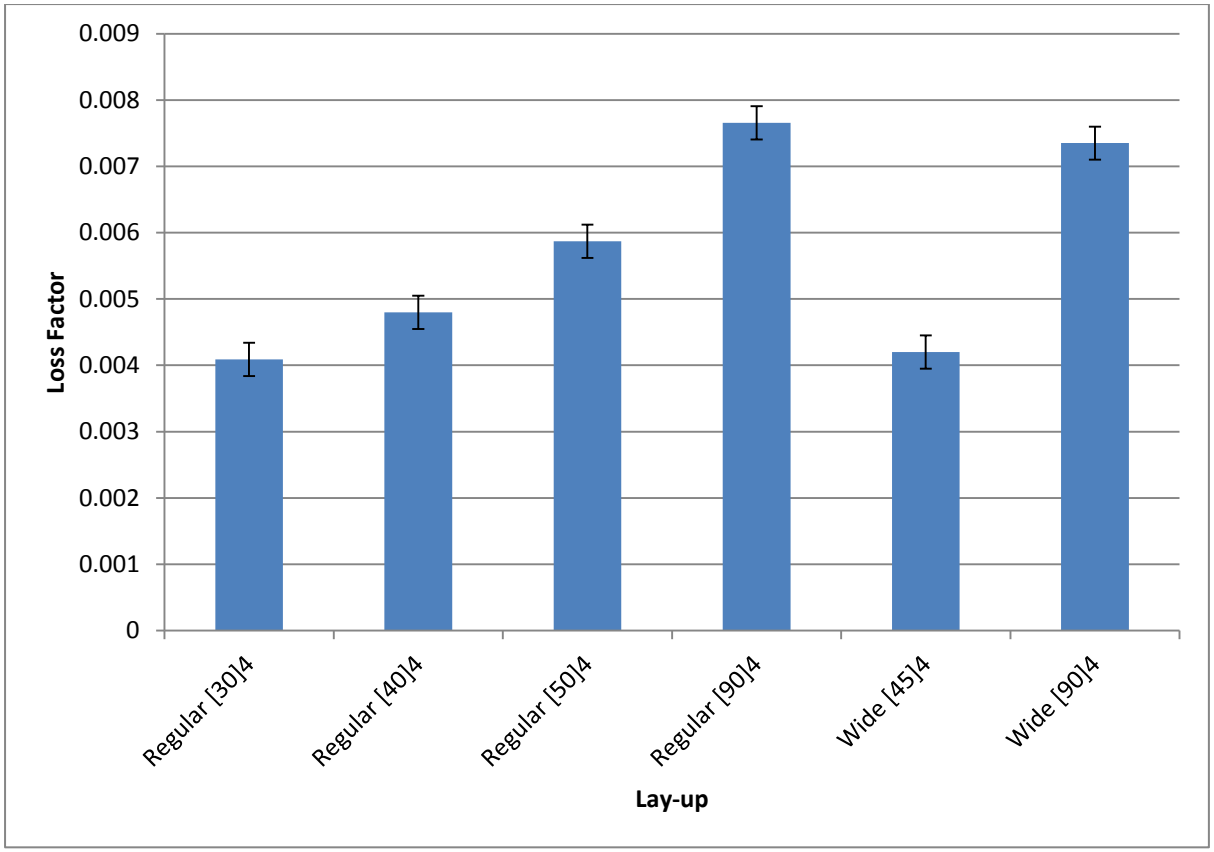

Figure 5.13: Experimental data of loss factor for regular (aspect ratio 2.16) and wide (aspect ratio 1.6) panels.

5.3. Summary

The dependence on strain rate of both modulus and damping have been characterised in this chapter for strain rates applicable to golf club shafts. The dependence has been analysed in terms of fibre orientation, stacking sequence and panel aspect ratio.

- The onset of strain-rate dependence appears to be similar for all orientations and stacking sequences analysed (around 0.4 s^{-1}), and is dictated by the matrix material. This is four times greater than the largest strain rate observed during a swing.
- The dependence on strain rate of the laminate (change in modulus/strain rate gradient) is strongly influenced by orientation and aspect ratio, with panels which show more

fibre dependent properties showing a reduced dependence on strain rate. For panels with large values of θ, the panel's modulus is lower and is more matrix dependent, and as such will show greater strain rate dependence.

- Panels fabricated with a seam (a resin-rich region comprising 20 % of the volume) showed an increase in strain-rate dependency for all off-axis panels. Onset remained constant. These seams are much greater than those typically seen in a golf shaft (< 5 %).
- Aspect ratio can alter the strain-rate dependency of a laminate, and as such laminates should be characterised in terms of fibre clamping conditions.
- No observable difference could be seen in the loss factor (η) of laminates at strain rates below 0.5 s^{-1}.
- The contribution of the individual plies on the overall damping is dependent on the position within the laminate as well as the orientation of other plies in the laminate.
- The total η has been broken down into it constituent parts (η_x, η_y and η_{xy}), and the source of these loss factors has been covered.
- Panels with varying aspect ratio will also show differing loss factors for a given fibre orientation, with a 45° panel with an aspect ratio of 1.6 showing the same loss factor as a 30° laminate with an aspect ratio of 2.16.

Overall, the static testing of a golf club shaft is sufficient at characterising the dynamic stiffness and damping characteristics. However, fibre orientation, stacking sequence and aspect ratio need to be considered when modelling the behaviour of flat panels.

6. Modelling of Damping and Modulus in Laminated Structure

This chapter covers the development of a model based on classical laminate theory, to predict, and optimise the modulus and damping of panels fabricated from various carbon composite systems with a range of orientations and stacking sequences. The full mathematical model can be found in Appendix A.

6.1. Obtaining flexural modulus and damping for a given stacking sequence.

All analysis of the mathematical models was carried out using Matlab R2007b (The MathWorks, Inc.). This model is based on Ni and Adams analysis [104] which uses classical laminate theory (CLT), in which, for thin laminates and small deflections, the modulus is a function of the angle at which the fibres are oriented away from the loading axis. Models based on this approach require several mechanical properties as inputs (E_1, E_2, G_{12}, v_{12}, η_1, η_2, and η_{12} of a 0° ply). Chapter 1 showed the how stress and strain within a composite gives a 6 x 6 stiffness matrix which can be reduced to a symmetric 3 x 3 matrix if no through stresses are assumed (this assumption becomes less valid for thicker laminates, section 6.3).

The elements of the reduced stiffness matrix, **C**, are given in Equation 6.1 to Equation 6.4.

$$C_{11} = \frac{E_1^2}{E_1 - v_{12}^2 E_2}.$$

Equation 6.1

$$C_{12} = \frac{v_{12} E_2 E_1}{E_1 - v_{12}^2 E_2} .$$

Equation 6.2

$$C_{12} = \frac{v_{12} E_2 E_1}{E_1 - v_{12}^2 E_2} .$$

Equation 6.3

$$C_{33} = G_{12} .$$

Equation 6.4

This matrix **C** is then used to derive the transformed stiffness matrix, ***c***, which is calculated for each ply. This allows the fibre orientation to be independent of the laminate orientation (x and y axis), and the fibres are now orientated in the 1-2 axis. The elements of the transformed stiffness matrix can be seen in Equation 6.5 to Equation 6.10.

$$c_{11} = C_{11} m^4 + 2\left(C_{12} + 2C_{33}\right) n^2 m^2 + C_{22} n^4 .$$

Equation 6.5

$$c_{22} = C_{11} n^4 + 2\left(C_{12} + 2C_{33}\right) n^2 m^2 + C_{22} m^4 .$$

Equation 6.6

$$c_{12} = \left(C_{11} + C_{22} - 4C_{33}\right) n^2 m^2 + C_{12} m^4 n^4 .$$

Equation 6.7

$$c_{33} = \left(C_{11} + C_{22} - 2C_{12} - 2C_{33}\right) n^2 m^2 + C_{33} n^4 m^4 .$$

Equation 6.8

$$c_{13} = \left(C_{11} - C_{12} - 2C_{33}\right) n m^3 + \left(C_{12} - C_{22} + 2C_{33}\right) n^3 m$$

Equation 6.9

$$c_{23} = \left(C_{11} - C_{12} - 2C_{33}\right) n^3 m + \left(C_{12} - C_{22} + 2C_{33}\right) n m^3$$

Equation 6.10

where $m = \cos(\Theta)$, $n = \sin(\Theta)$, and Θ is the angle between the fibre axis (1-2) and the panel axis (x-y).

From the transformed stiffness matrix the ***ABD*** matrices can be formed. This allows the tensile stiffness matrix (***A***), the bending stiffness matrix (***D***) and the coupling between these two (***B***) to be analysed for any given orientation. As the panels and laminates in this study are balanced and symmetric, there should be no tensile-bending coupling therefore ***B*** does not need to be considered. The matrices ***A*** and ***D*** can be seen in Equation 6.11 and Equation 6.12 respectively. It can be seen that ***A*** is simply the product of ***c*** and the lamina thickness (*t*). It is also evident in ***A*** that all plies would have an equivalent effect providing that each ply has the same thickness (Chapter 3.1 showed this is a reasonable assumption as ply thicknesses were seen to vary by approximately 5 %).

The matrix ***D*** does show a dependence on ply position, *w*, which is the ply weighting function, $w = z_1^3 - z_2^3$. The weighting function is based on the ply's thickness and distance away from the neutral axis during bending. Due to the weighting factor being a cubic relationship with

bending stiffness, the panel's flexural properties are likely to be heavily dictated by the outer plies.

$$\boldsymbol{A} = \begin{bmatrix} c_{11}\,t & c_{12}\,t & c_{13}\,t \\ c_{12}\,t & c_{22}\,t & c_{23}\,t \\ c_{13}\,t & c_{23}\,t & c_{33}\,t \end{bmatrix}$$

Equation 6.11

$$\boldsymbol{D} = \begin{bmatrix} c_{11}\,w & c_{12}\,w & c_{13}\,w \\ c_{12}\,w & c_{22}\,w & c_{23}\,w \\ c_{13}\,w & c_{23}\,w & c_{33}\,w \end{bmatrix}$$

Equation 6.12

where *w* is the ply weighting function. $w = z_1^3 - z_2^3$, z_1 and z_2 refer to the distance of the outer and inner surface of the ply to the neutral axis.

Using these matrices the longitudinal tensile and flexural moduli can be deduced (Equation 6.13 and Equation 6.14 respectively)

$$E_{x\ Tensile} = \frac{1}{H\,a_{11}}$$

Equation 6.13

$$E_{x\ Flexural} = \frac{12}{H^3\,d_{11}}$$

Equation 6.14

where *H* is the panel thickness. The matrices ***a*** and ***d*** are the inverse of the ***A*** and ***D*** matrices, respectively.

The flexural damping properties can also be derived from the ***ABD*** matrix (Equation 6.15 to Equation 6.18). It can be seen from these equations that the damping is the sum of the damping in each of the plies [67, 94, 104, 105]. The factor p/2 is used as the laminates are restricted to being balanced and symmetric, if an odd number of plies of like thickness are used then the ply about the neutral axis should be treated as two plies of half its thickness.

$$\eta_x = \frac{2}{3\,d_{11}} \sum_{k=1}^{\frac{p}{2}} \left(c_{11}^k d_{11} + c_{12}^k d_{12} + c_{13}^k d_{16}\right)\left(m_k^2 d_{11} + m_k n_k d_{13}\right) w_k \eta_1 m_k^2.$$

$$\eta_x = \frac{2}{3\,d_{11}} \sum_{k=1}^{\frac{p}{2}} \left(c_{11}^k d_{11} + c_{12}^k d_{12} + c_{13}^k d_{16}\right)\left(m_k^2 d_{11} + m_k n_k d_{13}\right) w_k \eta_1 m_k^2.$$

Equation 6.15

$$\eta_y = \frac{2}{3\,d_{11}} \sum_{k=1}^{\frac{p}{2}} \left(c_{11}^k d_{11} + c_{12}^k d_{12} + c_{13}^k d_{13}\right)\left(n_k^2 d_{11} - m_k n_k d_{13}\right) w_k \eta_2 n_k^2.$$

$$\eta_y = \frac{2}{3\,d_{11}} \sum_{k=1}^{\frac{p}{2}} \left(c_{11}^k d_{11} + c_{12}^k d_{12} + c_{13}^k d_{13}\right)\left(n_k^2 d_{11} - m_k n_k d_{13}\right) w_k \eta_2 n_k^2.$$

Equation 6.16

$$\eta_{xy} = \frac{2}{3\,d_{11}} \sum_{k=1}^{\frac{p}{2}} \left(c_{11}^k d_{11} + q_{12}^k d_{12} + c_{13}^k d_{13}\right)\left(2 m_k n_k d_{11}\right) - \left(m_k^2 n_k^2 d_{13}\right) w_k \eta_{12} m_k n_k.$$

$$\eta_{xy} = \frac{2}{3\,d_{11}} \sum_{k=1}^{\frac{p}{2}} \left(c_{11}^k d_{11} + q_{12}^k d_{12} + c_{13}^k d_{13}\right)\left(2 m_k n_k d_{11}\right) - \left(m_k^2 n_k^2 d_{13}\right) w_k \eta_{12} m_k n_k.$$

Equation 6.17

$Total\,\eta = \eta_x + \eta_y + \eta_{xy}.Total\,\eta = \eta_x + \eta_y + \eta_{xy}.$

Equation 6.18

where *p* is the number of plies, and *kth* term refers to each separate ply.

The model is summarised in Figure 6.1 and in full Matlab script in Appendix A.

Input Fibre Orientation.

- The model will ask for the lay-up of the panel in the form [θ_1 θ_2 θ_3 ..... θ_n]. There is no limit to the number of plies which is automatically calculated.

Material Properties.

- 7 material constants need to be input to define a material for this model (assuming anisotropy). E_1, E_2, G_{12}, ν_{12}, η_1, η_2, and η_{12} . A database can be made and a material selected by using the mat function.

Ply Thickness.

- This refers to the relative ply thickness, although physical thicknesses can be input it is not necessary. For example if the inner two plies of a for ply lay-up are twice as thick as the outer two then the command would be [1 2 2 1].

Ply Weighting Factor.

- Calculated as the distance away from the neutral axis for bending. This will only alter the D matrix, thus if a tensile calculation is need this is skipped.

Reduced Stiffness Matrix.

- For an anisotropic material a stiffness matrix can be reduced to C_{11}, C_{12}, C_{22} and C_{66}, assuming no stress in the σ_3 direction and no shearing in the τ_{23} and τ_{13} directions. (Hull and Clyne 1996)

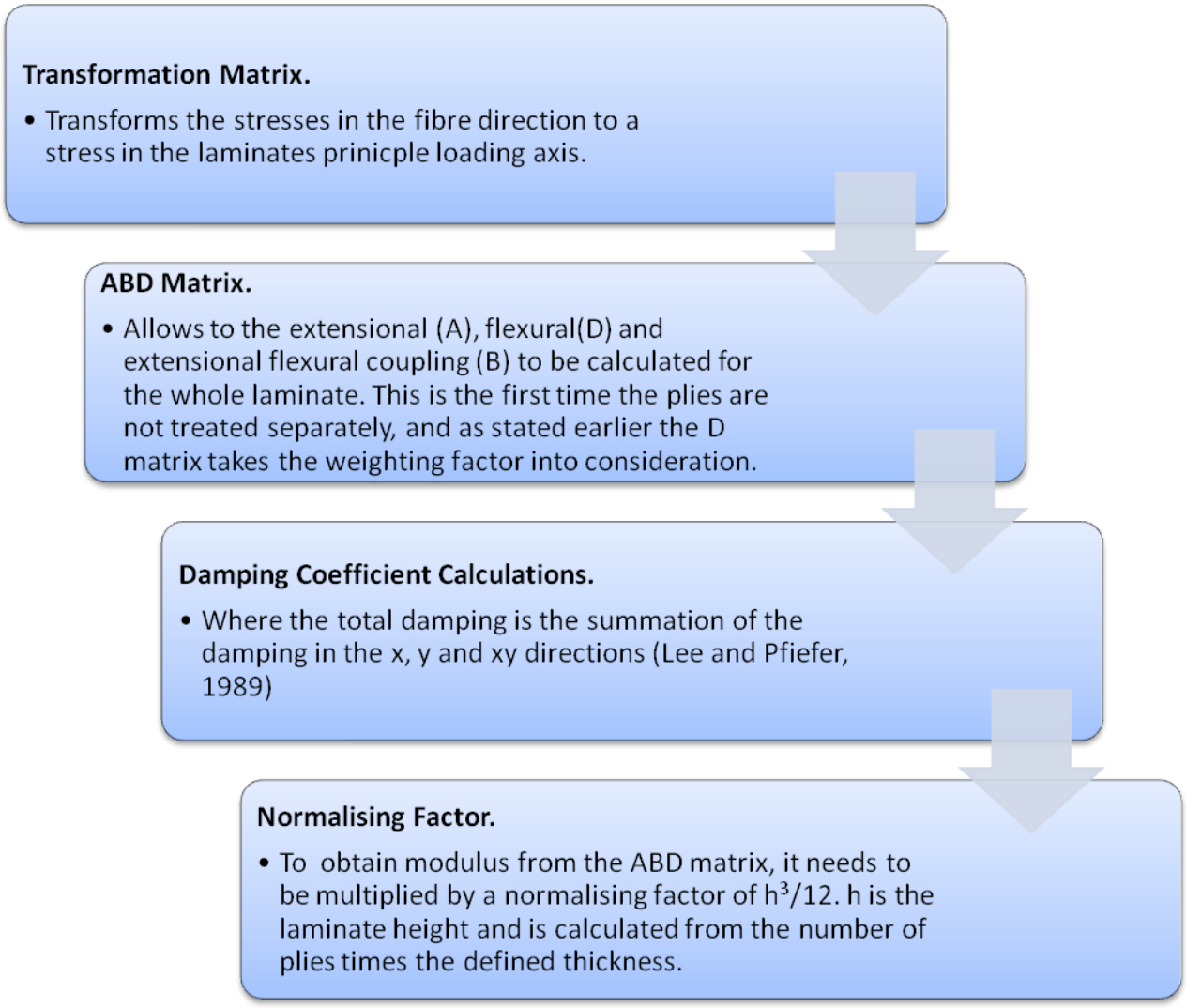

Figure 6.1: Flow diagram summarising the model steps used for predicting modulus and damping for a given composite ply stacking sequence.

The scheme illustrated in Figure 6.1 was then put into a user interface to demonstrate the dependence of both damping and modulus on orientation, and therefore help optimise the panel (optimisation in this case is in terms of maximising both stiffness and damping). A screen shot of the user interface can be seen in Figure 6.2; on the left the seven material constants are entered creating a graph to show how a unidirectional composite's loss factor and modulus

changes with orientation. On the right, the flexural modulus and damping for a specific lay-up can be calculated using the material constants input (

Table 6.1).

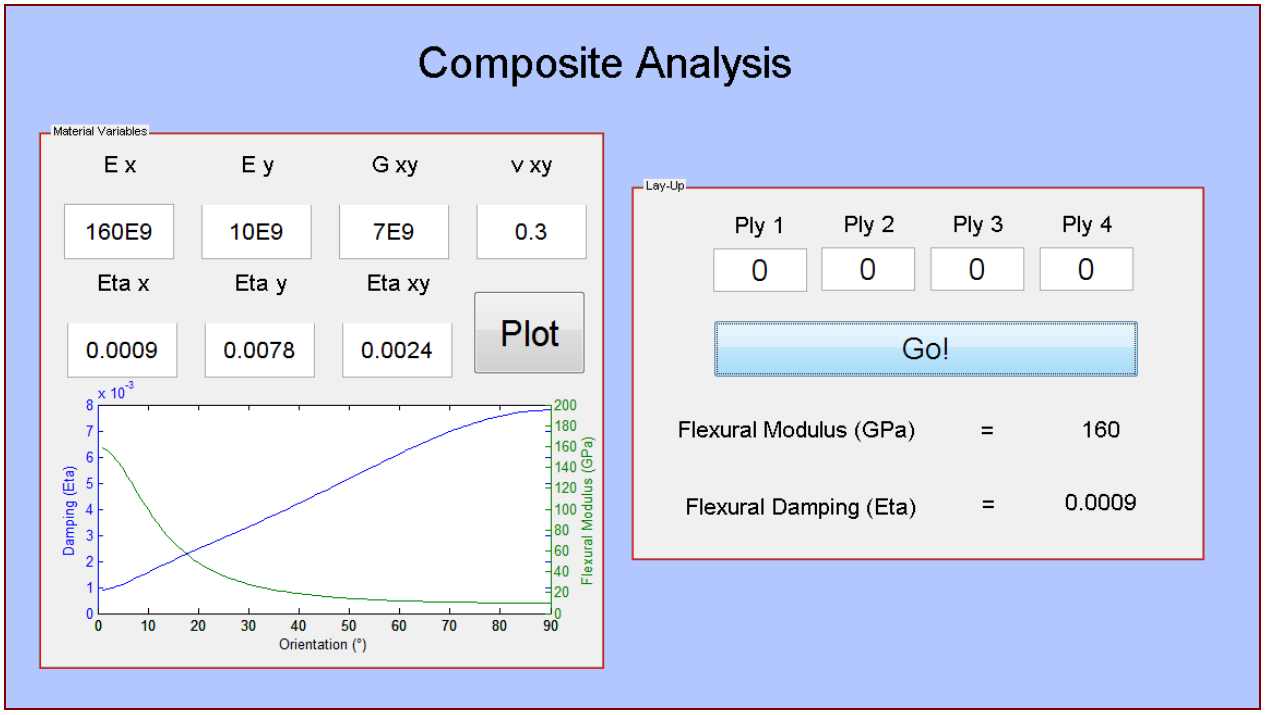

Figure 6.2: Screen shot of the user interface created for the flow diagram shown in Figure 6.1.

Table 6.1: Table of material properties of the composite systems used in testing and verification of the model (taken from a 0°, 90° laminates and a 0° lap laminate).

Composite	**VSM264/T800**	**MTM28-1/T800H**	**MTM28-1/T800H (Part cure)**
E_x (GPa)	**95 (±2)**	**160 (±2)**	**140 (±2)**
E_y (GPa)	**8 (±0.5)**	**10 (±0.5)**	**6 (±0.5)**
Gxy (GPa)	**5 (±0.5)**	**8 (±0.5)**	**4 (±0.5)**
v_{xy}	**0.25 (±0.03)**	**0.28 (±0.03)**	**0.25 (±0.03)**
η_x	**0.008 (±0.0005)**	**0.0007 (±0.0005)**	**0.0075 (±0.001)**
η_y	**0.012 (±0.001)**	**0.0083 (±0.001)**	**0.014 (±0.001)**
η_{xy}	**0.00105 (±0.001)**	**0.003 (±0.001)**	**0.012 (±0.001)**

Using the program shown in Figure 6.1, 16 different panels (same orientation and geometry to those used in Section 4.2) were tested to compare experimental with theoretical results. The experimental procedure for calculating loss factor was repeated from Section 4.2, modulus (E) was also calculated from this testing procedure using Equation 6.19, by measuring the fundamental bending frequency (f) of the panel during testing.

$$f = \frac{C_1}{2\pi}\sqrt{\frac{EI}{\rho A L^4}},$$

Equation 6.19

where C_1 is the clamping constant (3.52 in the clamped-free condition), is the density of the material, A is the cross-sectional area, I is the second moment of area about the panel's neutral axis, and L is the cantilever length.

The material constants (

Table 6.1) were obtained from tensile testing of a 0° and 90° laminate (120 by 30 mm and 4 plies thick) and shear testing of a 0° lap joint. A schematic diagram of the lap joint can be seen in Figure 6.3. A Kyowa biaxial strain gauge (type KFG) was used on the 0° panel to obtain the Poisson's ratio (ν_{xy}). The results for this series of tests were needed for each composite system that was modelled using this program (each test was carried out on 5 samples).

Figure 6.3: Schematic diagram of lap joint used to determine the shear properties of the composite systems used (with the loading axis in the x direction, and the laminate width and thickness in the y (into the page) and z directions respectively).

The model was designed in order to predict varying orientation as well as stacking sequence. Figure 6.4 shows that there is no noticeable difference (root mean square difference (RMSD) 0.00023) between experiment and theory for the MTM28-1/T800H composite system.

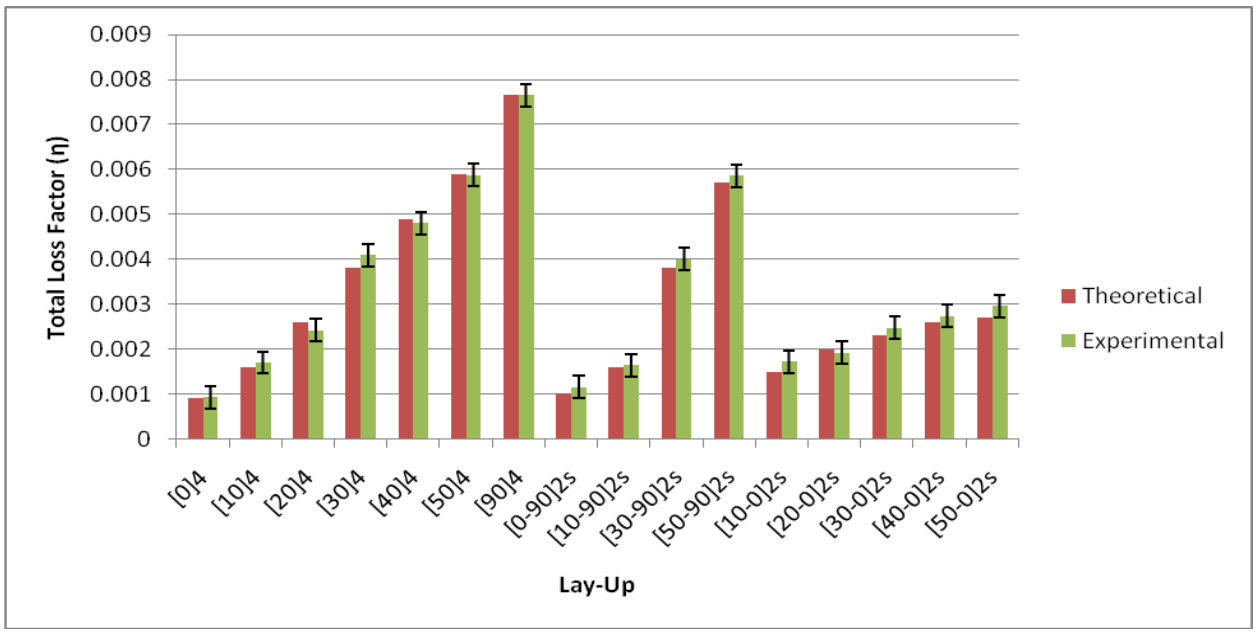

Figure 6.4: Theoretical and experimental loss factor for different stacking sequences fabricated from MTM28-1/T800H.

The model was validated against two other composite systems (VSM264/T800 and a part-cured MTM28-1/T800H). Figure 6.5 shows the same model used for the part-cured MTM28-1/T800H; no noticeable difference (RMSD 0.00019) can be seen between experimental and theoretical results. Comparison of Figure 6.5 with Figure 6.4 indicates that there is a significant increase in the damping overall for the part-cured panels, with a much reduced sensitivity to orientation. The increase from 0 to 90° in the part cured panels being just less than double compared to the 8.5 times increase for the same orientations in the fully cured panels. This is likely to be due to a weaker interface between the fibres and matrix as well as the reduced amount of cross-linking in the matrix for the part-cured panels (

Table 6.1 shows that the part-cured samples showed a noticeably lower shear modulus and a much greater shear damping, suggesting a weaker interface). A characteristic of a part-cured laminate is reduced ply adhesion, although little/no gap can be seen between plies from optical

analysis, the reduced cure cycle would have reduced inter-ply chain movement [106] as the viscosity levels are not reduced to as low a value as that for a full curing cycle, and, as such, the plies would be acting more independently leading to larger inter-ply losses. This would explain the consistently high values of damping, and the small change in damping with orientation, as total damping appears to be dictated by the inter-ply damping in this case. The model does however still hold for this scenario; this is due to the initial parameters being dictated from the 0° laminate of this material, and, as such, inter-ply damping is indirectly taken into consideration in the model. These trials were carried out to validate the model by changing the matrix properties whilst keeping fibre type the same.

Figure 6.6 and Figure 6.7 show the model used for VTM264/T800, a lower modulus variable temperature matrix carbon fibre composite. Again there is very good agreement between predicted and experimental modulus and damping. The damping of this composite is a lot greater than the MTM28-1/T800H composite measured before. The VTM264/T800 also shows a different trend in the damping, with no further increase in damping observed for orientations greater than 45°. By comparing the initial material property inputs, the difference in the damping dependence on orientation can be observed. VTM264/T800 has a much lower E_x than MTM28-1/T800H, this increases the dependency the panels properties on the matrix, as the difference between fibre and matrix modulus decreases. This increased dependency on matrix properties raises the loss factor at low fibre orientations. The values of η_{xy} and G_{xy} are both directly affected by the fibre/matrix interfacial properties. If fibre slippage occurs, then as a result the shear modulus, which relies on a good interface, will reduce. This increase in slippage results in higher levels of internal friction and therefore an increase in η_{xy} is seen, and it is this high level of η_{xy} which results in the 45° panel showing a similar loss factor to that of a 90° panel.

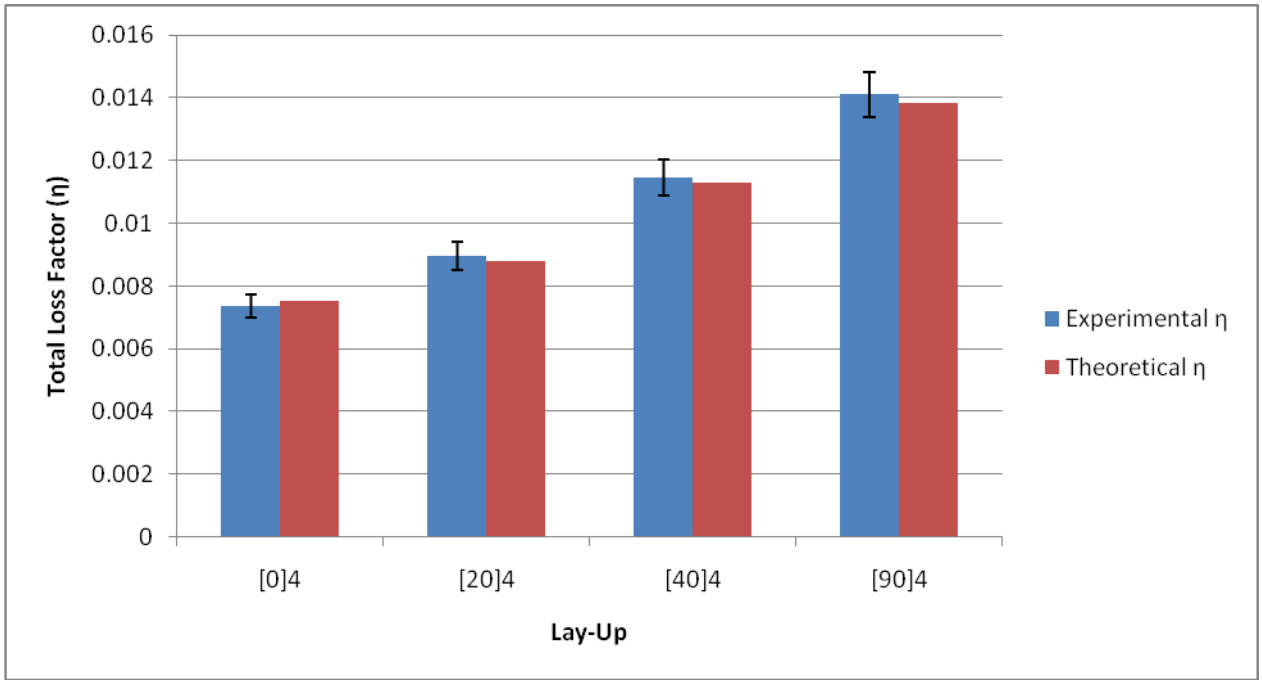

Figure 6.5:Theoretical and experimental loss factor values for orientations using part cured MTM28-1/T800H.

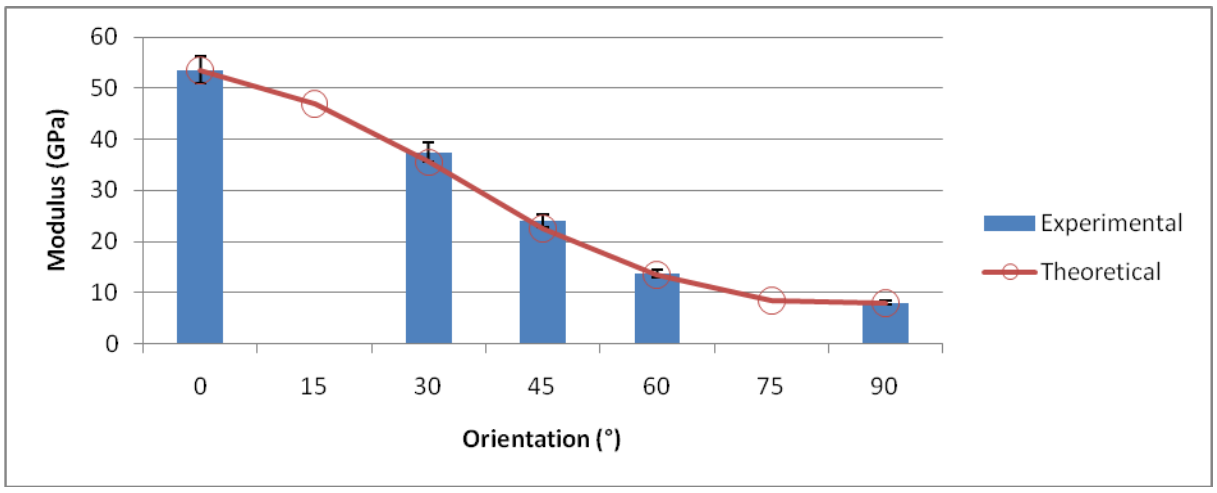

Figure 6.6: Experimental and theoretical predications of modulus for VTM264/T800.

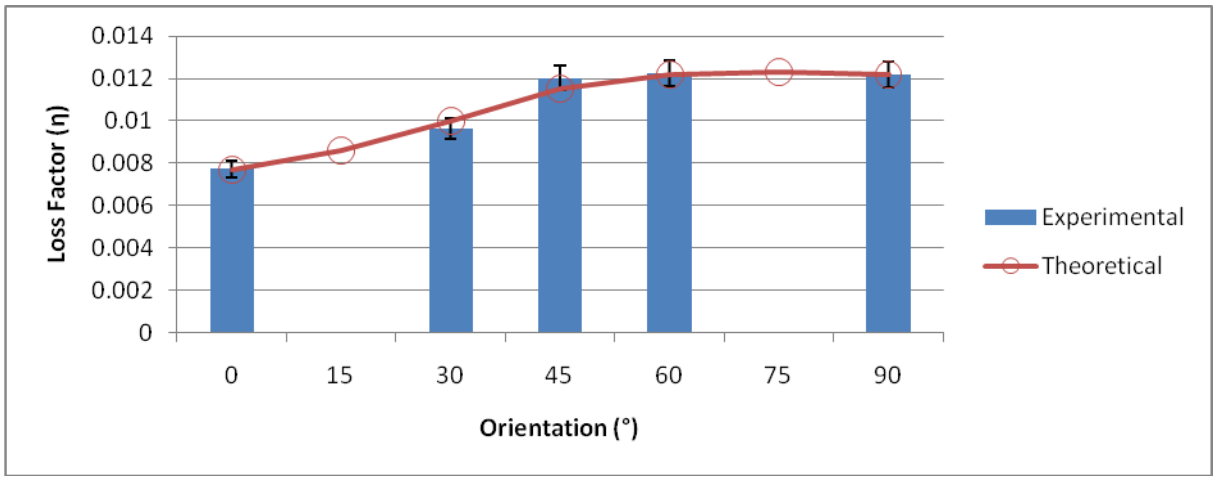

Figure 6.7: Experimental and theoretical predications of modulus for VTM264/T800.

The fabrication and testing of the panels was carried out in two stages; firstly 7 material properties were determined which gave material inputs for the unidirectional laminates. After this, blind testing was carried out for the remaining panels of the same composite system. Panels of varying orientation and stacking sequence were fabricated without any predictions being made. Once testing had been carried out, the model predictions were calculated and the values compared, Table 6.2. No noticeable difference (RMSD 0.00018) was observed between the results and the blind predictions. This is a good measure of the robustness of the model, as opposed to having a prediction already whilst testing.

Table 6.2: Experimental and theoretical values for modulus and damping of the blind testing of panels fabricated from MTM28-1/T800H.

Lay-Up	Predicted Modulus (GPa)	Experimental Modulus (GPa)	Predicted Damping	Experimental Damping
$[\pm 25°]_8$	82.3	84	0.000156	0.00162
$[\pm 55°]_8$	15.8	15	0.004669	0.0048
$[\pm 25° \pm 55°]_{4s}$	47.1	48	0.00211	0.0025

Lee *et al.* (1989) [58] also used an analysis based on CLT to predict loss factor in composites with varying moisture content. The model agreed very well provided that the material constant inputs agreed with the state that the model was to be used in. For example, a theoretical value of the total η agreed well (within 5% error) if E_x, Ey, G_{xy}, v_{xy}, η_x, η_y, and η_{xy}were all measured at the specific moisture content at that of the model prediction. A 50 % change could be seen in the total damping when moisture content increased from 0 to 0.8% (moisture content can be as high as 2.5 % depending on humidity [107, 108]), and therefore the model would not predict the change in damping if this had not been taken into consideration. Ni and Adams (1984) [104] used their model to predict the effect of changing outer ply orientation on modulus and damping. This agreed well with experimental results for both carbon fibre and glass fibre composites (less than 10 % discrepancy in both cases); the greatest difference was seen at intermediate orientations (30 – 40°) where experimental data show large loss factor values compared to the 90° orientation. The authors however did state that although plate theory was used in the model, the use of the narrow plates tested may contribute to some of the

discrepancies observed. Large disagreement (up to 50 %) could be seen when panels showed bending and twisting coupling due to the non-balanced nature of some of the laminates.

The test pieces used by Ni and Adams were simple panels, it is important to understand whether models based on this approach still hold when designing more complex composite components, in the case of this research, golf shafts. For three-dimensional applications such as golf club shafts, the fibres are not constrained to the x-y in their orientation and the plane of orientation will vary around the circumference of the shaft. Seams (Chapter 1.6) change the local stiffness and damping characteristics and therefore the model can show some level of discrepancy in areas significantly affected by seams.

6.2. Predicting stacking sequence for a given modulus range.

In many cases in design the stacking sequence of a laminate is the variable, and a specific modulus and damping are required. Current models and software [98, 104] rely on a predetermined stacking sequence to give the predicted mechanical properties. The following model (Figure 6.8) has been proposed to allow a user to get the specific stacking sequence required to obtain certain mechanical properties. The model also suggests possible other stacking sequences depending on whether E, η or the product of both needs to be optimised.

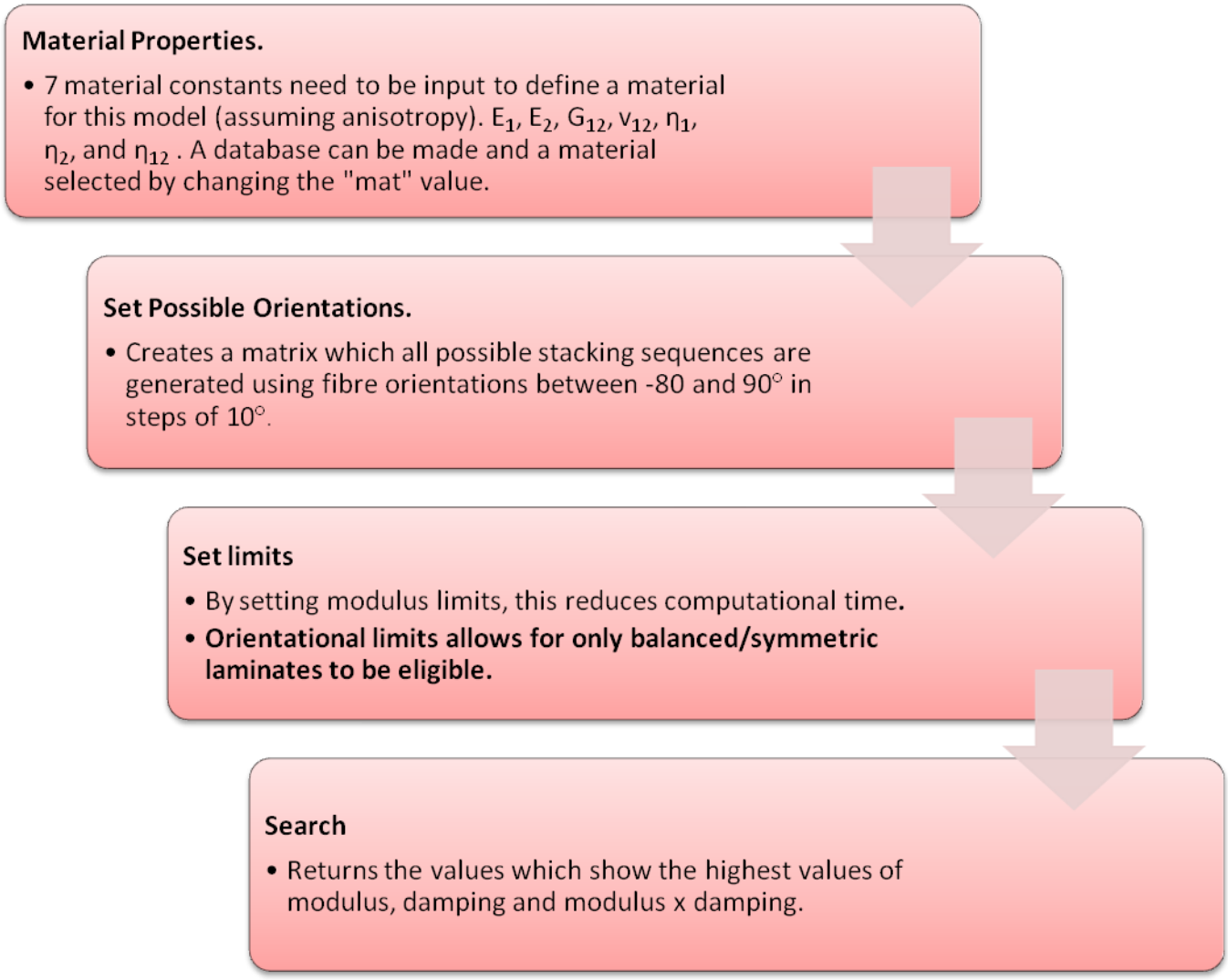

Figure 6.8: A schematic flow diagram of the method for calculating modulus and damping for possible combination of stacking sequence (orientation limited to nearest 10°).

A user interface was created for this model (Figure 6.9), in order that a user can input a modulus range to give a range of possible stacking sequences before optimising for E, η or the product $E\eta$. The top panel has an option to select material, this loads the material data that would have been previously saved from Figure 6.8, then the modulus range is input. This particular interface was designed specifically for an 8 ply composite, with the given lay-up being symmetrical about the last ply and an orientation resolution of 10° is used (although may

be changed if needed). No errors have been incorporated into the model. In other words, if two values are very close together, and experimentally one would not see a noticeable difference between them, the model still selects the stacking sequence with preferential properties. It is the user who should define their experimental error and therefore understand how large a change is needed to be noticeable. It should be noted however that if a range of 5 GPa is used, 1000s of possibilities of lay-ups will give the desired modulus (Figure 6.10), but only 3 of these will be shown in the interface (the greatest E, the greatest η and the greatest Eη).

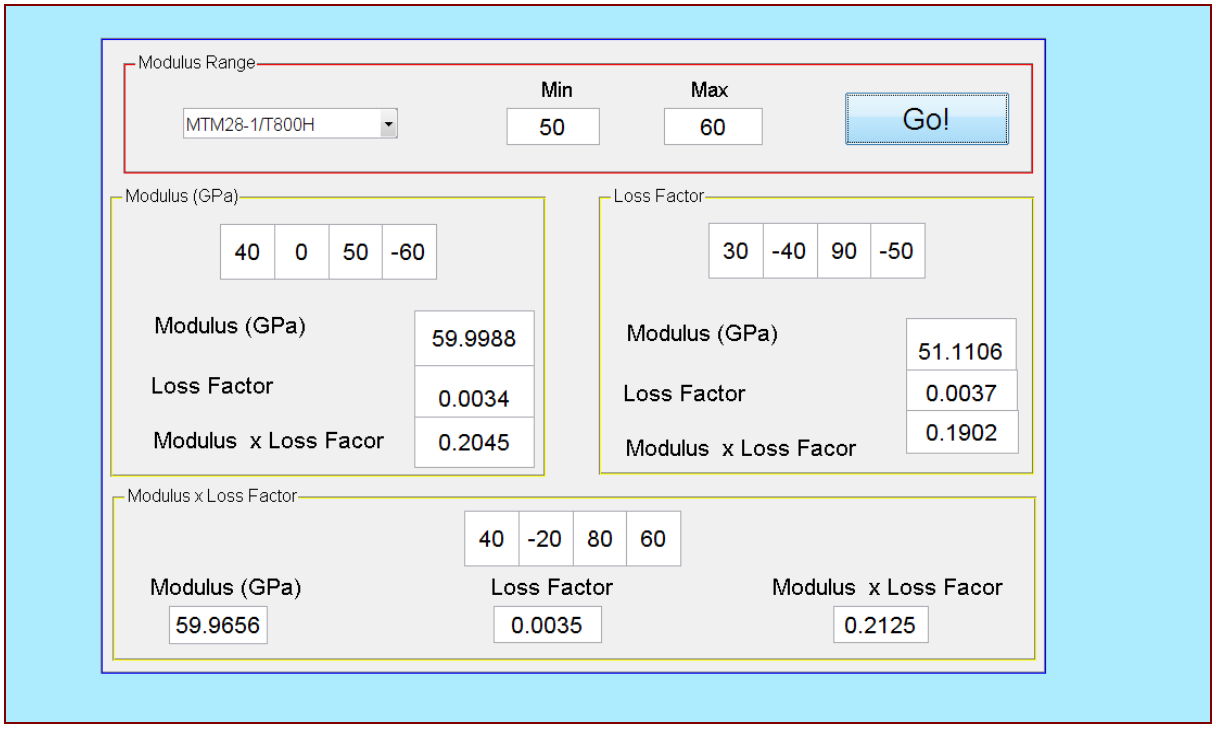

Figure 6.9: User interface for the optimal stacking sequence model.

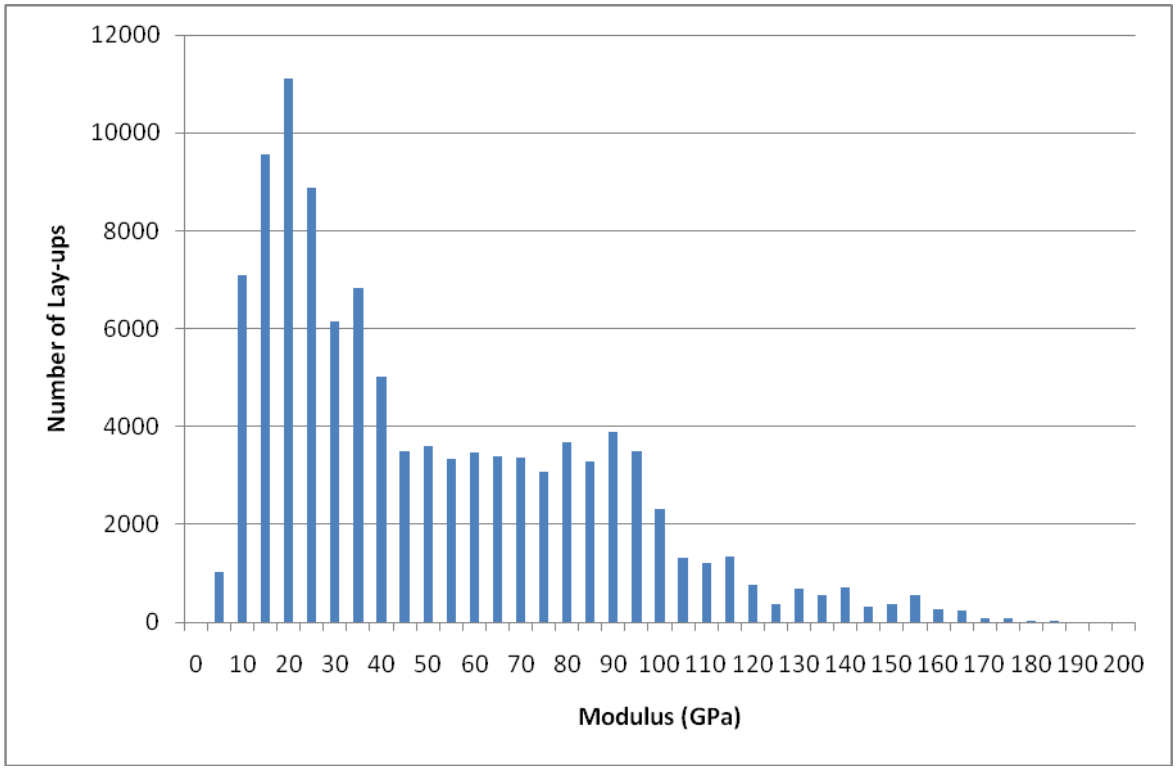

Figure 6.10: Histogram to show the number of possible lay-ups for a given modulus given a 5GPa variability.

Blind testing was also carried out for this section of the model. Panels of orientations seen in Figure 6.9 were fabricated (Table 6.3). Again no noticeable difference (RMSD 0.00021) between the predicted and experimental results was seen given the error of around 5-7 % (see Chapter 4.2).

Table 6.3: Predicted and experimental data from blind testing of panels from the optimisation model. Panels were fabricated from MTM28-1/T800H.

	[40 0 50 -60]2s	**[30 -40 90 -50]2s**	**[40 -20 80 60]2s**
Predicted Youngs Modulus (GPa)	**59.9**	**51.1**	**59.9**
Experimental Young's Modulus (GPa)	**61**	**49**	**58**
Predicted Loss Factor	**0.0034**	**0.0037**	**0.0035**
Experimental Loss Factor	**0.0032**	**0.004**	**0.0039**

6.3. Limitations of the models

6.3.1. *Stress and Strain Distribution*

Classical Laminate Theory (CLT) states that each lamina acts as a separate body [3, 57, 101], but it is also perfectly bonded to its neighbours. As well as being a contradiction in terms, this statement has a real effect on how the deformation of laminates is defined in any model. By defining that each of the plies acts separately states that, for a given applied force, each lamina will have a single value for stress through its thickness. Likewise, by stating that the laminae are perfectly bonded, this implies that strain must show no steps in strain variation through the thickness of the laminate and that at the neutral plane, strain equals zero (Figure 6.11 a and b).

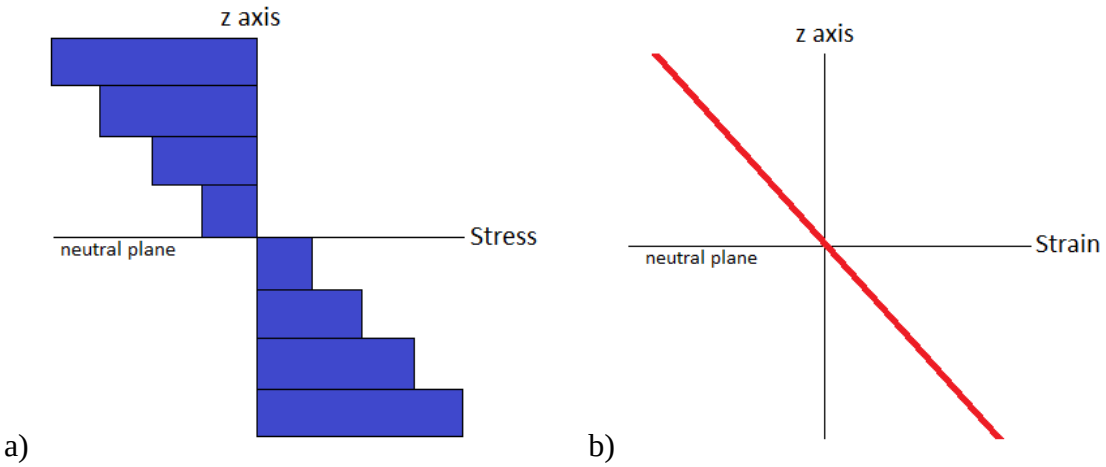

Figure 6.11: a) Stress and b) strain variation through the thickness of a ply according to CLT.

These assumptions are valid for thin laminate plates and where the stiffness difference between each ply is not too great, although both "thin" and "not too great" are qualitative terms and therefore need to be defined. An observation that backs up this theory is the failure mechanism of delamination. Delamination has been attributed to inter-laminar shearing, due to both the strain distribution and the differing laminae moduli of non-unidirectional panels [3, 109, 110]. This suggests that the resin-rich region (RRR) between plies undergoes shear strain and is likely to change the strain distribution to more smoothed stepped distribution as in Figure 6.11. Although this inter-ply shearing may alter the damping properties of a laminate, if these resin rich regions do not change in geometry from the laminates used for the material inputs, the affect should be minimised.

Singh and Gupta (1995)[111] compared CLT with other theoretical models, such as finite element models, and CLT consistently over-predicted the natural frequencies of the laminates with a length/thickness ratio of 10 (around 40 % higher), however with a length/thickness ratio of 100, a much better correlation was seen (with 5 %). Bosia *et al.* (2004) [112] investigated the strain distribution through-thickness of a laminate with varying length/height (*l*/*h*) and width/height (*w*/*h*) ratio in 0/90 balanced lay-ups using embedded fibre Bragg gratings sensors

in 8 x 1.25 mm ply laminates under three-point bend testing. The experimental data were compared to both finite element modelling (FEM) and CLT to predict the inter-ply strains. It was noted that FEM and experimental data agreed very well (±5 %), however CLT always under-predicted the strain (consistent with CLT predicting higher frequencies). However the uncertainty value assigned to the experimental data was only attributed to the uncertainty in the determination of the wavelength of the Bragg-peak shift; errors can also be attributed to the local strain around the Bragg grating (although Bosia *et al*. (2004) showed that this is not noticeable compared to the inter-laminar strains and was justified by using electronic speckle pattern interferometry). Errors could also arise from length over which the Bragg grating averages its readings (125 μm), which is approximately 1.5 % of the thickness of a ply. Bosia *et al.* also showed that strain remained linear through the panel for both *l/h* and *w/h* down to 10. Non-linearity was only observed in these cases directly under the loading points. Mulle *et al.* (2009) [113] used the same technique but with a more isotropic (0°, 45°,-45°,90°) lay-up consisting of 28 plies. Strain linearity was still seen through the laminate even at very high deflections (16 mm) in a three-point bend test (although strain was only monitored in 5 locations through the thickness). Some strain (2% of outer ply strain) was monitored at the neutral axis, but this is also likely to be due to the fact that the sensors have finite dimensions (approximately 125 μm diameter) and the neutral axis is actually infinitely thin. An acrylate coating of < 20 μm thickness is usually applied to the optical fibres to protect them from damage and atmospheric attack. In the studies cited, this coating had been stripped off to aid impregnation of the optical fibre into the composite lay-up.

It therefore appears that for *l/h* and *w/h* ratios greater than 10 then classical laminate theory still hold true, and likewise with the high stiffness differences between 0 and 90° plies, and any inter-laminar shearing that ±45° plies are likely to induce. Although these effects cannot be

completely disregarded, it would appear that for this research their effects will be consistent, but further investigation will be needed in order to define a point where these phenomena will start affecting the results of the model.

6.3.2. *Limit to Number of Plies*

At the moment the optimisation model is restricted to 8 ply, symmetric and balanced laminates to reduce the processing power needed; with 18 different orientations possible (-80° to 90° in increments of 10°) then the number of possible 4 ply laminates is 104976 (18^4), compared to a 16 ply which has over 11 million possibilities. The process will need to be adjusted to allow for any number of plies, thus giving specific stiffness not modulus which is more applicable in design. This model allows for no bending-extensional coupling, therefore panels that are not balanced and symmetric may fail to be predicted.

6.4. Summary

A model has been proposed to determine modulus and damping values of carbon fibre laminates of varying orientation and stacking sequence.

- Good agreement (<5 %) was seen between experimental and theoretical predictions for panels fabricated from three composite systems.
- Validation of the model was carried out in the form of blind testing, both for simple and for more complicated lay-ups.
- The proposed model relies on seven material inputs in order to predict all laminate configurations (E_x, E_y, G_{xy}, ν_{xy}, η_x, η_y, and η_{xy}). These were obtained from mechanical testing of a 0° panel for the properties in the x and y directions, and the testing of a lap joint to obtain shear properties.

- An optimisation interface has been proposed in order to obtain a stacking sequence to give maximum E, η or the product of both.
- Classical laminate theory has been shown to be sufficient in characterising the modulus and damping of the panels tested, although, as has been stated, that application of the model to panels with width/thickness ratios of less than 10 may give greater discrepancy.

7. Commercial Shafts

In order to apply the model presented in Chapter 6 to commercial shafts, it was necessary to catalogue the structures and mechanical properties for a range of commercial shafts. In particular, the aspect of reproducibility, i.e. manufacturing tolerances, needed to be determined. This chapter includes details of the inter- and intra-Batch stiffness and damping variations as well as along the shafts' length and around their circumference. The mechanical property assessments are related to the effects of shaft geometry, defects and lay-ups. A full list of the shafts tested can be seen in Table 7.1.

Table 7.1: Details on the commercial shafts selected for mechanical testing

Shaft Batch	Number of Shafts	Manufacturers Stiffness Rating	Notes
A	3	Regular Flex	
B	1	Regular Flex	Triangular section
C	1	Ladies Flex	
D	1	Regular Flex	
E	1	Regular Flex	Triangular section
F	6	Regular Flex	
G	1	Stiff Flex	
H	1	Regular Flex	Parallel sided

7.1. Optical Analysis

7.1.1. *Microstructure and defects*

Shafts were sectioned transversely at positions 70 mm from each end, which were used to obtain tip and butt microstructures.

Batches A and F were sectioned at the tip and butt ends. The acquired samples were mounted in DuroFix (a cold mounting resin) and polished to a 1 μm diamond paste finish.

Figure 7.1 shows the butt sections, at 0° (defined by the position of the manufacturer's logo on the circumference).

Figure 7.1 and Figure 7.2 shows cross-sectional images of Batch A (images from Batch F can be seen in Appendix B). Table 7.1 and Table 7.2 show the fibre orientation and ply properties for Batches A and F. Both Batches were fabricated from 6µm diameter circular cross-sectioned fibres. It can be seen that apart from the fibres orientation, that Batch A and F show similar characteristics in terms of ply thickness, volume fraction and inter-ply RRR, however the fibre orientation varies, with Batch F using 15° plies on the outer surface compared to the 0° fibres used in Batch A. It was noted that the inter-ply resin-rich regions were more prominent with an orientation mismatch between neighbouring plies. Figure 7.1 shows the plies on the left (±45°) show a larger inter-ply resin-rich region in comparison to the plies on the right (0°), where fibres are not constrained to move between plies, unlike in the 45° sections.

Table 7.2: Average fibre orientation* for the butt and tip sections for Batches A and F.

	Ply Number (1st ply refering to the outermost ply)															
Batch	**1**	**2**	**3**	**4**	**5**	**6**	**7**	**8**	**9**	**10**	**11**	**12**	**13**	**14**	**15**	**16**
A - Tip	0	0	0	45	45	45	45	45	/	/	/	/	/	/	/	/
A -Butt	0	0	0	0	0	0	0	45	45	45	45	45	0	0	0	0
F - Tip	15	15	15	25	25	45	45	45	/	/	/	/	/	/	/	/
F - Butt	15	15	15	15	15	15	25	25	25	45	45	45	45	15	15	15

* fibre orientation varied by ±3° in all sections.

Table 7.3: Microstructural analysis of Batches A and F.

Batch	Intra-ply volume fraction	Average Ply Thickness (µm)	Average Inter-ply RRR (µm)
A	0.56 (±0.05)	190 (± 10)	20 (± 5)
F	0.57 (±0.06)	190 (± 12)	20 (± 7)

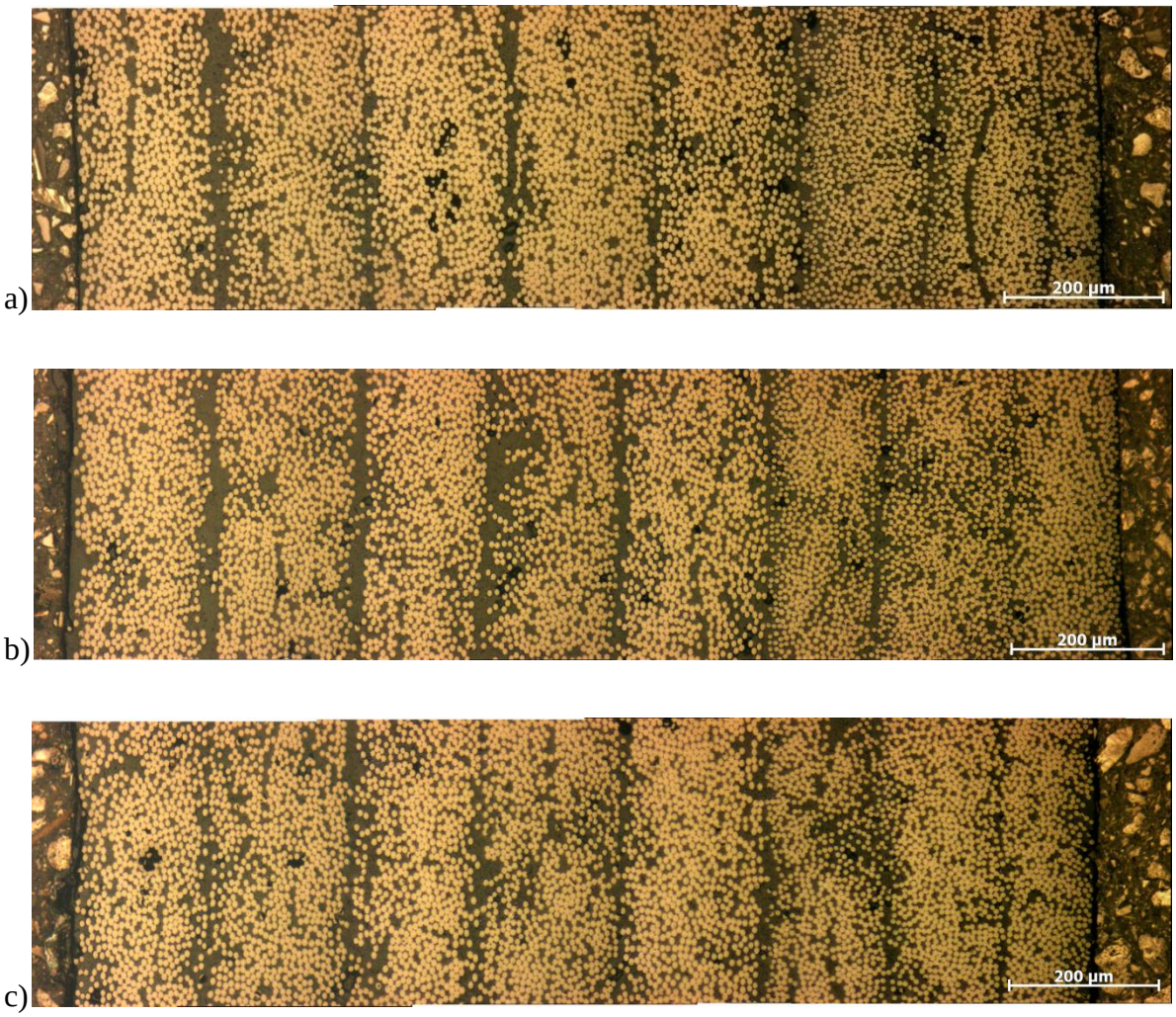

Figure 7.1: Through-thickness optical sections of the butt for shafts a) A1, b) A2 and c) A3.The outer surface of the shaft is at the right of the image.

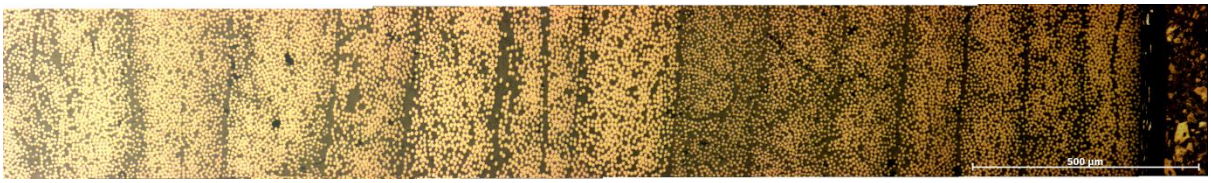

Figure 7.2: Micrograph of the tip end of A1. The outer surface of the shaft is at the right of the image.

Evidence of seams which can be found in the commercial shafts can be seen in Figure 7.3 to Figure 7.6. Seams are formed when a void is filled during the cure cycle of the composite [4], as the matrix has a low viscosity during this phase then it can fill the area easily, but the fibres cannot leaving this as a low stiffness resin-rich region. The size of the seam depends on how easily the fibres can move into that area and the size of the original void (affected by ply thickness and degree of alignment of the ends of ply sheets during assembly).

The characteristics of the seams fall into three main groups:

- Presence of 0° fibres on either side of the seam. As there are some plies which fall in the same axis as the seam (along the length of the shaft) then the resin-rich region (RRR) which is produced is very small (Figure 7.6), this is due to the fibres moving to occupy this area during period of low matrix viscosity during the curing cycle. If all fibres present around the seam are 0° then there is almost no RRR present (Figure 7.4).
- No 0° plies present either side of the seam. As no fibres are aligned with the seam, then the fibres cannot easily fill the void. This is the common type of seam as a ±θ° lay-up is used widely, and as such the void is trapped between two plies of

constrained fibres. This results in loss in stiffness at certain points around the shaft's circumference (Figure 7.3).

- Transition between two plies. Very rare and stringent efforts are made to avoid these. The gap between the end of one ply and the beginning of another causes a discontinuity in the ply, which is resin-filled, as well as causing a large amount of distortion can be seen in neighbouring plies (Figure 7.5)

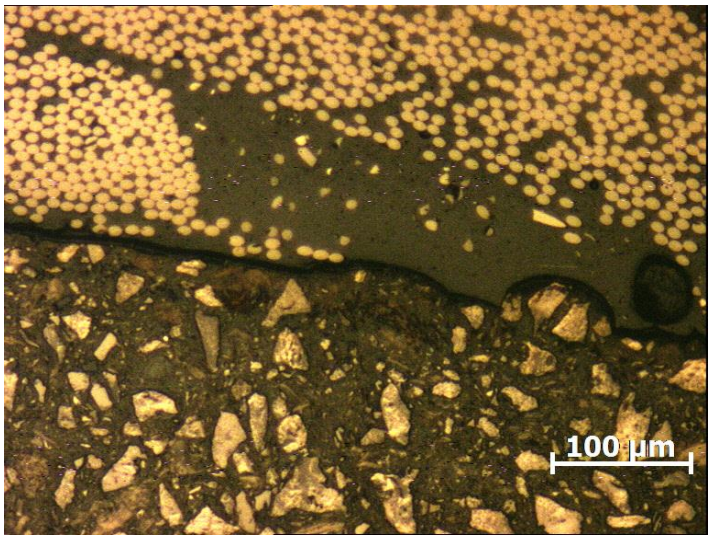

Figure 7.3: Micrograph shows a seam on the inner wall of A1.

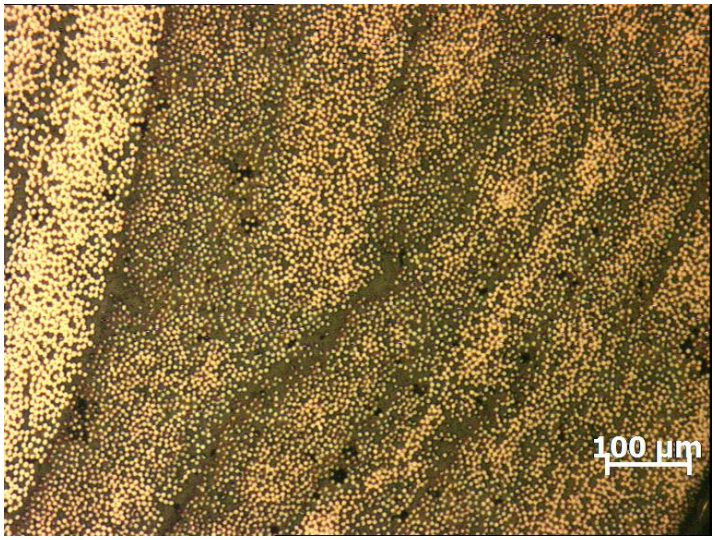

Figure 7.4: Micrograph showing a seam in the 0° plies of A2.

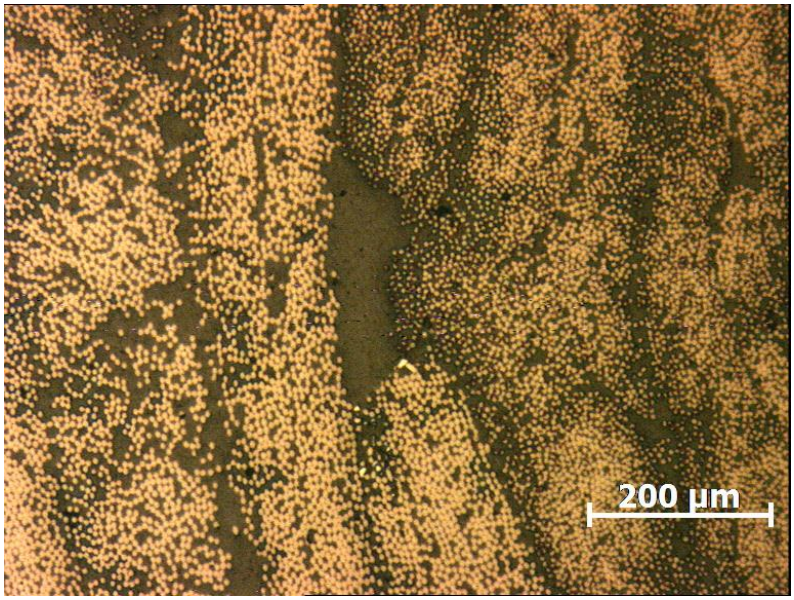

Figure 7.5: A seam created where a 0 and 45° ply where two plies ended in A3.

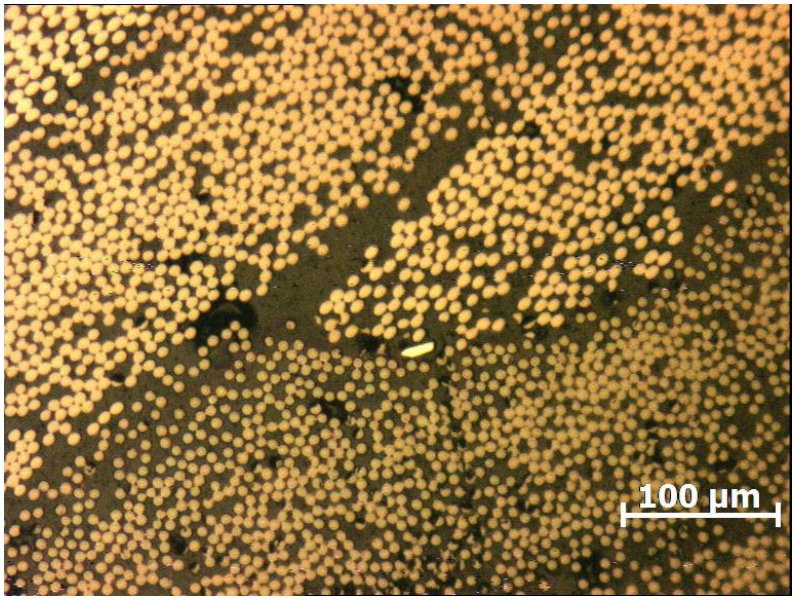

Figure 7.6: A seam showing the introduction of a 45° ply in A1.

The positions of the seams in all three shafts from Batch A were mapped in terms of orientation around the circumference and the plies in between which it fell. This was carried out both at the tip and the butt. All butt sections appear very similar, not quite evenly distributed but no particular area shows a high density of seams. Shaft A1 at the tip however does show a large collection of 5 seams within a 40° distance around the circumference, with shaft A2 showing the most even distribution of seams (Figure 7.7). This was used when stiffness testing in order to determine the effect that the size and distribution of the seams had on the stiffness variation of a shaft around its circumference.

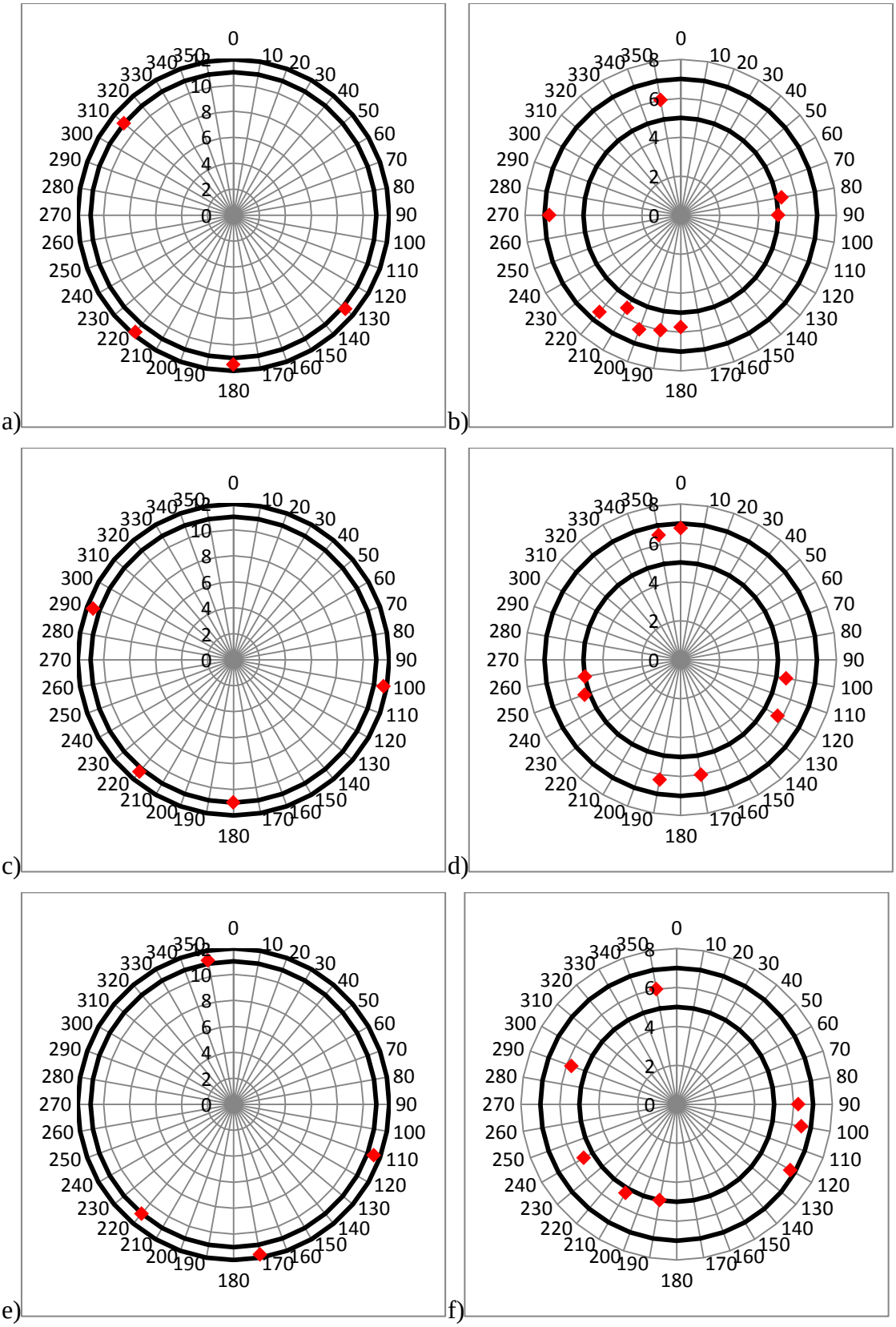

Figure 7.7: Seam locations for the three shafts from Batch A a) A1 butt, b)A1 tip, c)A2 butt, d) A2 tip, e) A3 butt, f) A3 tip. The thick black lines refer to the outer and inner wall of the shaft.

7.2. *Mechanical Properties of Commercial Shafts*

7.2.1. *Outer Diameter*

The shafts' outer diameters are plotted in Figure 7.8. It can be seen in all cases except for H1 that an outer diameter of around 8.5 - 9.5 mm can be seen at the tip and about 15 mm at the butt. H1 is a parallel-sided shaft, but it is apparent from observation that there is some tip stiffening so the stiffness would not be expected to remain constant along its length.

The B1 and E1 shafts both have a section which is triangular. The point at which it changes is apparent from Figure 7.8 (approximately 500 mm for both).

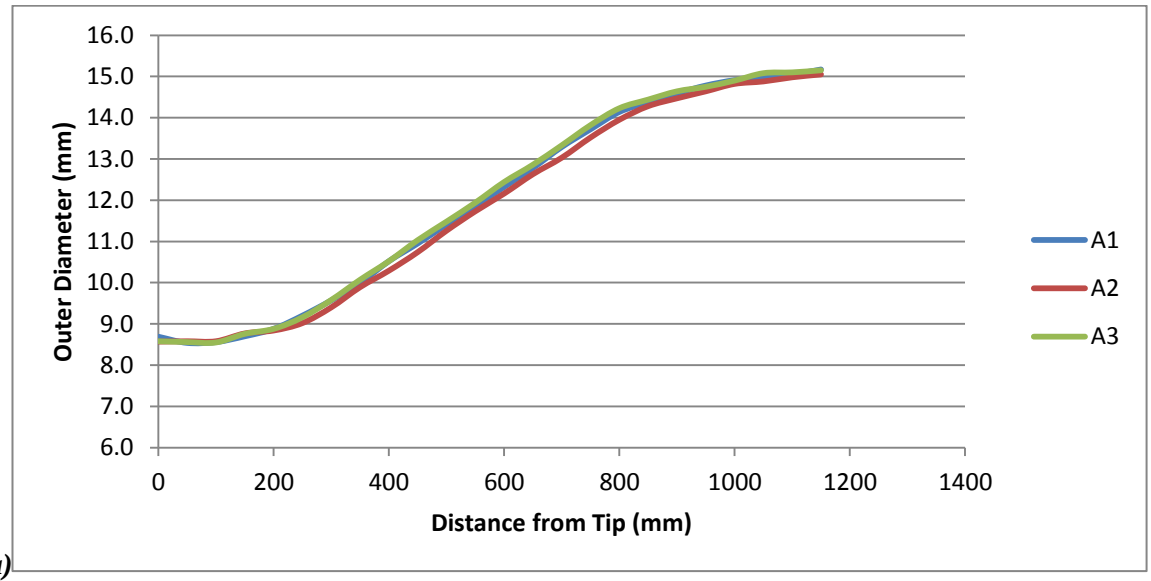

a)

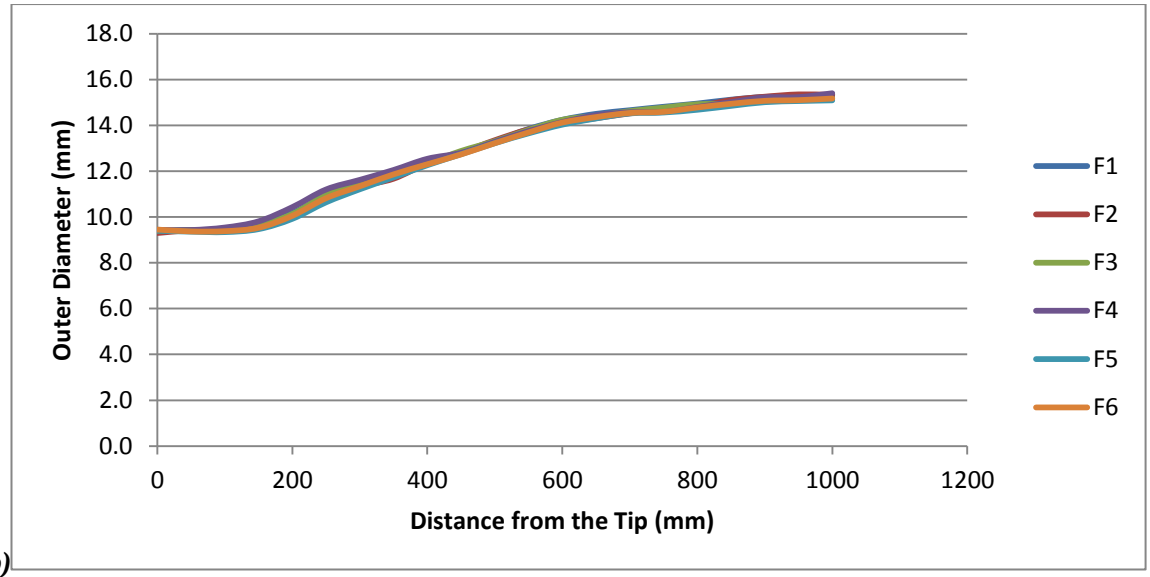

b)

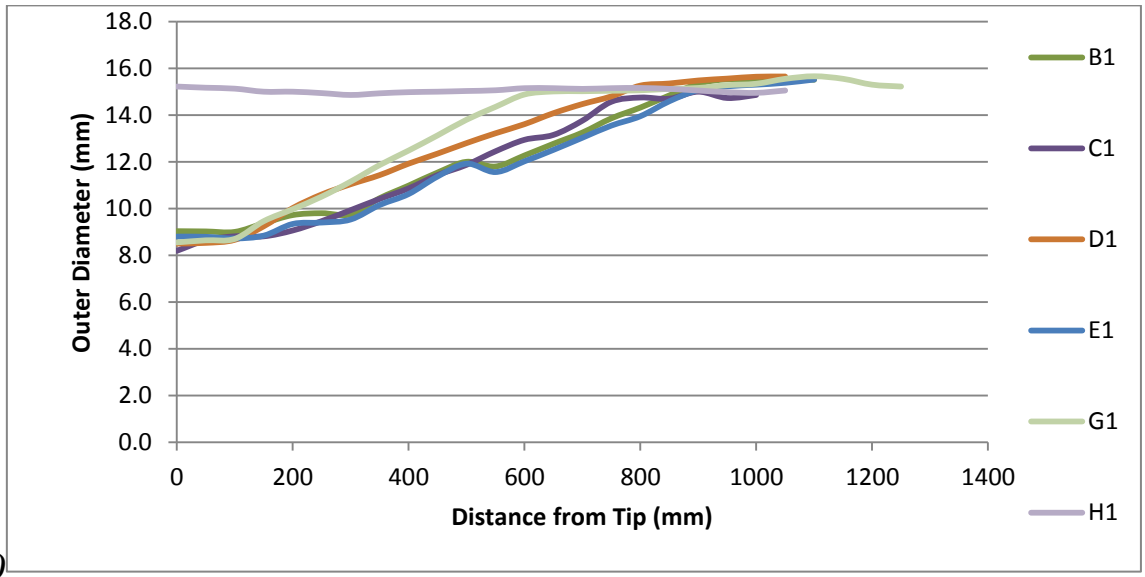

c)

Figure 7.8: Outer diameter profiles for a) A1-3, b) F1-6 and c) the remaining shafts.

7.2.2. *Stiffness and damping along the length of the shaft*

In this section the distance from the tip refers to the loading point. For example if 150 mm is stated as the distance from the tip, then the section being tested will be the 150-635 mm section along the shaft (485 mm cantilever length).

Figure 7.9 shows the change in stiffness along the length of the shaft for the shafts from Batch A. It can be seen that there is very little difference between the three shafts (no greater than 5%) with most discrepancy towards the butt end.

The stiffness profile shows a similar trend to that in outer diameter, with a lower gradient at the tip and butt. A much steeper gradient in stiffness can be seen at the section which covers the greatest change in outer diameter (Figure 7.10). The stiffness is very consistent intra-Batch, with only the butt end of A2 showing a slightly higher stiffness.

The hysteresis however does show a significantly different trend to that of stiffness (Figure 7.11), with a large change in damping at the tip, and then a plateau starts around 350 mm. This plateau shows that no change in material properties is occurring here. Therefore as the stiffness is still increasing dramatically in this region it is most likely that this increase in stiffness is dominated by the change in outer diameter (Figure 7.10a).

The intra-Batch variation of these shafts in damping is much greater than with stiffness, with A1 showing almost double the amount of damping at the tip than A3 and A2 in between. These shafts were tested in the 0° orientation, and as such the greatest stresses will be on the top surface (tension) and bottom surface (compression), and as such seams in these locations will have a greater affect on the mechanical properties in this orientation. As it can be seen in Figure 7.7 A1 has six seams in the region of influence (taken as 315-45° and 135-225°), A2 has four and A3 has three. This trend can be seen in the difference in tip damping, where a noticeable difference occurred between all three shafts.

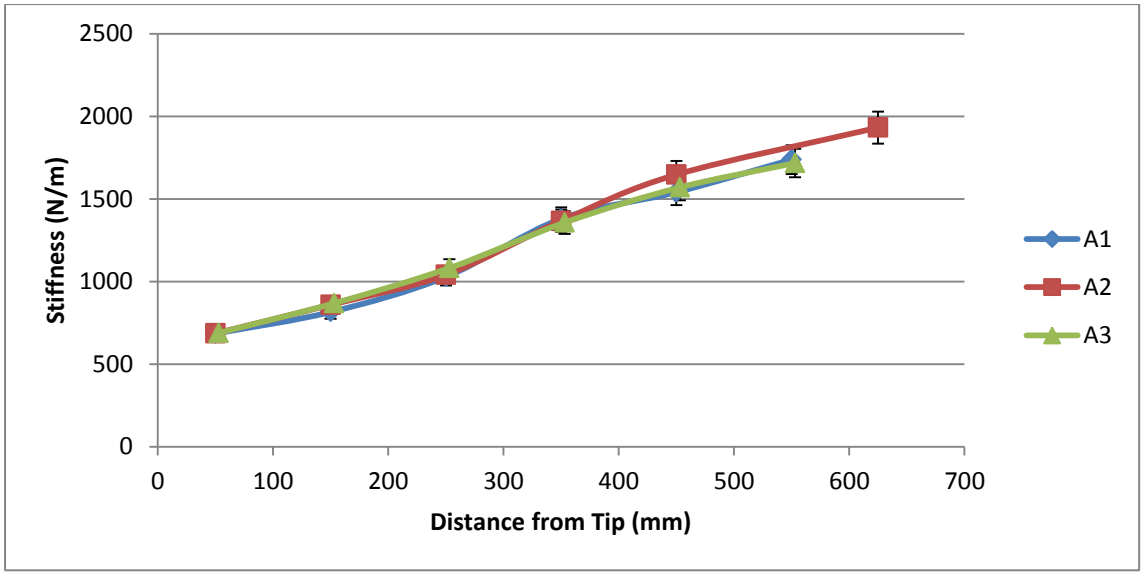

Figure 7.9: Change in stiffness along the length of the shaft for shafts A1-3.

a)

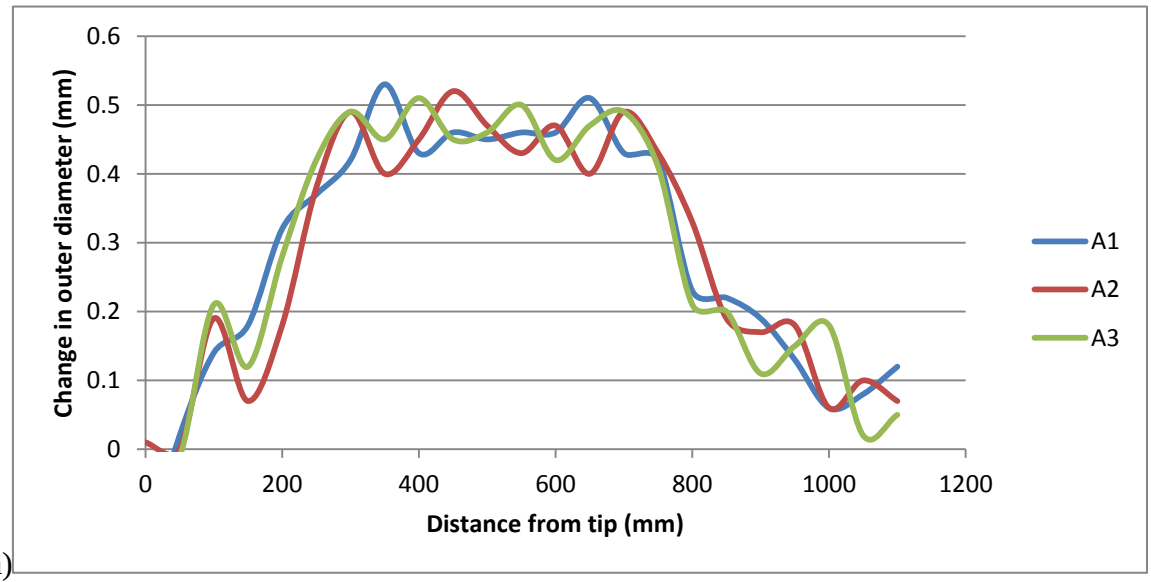

b)

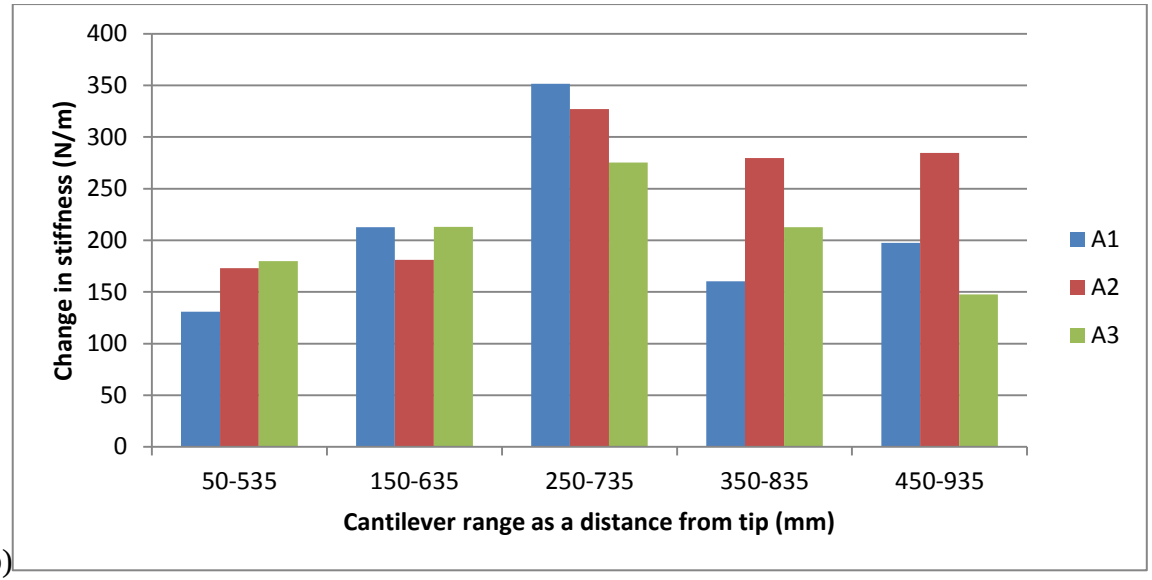

Figure 7.10: The change in a) outer diameter and b) stiffness along the length of shafts A1-3.

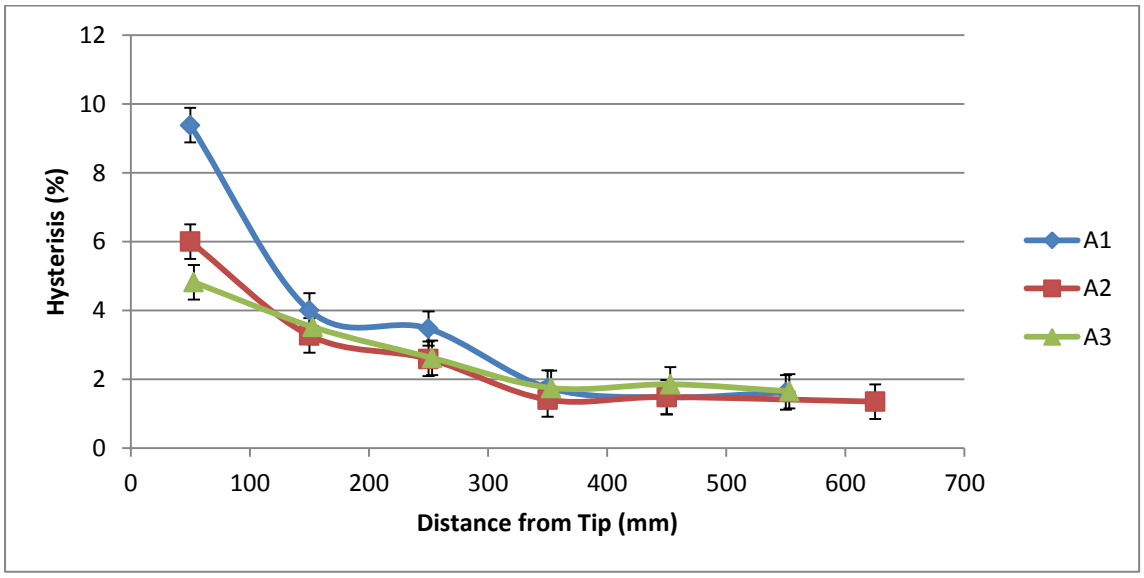

Figure 7.11: Change in hysteresis along the length of the shaft for shafts A1-3.

F1-6 show a greater intra-Batch scatter in stiffness (up to 11% difference), however, each shaft maintains the same trend i.e. the stiffest shaft is above the Batch average in stiffness along the entire length (Figure 7.12). Batch F shows a generally lower tip hysteresis than Batch A but still show a large scatter (hysteresis values ranging 2.5 - 6 % as seen in Figure

7.14). The damping reduces less than Batch A along the length, but, with damping ranging from 1.2 - 2.2 %, the average is similar to that for Batch A.

Figure 7.13 shows the frequency traces from F2, 3, 4 and 6. Firstly it is apparent that the order of stiffnesses agrees well with the shaft deflection testing, with F6 being the stiffest and F3 being the least stiff. It is important to note how the stiffness alters around the circumference, such that a stiffer shaft when tested at one orientation could be one of the least stiff if tested in another orientation. This is shown by the order of stiffnesses at 0° and 140°, Figure 6.13.

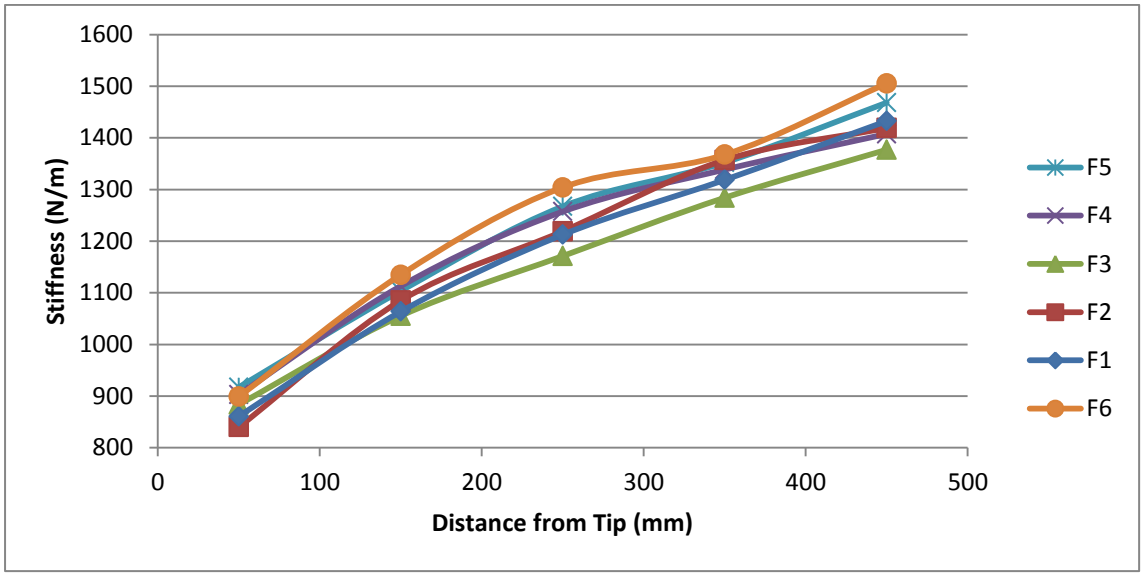

Figure 7.12:Change in stiffness along the length of the shaft for Batch F.

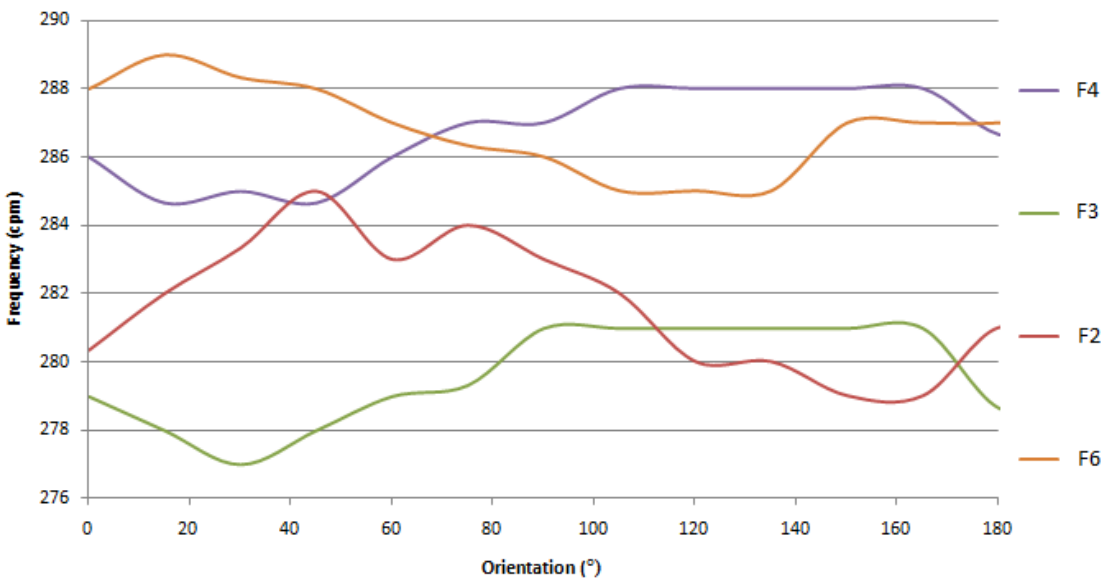

Figure 7.13: Frequency testing results for F2, F3, F4 and F6. 0° refers to the point at which the deflection test was taken.

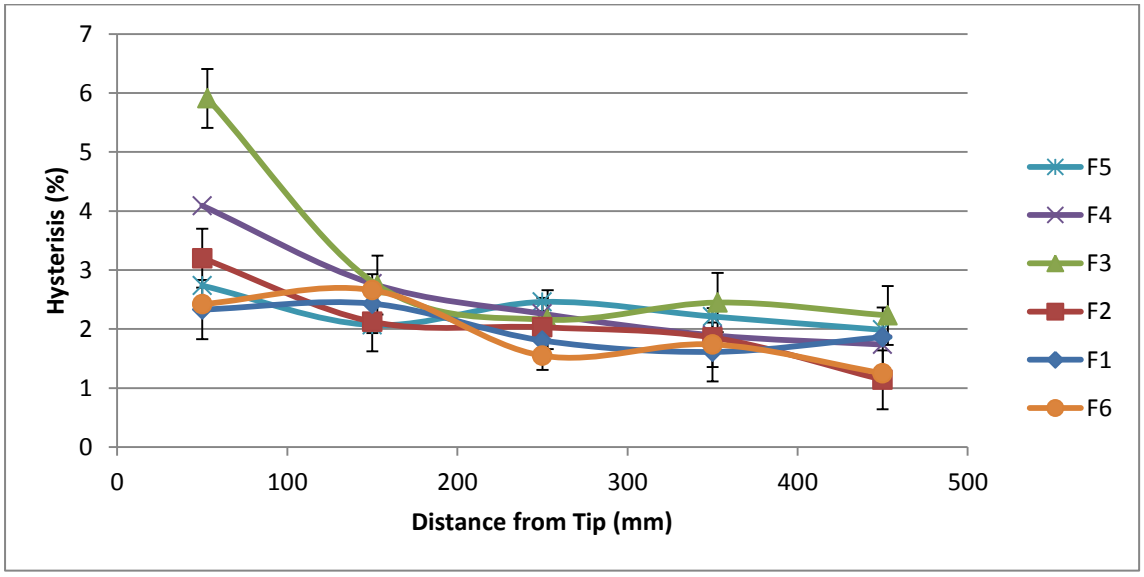

Figure 7.14:Change in hysteresis along the length of the shaft for Batch F.

The remaining shafts show quite different trends, Figure 7.15 and Figure 7.16. Firstly the two shafts with a triangular section (B1 and E1) show a greater change in stiffness from 350 to the butt, than the other shafts do (Figure 7.15). Figure 7.8 shows that, for both shafts, the triangular section finishes at around 500 - 550 mm from the tip, which correlates well with

the increase in the stiffness, suggesting either the transition between the two or the triangular section reduces the stiffness. Both these shafts show a very constant damping, with the E1 showing a noticeable decrease in damping only at 550 mm away from the tip (after the triangular section).

The ordering of the shafts matches the manufactures stiffness rating quite well with the stiffest shaft being the G1, which is the only "Stiff" shaft, and the C1 is the least stiff and is the only "Ladies" flex shaft.

With the exception of the H1, all shafts have a higher damping at the tip and plateau towards the butt. This is likely to be attributed to the tip stiffening used so that the head can be attached [4]. The additional plies are predominantly low angle plies (0° in Batch A, 15° in Batch F) therefore a lower damping would be expected. The increase in damping is likely to be due to the high number of seams (Figure 7.7) due to the addition of the plies, or due to a feature called ply drop-off. Ply drop-off is essentially a seam normal to the loading axis and is formed when a ply is only used for part of the length of the shaft, in this case extra plies have been used to stiffen up the tip. Fish and Lee (1989) [54] investigated how inter-lamina stress changes when panels show internal ply drops. It was seen that clear increases of around 40 % in inter-lamina stresses are present at the end of a ply which has finished before the end of the laminate. This effect is intensified when the ply which has finished is a stiffer ply than the two either side of it (50 % in inter-lamina stress), this results in the shifting of the load, whereas for a less stiff ply, the plies either side would be carrying the majority of the load resulting in very little load transfer from the drop off. This would be a possible explanation for the high level of damping at the tip where a lower level would be expected. So, in opposition to the usual composite mechanics the addition of low fibre angle plies has increased both stiffness and damping in this case.

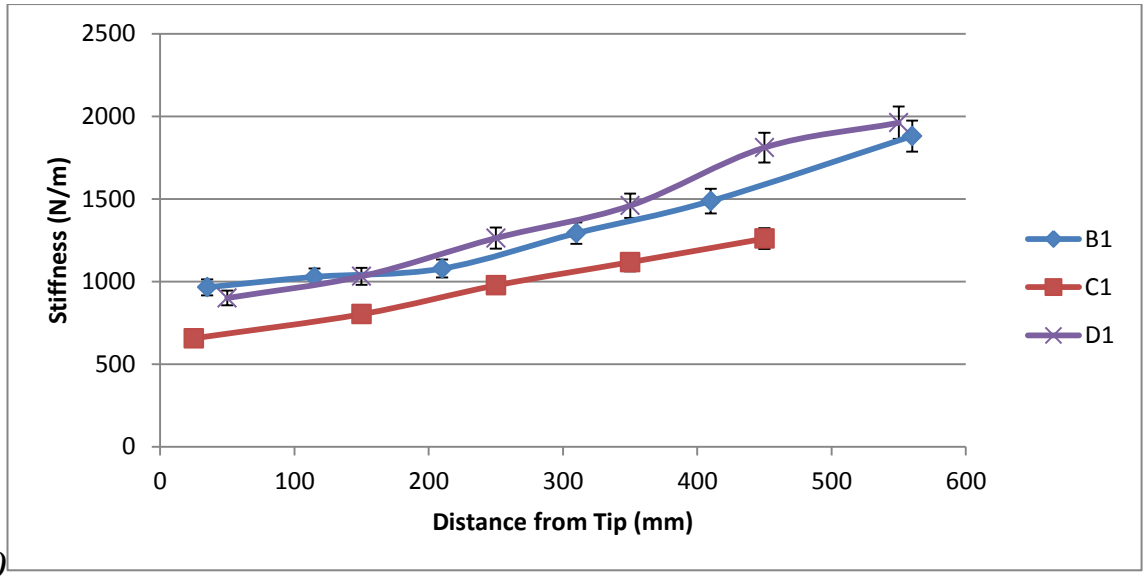

a)

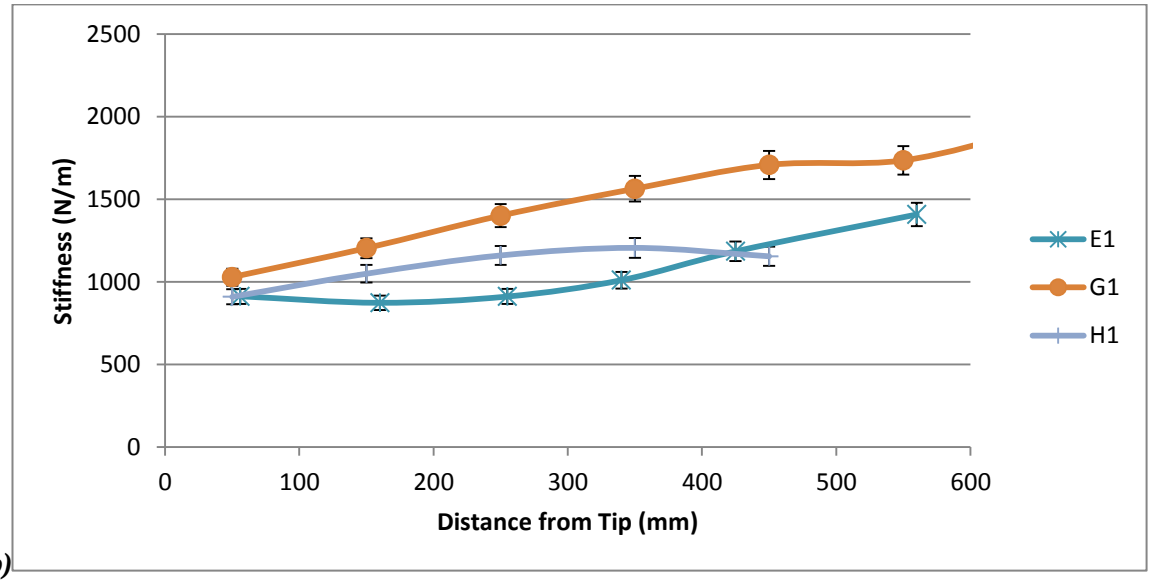

b)

Figure 7.15: Change in stiffness along the length of the shaft a) B1, C1 and D1 b) E1,G1 and H1.

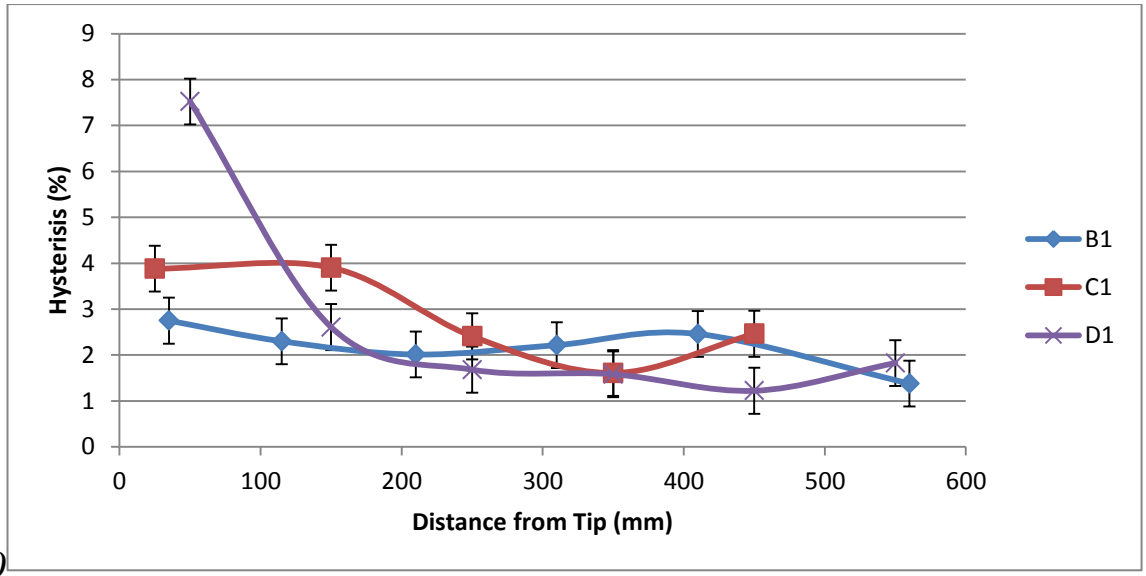

a)

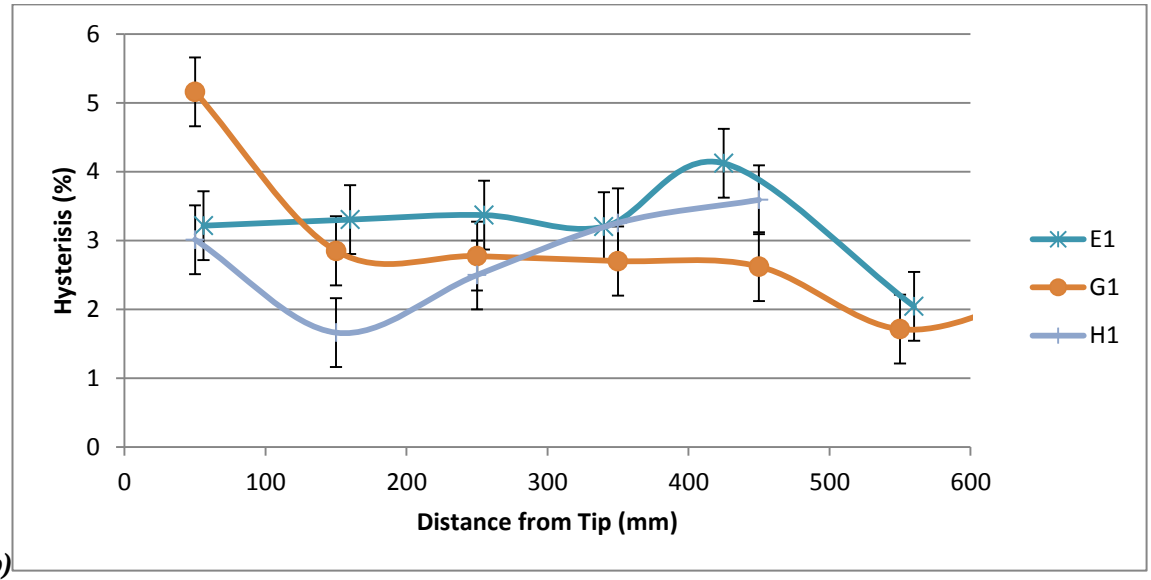

b)

Figure 7.16: Change in hysteresis along the length of the shaft a)B1, C1 and D1 b) E1,G1 and H1.

7.3. Implications of shaft variation on the model inputs

7.3.1. *Thickness variation*

The shafts analysed in this section have shown up to a 5 % in ply thickness variation. With stiffness showing a cubic relationship to thickness (Equation 5.13) in bending. For flat panels this 5 % variation would cause a relatively large (compared to experimental error) difference

in predicted stiffness value. However, due to the geometry of shafts, the wall thickness is a minor constituent of the total shaft diameter (around 40 % at the tip, and 15 % at the butt), and therefore the variation in wall thickness will result in a much smaller variation in stiffness.

7.3.2. *Inter-ply resin rich region*

Emphasised in off-axis lay-ups, inter-ply RRR arise from the reduced flows of fibres between plies. The inter-ply RRR found in Batches A and F were found to be over 10 % of a plies thickness in some cases. The model presented in Chapter 6 calculates the mechanical properties from 7 material inputs, these are obtained from 3 panels. Therefore if the inter-ply RRR is consistent across all components manufactured from that composite system, then the inter-ply RRR would be accounted for. The problem arises with the severity of the inter-ply RRR changing with fibre orientation, the model presented here cannot account for this at the moment and future amendments to the model will need to incorporate this. One method to account for these defects would be to add additional plies (20 μm thick) with material properties based on that of the matrix.

7.3.3. *Seams*

Seams will essentially have the same influence on the mechanical properties as the inter-ply RRR, however the prediction of this form of defect is out of the scope of the models capabilities. These areas of high resin content are quiet unpredictable, and as seen in this section can appear in many forms. Many factors can contribute to the severity of seams, such as fibre orientation, cure cycle, curing pressure, constituent material properties and the geometry of the artefact [4]. In the case of this, a flat panel with an incorporated seam may not characterise one found in a shaft. To take this model further the model presented in this

work will need to be incorporate into a finite element model (FEM). Further analysis of the effect of seams on the mechanical properties of shafts will be examined in Chapter 7.

As well as the size of the seam, its location within the shaft wall will change the degree to which it will cause discrepancy with the model, with seams closer to the surface having a greater affect than those towards the centre. It has been shown that the outer plies of commercial shafts tend to be low angle fibre orientations (for improved stiffness), fibres at lower orientation have been shown to have less sever seams, and therefore the more sever seams will be seen in the regions where they have less of an effect (closer to the centre).

7.3.4. *.Seam distribution*

Whereas the seam severity cannot be predicted in this model, seam distribution can be predicted based on the lay-up process, by knowing the width of the pre-preg used, the position of the seam within the shaft can be predicted. Therefore if the severity of a seam can be modelled, this can be placed into the correct position within a shaft.

7.3.5. *Manufacturers variation*

Another aspect that can alter the applicability of the model, is the variation due to manufacturing. Earlier in the chapter intra-Batch variation could be seen as high as 11 % in stiffness, and damping was seen to increase by almost double at the tip in some shafts within a Batch. These variations can be attributed to several factors other than those already mentioned. These include, material properties (inconsistencies in cure cycle) and fibre angle (inaccuracies with the fabrication). Of these two fibre orientation can have a larger effect (cure cycles are usually thermostatically controlled, and has minimal human error [17]). It was shown that fibre orientation can vary by ±3° of the average (assumed to be the desired)

angle. This variation can have a noticeable change on the material properties depending on the angle. For example (based on the properties of MTM28-1/T800H) a 5° panel will have a 10 % greater modulus than that of an 11° panel (6° manufacturers variability), and could account for the high variation in mechanical properties within a batch. However this effect is much smaller at higher angles (less than 0.5 % variation from 84 to 90° panels). Therefore the model should be used with the consideration that its effectiveness is only as good as the fabrication consistency.

8. Fabricated Shafts

In order to identify how applicable the model presented in Chapter 6 is for golf club shafts, several shafts of varying orientations were fabricated. This chapter discusses factors which may result in discrepancies between predicted and measured stiffness and damping values. For the shafts presented in this chapter, 0° was defined from a line on the inner silicone tube which was face up during the curing process (this bares no correlation to any microstructural details).

8.1. Optical Analysis

Details of the fabrication of the shafts used for this section (Table 3.4) are given in Chapter 2.3. All shafts fell within the acceptable limit for the orientation (± 2°) and therefore no shafts were discarded (Table 8.2).

Table 8.1: List of fabricated shafts and their orientations.

Shaft Number	Orientation (°)
1	0
2	0
3	0
4	±30
5	±30
6	±45
7	±45
8	±45

Figure 8.1 to Figure 8.7 show cross-sectional micrographs of the fabricated shafts. All shafts had an intra-ply volume fraction of 0.56 (± 0.03), however there is a noticeable change in the resin-rich region (RRR) between plies, more apparent in shafts 45-II and 45-III (Figure 8.6 and Figure 8.7). This can be seen in Table 8.3, where the RRR is almost double in area in 45-III compared to that of 45-I. This is evidence of manufacturing variability as these should be

nominally identical shafts. This can also be seen with the 0° shafts showing a much smaller inter-ply RRR than the 30 and 45° shafts. The 0° shaft also showed negligible areas of excess resin at the seams suggesting the on-axis fibres filled in the seam gaps more readily. It can also be seen that with increasing fibre orientation the average seam area (Figure 8.8 to Figure 8.12, Table 8.3) increased. The shaft 45-I showed a significantly higher average seam size than the other two 45° shafts, however this shaft also shows a noticeably lower inter-ply RRR than the other 45° shafts. This would suggest that the seam will have a very local affect in shaft 45-I. Both shaft 45-II and shaft 45-III show a large RRR going along the ply from the seam (Figure 8.11 and Figure 8.12). It should be noted that during the manufacturing process that the laying up of 45° shafts resisted the wrapping more than the other lay-ups, due to its higher transverse stiffness (see Chapter 3), this will also be the case during the cure cycle, where the off-axis fibres resist the pressure exerted by the vacuum bag. This could explain the large RRR measured in the 45° shafts (both as seams and as inter-ply RRR) and the slight increase in the wall thickness. The shaft 30-I shows both a smaller seam and no apparent increase in RRR near the seam compared to the 45° shafts (Figure 8.9).

The model presented calculates the stiffness and damping of laminates based on 7 material properties taken for sample laminates. Therefore if defects such as seams and inter-ply resin rich regions are not consistent across all shafts, deviations away from the theoretical values will occur. Errors attributed to wall thickness variation are likely to be small considering the small deviation (approx 3 %) the batch for shafts show.

Table 8.2: Fibre aspect ratios and wall thicknesses taken from optical microscopy.

Shaft	Average Feret Ratio	Average Wall Thickness (μm)
0-I	1	810 ± 10
0-II	1	805 ± 10
0-III	1	807 ± 10
30-I	0.85	810 ± 10
45-I	0.7	825 ± 10
45-II	0.71	833 ± 10
45-III	0.71	835 ± 10

Table 8.3: Ply, inter-ply and seam dimensions for the fabricated shafts.

Shaft	Average Ply Thickness (μm)				Maximum width of inter-ply RRR (μm)*	Average Seam Area (mm^2)
	1	2	3	4		
0-I	201	195	200	195	12	/
0-II	210	205	201	197	10	/
0-III	207	210	201	200	10	/
30-I	205	204	196	198	26	0.032
45-I	194	217	192	214	28	0.085
45-II	214	214	197	204	36	0.054
45-III	203	212	173	192	57	0.056

*Minimum width was not stated as inter-ply RRR may not exist in defect free regions, and thus the minimum will be 0 μm.

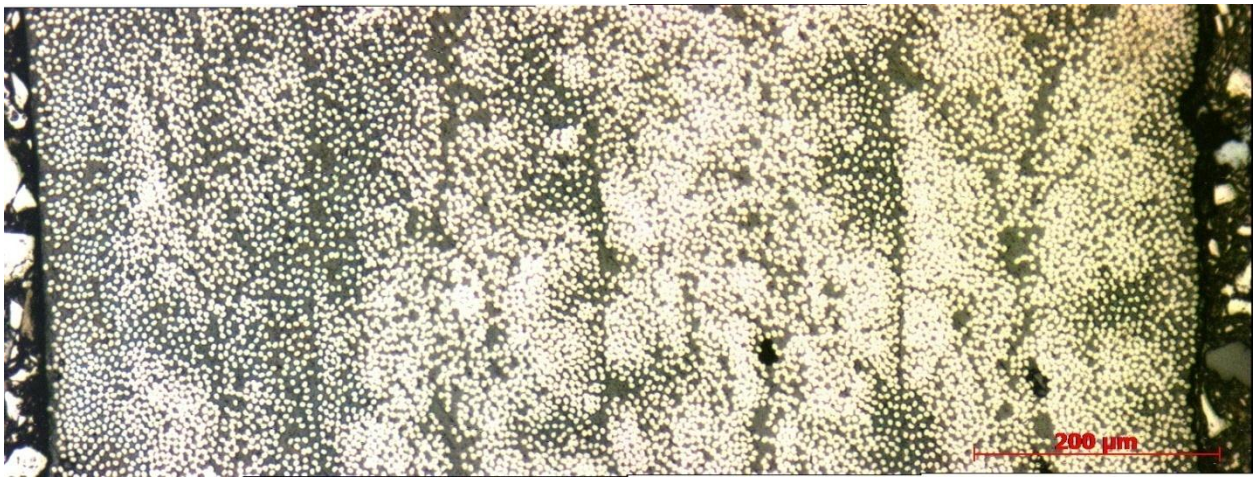

Figure 8.1: Micrograph of the shaft wall of 0-I at 180°.

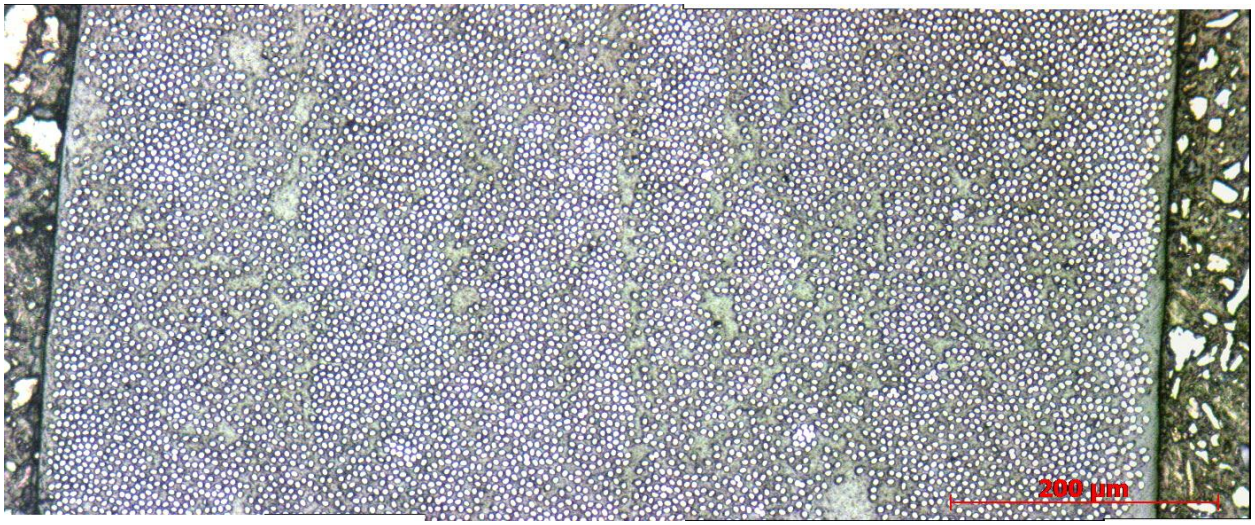

Figure 8.2: Micrograph of the shaft wall of 0-II at 180°.

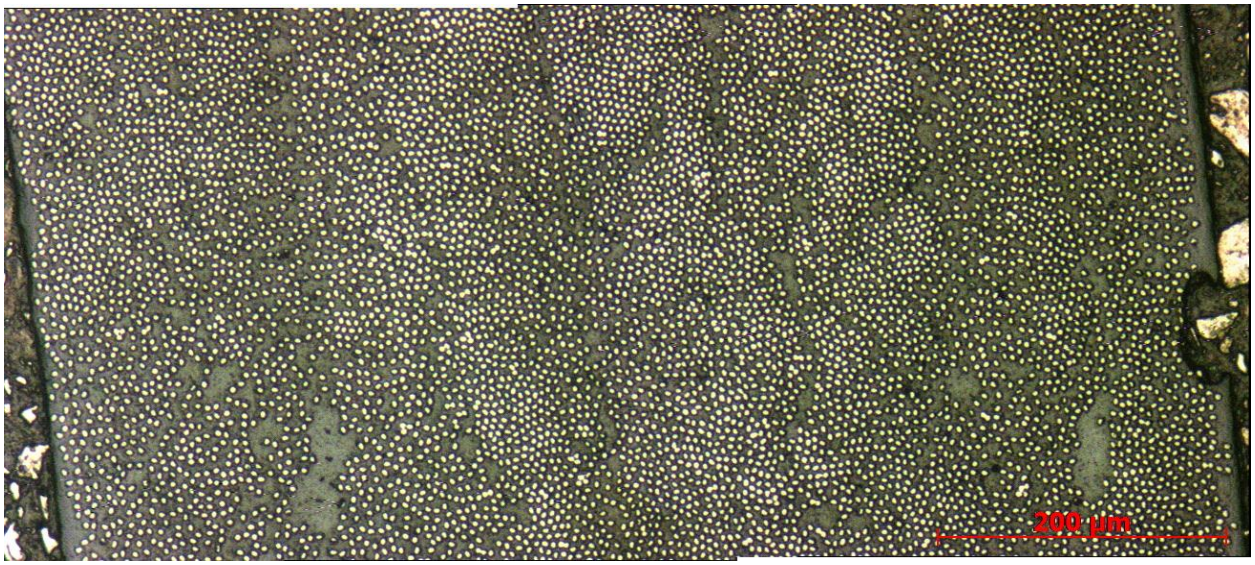

Figure 8.3: Micrograph of the shaft wall of 0-IIIat 180°.

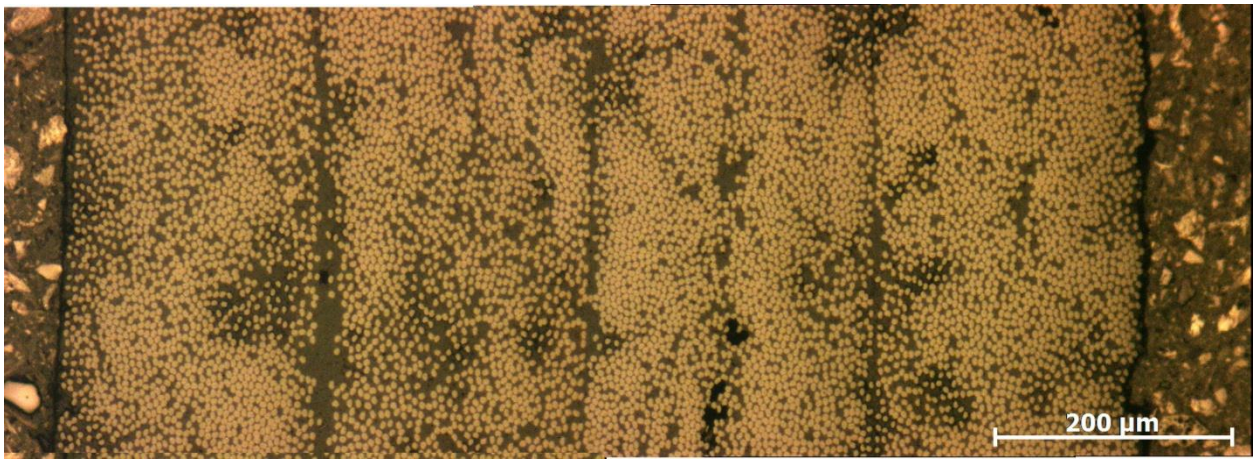

Figure 8.4: Micrograph of the shaft wall of 30-I at 180°.

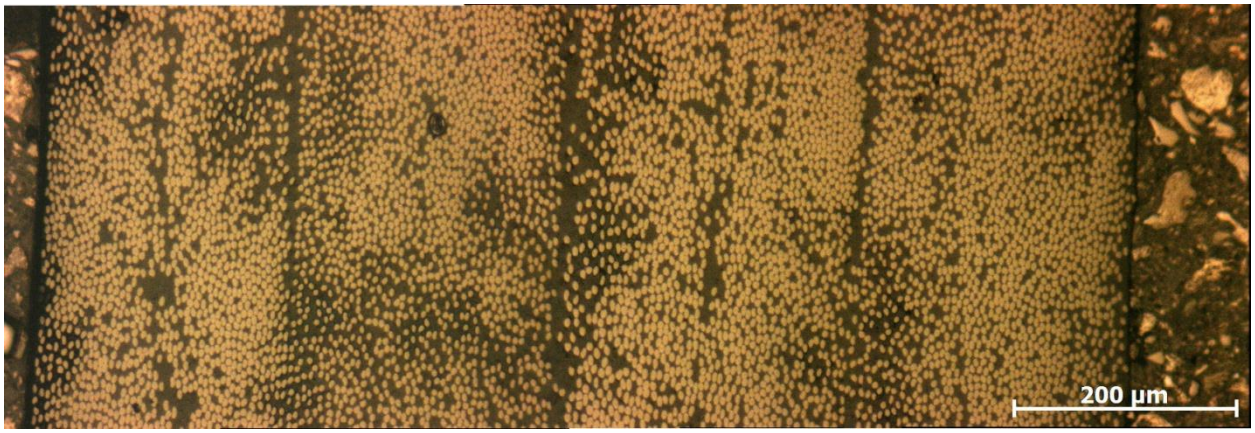

Figure 8.5: Micrograph of the shaft wall of 45-I at 180°.

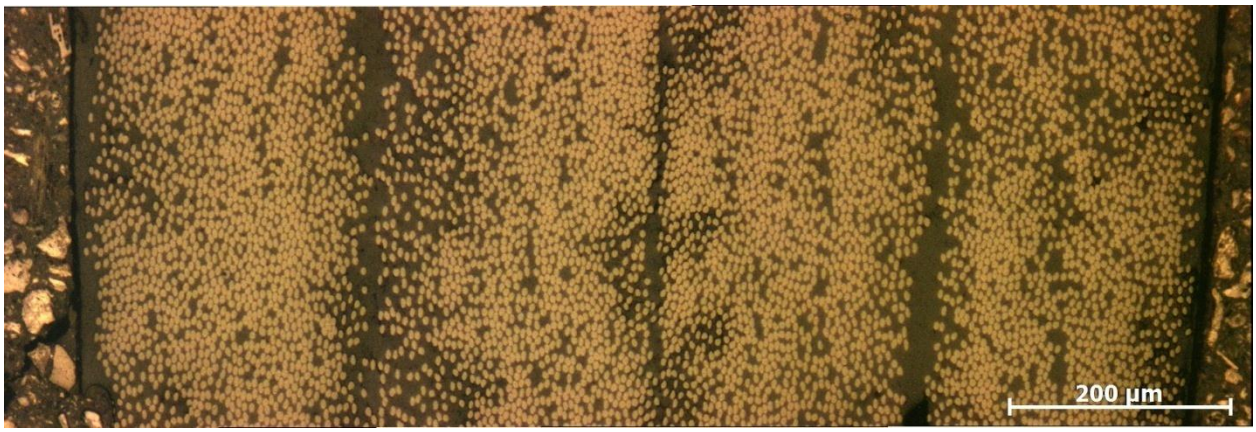

Figure 8.6: Micrograph of the shaft wall of 45-II at 180°.

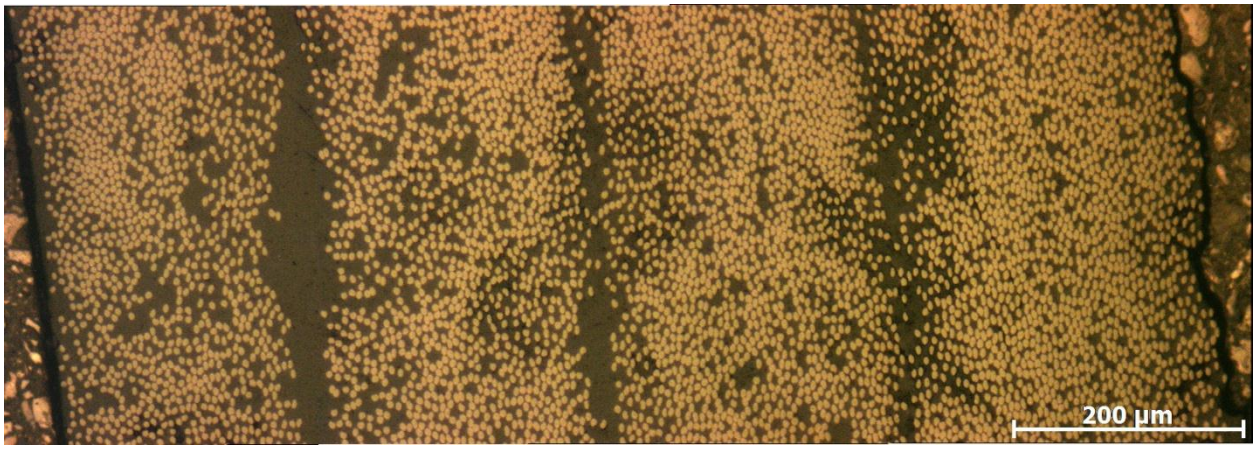

Figure 8.7: Micrograph of the shaft wall of 45-III at 180°.

Figure 8.8: Micrograph of seam found in shaft 0-II.

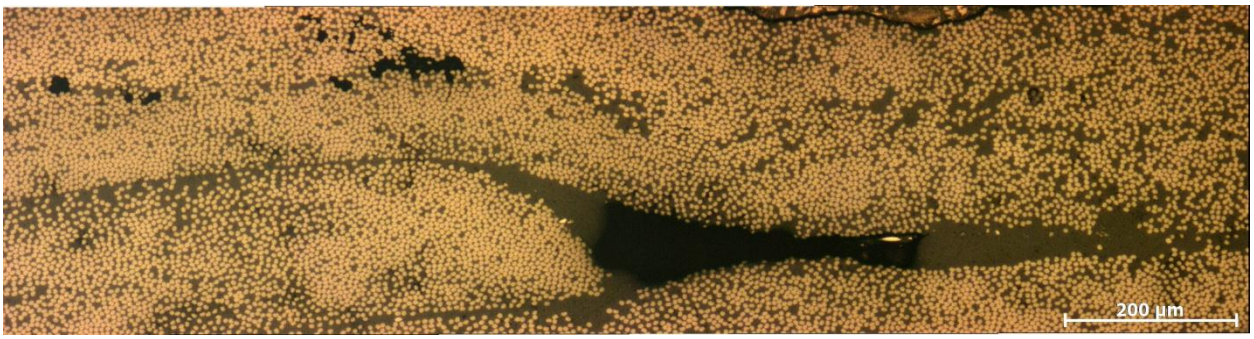

Figure 8.9: Micrograph of seam found in shaft 30-I.

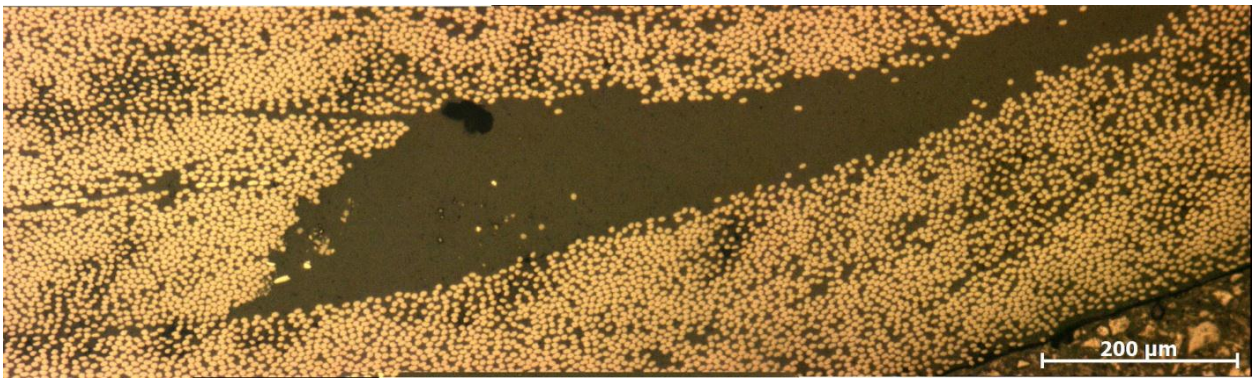

Figure 8.10: Micrograph of seam found in shaft 45-I.

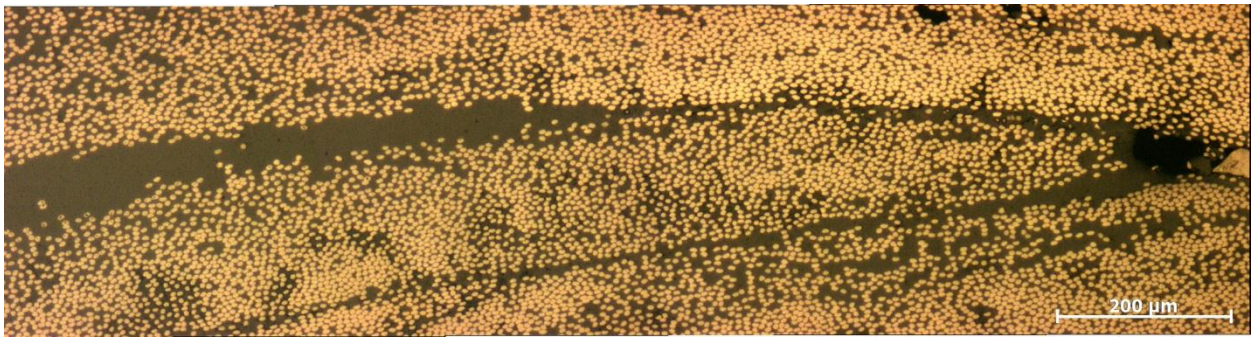

Figure 8.11*: *Micrograph of seam found in shaft 45-II.

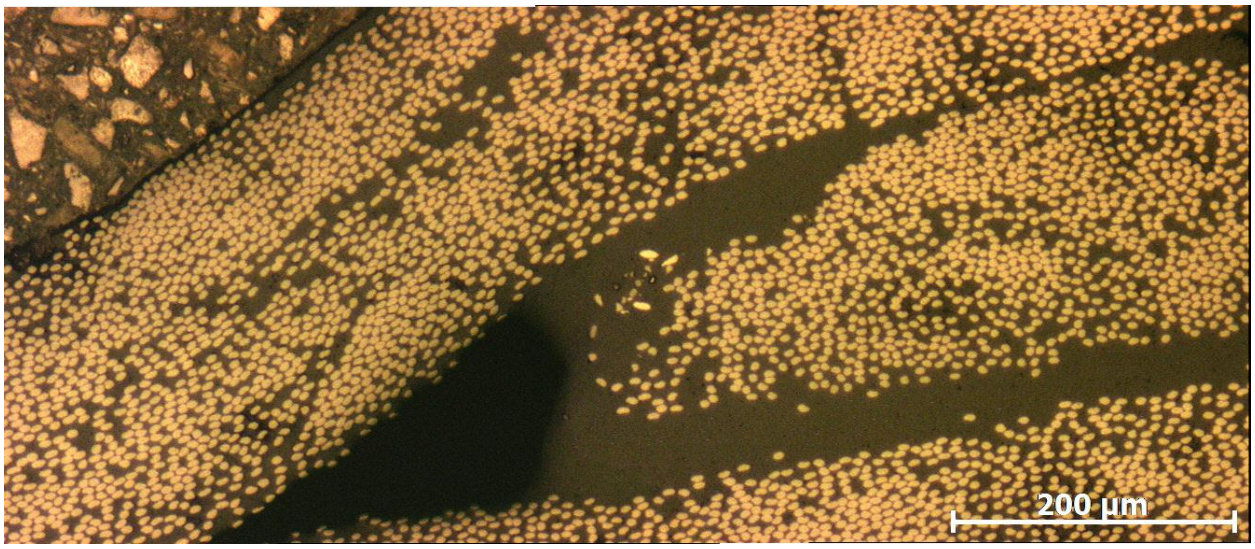

Figure 8.12: Micrograph of seam found in shaft 45-III.

Shaft 0-I has a large crack going through the entire thicknesses of the wall (Figure 8.13). This only extends 10 mm up the length of the shaft but was at the point of loading (possibly caused by the loading due to the poor transverse properties). This crack is present at 230° on the circumference.

Figure 8.13: Micrograph of crack found in shaft 0-I

Figure 8.14 shows the locations of the seams in the manufactured shafts, these shall be referred to for the remained of the chapter. They all show similar seam distribution (grouped in pairs with less than 100° between the pairs), but as 0° was assigned randomly their relative position varied between all the shafts. A summary of the seam distribution and sizes can be seen in Table 8.4. Due to the nature of the bend testing these shafts underwent, the seams will contribute greatest on both the upper and lower (tensile and compressive) surfaces of the shafts, and as such a reduction in stiffness (and increase in damping) would be expected not only with the shaft orientated in line with a seam, but also 180° afterwards, giving a sinusoidal distribution of stiffness and damping around the circumference.

a)

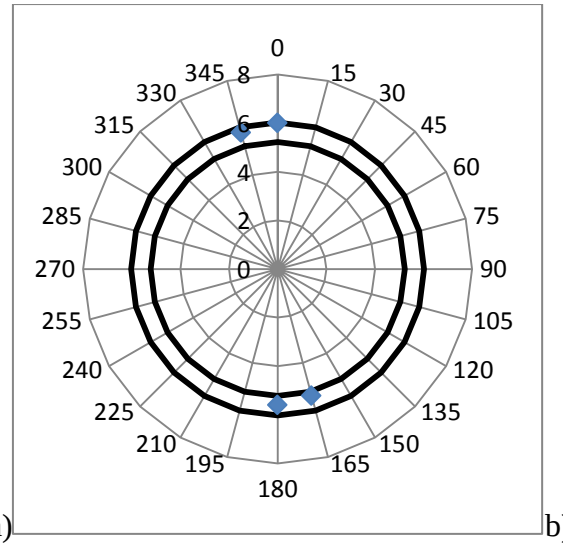
0
15
30
45
60
75
90
105
120
135
150
165
180
195
210
225
240
255
270
285
300
315
330
345
8
6
4
2
0

b)

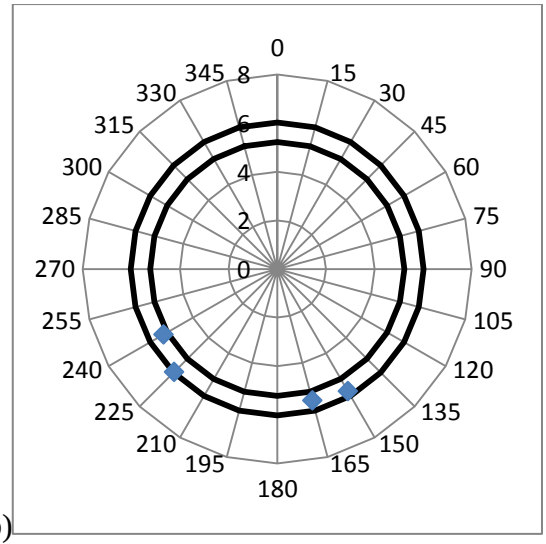
0
15
30
45
60
75
90
105
120
135
150
165
180
195
210
225
240
255
270
285
300
315
330
345
8
6
4
2
0

c)

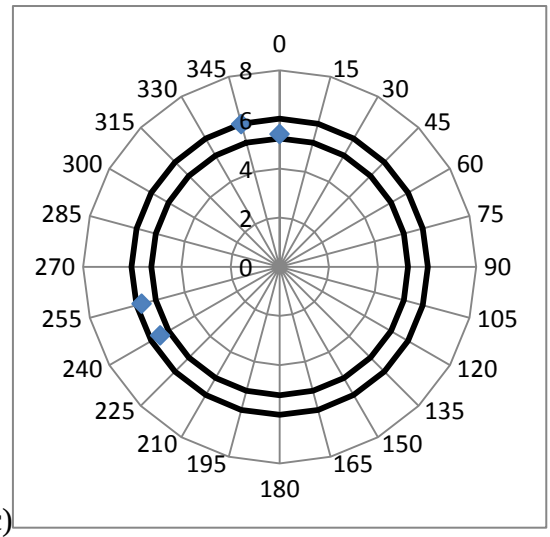
0
15
30
45
60
75
90
105
120
135
150
165
180
195
210
225
240
255
270
285
300
315
330
345
8
6
4
2
0

d)

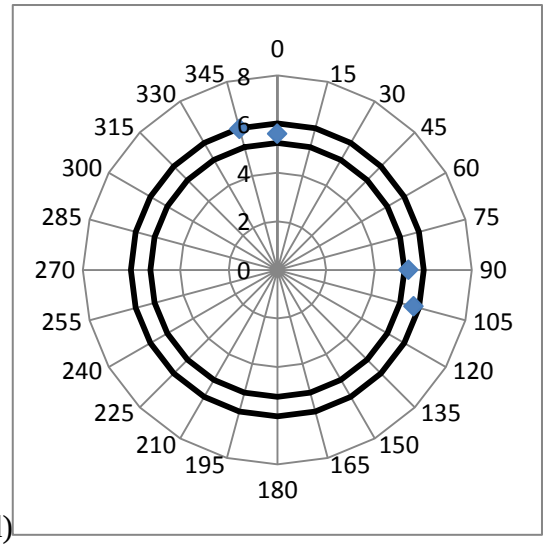
0
15
30
45
60
75
90
105
120
135
150
165
180
195
210
225
240
255
270
285
300
315
330
345
8
6
4
2
0

e)

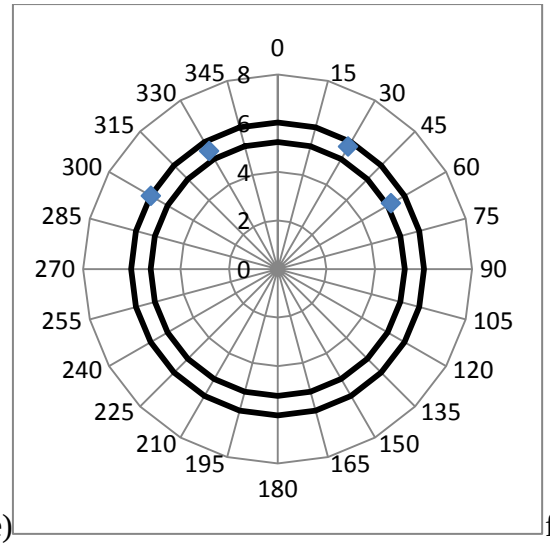

f)

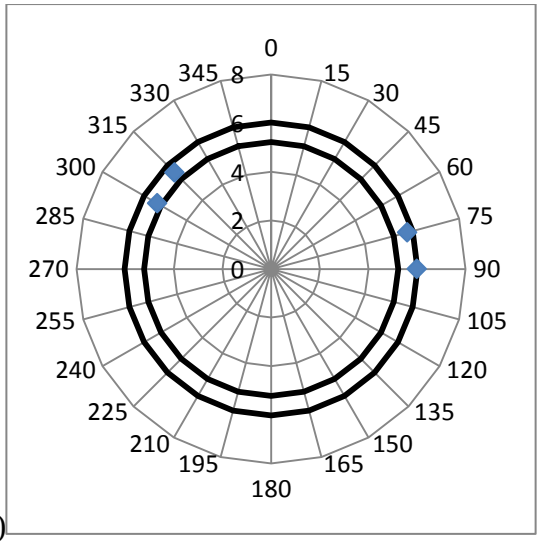

g)

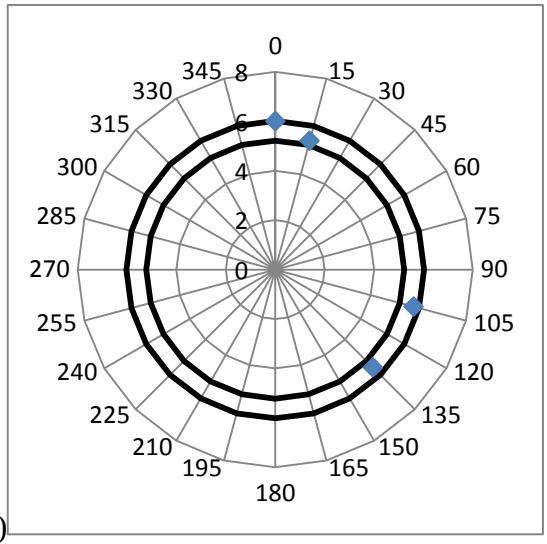

Figure 8.14: Seam locations for shafts a) 0-I, b) 0-II, c) 0-III, d) 30-I, e) 45-I, f) 45-II, and g) 45-III. The area between the black lines is the shaft wall, the radial component of the graph refers to the orientation around the circumference and the radar axis shows the distance from the centre point (mm).

Table 8.4: Summary of seam size and location in the seven fabricated shafts.

	Position of Seam (°)				Average Seam Area (μm^2)
	1	2	3	4	
0-I	0	165	180	345	/
0-II	150	165	225	240	/
0-III	0	240	255	345	/
30-I	0	90	105	345	0.032
45-I	30	60	300	330	0.085
45-II	75	90	300	315	0.054
45-III	0	15	105	135	0.056

8.2. The Stiffness Variation of Fabricated Shafts

As the shaft variation has been analysed optically, then any variation in mechanical properties around the circumference can be compared to the microstructure in the same location.

Figure 8.15 shows the stiffness of all fabricated shafts as a function of the orientation around the circumference. Firstly it is apparent that there is reasonable consistency between shafts of the same orientation (further details to follow). Using the model proposed in Chapter 6, predicted modulus values were obtained for each lay-up. Shaft stiffness was then predicted by using Equation 8.1.

$$Stiffness = \frac{3EI}{L^3},$$

Equation 8.1

where E is the modulus obtained from the model, I is the second moment of area and L is the cantilever length at which the shaft was tested.

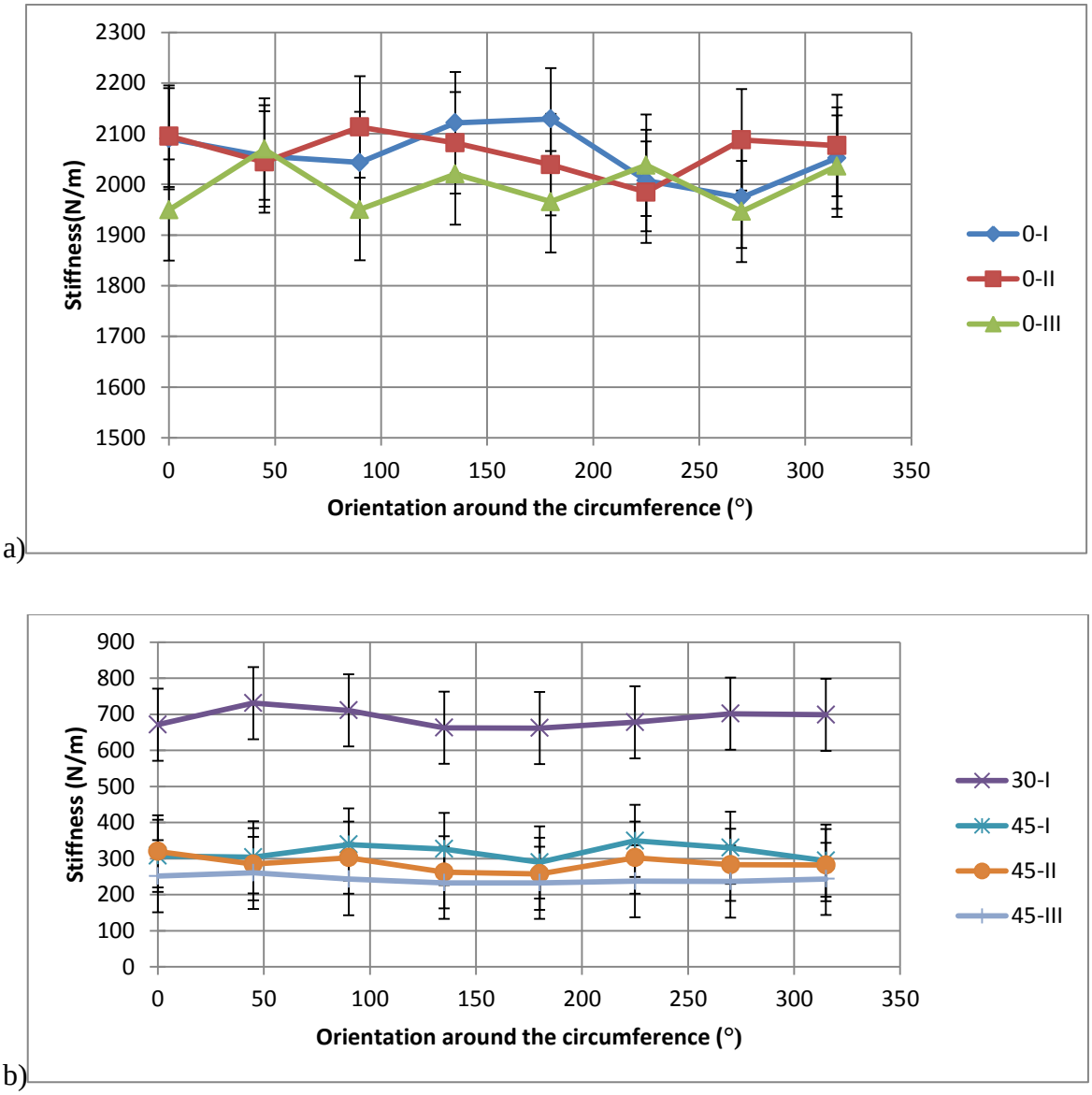

Figure 8.15: Stiffness (N/m) variation around the circumference of all fabricated shafts.

Figure 8.15 shows the stiffness variation around the circumference for all the shafts tested. Shaft 0-I shows a significant drop of about 5 % in the location of the crack (230°). Overall it appears that seams do not have a significant effect (within experimental error) on the stiffness

around the shaft. This can be attributed to several factors. The three 0° shafts showed that, at the position where a ply finishes, little or no resin-rich region could be seen, therefore although the fibres have moved to fill the void, a more uniform volume fraction of fibres could be seen through the cross-section. The 30° and 45° shafts both contained resin-rich regions (both as seams and as inter-ply RRR) and, as such, their properties should be dictated by this. However the difference in modulus between pure resin and the 30 and 45° plies is relatively small when compared to that of a 0° ply (see Chapter 3.2), and it is this discrepancy between the plies modulus and that of the resin which (along with its geometry) defines the severity of the change in mechanical properties around the shaft. The off-axis nature of the 30 and 45° shafts will also act to distribute the load around the shaft, and thus only passing over the seam, rather than travelling along it.

Referring to Figure 8.16, there is very good agreement between the predicted and average experimental results for these shafts in terms of stiffness. The modulus value was obtained by assuming that the shaft was a flat panel, with a lay-up twice the thickness of that of the shaft wall and symmetric about the centre plies. For example, the 30° shaft was input as [30 -30 30 -30 -30 30 -30 30].

The problem with this approach is that this does not take into account the three-dimensional space in which the fibres are orientated and treats fibre orientation as a two-dimensional variable. This can be seen in Figure 8.16 and Figure 8.18 where the off-axis fibre at 0° is orientated in the x-y plane (as modelled), however at 90°around the circumference the fibre is now in the x-z plane (not modelled). This is not a consideration when dealing with isotropic materials such as metallics as there is no difference in mechanical properties in the different planes. It does seem however, that the model still agrees well within the accuracy of the component data. This is likely to be attributed to the fact that at the point of greatest

misorientation of the fibre (at 90 and 270° when in bending) these points lie along the neutral axis and thus have very little effect on the overall stiffness, and at 0 and 180° (the greatest influence on stiffness), the fibres are orientated in the correct plane (x-y), and therefore the shaft's overall characteristic will represent these closer.

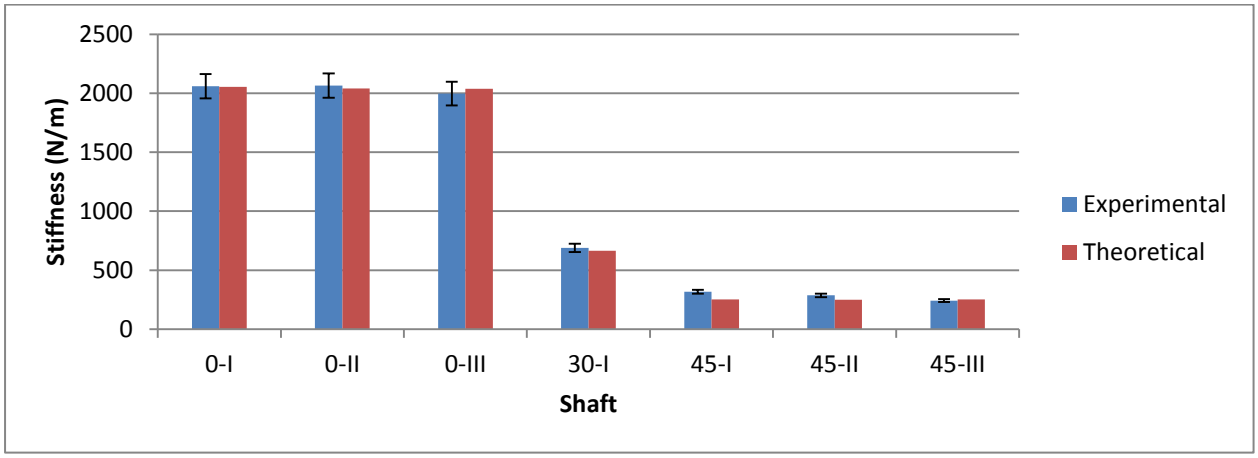

Figure 8.16: Experimental and predicted stiffnesses for all fabricated shafts.

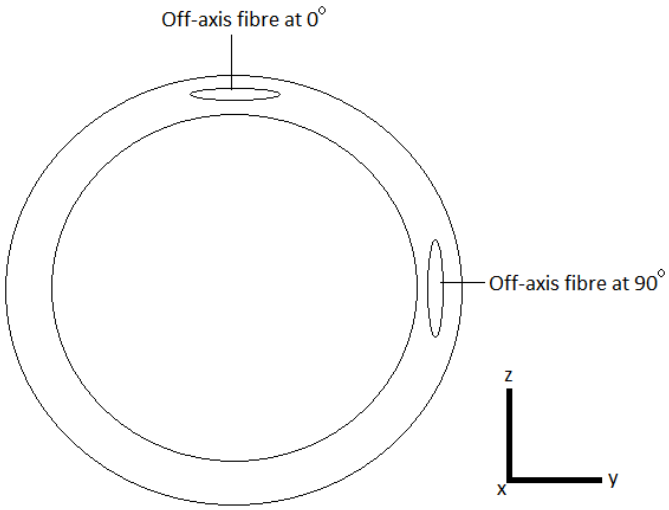

Figure 8.17: Schematic diagram showing the mis-orientation of fibres around the circumference of a shaft.

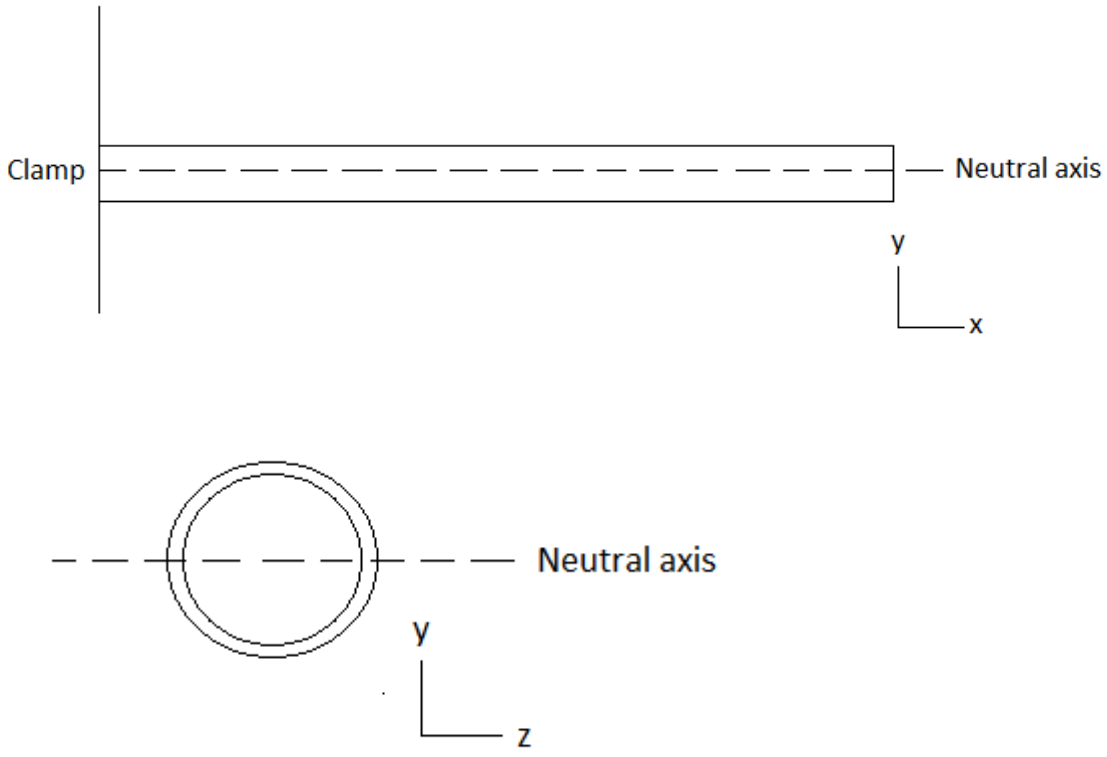

Figure 8.18: Schematic diagram showing the neutral axis of a shaft bending in the y axis from a) side view and b) cross-section view.

Composite analysis not carried out using finite element modelling (FEM) uses this same basis, namely simple beam theory [92, 114]. After the stacking sequence has been determined, the ***D***-matrix (the flexural stiffness matrix derived from the stacking sequence) is calculated and the modulus is obtained. The modulus is simply multiplied by the shape factor to get an overall bending stiffness (assuming pure bending, which is reasonable due to the large length/thickness ratio of the shaft [105]). This is treating the stacking sequence as a single solid anisotropic material [66]. However, it has presented here that the error involved in using this technique is quite small as the model still predicts accurately. It should be noted that this may not still hold true for tapered shafts.

8.3. The Damping Variation of Fabricated Shafts

Figure 8.19 shows the variation in loss factor with position around the shaft circumference for all the shafts tested. It can be seen that there is less difference between the 0° and 45° shafts for damping than was seen for stiffness. It can also be seen however, that shafts of similar lay-up show a greater variation than was seen for stiffness.

Shafts 0-II and 0-III both have a very sinusoidal shape to their loss factor curves. This clearly shows the influence of the seams. Shaft 0-II has seams in the region of about 150° and 230°, and as such symmetry suggests that this will also affect 45° and 345°. This can be seen clearly as the seams double the damping in that region. This can also be seen in shaft 0-III where seams were present at 0° and 250° and therefore will also affect 180° and 70°, clear peaks in damping can be seen in these regions. The shaft 0-I shows a much higher damping than the other two 0° shafts, which is most likely to be caused by the crack, as motion of any kind would generate high frictional losses at such a point, the effect of which would not necessarily be localised to that area. In the range 220° to 315° there is a noticeable increase in damping (crack position was approximately 230°).

The 30° and 45° shafts show no loss factor dependence on seam location. The shaft 45-III seems to have up to a 50 % greater damping than the other two 45° shafts. There are no appreciable differences in microstructure beyond a much larger RRR between all the plies (Table 8.2 and Table 8.3) and as such it is reasonable to attribute this change in damping to the size of this region (a correlation between inter-ply RRR and average loss factor can be seen in Table 8.5), although this may not decrease the stiffness by a noticeable amount.

Table 8.5: Average loss factor for the fabricated shafts, with measurements of excess resin regions.

Shaft	Average Loss Factor (η)	Maximum width of inter-ply RRR (μm)*	Average Seam Area (mm^2)
0-I	0.008	12	/
0-II	0.005	10	/
0-III	0.006	10	/
30-I	0.0065	26	0.032
45-1	0.0077	28	0.085
45-II	0.01	36	0.054
45-III	0.013	57	0.056

Poor agreement can be seen between the predicted and experiment values of loss factor for the shafts (root mean square difference (RMSD) of 0.0026) with the greatest discrepancies being seen in the shafts 0-I and 45-III (Figure 8.20), and the reason for this has been covered previously. However, the model does not sufficiently predict the loss factor of all the remaining shafts, with model consistently under estimating the damping of the shaft, as the model has no feature to compensate for the effect of seam. If only the loss factor values away from the seams were compared to the value obtained from the model (trough values), Figure 8.21, then the experimental and theoretical agree much better (RMSD of 0.0003) excluding shafts 0-I and 45-III.

a)

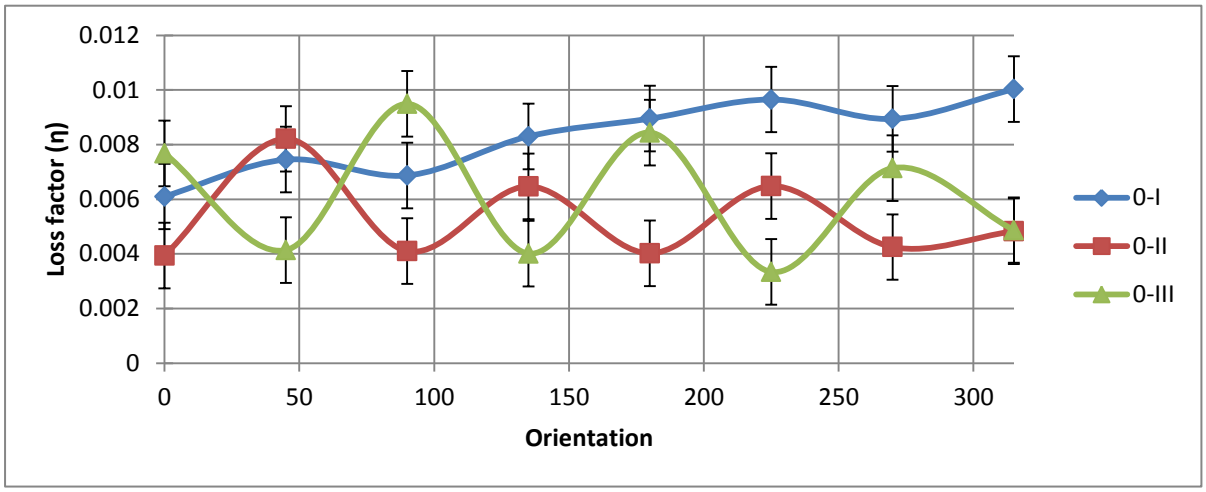

b)

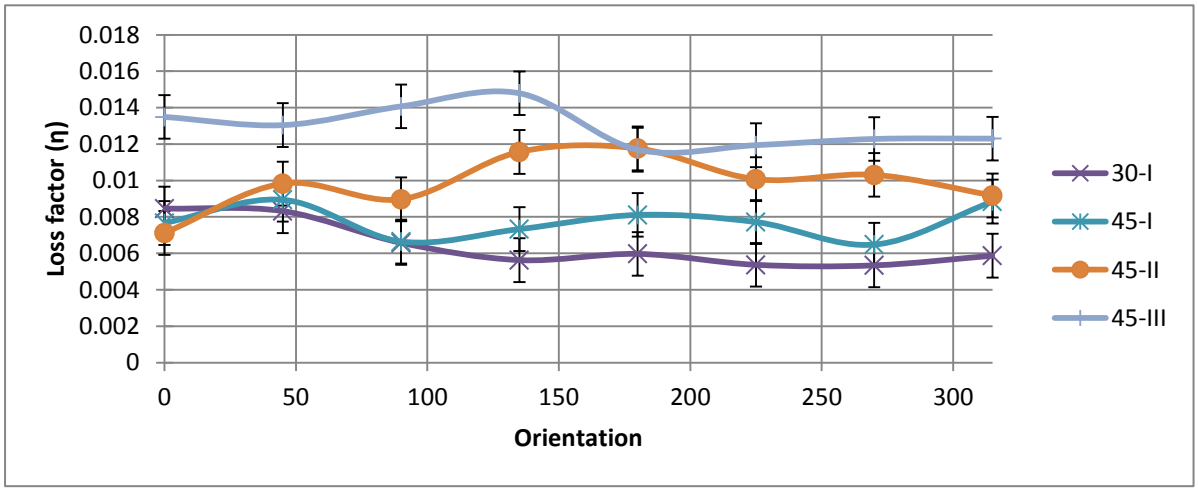

Figure 8.19: Loss factor (η) variation around the circumference for all fabricated shafts.

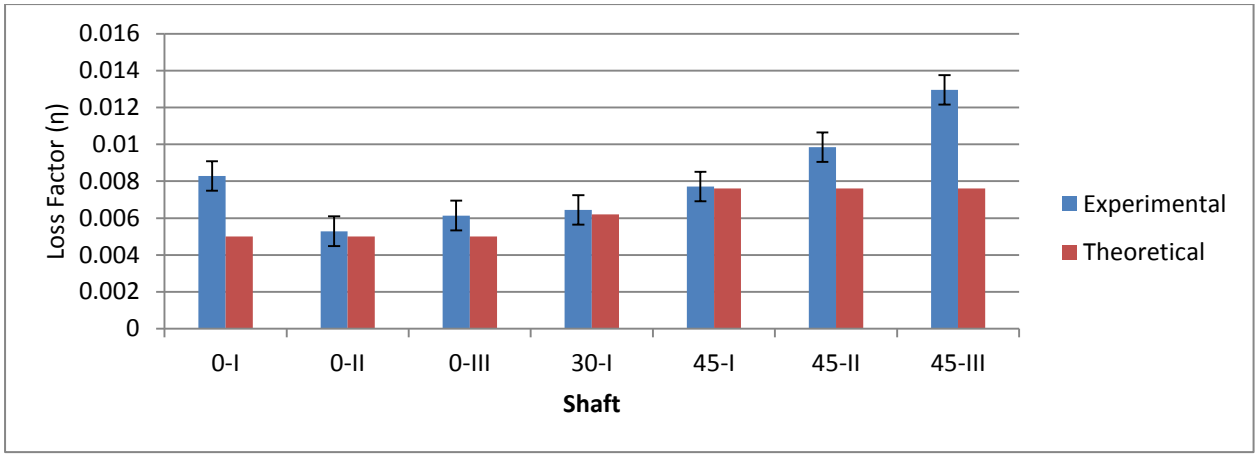

Figure 8.20: Experimental and predicted loss factor for all fabricated shafts.

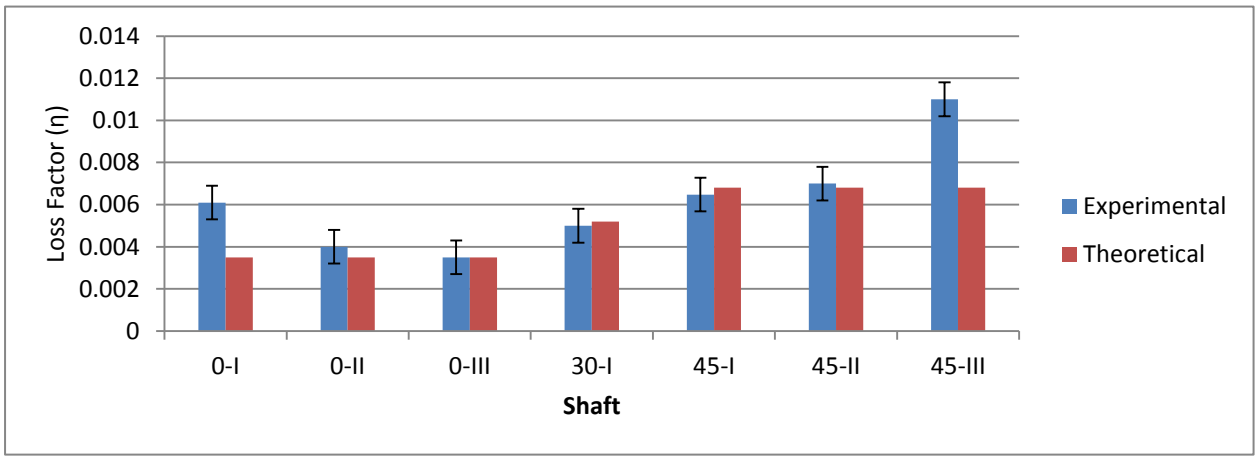

Figure 8.21: Experimental and predicted loss factor for all fabricated shafts neglecting the seam.

8.4. The Influence of Seams

As it has been stated above, the stiffness profile around the shafts' circumference showed that seams showed very little change (< 5%) however the presence of seams resulted in discrepancies in predicting the damping of the shafts.

Table 8.6 shows the variation of the nominal damping and stiffness around the shaft. All stiffness variations fell within a 5% range, however the variation is damping is much greater. It can also be seen that the 0° shafts showed a much greater variation due to the seams. Figure

8.22 shows how the nominal stiffness and damping changes around the circumference of the shaft along with the position of the seams. This shows clearly the effect/presence of the seams. Shafts 0-II and 0-III show a large peak in damping in the areas of the seam. Stiffness varies very little in all shafts whether a seam is present or not compared to damping which shows up to 180% increase when a seam is present (Figure 8.23). It can also be seen that the off-axis orientated shafts show much less variation in both stiffness and damping around the shaft (Table 8.7 and Figure 8.22e-g), due to both modulus and damping showing similar properties in the a 45° ply and pure resin, compared to that of a 0° ply. The off-axis fibres of a 45° ply are also likely to divert the load away from the seams, giving a more uniform distribution around the shaft.

Shafts 0-II and 0-III both show a prominent effect of the seams on damping, by comparing these two shafts in Figure 8.22 it can be seen that the seams line up very well with the points of highest damping, it can also be seen that the seams have an effect both on top and underneath the shaft (tension and compression) whilst it is being loaded in bending, but there seems a slight increase in the damping when the seam is in compression. This is due to the high losses during buckling of the polymer chains during compressive loading, rather than the recoverable stretching exhibited in tension, although rotation on pendant groups is still present in both [115].

Table 8.6: The variation of the nominal stiffness and damping around the circumference for all shaft lay-ups

Shaft lay-up	Variation in nominal damping (RMSD)	Variation in nominal stiffness (RMSD)
0°	0.28	0.02
±30°	0.18	0.03
±45°	0.11	0.05

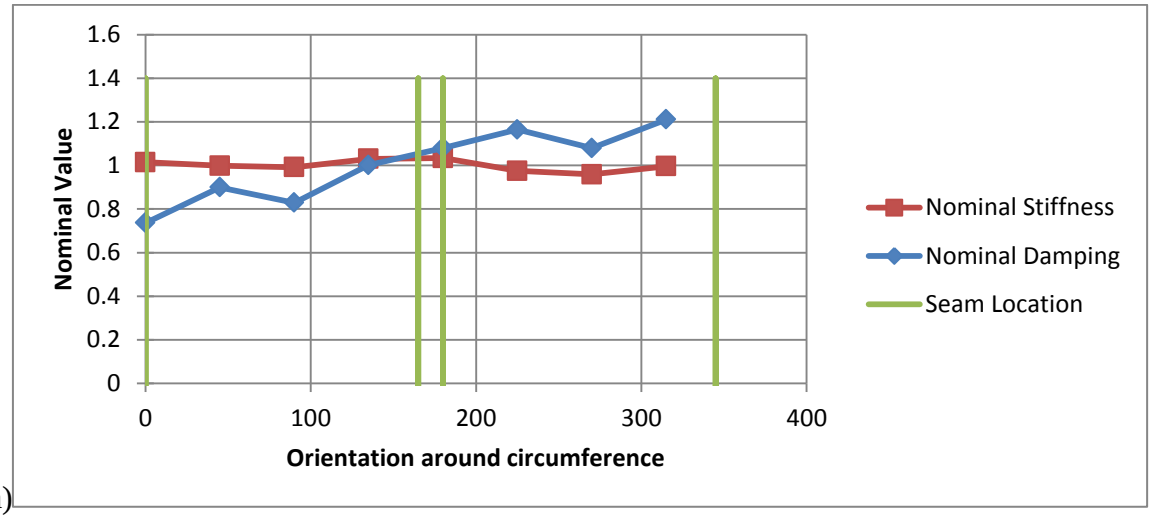

a)

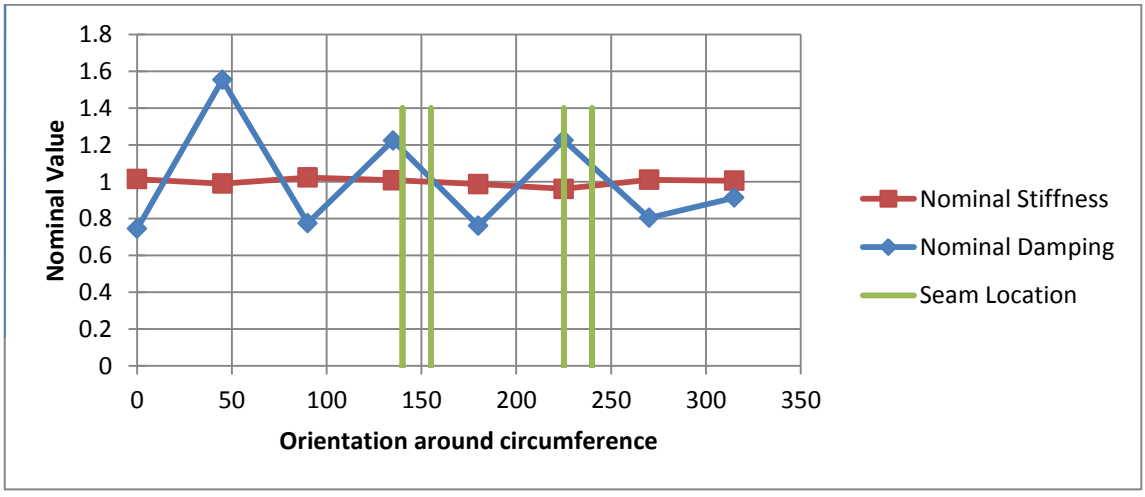

b)

c)

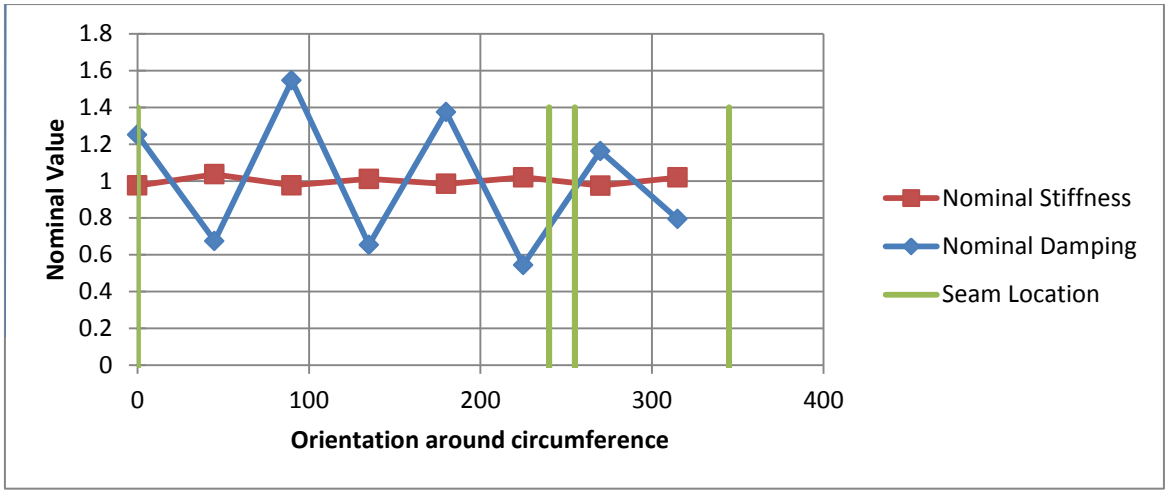
1.8
1.6
1.4
1.2
1
0.8
0.6
0.4
0.2
0
Nominal Value
0
100
200
300
400
Orientation around circumference
Nominal Stiffness
Nominal Damping
Seam Location

d)

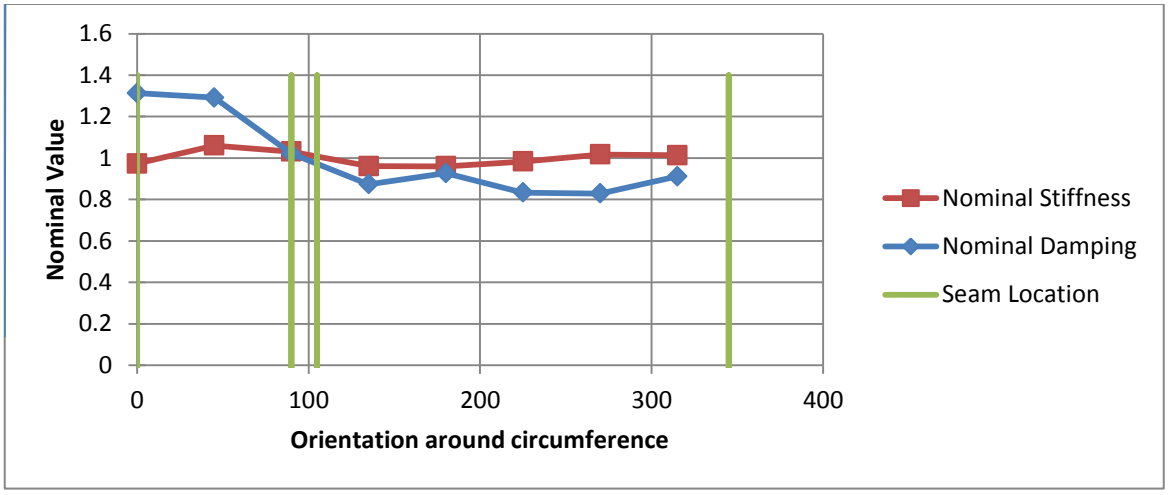
1.6
1.4
1.2
1
0.8
0.6
0.4
0.2
0
Nominal Value
0
100
200
300
400
Orientation around circumference
Nominal Stiffness
Nominal Damping
Seam Location

e)

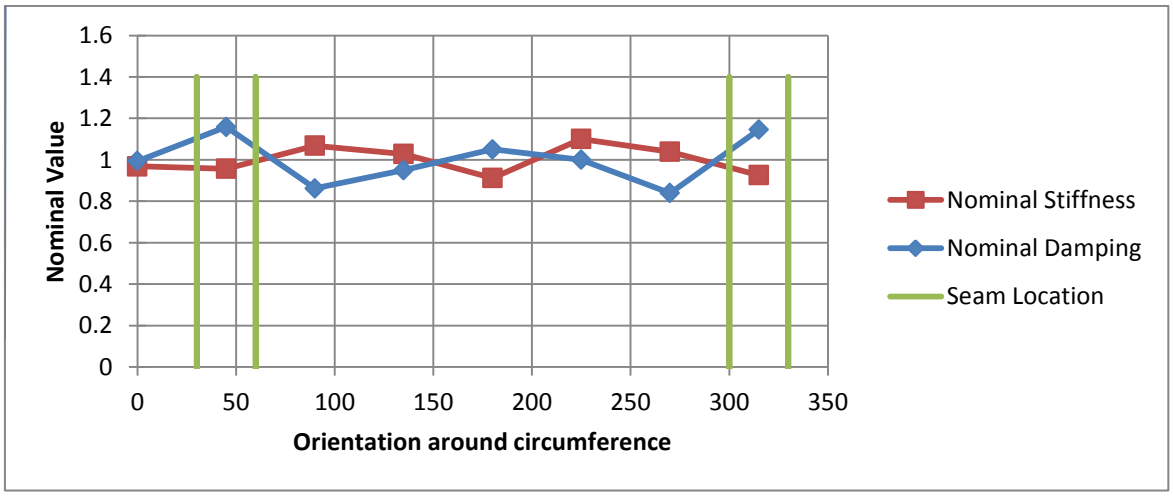
1.6
1.4
1.2
1
0.8
0.6
0.4
0.2
0
Nominal Value
0
50
100
150
200
250
300
350
Orientation around circumference
Nominal Stiffness
Nominal Damping
Seam Location

f)

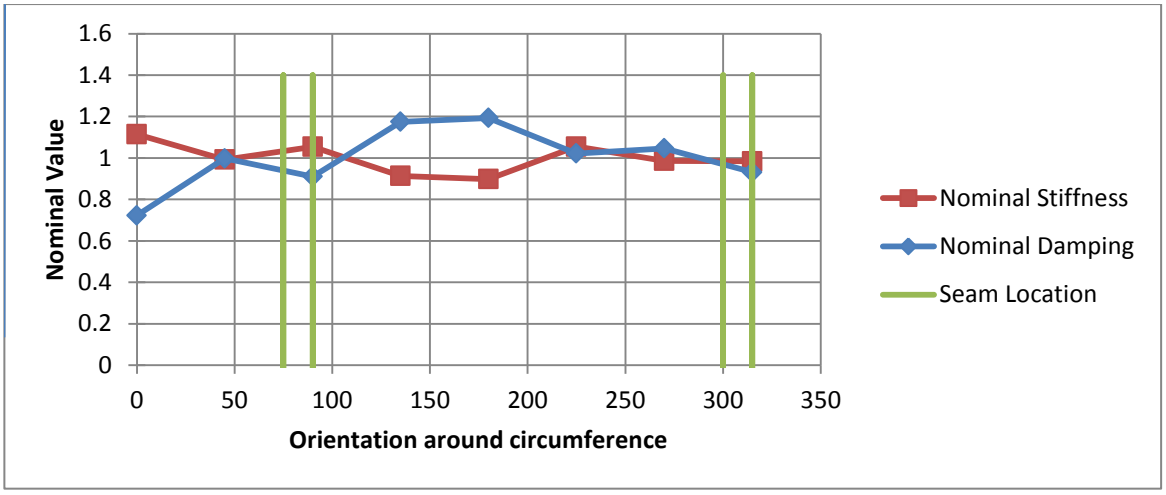

g)

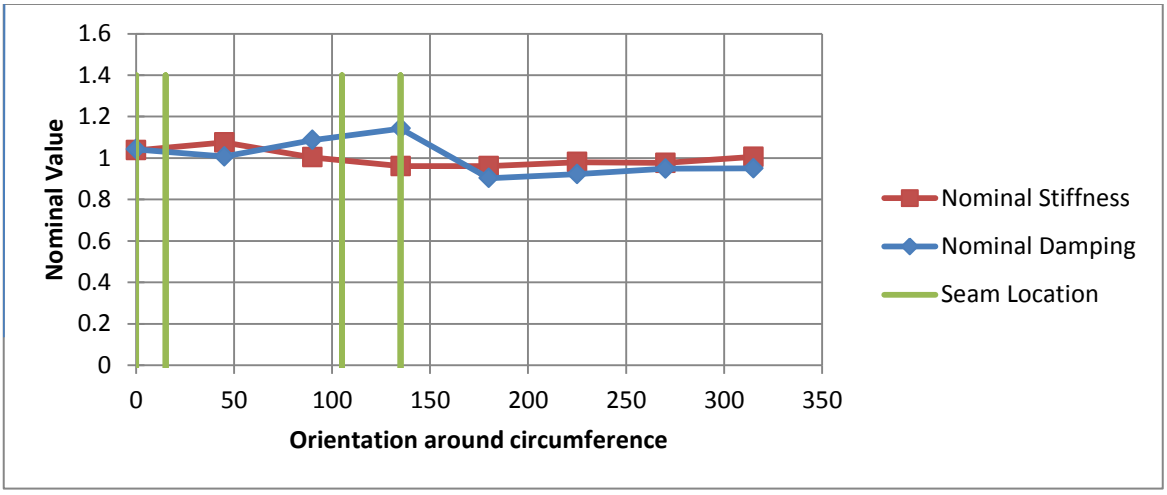

Figure 8.22: Radial charts showing the nominal stiffness (red line) and nominal damping (blue line) around the circumference of the shaft for a) shaft 0-I, b) shaft 0-II, c) shaft 0-III, d) shaft 30-I, e)shaft shaft 45-I, f) shaft 45-II and g) shaft 45-III.

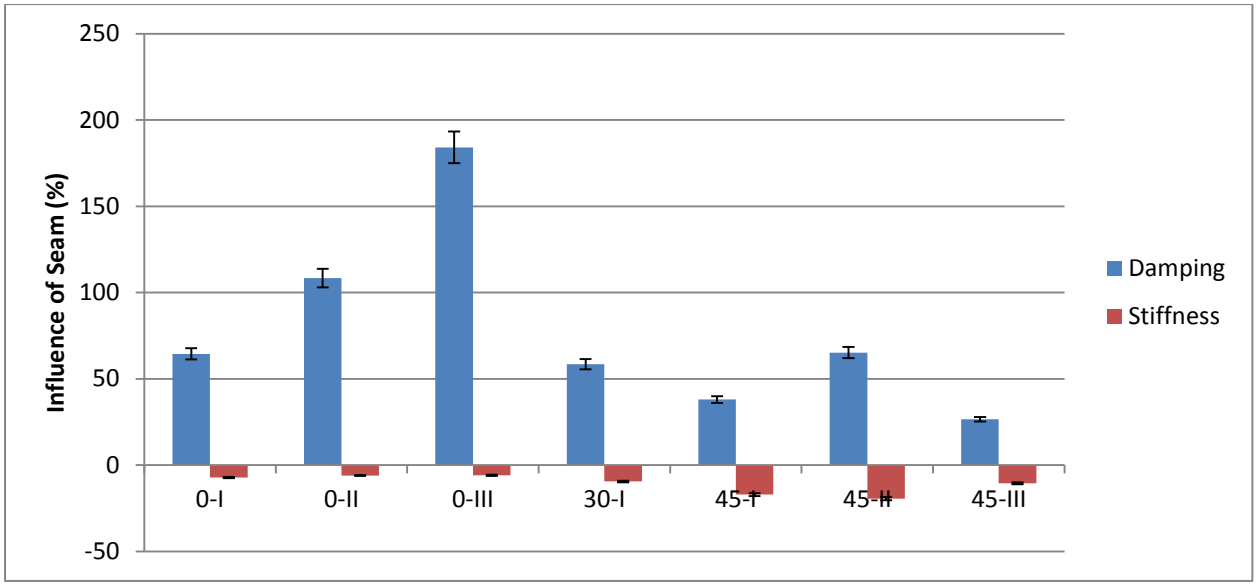

Figure 8.23: Average change in mechanical properties due to the presence of a seam (average peak/trough change)

In order to clearly understand the effects of the seam, an 8 ply panel of 0° orientation was fabricated with a 2 ply drop off seam along the loading axis. It has to be pointed out that this is an over-exaggerated situation and very rarely will shafts exhibit a 2 ply drop off (Figure 8.24).

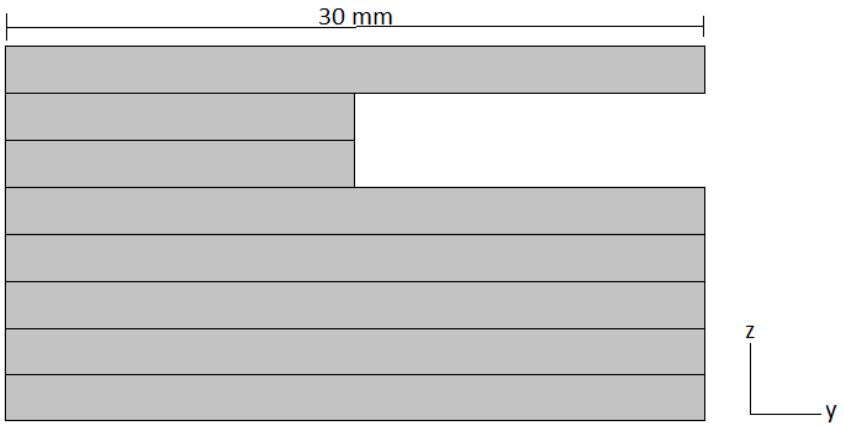

Figure 8.24: Schematic diagram of panel fabricated with a seam.

From Table 8.7 and Figure 8.25 it can be seen there is a large difference between the stiffness and damping of a seamed and non-seamed panel. The stiffness however falls between the expected values of an 8 and 6 ply panel, so the stiffness loss seems to be attributed to the loss of thickness. This however cannot be said for damping. Both a 6 and 8 ply panel would show the same loss factor for a balanced unidirectional composite. It is evident however that by introducing a seam the loss factor increases by more than double, showing that the excess resin greatly increases damping while having less of an effect on the stiffness. Although the presence of a seam has been shown to change the damping in CFCs, quantification of these defects in order to accommodate them in the model would be difficult without FEM due to varying sizes and contribution to the overall mechanical properties, as seen throughout this chapter.

The position of the seam was also investigated and shows that having the seam on the compressive side during bending will show a reduced effect compared to having the seam in tension. Mujika et al. (2006) [62] compared the compressive and tensile modulus of a carbon/carbon composite in bending, finding up to a 5 % difference between the two, with the tensile side being the stiffer. This suggests that having a resin-rich region on the tensile side of a beam would result in a greater reduction in stiffness than if it were on the compressive side, as has been shown in this research. This trend is likely to be attributed the tendency of micro-buckling in carbon fibre composites in compression [62, 76, 77].

Table 8.7: Comparison of the presence and location of a seam in a 0° panel.

Panel	**Damping (η)**	**Stiffness (N/m)**
No Seam	0.000773	51342
Seam Compression	0.001721	38036
Seam Tension	0.001567	28271

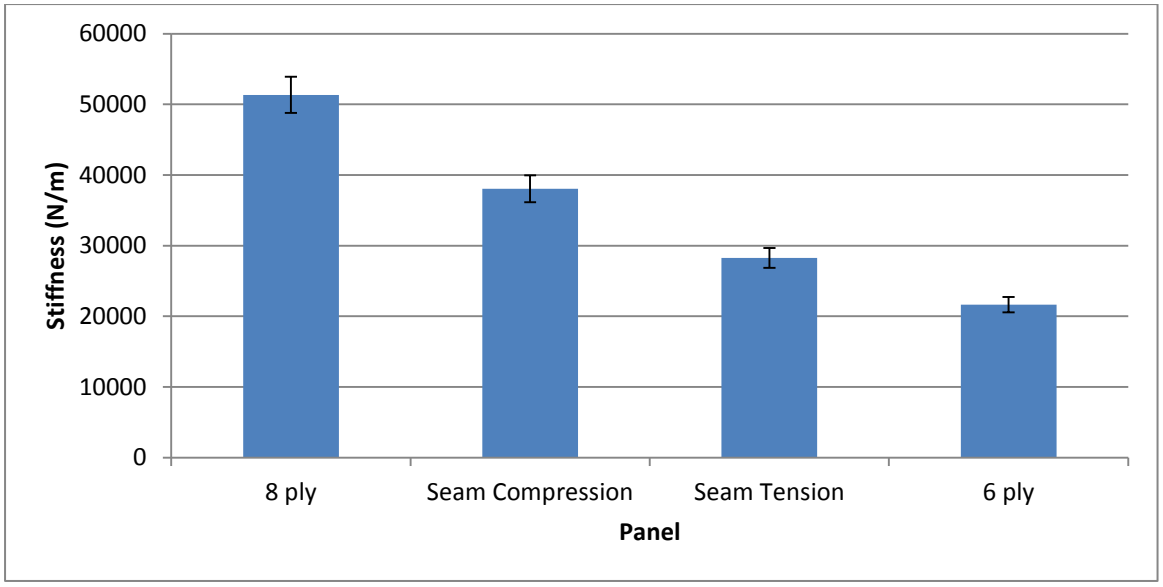

Figure 8.25: Stiffness comparison of seamed panels to an 8 and 6 ply panel.

8.5. Summary

This chapter has assessed the applicability of the proposed model from Chapter 6 on parallel-sided shafts of various lay-ups.

- Although the model predicts the shafts stiffness through taking the shaft lay-up as a flat panel, there is no noticeable difference between experimental and predicted stiffnesses.
- Damping showed a greater discrepancy with predicted values, although a better agreement could be seen when the areas which included a seam were neglected.

The 0° shafts showed a much greater influence of seams on damping, although stiffness was less sensitive to seam in all cases.

9. Conclusions

The primary purpose of this research was to find whether current testing of golf club shafts sufficiently characterises the dynamic performance of the shaft during a swing. Secondly, composite stiffness and damping performance was determined as a function of lay-up, defects and strain rate for flat panels and shafts both experimentally and by modelling. The following conclusions were found:

1. No noticeable change in modulus was seen at strain rates applicable to golf club shafts. All panels tested strain rate sensitivity onset occurred at around 0.4 s^{-1}. Panels which had 0° plies present showed no noticeable change in modulus over the whole range of strain rates tested (0.0001 – 1 s^{-1}).
2. The dependence on strain rate of the laminate (change in modulus/strain rate gradient) is strongly influenced by orientation and aspect ratio, with panels which show more fibre dependent properties showing a reduced dependence on strain rate. For panels with large values of θ, the panels' modulus is lower and is more matrix dependent, and as such will show greater strain rate dependence.
3. Two 20° panels of the same fibre interfacial area, but with different aspect ratios (length/width) showed different strain rate sensitivities. The short wide panel (aspect ratio 1.5) showed a higher stiffness and lower strain rate sensitivity when compared to a panel with an aspect ratio of 2.6.

4. No change in damping was seen through the range of strain rates applicable to golf club shafts. Although a clear dependence of damping on fibre orientation on damping was seen, strain rates up to 0.2 s^{-1} caused no noticeable change in the damping of the panels.
5. For strain rates applicable to golf club shafts no noticeable change in stiffness or damping could be seen for a range of flat panel laminates, suggesting that current quasi-static testing of a shaft is sufficient in characterising its dynamic performance.
6. Ni and Adams damping analysis (1984) was used to create software to predict and optimise modulus and damping. The model was validated against three composite systems at varying orientations and stacking sequences (data sets showed a RMSD of less than 5 %). The software agreed well with experimental data. The optimising software provides a stacking sequence that will optimise modulus, damping or modulus x damping.
7. Commercial shafts were tested for both stiffness and damping. Intra-batch variation in the form of relatively large scatter between shafts, with loss factor varying between 0.004 and 0.0095 at the tip was found.
8. The stiffness and damping of fabricated shafts was measured and compared to predictions from the model. The model accurately predicted the stiffness of the shafts however the model failed to predict the damping of the shafts when comparing to the average values taken. When damping was compared to the lower values measured the model agreed well except in two cases, which have been attributed to shafts' flaws (cracks or excess inter ply resin). This shows that although the damping can be predicted in areas of no seams,

the seam effects are so dominant that the overall shaft is unable to be predicted unless some function for the seam is introduced.

9. Seams increased damping by almost 200 % compared to decreasing the stiffness by no more than 18 %. This was found in a 0° shaft which has a greater difference in longitudinal modulus in areas with and without fibres. This shows damping is more sensitive to such defects than stiffness.
10. Both the interply resin-rich region (RRR) and average seam size increased with increased fibre orientation from the loading axis in the fabricated shaft. The 0° shaft showed almost no measurable seams and an interply RRR similar to that found in a flat panel, however off-axis shafts showed a resistance to being wrapped around the mandrel and a greater interply RRR was seen.
11. Panels fabricated with a seam present showed that, although the stiffness value falls between the predicted values for the thickness of the two halves, damping almost doubled due to the defect. It was also shown that the seam had a greater effect when in tension than compression.

10. Future work

1. The effect of seams needs to be fully understood in order to put them into a model. Therefore the affect of orientation and shaft diameter on seam size needs to be investigated. This will need to be carried out as a flat panel, much the same as the research presented here. This is likely to need Finite Element Modelling (FEM) based on the presented model.

2. The work that has been presented has investigated parallel-sided shafts and does not entirely represent a tapered golf shaft. Tapering by means of altering outer diameter and/or wall thickness introduces other factors which will change the stiffness profile along the length of the shaft, as seen in the commercial shafts.
    a. Having a mismatch of plies at either end of the shaft means that ply drop off is present. The means by which the load is transferred may result in an increase in damping due to the reduced amount of continuous fibres from tip to butt.
    b. Changing the diameter at a single end of the shaft changes the basis of the co-ordinate system used. So, although the transfer from flat panel to tube showed no noticeable problems with modelling, the move to tapered shafts needs to be validated as well. This is because the tube showed characteristics similar to the panels i.e. the areas of critical influence (top and bottom surface of the tube) essentially show the same orientation as in a flat panel, however if the shaft is then tapered, defining a 0° fibre would indeed be 0° when using the x-y plane used for the panels, but it will show an offset in the z-axis by the angle of taper of the shaft.

3. Once points 2a and b have been addressed, this will allow for the tailoring of shafts. Producing shafts with the same stiffness and mass but with varying damping properties, allowing beginners and the elderly to play more comfortably and for longer. This can be achieved by altering lay-up down the shaft and introducing plies to influence the stiffness, damping and kick point in areas which directly control these attributes.

4. Hybrid shafts (part metallic - part composite) have started coming into the market and although the model presented can cope with metallic materials, the interface between the two is yet to be characterised. The effect is likely to be similar to the ply drop off effect mentioned in point 2a but on a greater scale if not investigated thoroughly.

11. Appendix A

11.1. Analysis of Unidirectional Composites

```
v1=zeros(90,4);
v2=zeros(90,4);

for X=1:1:90;
T=[X -X];

Mat=3;

MaterialData=zeros(4,7); % (E1, E2, v12, G12, Eta1, Eta2, Eta12)
MaterialData(1,1:end)=[165E9,3E9,0.3,6E9,0.0062,0.0145,0.007]; %T800H-MTM28-
1.
MaterialData(2,1:end)=[185E9,6E9,0.3,6E9,0.0008,0.0078,0.0024]; %T800-VTM264.
MaterialData(3,1:end)=[60E9,10E9,0.3,10E9,0.0145,0.0145,0.0145]; %Adhesive
Film.
MaterialData(4,1:end)=[1,1,0,0,1,1,1]; %Air.

EL=(MaterialData(Mat,1))';
ET=(MaterialData(Mat,2))';
vLT=(MaterialData(Mat,3))';
GLT=(MaterialData(Mat,4))';
etaL=(MaterialData(Mat,5))';
etaT=(MaterialData(Mat,6))';
etaLT=(MaterialData(Mat,7))';


[R,P]=size(T);
t=0.000125;


S=(1:P/2).*t;
s=S-t;
w1=(S.^3)-(s.^3);
w2=fliplr(w1);
w=[w2 w1]; % weighting factor for panels in bending


% reduced stiffness matrix
Q1=EL/((EL-((vLT.^2).*ET))./EL);%(Q11)
Q2=(vLT.*ET)/((EL-((vLT.^2).*ET))./EL);%(Q12)
Q3=ET./((EL-((vLT.^2).*ET))./EL);%(Q22)
Q4=GLT;%(Q33)

m=cosd(T);
```

```
n=sind(T);
m2=m.^2;
n2=n.^2;
m3=m.^3;
n3=n.^3;
m4=m.^4;
n4=n.^4;

q=zeros(3,3);
q11=(Q1.*m4)+((2.*(Q2+(2.*Q4))).*n2.*m2)+(Q3.*n4);
q22=(Q1.*n4)+((2.*(Q2+(2.*Q4))).*n2.*m2)+(Q3.*m4);
q12=((Q1+Q3-(4.*Q4)).*n2.*m2)+(Q2.*(m4+n4));
q33=((Q1+Q3-(2.*Q2)-(2.*Q4)).*n2.*m2)+(Q4.*(m4+n4));
q13=((Q1-Q2-(2.*Q4)).*n.*m3)+((Q2-Q3+(2.*Q4)).*n3.*m);
q23=((Q1-Q2-(2.*Q4)).*n3.*m)+((Q2-Q3+(2.*Q4)).*n.*m3);


A=zeros(3,3);
A(1,1)=sum(q11.*t);
A(1,2)=sum(q12.*t);
A(1,3)=sum(q13.*t);
A(2,1)=A(1,2);
A(2,2)=sum(q22.*t);
A(2,3)=sum(q23.*t);
A(3,1)=A(1,3);
A(3,2)=A(2,3);
A(3,3)=sum(q33.*t);

a=inv(A);

D=zeros(3,3);
D(1,1)=sum(q11.*w);
D(1,2)=sum(q12.*w);
D(1,3)=sum(q13.*w);
D(2,1)=D(1,2);
D(2,2)=sum(q22.*w);
D(2,3)=sum(q23.*w);
D(3,1)=D(1,3);
D(3,2)=D(2,3);
D(3,3)=sum(q33.*w);
D=D./3;
d=inv(D);


x1a=((q11.*d(1,1))+(q12.*d(1,2))+(q13.*d(1,3))).*((m2.*d(1,1))+(m.*n.*d(1,3))
).*m2.*etaL.*w;
x1b=(sum(x1a))/2;
x1c=2/(d(1,1)*3)*x1b;

x2a=((q11.*d(1,1))+(q12.*d(1,2))+(q13.*d(1,3))).*((n2.*d(1,1))-
(m.*n.*d(1,3))).*n2.*etaT.*w;
x2b=(sum(x2a))/2;
```

```
x2c=2/(d(1,1)*3)*x2b;

x3a=((q11.*d(1,1))+(q12.*d(1,2))+(q13.*d(1,3))).*((2.*m.*n.*d(1,1))-((m2-
n2).*d(1,3))).*m.*n.*etaLT.*w;
x3b=(sum(x3a))/2;
x3c=2/(d(1,1)*3)*x3b;


Eta=(x1c+x2c+x3c)
Static_Flexural_Modulus_GPaL=((12/(((t*P)^3)*d(1,1))))/1000000000
Static_Flexural_Modulus_GPaT=((12/(((t*P)^3)*d(2,2))))/1000000000;
Static_Flexural_Modulus_GPaLT=((12/(((t*P)^3)*d(3,3))))/1000000000;
```

11.2. Database

```
MaterialData=[165E9,3E9,0.3,6E9,0.0062,0.0145,0.007]; %T800-VTM264.
EL=(MaterialData(1,1))';
ET=(MaterialData(1,2))';
vLT=(MaterialData(1,3))';
GLT=(MaterialData(1,4))';
etaL=(MaterialData(1,5))';
etaT=(MaterialData(1,6))';
etaLT=(MaterialData(1,7))';

Theta=-80:10:90;
P4=18^4;
P3=18^3;
P2=18^2;
P=18;

Matrix=zeros(7, P4);

L1(1,1:P3)=-80;
L1(1,(P3+1):(2*P3))=-70;
L1(1,((2*P3)+1):(3*P3))=-60;
L1(1,((3*P3)+1):(4*P3))=-50;
L1(1,((4*P3)+1):(5*P3))=-40;
L1(1,((5*P3)+1):(6*P3))=-30;
L1(1,((6*P3)+1):(7*P3))=-20;
L1(1,((7*P3)+1):(8*P3))=-10;
L1(1,((8*P3)+1):(9*P3))=0;
L1(1,((9*P3)+1):(10*P3))=10;
L1(1,((10*P3)+1):(11*P3))=20;
L1(1,((11*P3)+1):(12*P3))=30;
L1(1,((12*P3)+1):(13*P3))=40;
L1(1,((13*P3)+1):(14*P3))=50;
L1(1,((14*P3)+1):(15*P3))=60;
L1(1,((15*P3)+1):(16*P3))=70;
L1(1,((16*P3)+1):(17*P3))=80;
```

```
L1(1,((17*P3)+1):(18*P3))=90;

L2(1,1:P2)=-80;
L2(1,(P2+1):(2*P2))=-70;
L2(1,((2*P2)+1):(3*P2))=-60;
L2(1,((3*P2)+1):(4*P2))=-50;
L2(1,((4*P2)+1):(5*P2))=-40;
L2(1,((5*P2)+1):(6*P2))=-30;
L2(1,((6*P2)+1):(7*P2))=-20;
L2(1,((7*P2)+1):(8*P2))=-10;
L2(1,((8*P2)+1):(9*P2))=0;
L2(1,((9*P2)+1):(10*P2))=10;
L2(1,((10*P2)+1):(11*P2))=20;
L2(1,((11*P2)+1):(12*P2))=30;
L2(1,((12*P2)+1):(13*P2))=40;
L2(1,((13*P2)+1):(14*P2))=50;
L2(1,((14*P2)+1):(15*P2))=60;
L2(1,((15*P2)+1):(16*P2))=70;
L2(1,((16*P2)+1):(17*P2))=80;
L2(1,((17*P2)+1):(18*P2))=90;

L3(1,1:P)=-80;
L3(1,(P+1):(2*P))=-70;
L3(1,((2*P)+1):(3*P))=-60;
L3(1,((3*P)+1):(4*P))=-50;
L3(1,((4*P)+1):(5*P))=-40;
L3(1,((5*P)+1):(6*P))=-30;
L3(1,((6*P)+1):(7*P))=-20;
L3(1,((7*P)+1):(8*P))=-10;
L3(1,((8*P)+1):(9*P))=0;
L3(1,((9*P)+1):(10*P))=10;
L3(1,((10*P)+1):(11*P))=20;
L3(1,((11*P)+1):(12*P))=30;
L3(1,((12*P)+1):(13*P))=40;
L3(1,((13*P)+1):(14*P))=50;
L3(1,((14*P)+1):(15*P))=60;
L3(1,((15*P)+1):(16*P))=70;
L3(1,((16*P)+1):(17*P))=80;
L3(1,((17*P)+1):(18*P))=90;

L4=-80:10:90;

Matrix(1,1:end)=L1;
Matrix(2,1:end)=[L2 L2 L2 L2 L2 L2 L2 L2 L2 L2 L2 L2 L2 L2 L2 L2 L2 L2];
Matrix(3,1:end)=ones(1,324)*L3
Matrix(4,1:end)= ones(1,5832)*L4;


for T1=-80:10:90;
    for T2=-80:10:90;
        for T3=-80:10:90;
            for T4=-80:10:90;
```

```
T=[T1 T2 T3 T4];
[R,p]=size(T);
t=0.000125;
S=(1:p/2).*t;
s=S-t;
w1=(S.^3)-(s.^3);
w2=fliplr(w1);
w=[w2 w1]; % weighting factor for panels in bending


% reduced stiffness matrix
Q1=EL/((EL-((vLT.^2).*ET))./EL);%(Q11)
Q2=(vLT.*ET)/((EL-((vLT.^2).*ET))./EL);%(Q12)
Q3=ET./((EL-((vLT.^2).*ET))./EL);%(Q22)
Q4=GLT;%(Q33)

m=cosd(T);
n=sind(T);
m2=m.^2;
n2=n.^2;
m3=m.^3;
n3=n.^3;
m4=m.^4;
n4=n.^4;

q=zeros(3,3);
q11=(Q1.*m4)+((2.*(Q2+(2.*Q4))).*n2.*m2)+(Q3.*n4);
q22=(Q1.*n4)+((2.*(Q2+(2.*Q4))).*n2.*m2)+(Q3.*m4);
q12=((Q1+Q3-(4.*Q4)).*n2.*m2)+(Q2.*(m4+n4));
q33=((Q1+Q3-(2.*Q2)-(2.*Q4)).*n2.*m2)+(Q4.*(m4+n4));
q13=((Q1-Q2-(2.*Q4)).*n.*m3)+((Q2-Q3+(2.*Q4)).*n3.*m);
q23=((Q1-Q2-(2.*Q4)).*n3.*m)+((Q2-Q3+(2.*Q4)).*n.*m3);


A=zeros(3,3);
A(1,1)=sum(q11.*t);
A(1,2)=sum(q12.*t);
A(1,3)=sum(q13.*t);
A(2,1)=A(1,2);
A(2,2)=sum(q22.*t);
A(2,3)=sum(q23.*t);
A(3,1)=A(1,3);
A(3,2)=A(2,3);
A(3,3)=sum(q33.*t);

a=inv(A);

D=zeros(3,3);
D(1,1)=sum(q11.*w);
D(1,2)=sum(q12.*w);
D(1,3)=sum(q13.*w);
```

```
D(2,1)=D(1,2);
D(2,2)=sum(q22.*w);
D(2,3)=sum(q23.*w);
D(3,1)=D(1,3);
D(3,2)=D(2,3);
D(3,3)=sum(q33.*w);
D=D./3;
d=inv(D);


x1a=((q11.*d(1,1))+(q12.*d(1,2))+(q13.*d(1,3))).*((m2.*d(1,1))+(m.*n.*d(1,3))
).*m2.*etaL.*w;
x1b=(sum(x1a))/2;
x1c=2/(d(1,1)*3)*x1b;

x2a=((q11.*d(1,1))+(q12.*d(1,2))+(q13.*d(1,3))).*((n2.*d(1,1))-
(m.*n.*d(1,3))).*n2.*etaT.*w;
x2b=(sum(x2a))/2;
x2c=2/(d(1,1)*3)*x2b;

x3a=((q11.*d(1,1))+(q12.*d(1,2))+(q13.*d(1,3))).*((2.*m.*n.*d(1,1))-((m2-
n2).*d(1,3))).*m.*n.*etaLT.*w;
x3b=(sum(x3a))/2;
x3c=2/(d(1,1)*3)*x3b;
Eta=(x1c+x2c+x3c);
Static_Flexural_Modulus_GPaL=((12/(((t*p)^3)*d(1,1))))/1000000000;


Matrix(5,((((T1+80)/10)*P3)+(((T2+80)/10)*P2)+(((T3+80)/10)*P)+(((T4+80)/10))
+1))=Static_Flexural_Modulus_GPaL;
Matrix(6,((((T1+80)/10)*P3)+(((T2+80)/10)*P2)+(((T3+80)/10)*P)+(((T4+80)/10))
+1))=Eta;
Matrix(7,1:P4)=(Matrix(5,1:P4)).*((Matrix(6,1:P4)));

            end
        end
    end
    pause(0.00001)
    progressbar(T1/18);
end

save T800-VTM264.dat Matrix -ascii
```

11.3. Stacking Optimiser

```
Matrix=importdata(T800-VTM264.dat');
P4=18^4;
```

```
Matrix(8,1:P4)=0;

StackingList=zeros(P4,7);
Matrix(8,1:P4)=0;

for V1=1:1:P4

if ((Matrix(5,V1))>0) && ((Matrix(5,V1))<100);
    Matrix(8,V1)=1;
end

if Matrix(8,V1)==1;
    StackingList(V1,1:end)=[Matrix(1,V1), Matrix(2,V1), Matrix(3,V1),
Matrix(4,V1), Matrix(5,V1), Matrix(6,V1), Matrix(7,V1)];

end
pause(0.00001);
progressbar(V1/104976);
end

Stiff1=sortrows(StackingList,5);
Stiff2=flipud(Stiff1);

TopStiffness=Stiff2(1:20,1:end);


StackingList=zeros(P4,7);
Matrix(9,1:P4)=0;
for V1=1:1:P4

if ((Matrix(6,V1))>0) && ((Matrix(6,V1))<1);
    Matrix(9,V1)=1;
end

if Matrix(9,V1)==1;
    StackingList(V1,1:end)=[Matrix(1,V1), Matrix(2,V1), Matrix(3,V1),
Matrix(4,V1), Matrix(5,V1), Matrix(6,V1), Matrix(7,V1)];

end
end

Damp1=sortrows(StackingList,6);
Damp2=flipud(Damp1);

TopDamping=Damp2(1:20,1:end);


disp('Top Stiffness')
TopStiffness(1,1:4)
disp('Top Damping')
TopDamping(1,1:4)
```

12. Appendix B

a) 

b) 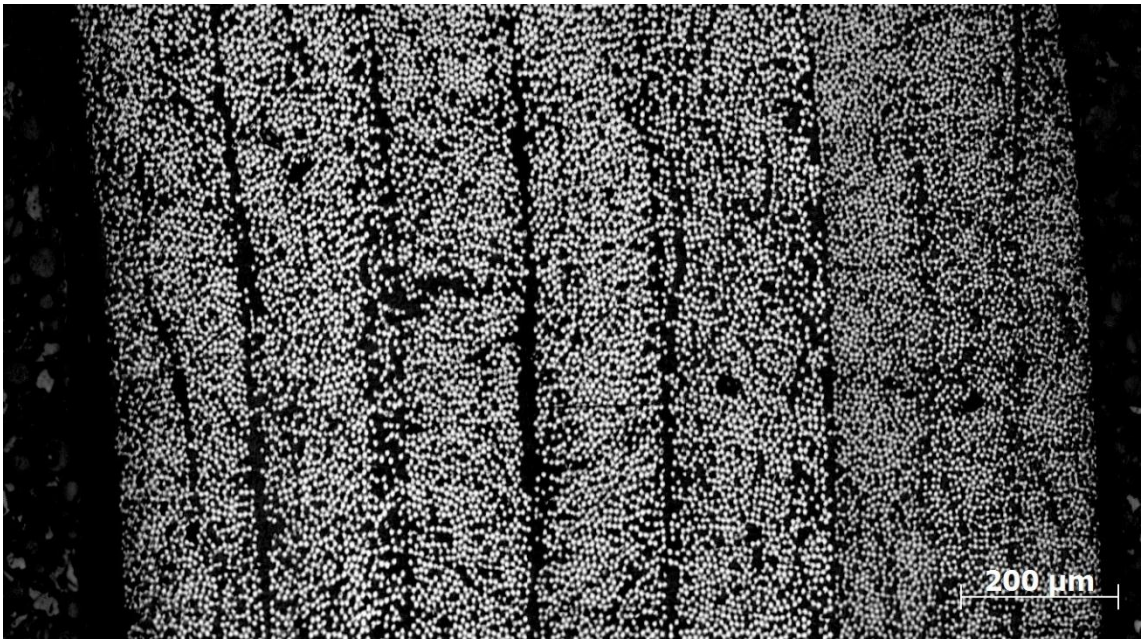

c) 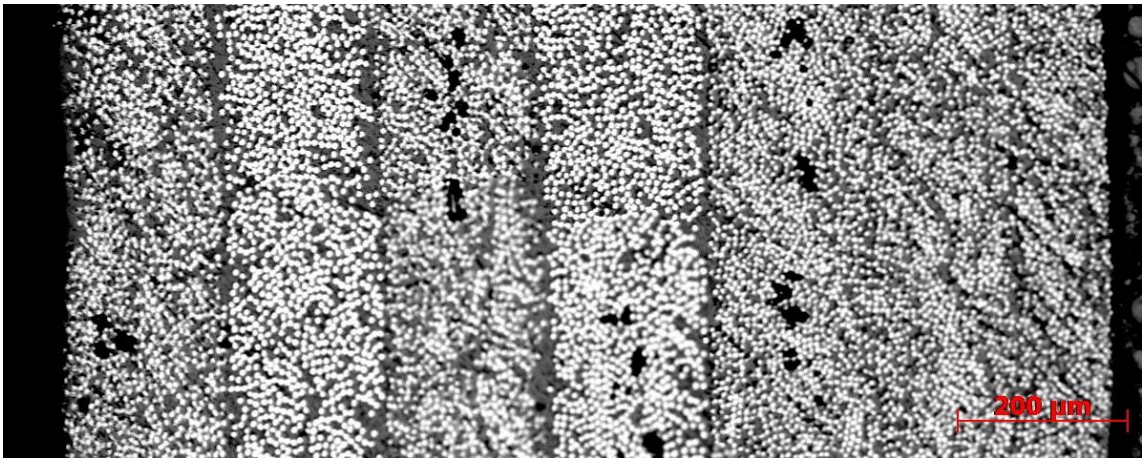

Figure 9.1: Through-thickness optical sections of the butt for shafts a) F2, b) F3 and c) F6.The outer surface of the shaft is at the right of the image.

a) 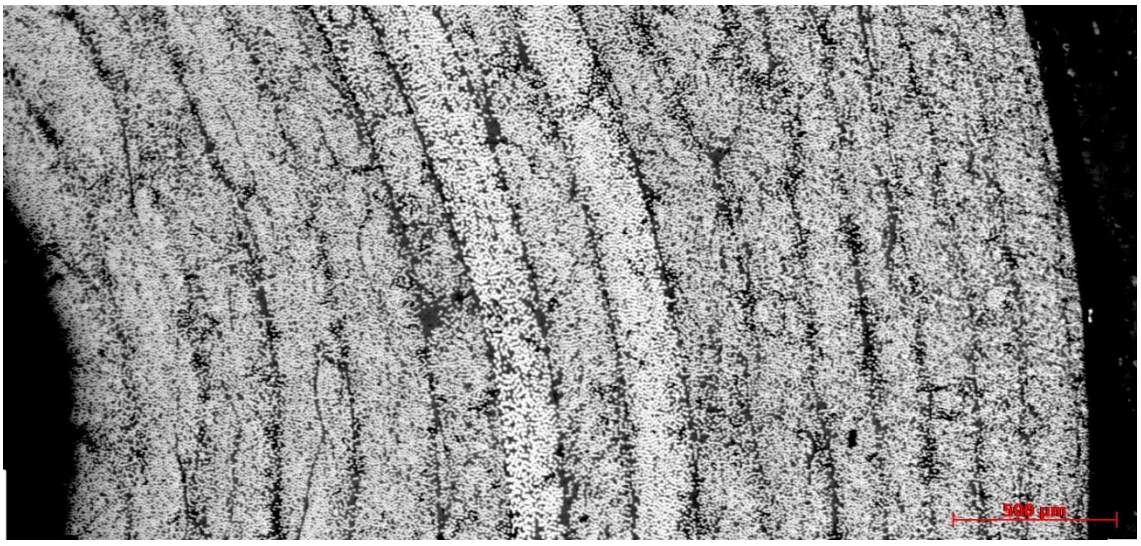

b)

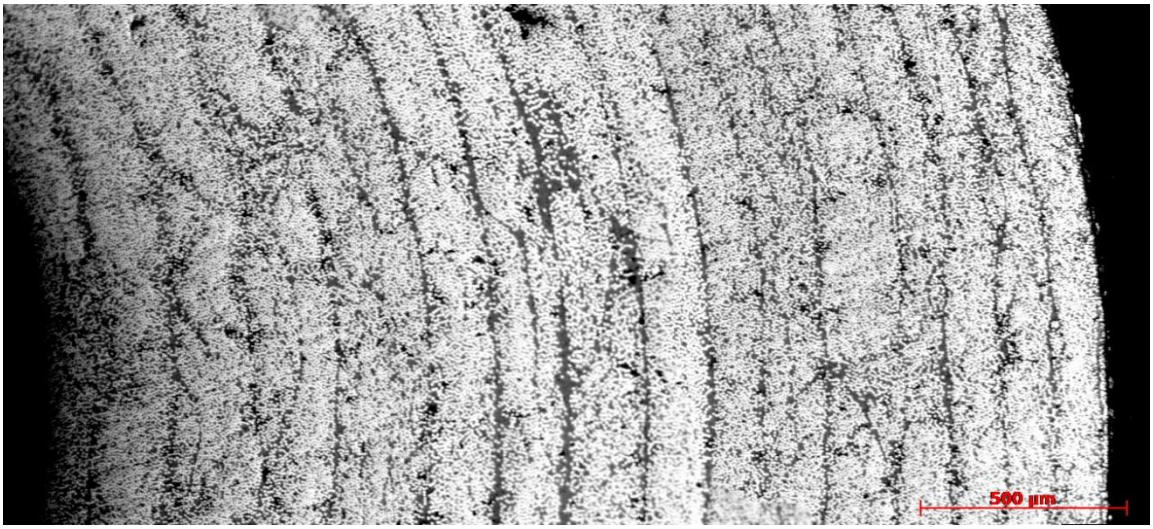

c)

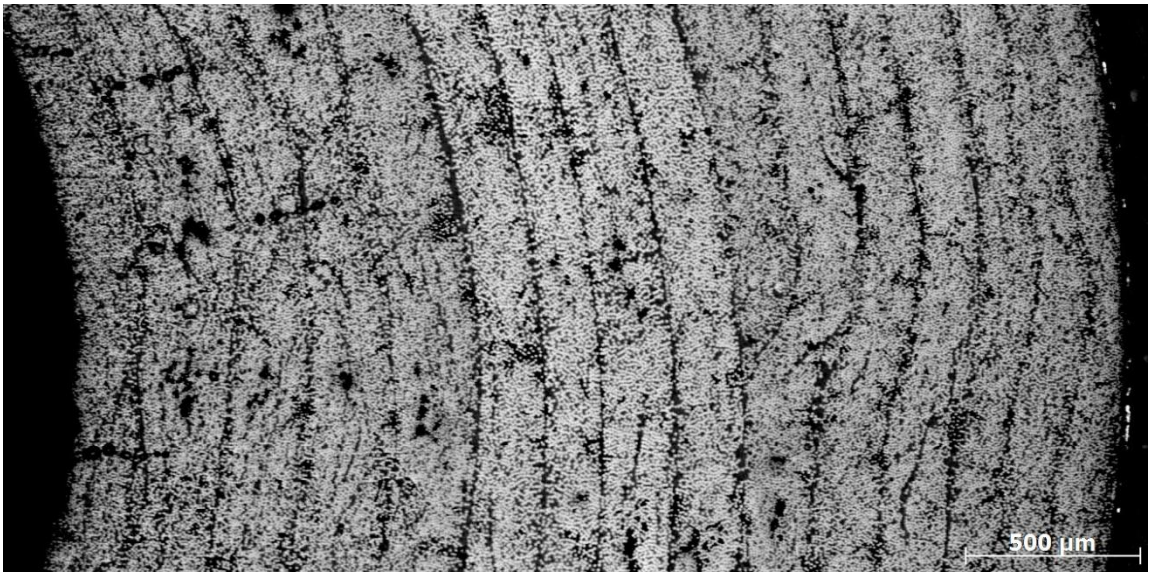

Figure 9.2: Through-thickness optical sections of the butt for shafts a) F2, b) F3 and c) F6.The outer surface of the shaft is at the right of the image.

13. References

1. Summitt, J., *The Modern Guide To Shaft Fitting*. 2 ed. 2000, Newark, Ohio: Dynacraft golf products, Inc. 110.

2. Hull, D., *An Introduction to Composite Materials*. 1981: Cambridge University Press. 242.

3. Hull, D. and T.W. Clyne, *An Introduction to Composite Materials*. 2nd Edition ed. 1996: Cambridge University Press.

4. Huntley, M., *Comparison of Static and Dynamic Carbon Fibre Composite Golf Club Shaft Properties and their Dependence on Structure (PhD thesis)*. 2007: University of Birmingham.

5. Huntley, M., C. Davis, M. Strangwood, and S. Otto, *Comparison of the static and dynamic behaviour of carbon fibre composite golf club shafts*, in *IMechE* 2006: Part L: J. Materials: Design and Applications.

6. *ASTM D 3039-00*, in *Standard test method for tensile properties of polymer matrix composite materials*. 2000, American Society for Testing and Matrials, West Conshohocken, PA. p. pp. 105-117.

7. Strangwood, M., *Equipment Technology - The Shaft*, in *The Proffessional Golfers' Association Trainee Dipoma Programme*. 2003, PGA: The Belfry.

8. Butler, H. and D. Winfield, *What shaft is best for you?*, in *Golf, The scientific way*, A. Cochran, Editor. 1995, Volvo: Hemel Hempstead.

9. Summitt, J., *Shaft Fitting Addendum*. 2004, Newark, Ohio: Dynacraft Golf Products, Inc.

10. Summitt, J., *2010 Shaft Fitting Addendum*. 2010, Newark, Ohio, Dynacraft golf products, Inc.: Hireko Golf.

11. Butler, J.H. and D.C. Winfield. *The Dynamic Performance of the Golf Shaft During the Downswing*. in *Science and Golf II*. 1994. St Andrews, Scotland: E & FN Spon.

12. Lee, N., M. Erickson, P. Cherveny, and Callaway-Golf-Company, *Measurement of the behaviour of a golf club during the golf swing*, in *Science and Golf IV*. 2002, Routledge publishing: St Andrews, Scotland. p. 374-386.

13. Horwood, G., *Flexes, Bend Points and Torques.*, in *Golf - the scientific way*, A. Cochran, Editor. 1995, Ashton Publishing Group: Hemel Hempstead. p. 103-108.

14. Newman, S., S. Clay, and P. Strickland. *The dynamic flexing of a golf club shaft during a typical swing*. in *Mechatronics and Machine Vision in Practice*. 1997.

15. Braunwart, P.R., *Experimental and Analytical Examination of Golf Club Dynamics (PhD Thesis)*. Department of Mechanical Engineering. 1998, Blacksburg, Virginia.

16. Friswell, M.I., J.E. Mottershead, and M.G. Smart, *Dynamic models of golf clubs.* Sports Engineering, 1998. **1**(1): p. 41-50.

17. Cheong, S.K., K.W. Kang, and S.K. Jeong, *Evaluation of the mechanical performance of golf shafts.* Engineering Failure Analysis, 2006. **13**: p. 464 - 473.

18. Brouillette, M., *On measuring the flexural rigidity distribution of golf shafts*, in *Science and Golf IV*, E. Thain, Editor. 2002, Routledge publishing: St Andrews, Scotland. p. 387-401.

19. Chou, A. and O.C. Roberts. *Golf shaft flex point - an analysis of measurement techniques*. in *Science and Golf II: Preceeding of the world scientific congress of golf*. 1994. St Andrews: E & FN Spon.

20. Wallace, E.S., S.R. Otto, and A. Nevill, *Ball launch conditions for skilled golfers using drivers of different lengths in an indoor testing facility*. Journal of Sports Sciences, 2007. **25**(7): p. 731 - 737.

21. Betzler, N., *The Effect of Differing Shaft Dynamics on the Biomechanics of the Golf Swing*. 2010, Edinburgh Napier University: Edinburgh.

22. Kenny, I., E. Wallace, D. Brown, and S. Otto, *Validation of a Full-Body Computer Simulation of the Golf Drive for Clubs of Differing Length*, in *The Engineering of Sport 6*, E.F. Moritz and S. Haake, Editors. 2006, Springer. p. 11-16.

23. Mizoguchi, M. and T. Hashiba, *Matching of the Shaft Length of a Golf Club to an Individual's Golf Swing Motion*, in *The Engineering of Sport 4*, S. Ujihashi and S.J. Haake, Editors. 2002, Blackwell Publishing. p. 695-700.

24. Wishon, T.W., *Modern shaft fitting - Combining flex and torque*, in *Golf, The scientific way*, A. Cochran, Editor. 1995, Volvo: Hemel Hempstead. p. 281.

25. R&A, *A Guide to the Rules on Clubs and Balls*. 2nd ed. 2005: The Royal and Ancient Golf Club of St Andrews and The United States Golf Association.

26. R&A, *Rules of Golf and the Rules of Amateur Status: 2008-2011*. 31st ed. 2008: The Royal and Ancient Golf Club of St Andrews and The United States Golf Association.

27. Betzler, N., *Static and Dynamic Characterisation of Golf Shafts (Unpublished)*. 2007, Napier University.

28. Horwood, G.P., *Golf shafts - a technical perspective*, in *Science and Golf II*, A.J. Cochran and M.R. Farrally, Editors. 1994, E & FN Spon: St Andrews, Scotland.

29. MacKenzie, S.J., *Understanding the Role of Shaft Stiffness in the Golf Swing*. 2005, University of Saskatchewan: Saskatoon.

30. Penner, A.R., *The physics of golf.* Reports on Progress in Physics, 2003(2): p. 131.

31. Betzler, N., M. Strangwood, E. Wallace, and S.R. Otto. *The Static and Dynamic Behaviour of Carbon Fibre Composites used in Golf Club Shafts*. in *Paper presented at the 17th International Conference on Composite Materials*. 2009. Edinburgh, UK.

32. Staab, G.H., *Laminar Composites*. 1999: Elsevier.

33. Agarwal, B.D., L.J. Broutman, and K. Chandrashekhara, *Analysis and performance of fiber composites*. 3rd ed. 2006, Hoboken, New Jersey: John Wiley and Sons Inc. 562.

34. Chung, D.D.D.L., *Carbon Fiber Composites*. 1994: Elsevier.

35. Goodman, S.H., *Handbook of Thermoset Plastics*. 2nd ed. 1998: Noyes Publications.

36. Qi, H.J., K. Joyce, and M.C. Boyce, *Durometer hardness and the stress-strain behavior of elastomeric materials.* Rubber Chemistry and Technology, 2003. **76**(2).

37. Cowie, J.M.G., *Polymers: Chemistry and Physics of Modern Materials*. 2nd ed. 1991: Chapman and Hall.

38. May, C.A., *Epoxy Resins: Chemistry and Technology*. 2 ed, ed. C.A. May. 1988, New York: Marcel Dekker.

39. Adams, R.C., S. Advani, D.E. Alman, and F.R. Andressen, *Composites*, in *ASM Handbook*, D.B. Miracle and S.L. Donaldson, Editors. 2001, ASM International.

40. Bogan, S.D. and M.K. Hinders, *Dynamic Stress Concentrations in Fiber-Reinforced Composites with Interface Layers.* Journal of Composite Materials, 1993. **27**(13): p. 1272.

41. Roselman, I.C. and D. Tabor, *The friction and wear of individual carbon fibres* Journal of applied Physics, 1977. **10**.

42. Chamis, C.C., *Mechanics of load transfer at the interface*. Composite Materials, ed. E.P. Plueddemann. Vol. 6. 1974: Academic Press.

43. Chamis, C.C., *Polymer Composite Mechanics Review — 1965 to 2006.* Journal of Reinforced Plastics and Composites, 2007. **26**(10): p. 987.

44. Pitkethly, M.J. and J.B. Doble, *Characterizing the fibre/matrix interface of carbon fibre-reinforced composites using a single fibre pull-out test.* Composites Science and Technology, 1990. **21**(5): p. 389.

45. Zhong, W. and N. Pan, *A Computer Simulation of Single Fibre Pull out Process in a Composite.* Journal of Composite Materials, 2003. **37**(21): p. 1951.

46. Sakai, M., R. Matsuyama, and T. Miyajima, *The pull-out and failure of a fiber bundle in a carbon fiber reinforced carbon matrix composite.* Carbon, 2000. **38**: p. 2123.

47. Piggott, M.R. and D. Andison, *The Carbon Fibre-Epoxy Interface.* Journal of Reinforced Plastics and Composites, 1987. **6**(3): p. 290-302.

48. Wadsworth, N.J. and I. Spilling, *Load transfer from broken fibres in composite materials.* BRIT. J. APPL. PHYS., 1968. **1**: p. 1049 - 1058.

49. Bouette, B., C. Cazeneuve, and C. Oytana, *Effect of strain rate on interlaminar shear properties of carbon/epoxy composites.* Composites Science and Technology, 1992. **45**: p. 313.

50. Choi, H. and F. Chang, *A Model for Predicting Damage in Graphite/Epoxy Laminated Composites Resulting from Low-Velocity Point Impac.* Journal of Composite Materials, 1992. **26**(14): p. 2134.

51. Gubran, H.B.H. and K. Gupta, *The effect of stacking sequence and coupling mechanisms on the natural frequencies of composite shafts.* Journal of Sound and Vibration, 2005. **282**(1-2): p. 231-248.

52. Ni, R.G. and R.D. Adams, *The Damping and Dynamic Moduli of Symmetric Laminated Composite Beams; Theoretical and Experimental Results.* Journal of Composite Materials, 1984. **18**.

53. Ha, S.K. and G.S. Springer, *Nonlinear Mechanical Properties of a Thermoset Matrix Composite at Elevated Temperatures.* Journal of Composite Materials, 1989. **23**(11): p. 1130-1158.

54. Fish, J.C. and S.W. Lee, *Delamination of tapered composite structures.* Engineering Fracture Mechanics, 1989. **34**(1): p. 43-54.

55. Gill, R.M., *Carbon fibres in Composite Materials*. 1972, London: The Butterworth Group. pp90-91.

56. Harkati, E.H., A. Bezazi, F. Scarpa, K. Alderson, and A. Alderson, *Modelling the influence of the orientation and fibre reinforcement on the Negative Poisson's ratio in composite laminates.* Phys. Stat. Sol. (b), 2007. **244**(3): p. 883-892.

57. Jones, R., *Mechanics of Composite Materials*. 1975: Scripta Book Company.

58. Lee, C.Y., M. Pfeifer, B.S. Thompson, and M.V. Gandhi, *The Characterization of Elastic Moduli and Damping Capacities of Graphite/Epoxy Composite Laminated Beams in Hygrothermal Environments.* Journal of Composite Materials, 1989. **23**(8): p. 819-845.

59. Melanitis, N., C. Galiotis, P.L. Tetlow, and C.K.L. Davies, *Fragmentation Studies on Carbon Fibre/Epoxy Systems Interfacial Shear Stress Distribution in Model Composites Part 2:*. Journal of Composite Materials, 1992. **26**: p. 574.

60. Montes-Moran, M.A. and R.J. Young, *Raman spectroscopy study of high modulus carbon fibres: effects of plasma-treatment on the interfacial properties of single fibre-epoxy composites. Part II: Characterisation of the fibre-matrix interface.* Carbon, 2002. **40**: p. 857.

61. Mujika, F., *New Considerations on the Stress Field in an Off-axis Tensile Test.* Journal of Composite Materials, 2005. **39**(21): p. 1909.

62. Mujika, F., N. Carbajal, A. Arrese, and I. Mondragon, *Determination of tensile and compressive moduli by flexural tests.* Polymer Testing, 2006. **25**(6): p. 766-771.

63. Naik, A., N. Abolfathi, G. Karami, and M. Ziejewski, *Micromechanical Viscoelastic Characterization of Fibrous Composites.* Journal of Composite Materials, 2008. **42**(12): p. 1179.

64. Stecenko, T.B. and M.M. Stevano, *Variation of Elastic Moduli with Strain in Carbon/Epoxy Laminates.* Journal of Composite Materials, 1990. **24**: p. 1152 - 1158.

65. Zako, M., K. Matsumoto, Y. Nakanishi, and N. Matsumoto, *Identification of equivalent elastic parameters of triaxial woven fabric composites for golf shafts.* Science and Engineering of Composite Materials, 2004. **11**(2-3): p. 209 - 215.

66. *CoDA v3.1(Help Documentation - Appendix D)*: Anaglyph Ltd. National Physical Laboratory. London. UK.

67. Adams, R.D. and D.G.C. Bacon, *Effect of Fibre Orientation and Laminate Geometry on the Dynamic Properties of CFRP*. Journal of Composite Materials, 1973. **7**(4): p. 402.

68. Adams, R.D. and D.G.C. Bacon, *The Dynamic Properties of Unidirectional Fibre Reinforced Composites in Flexure and Torsion.* Journal of Composite Materials, 1973. **7**(53).

69. Avallone, E.A., T. Baumeister, and A.M. Sadegh, *Marks' Standard Handbook for Mechanical Engineers*. 11th ed. 2007: McGraw-Hill

70. Matthews, F.L. and R.D. Rawlings, *Composite materials: Engineering and science*. 1999, Cambridge: Woodhead publishing limited. 470.

71. Findley, W.N., J.S. Lai, and K. Onaran, *Creep and Relaxation of Nonlinear Viscoelastic Materials: With an Introduction to Linear Viscoelasticity*. 1989: Dover Publications.

72. Ward, I.M. and J. Sweeney, *An Introduction to the Mechanical Properties of Solid Polymers*. 2 ed. 2004, London, UK: Wiley and Sons, Ltd.

73. Painter, P.C. and M.M. Coleman, *Essentials of Polymer Science and Engineering*. 2009: DEStech Publications.

74. Sperling, L.H., *Introduction to Physical polymer Science*. 2006: A John Wiley & Sons, Inc.

75. Hsiao, H.M. and I.M. Daniel, *Strain rate behavior of composite materials.* Composites Part B: Engineering, 1998. **29**(5): p. 521-533.

76. Groves, S.E. and A.L. Highsmith, *Compression response of composite structures*. 1994: ASTM International.

77. Groves, S.E., R.J. Sanchez, R.E. Lyon, and A.E. Brown, *In Composite Materials: Testing and Design*, ed. P.A.S.o.T.a. Materials. Vol. 11. 1993: ASTM International.

78. Gilat, A., R.K. Goldberg, and G.D. Roberts, *Experimental study of strain-rate-dependent behavior of carbon/epoxy composite.* Composites Science and Technology, 2002. **62**(10-11): p. 1469-1476.

79. Gilat, A., R.K. Goldberg, and G.D. Roberts, *Strain Rate Sensitivity of Epoxy Resin in Tensile and Shear Loading.* Journal of Aerospace Engineering, 2007. **20**(2): p. 75-89.

80. Vinson, J.R. and E. Woldesenbet, *Fiber Orientation Effects on High Strain Rate Properties of Graphite/Epoxy Composites.* Journal of Composite Materials, 2001. **35**: p. 509 - 513.

81. McClung, A.J.W. and M.B. Ruggles-Wrenn, *The rate (time)-dependent mechanical behavior of the PMR-15 thermoset polymer at elevated temperature.* Polymer Testing, 2008. **27**(7): p. 908-914.

82. Goldberg, R.K., G.D. Roberts, and A. Gilat, *Incorporation of mean stress effects into the micromechanical analysis of the high strain rate response of polymer matrix composites.* Composites: Part B, 2003. **34**: p. 151 -165.

83. Goldberg, R.K. and D.C. Stouffer, *Strain Rate Dependent Analysis of a Polymer Matrix Composite Utilizing a Micromechanics Approach.* Journal of Composite Materials, 2002. **36**(7): p. 773

84. Bergstrom, J.S. and M.C. Boyce, *Deformation of Elastomeric Networks: Relation between Molecular Level Deformation and Classical Statistical Mechanics Models of Rubber Elasticity* Macromolecules, 2001. **34**: p. 614 - 626.

85. Haque, A. and M. Ali, *High Strain Rate Responses and Failure Analysis in Polymer Matrix Composites – An Experimental and Finite Element Study.* Journal of Composite Materials, 2005. **39**(5): p. 423.

86. Jacob, G.C., J.M. Starbuck, J.F. Fellers, S. Simunovic, and R.G. Boeman, *Strain Rate Effects on the Mechanical Properties of Polymer Composite Materials.* Journal of Applied Polymer Science, 2004. **94**: p. 296-301.

87. Jadhav, A., *High Strain Rate Properties of Polymer Matrix Composites*. 2003, Louisiana State University.

88. Lakes, R., *Viscoelastic Materials*. 2009: Cambridge University Press.

89. Lakes, R.S., *High Damping Composite Materials: Effect of Structural Hierarchy.* Journal of Composite Materials, 2002. **36**(3): p. 287-297.

90. Crane, R.M. and J. John W. Gillespie, *Characterization of the Vibration Damping Loss Factor of Glass and Graphite Fiber Composites.* Composites Science and Technology, 1991. **40**: p. 355-375.

91. Cebon, D. and M.F. Ashby, *Material Selection for Precision Equipment.* Meas. Science and Technology, 1994. **5**: p. 296 - 306.

92. Ashby, M.F., *Materials selection in mechanical design*. 2nd ed. 1999: Butterworth-Heinemann. 501.

93. Main, I.G., *Vibrations and Waves in physics*. 1978: Cambridge University Press.

94. Kadioglu, F., *Measurement of Dynamic Properties of Composites in Vibration by Means of a Non-contact Mechanism.* Journal of Reinforced Plastics and Composites, 2009. **28**(12): p. 1459-1467.

95. Shokrieh, M.M. and A. Najafi, *An Experimental Evaluation of Micromechanical Approaches for Damping Characterization of Polymer Matrix Composites.* Journal of Composite Materials, 2008. **42**(24): p. 2599-2613.

96. Deng, S. and L. Ye, *Influence of Fibre-Matrix Adhesion on Mechanical Properties of Graphite/Epoxy Composites: III. Impact and Dynamic Mechanical Properties.* Journal of Reinforced Plastics and Composites, 2000. **19**(9): p. 689-703.

97. Tong, L., A.P. Mouritz, and M.K. Bannister, *3D Woven Composites*, in *3D Fibre Reinforced Polymer Composites*. 2002, Elsevier Science: Oxford. p. 107-136.

98. *CoDA v3.1*, Anaglyph Ltd. National Physical Laboratory. London. UK.

99. Betzler, N. and C.Slater. *The Static and Dynamic Behaviour of Carbon Fibre Composites Used in Golf Club Shafts*. in *ICCM 17*. 2009. Edinburgh.

100. Chen, A.S. and F.L. Matthews. *Biaxial Flexural Fatigue of Composite Plates*. in *ICCM 9*. 1993. Madrid.

101. Berthelot, J.-M., *Damping analysis of laminated beams and plates using the Ritz method.* Composite Structures, 2006. **74**(2): p. 186-201.

102. Slater, C., N. Betzler, S. Otto, and M. Strangwood. *The Static and Dynamic Behaviour of Carbon Fibre Composites*

used in Golf Club Shafts. in *4th APCST - The Impact of Technology on*

Sport III. 2009. Honolulu, Hawaii.

103. Jones, D.I.G., *Handbook of Viscoelastic Vibration Damping*. 2001, Chichester, UK: John Wiley and Sons Ltd.

104. Ni, R.G. and R.D. Adams, *The Damping and Dynamic Moduli of Symmetric Laminated Composite Beams--Theoretical and Experimental Results.* Journal of Composite Materials, 1984. **18**(2): p. 104-121.

105. Alam, N. and N.T. Asnani, *Vibration and Damping Analysis of Fibre Reinforced Composite Material Plates.* Journal of Composite Materials, 1986. **20**(1): p. 2-18.

106. Davies, P. and G. Evrard, *Accelerated ageing of polyurethanes for marine applications.* Polymer Degradation and Stability, 2007. **92**(8): p. 1455-1464.

107. Joshi, O.K., *The effect of moisture on the shear properties of carbon fibre composites.* Composites, 1983. **14**(3): p. 196-200.

108. Selzer, R. and K. Friedrich, *Mechanical properties and failure behaviour of carbon fibre-reinforced polymer composites under the influence of moisture.* Composites Part A: Applied Science and Manufacturing, 1997. **28**(6): p. 595-604.

109. Ageorges, C., L. Ye, and M. Hou, *Advances in fusion bonding techniques for joining thermoplastic matrix composites: a review.* Composites Part A: Applied Science and Manufacturing, 2001. **32**(6): p. 839-857.

110. Liu, P.F., S.J. Hou, J.K. Chu, X.Y. Hu, C.L. Zhou, Y.L. Liu, J.Y. Zheng, A. Zhao, and L. Yan, *Finite element analysis of postbuckling and delamination of composite laminates using virtual crack closure technique.* Composite Structures, 2011. **93**(6): p. 1549-1560.

111. Singh, S.P. and K. Gupta, *Experimental Studies on Composite Shafts*, in *International Conference on Advances in Mechanical Engineering*. 1995, IISc: Bangalore. p. 1205-1220.

112. Bosia, F., M. Facchini, J. Botsis, T. Gmür, and D. de'Sena, *Through-the-thickness distribution of strains in laminated composite plates subjected to bending.* Composites Science and Technology, 2004. **64**(1): p. 71-82.

113. Mulle, M., R. Zitoune, F. Collombet, L. Robert, and Y.H. Grunevald, *Embedded FBGs and 3-D DIC for the stress analysis of a structural specimen subjected to bending.* Composite Structures, 2009. **91**(1): p. 48-55.

114. Young, W.C., *Roark's formulas for stress and strain*. 6th ed. 1989: McGraw-Hill International Editions.

115. Nagy, P.M., A. Juhász, G. Vörös, A. Tóth, and T. Ujvári, *Internal friction measurement on polymers by low-frequency cyclic Vickers microindentation test.* Materials Science and Engineering A, 2004. **387-389**: p. 525-530.